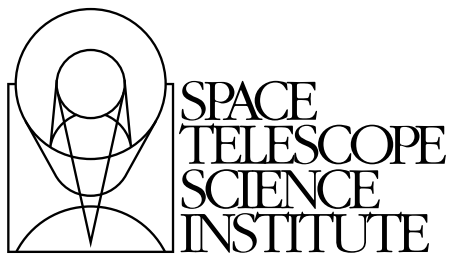


---

Version 5.0  
October 2004

# Advanced Camera for Surveys Instrument Handbook for Cycle 14



Space Telescope Science Institute  
3700 San Martin Drive  
Baltimore, Maryland 21218  
[help@stsci.edu](mailto:help@stsci.edu)

## User Support

For prompt answers to any question, please contact the STScI Help Desk.

- **E-mail:** [help@stsci.edu](mailto:help@stsci.edu)
- **Phone:** (410) 338-1082  
(800) 544-8125 (U.S., toll free)

## World Wide Web

Information and other resources are available on the ACS World Wide Web site:

- **URL:** <http://www.stsci.edu/hst/acs>

## Revision History

Version	Date	Editors
5.0	October 2004	Pavlovsky, C., Biretta, J., Bohlin, R., Cox, C., Fruchter, A., Giavalisco, M., Gilliland, R., Gonzaga, S., Hack, W., Heyer, I., Hook, R., Jogee, S., Koekemoer, A., Krist, J., Mack, J., Mutchler, M., Platais, V., Riess, A., Sirianni, M., Van der Marel, R., Welty, A., Ford, H., Illingworth, G., Blakeslee, J., Clampin, M., Martel, A., Meurer, G., Walsh, J., Pasquali, A., Pirzkal, N.
4.0	October 2003	Pavlovsky, C., et al.
3.0	October 2002	Pavlovsky, C., et al.
2.1	July 2001	Pavlovsky, C., et al.
2.0	June 2001	Suchkov, A., et al.
1.0	June 2000	Jedrzejewski, R., et al.

## Citation

In publications, refer to this document as:

Pavlovsky, C., et al. 2004, "ACS Instrument Handbook", Version 5.0, (Baltimore: STScI).

Send comments or corrections to:  
Space Telescope Science Institute  
3700 San Martin Drive  
Baltimore, Maryland 21218  
E-mail: [help@stsci.edu](mailto:help@stsci.edu)

# Acknowledgments

The technical and operational information contained in this Handbook is the summary of the experience gained by members of the STSci ACS Branch, the ACS group at ST-ECF and by the ACS IDT. The ACS IDT is Holland Ford (PI), Garth Illingworth (Deputy PI), George Hartig, Mark Rafal, Frank Bartko, Tom Broadhurst, Bob Brown, Chris Burrows, Ed Cheng, Mark Clampin, Jim Crocker, Paul Feldman, Marijn Franx, David Golimowski, Randy Kimble, John Krist Tom La Jeunesse, Mike Lesser, Doug Leviton, George Miley, Marc Postman, Piero Rosati, Bill Sparks, Pam Sullivan, Zlatan Tsvetanov, Paul Volmer, Rick White, Bob Woodruff, David Ardila, Narciso Benitez, John Blakeslee, Rychard Bouwens, Larry Bradley, Nicholas J.G. Cross, Ricardo Demarco, Tomotsugu Goto, Caryl Gronwall, Brad Holden, Nicole Homeier, André Martel, Simona Mei, Felipe Menanteau, Gerhardt Meurer, Veronica Motta, Marco Sirianni and Hien Tran. The ST-ECF ACS group is Jeremy Walsh, Anna Pasquali and Norbert Pirzkal. The contributions of Warren Hack, Alan Welty and Susan Rose are also greatly appreciated.

## ACS Instrument Branch at STSci

Name	Title	Phone	e-mail
Roeland Van der Marel	Instrument Scientist	(410)338-4931	marel@stsci.edu
John Biretta	Instrument Scientist	(410)338-4917	biretta@stsci.edu
Ralph Bohlin	Instrument Scientist	(410) 338-4804	bohlin@stsci.edu
Andrew Fruchter	Instrument Scientist	(410) 338-5018	fruchter@stsci.edu
Mauro Giavalisco	Instrument Scientist	(410) 338-4804	mauro@stsci.edu
Ron Gilliland	Instrument Scientist	(410)338-4366	gillil@stsci.edu
Shardha Jogee	Instrument Scientist	(410) 338-4349	jogee@stsci.edu
Anton Koekemoer	Instrument Scientist	(410) 338-4815	koekemoer@stsci.edu
Adam Riess	Instrument Scientist	(410) 338-4509	ariess@stsci.edu
Marco Sirianni	Instrument Scientist	(410) 338-4810	sirianni@stsci.edu
Colin Cox	Systems Analyst	(410) 338-4792	cox@stsci.edu
Richard Hook (ST-ECF/ESO)	Science Software Specialist	(410)338-4980	hook@stsci.edu
John Krist	Optical Analyst	(410) 338-4901	krist@stsci.edu
Shireen Gonzaga	Data Analyst	(410)338-4412	shireen@stsci.edu
Inge Heyer	Data Analyst	(410)338-5017	heyer@stsci.edu
Jennifer Mack	Data Analyst	(410)338-4565	mack@stsci.edu
Max Mutchler	Data Analyst	(410) 338-1321	mutchler@stsci.edu
Cheryl Pavlovsky	Data Analyst	(410) 338-4339	cheryl@stsci.edu
Vera Platais	Data Analyst	(410) 338-4339	verap@stsci.edu



# Table of Contents

<b>Acknowledgments</b> .....	iii
ACS Instrument Branch at STScI .....	iii

---

<b>Part I: Introduction</b> .....	1
-----------------------------------	---

<b>Chapter 1: Introduction</b> .....	3
1.1 Purpose .....	4
1.1.1 Document Conventions .....	4
1.1.2 Examples Used in this Handbook .....	4
1.2 Handbook Layout .....	5
1.3 Preparing an Observing Proposal with ACS .....	8
1.4 The Help Desk at STScI .....	9
1.5 The ACS Web Site and Supporting Information .....	9

<b>Chapter 2: Special Considerations for Cycle 14</b> .....	11
2.1 ACS is a Maturing Instrument .....	11
2.2 SBC Scheduling Policies .....	12
2.3 Prime and Parallel Observing with the SBC .....	12
2.4 Policy for Auto-Parallel Observations .....	14
2.5 Use of Available-but-Unsupported Capabilities .....	14
2.6 Data Volume Constraints .....	16
2.7 Charge Transfer Efficiency .....	16
2.8 Two-gyro Guiding .....	17
2.9 Status of STIS .....	18

---

<b>Part II: User's Guide</b> .....	19
<b>Chapter 3: Introduction to ACS</b> .....	21
3.1 Instrument Capabilities .....	21
3.2 Instrument Design .....	22
3.2.1 Detectors .....	23
3.2.2 ACS Optical Design .....	24
3.3 Basic Instrument Operations .....	28
3.3.1 Target Acquisitions .....	28
3.3.2 Typical ACS Observing Sequence .....	28
3.3.3 Data Storage and Transfer .....	28
3.3.4 Parallel Operations .....	29
3.4 Designing an ACS Observing Proposal .....	29
3.4.1 Identify Science Requirements and Define ACS Configuration .....	32
3.4.2 Determine Exposure Time and Check Feasibility .....	33
3.4.3 Identify Need for Additional Exposures .....	34
3.4.4 Determine Total Orbit Request .....	34
<b>Chapter 4: Imaging</b> .....	35
4.1 Imaging Overview .....	35
4.2 Which Instrument to Use? .....	41
4.2.1 Comparison of ACS and WFPC2 .....	42
4.2.2 Comparison of ACS and NICMOS .....	43
4.2.3 Comparison of ACS and STIS .....	44
4.3 Caveats for ACS Imaging .....	46
4.3.1 Throughputs and Limiting Magnitudes .....	47
4.3.2 Limiting Magnitudes .....	48
4.3.3 Signal-To-Noise Ratios .....	49
4.3.4 Saturation .....	49
4.4 Wide Field Optical CCD Imaging .....	49
4.4.1 Filter Set .....	50
4.4.2 Long Wavelength Halo Fix .....	51

4.5 High-Resolution Optical and UV Imaging.....	51
4.5.1 Filter Set .....	52
4.5.2 Multiple Electron Events .....	52
4.5.3 Red Leaks.....	52
4.6 Ultraviolet Imaging with the SBC.....	53
4.6.1 Filter Set .....	53
4.6.2 Bright-Object Limits .....	54
4.6.3 Optical Performance .....	54
4.6.4 Red Leaks.....	54
4.7 ACS Point Spread Functions .....	54
4.7.1 CCD Pixel Response Function .....	55
4.7.2 Model PSFs .....	55
4.7.3 Encircled Energy.....	56
4.7.4 Geometric Distortions .....	58
4.7.5 PSFs at Red Wavelengths and the UV.....	59
4.7.6 Residual Aberrations .....	59
4.8 Two-Gyro Guiding.....	62

## **Chapter 5: Polarimetry, Coronagraphy and Prism/Grism Spectroscopy..... 63**

5.1 Polarimetry.....	63
5.2 Coronagraphy .....	69
5.2.1 Coronagraph Design.....	70
5.2.2 Acquisition Procedure and Pointing Accuracy.....	72
5.2.3 Vignetting and Flat Fields .....	73
5.2.4 Coronagraphic Performance.....	74
5.2.5 Residual Light Subtraction.....	78
5.2.6 The Off-Spot PSF .....	82
5.2.7 Occulting Spot Motions.....	84
5.2.8 Planning ACS Coronagraphic Observations.....	85
5.2.9 Choice of Filters for Coronagraphic Observations .....	88

5.3 Grism/Prism Spectroscopy .....	88
5.3.1 WFC G800L .....	89
5.3.2 HRC G800L .....	91
5.3.3 HRC PR200L .....	92
5.3.4 SBC PR110L .....	94
5.3.5 SBC PR130L .....	94
5.3.6 Observation Strategy .....	95
5.3.7 Extraction and Calibration of Spectra .....	98

## Chapter 6: Exposure-Time

<b>Calculations</b> .....	101
6.1 Overview .....	101
6.1.1 The ACS Exposure Time Calculator .....	101
6.2 Determining Count Rates from Sensitivities .....	102
6.2.1 Imaging .....	105
6.2.2 Spectroscopy .....	107
6.3 Computing Exposure Times .....	108
6.3.1 Calculating Exposure Times for a Given Signal-to-Noise .....	109
6.3.2 Exposure Time Estimates for Red Targets in F850LP .....	110
6.3.3 Two-Gyro Guiding .....	111
6.4 Detector and Sky Backgrounds .....	111
6.4.1 Detector Backgrounds .....	112
6.4.2 Sky Background .....	112
6.5 Extinction Correction .....	117
6.6 Exposure-Time Examples .....	118
6.6.1 Example 1: WFC Imaging a Faint Point Source .....	119
6.6.2 Example 2: SBC Objective Prism Spectrum of a UV Spectrophotometric Standard Star .....	120
6.6.3 Example 3: WFC VIS Polarimetry of the Jet of M87 .....	120
6.6.4 Example 4: SBC imaging of Jupiter's Aurora at Lyman-alpha .....	121
6.6.5 Example 5: Chronographic imaging of the Beta-Pictoris Disk .....	121
6.7 Tabular Sky Backgrounds .....	122

<b>Chapter 7: Feasibility and Detector Performance .....</b>	<b>125</b>
7.1 The CCDs .....	125
7.1.1 Detector Properties .....	125
7.1.2 CCD Spectral Response .....	127
7.1.3 Quantum Efficiency Hysteresis .....	127
7.1.4 CCD Long-Wavelength Fringing .....	127
7.1.5 Optical Performance .....	127
7.1.6 Readout Format .....	128
7.1.7 Analog-To-Digital Conversion .....	128
7.1.8 Flat Fields .....	129
7.2 CCD Operations and Limitations .....	131
7.2.1 CCD Saturation: the CCD Full Well .....	131
7.2.2 CCD Shutter Effects .....	132
7.2.3 Readnoise .....	133
7.2.4 Dark Current .....	134
7.2.5 Cosmic Rays .....	136
7.2.6 Hot Pixels .....	137
7.2.7 Charge Transfer Efficiency .....	140
7.2.8 UV Light and the HRC CCD .....	142
7.3 The SBC MAMA .....	142
7.3.1 MAMA Properties .....	142
7.3.2 SBC Spectral Response .....	144
7.3.3 Optical Performance .....	145
7.4 SBC Operations and Limitations .....	145
7.4.1 MAMA Overflowing the 16 Bit Buffer .....	145
7.4.2 MAMA Darks .....	146
7.4.3 SBC Signal-to-Noise Ratio Limitations .....	147
7.4.4 SBC Flatfield .....	148
7.4.5 SBC Nonlinearity .....	149

7.5 SBC Bright-Object Limits.....	149
7.5.1 Overview.....	149
7.5.2 Observational Limits .....	150
7.5.3 How Do You Determine if You Violate a Bright Object Limit? .....	152
7.5.4 Policy and Observers' Responsibility in Phase I and Phase II .....	152
7.5.5 What To Do If Your Source is Too Bright for Your Chosen Configuration? .....	154
7.5.6 Bright-Object Protection for Solar System Observations .....	154

## **Chapter 8: Observing Techniques** ..... 157

8.1 Operating Modes.....	157
8.1.1 WFC ACCUM Mode .....	158
8.1.2 HRC ACCUM Mode.....	160
8.1.3 SBC ACCUM Mode .....	161
8.1.4 HRC ACQ Mode .....	162
8.2 Patterns and Dithering .....	162
8.2.1 How to Obtain Dithered Data.....	163
8.2.2 Supported Patterns.....	164
8.2.3 How to Combine Dithered Observations .....	164
8.2.4 How to Determine the Offsets.....	165
8.3 A Road Map for Optimizing Observations.....	165
8.4 CCD Gain Selection .....	168
8.4.1 WFC Gain .....	168
8.4.2 HRC Gain .....	169
8.5 ACS Apertures .....	169
8.5.1 WFC Apertures .....	169
8.5.2 Ramp Filter Apertures.....	171
8.5.3 The Small Filter Apertures .....	173
8.5.4 Polarizer Apertures .....	175
8.5.5 HRC Apertures .....	175
8.5.6 SBC Apertures.....	175
8.6 Fixing Orientation on the Sky .....	177
8.6.1 Determining Orientation for Phase II .....	181
8.7 Parallel Observations .....	181
8.7.1 Parallel Observing .....	181
8.8 Two-Gyro Guiding.....	186

<b>Chapter 9: Overheads and Orbit-Time Determination</b>	187
9.1 Overview	187
9.2 ACS Exposure Overheads	188
9.2.1 Subarrays	191
9.3 Orbit Use Determination Examples	192
9.3.1 Sample Orbit Calculation 1:	192
9.3.2 Sample Orbit Calculation 2	193
9.3.3 Sample Orbit Calculation 3:	193
9.3.4 Sample Orbit Calculation 4:	194
9.3.5 Sample Orbit Calculation 5:	196

## **Part III: Supporting Material** ..... 197

<b>Chapter 10: Imaging Reference Material</b>	199
10.1 Introduction	200
10.2 Using the Information in this Chapter	200
10.2.1 Sensitivity Units and Conversions	200
10.2.2 Signal-To-Noise	201
10.2.3 Point Spread Functions	202
10.3 Distortion in the ACS	248
10.3.1 WFC	249
10.3.2 HRC	251
10.3.3 SBC	252
10.3.4 Summary	254

## **Part IV: Calibration** ..... 255

<b>Chapter 11: Pipeline Calibration</b>	257
11.1 Overview	257
11.1.1 On The Fly Reprocessing (OTFR)	257
11.1.2 When is OTFR not Appropriate or Sufficient?	258
11.1.3 Distortion Correction and Dither Combining	261

11.2 ACS Pipeline .....	263
11.3 ACS Data Products .....	266
11.4 System Requirements for ACS Data .....	269
<b>Chapter 12: Calibration Accuracies</b> .....	273
12.1 Summary of Accuracies .....	273
<b>Chapter 13: Calibration Plans</b> .....	277
13.1 Ground Testing and Calibration .....	278
13.2 SMOV Testing and Calibration .....	278
13.3 Cycle 11 Calibration .....	280
13.3.1 Calibration Priorities .....	280
13.4 Cycle 12 Calibration .....	282
13.5 Cycle 13 Calibration .....	284
13.6 Cycle 14 Calibration .....	285
<b>Glossary</b> .....	287
<b>Index</b> .....	291



PART I:

# Introduction

---

The Chapters in this Part explain how to use this Handbook, where to go for help, and special considerations for using ACS in Cycle 14.





## CHAPTER 1:

# Introduction

### In this chapter. . .

1.1 Purpose / 4
1.2 Handbook Layout / 5
1.3 Preparing an Observing Proposal with ACS / 8
1.4 The Help Desk at STScI / 9
1.5 The ACS Web Site and Supporting Information / 9

The Advanced Camera for Surveys (ACS) is a third-generation instrument that was installed in the Hubble Space Telescope during Servicing Mission 3B, March 7, 2002. Its primary purpose is to increase the discovery efficiency of imaging with HST by providing a combination of detector area and quantum efficiency that surpasses that available from previous instruments by a factor of 10 or so. It consists of three independent cameras that provide wide-field, high resolution and ultraviolet imaging capability respectively, with a broad assortment of filters designed to address a large range of scientific goals. Additional coronagraphic, polarimetric and grism capabilities make this a versatile and powerful instrument. This Instrument Handbook provides instrument-specific information you will need to propose for ACS observations (Phase I), design accepted programs (Phase II), and understand ACS in detail. The companion ACS Data Handbook describes how to deal with ACS data once it has been obtained.

This Chapter explains the layout of the present Handbook and describes how to use the Help Desk at STScI and the STScI ACS World Wide Web pages to get help and further information. Instrument and operating updates will be posted on the ACS Web pages.

## 1.1 Purpose

The *ACS Instrument Handbook* is the basic reference manual for the Advanced Camera for Surveys, and describes the instrument's properties, performance, operations and calibration. The Handbook is maintained by scientists at STScI. Additional information has been provided by the Investigation Definition Team, led by Dr. Holland Ford of Johns Hopkins University, and by the principal contractors, Ball Aerospace.

We have designed the document to serve three purposes:

- To provide instrument-specific information for preparing Cycle 14 Phase I observing proposals using ACS.
- To provide instrument-specific information to support the design of Phase II proposals for accepted ACS programs, in conjunction with the Phase II Proposal Instructions.
- To provide technical information about the operation and expected performance of the instrument, which can help in the understanding of problems and in the interpretation of data acquired with ACS.

### 1.1.1 Document Conventions

This document follows the usual STScI convention in which terms, words and phrases which are to be entered by the user in a literal way on an HST proposal are shown in a typewriter font (e.g., ACS/WFC, F814W). Names of software packages or commands are given in bold type (e.g., **calacs**).

Wavelength units in this Handbook are in Angstroms ( $\text{\AA}$ ), and fluxes are generally given in  $\text{erg cm}^{-2}\text{s}^{-1}\text{\AA}^{-1}$ .

### 1.1.2 Examples Used in this Handbook

To illustrate the use of ACS, we have devised a set of representative programs that cover a range of its capabilities. We hope that they will prove helpful to users both in determining the capabilities of the instrument and in writing a proposal to request HST time. The examples are:

1. Wide Field Channel imaging of a faint point source.
2. Solar Blind Channel (SBC) prism spectroscopy of a faint standard star.
3. Polarimetry of the jet of M87.
4. SBC imaging of Jupiter's aurora.
5. Coronagraphy of the circumstellar disk of  $\beta$  Pic.

---

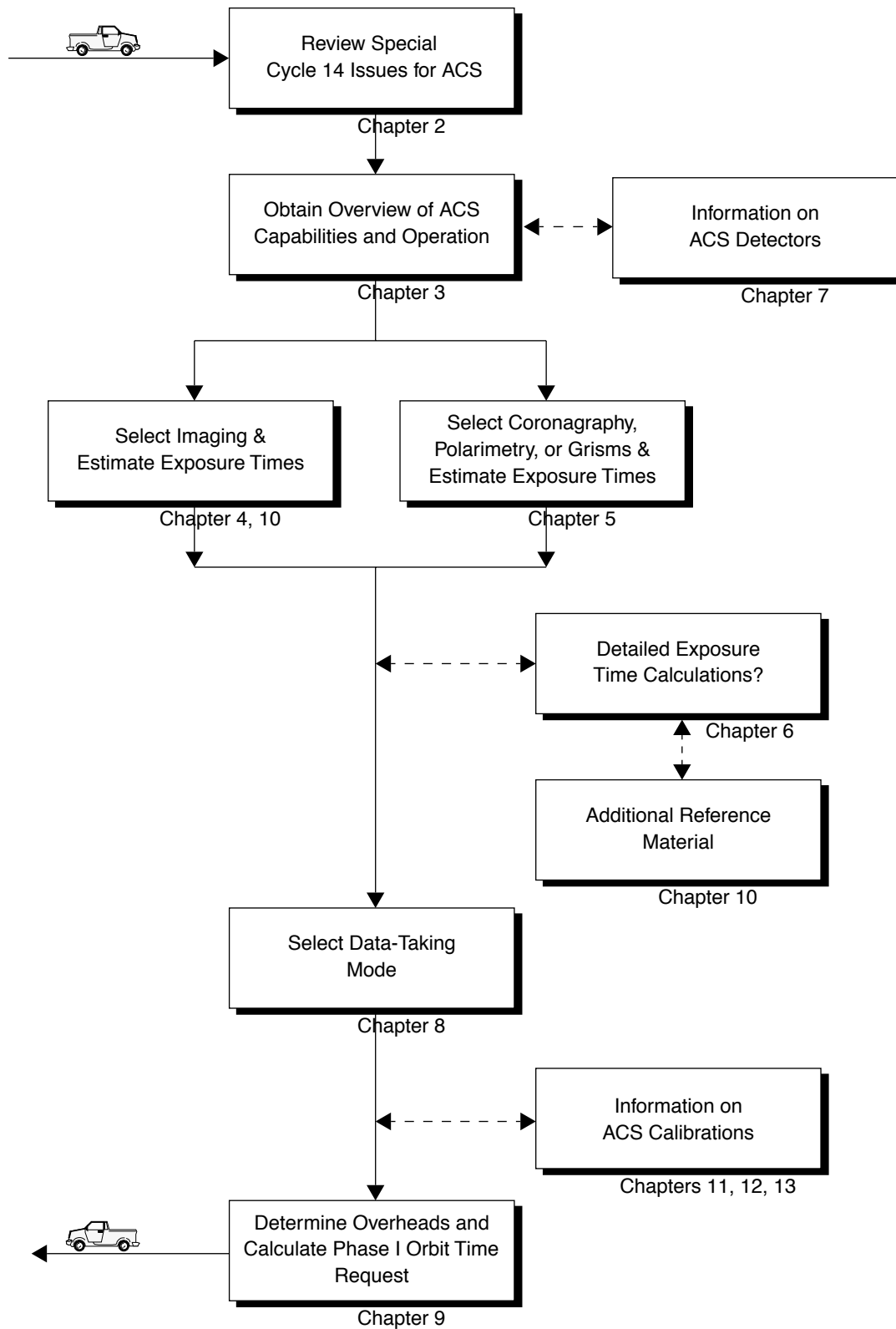
## 1.2 Handbook Layout

To guide you through ACS's capabilities and help optimize your scientific use of the instrument we have divided this handbook into four parts:

- Part I - Introduction
- Part II - User's Guide
- Part III - Supporting Material
- Part IV - Calibration

Figure 1.1 provides a roadmap to navigating this Handbook.

Figure 1.1: ACS Handbook Roadmap for Proposal Preparation



The chapters of this Handbook are as follows:

- Part I - Introduction
  - Chapter 1 - *Introduction*, includes information about getting help.
  - Chapter 2 - *Special Considerations for Cycle 14*, describes special policy considerations for using ACS during Cycle 14.
- Part II - User's Guide
  - Chapter 3 - *Introduction to ACS*, provides an introduction to ACS's capabilities. A discussion is provided to help guide you through the technical details you need to consider in choosing the optimum ACS configuration and in determining the number of orbits to request.
  - Chapter 4 - *Imaging*, provides a description of ACS's imaging capabilities, including camera resolutions and sensitivities.
  - Chapter 5 - *Polarimetry, Coronagraphy and Prism/Grism Spectroscopy*, provides detailed information on these specialized observation modes.
  - Chapter 6 - *Exposure Time Calculations*, describes how to perform signal-to-noise calculations, either by using pencil and paper, or by using software tools that are provided on the World Wide Web.
  - Chapter 7 - *Feasibility and Detector Performance*, provides a description of the three detectors and their physical characteristics, capabilities and limitations, including saturation, linearity and bright object limits.
  - Chapter 8 - *Observing Techniques*, describes some methods that can be used to obtain the best science from ACS, including dithering and the use of pre-defined patterns that mitigate the effects of detector imperfections.
  - Chapter 9 - *Overheads and Orbit Time Determination*, provides information to convert from a series of planned science exposures to an estimate of the number of orbits, including spacecraft and ACS overheads. This chapter applies principally to the planning of Phase I proposals.
- Part III - Supporting Material
  - Chapter 10 - *Imaging Reference Material*, provides summary information and filter transmission curves for each imaging filter.
- Part IV - Calibration
  - Chapter 11 - *Pipeline Calibration*, briefly describes the processing of ACS data by the STScI pipeline and the products that are sent to observers.

- Chapter 12 - *Expected Calibration Accuracies*, summarizes the accuracies expected for ACS data calibrated by the STScI pipeline.
- Chapter 13 - *Calibration Plans*, provides an overview of the current state of ACS calibration, including changes resulting from the Servicing Mission Observatory Verification (SMOV) and Cycle 11 and 12 calibration programs and plans for Cycle 13 and 14 calibration.

---

## 1.3 Preparing an Observing Proposal with ACS

Use the *ACS Instrument Handbook* together with the *Hubble Space Telescope Call for Proposals for Cycle 14* (CP) when assembling your ACS Phase I proposal. In addition the *HST Primer* provides a basic introduction to the technical aspects of HST and its instruments, and explains how to calculate the appropriate number of orbits for your Phase I observing time requests. The CP provides policies and instructions for proposing; the *ACS Instrument Handbook* contains detailed technical information about ACS, describing its expected performance, and presenting suggestions for use. The next Chapter in the Handbook describes special considerations for Cycle 14.

If your Phase I proposal is accepted, you will be asked to submit a Phase II proposal in which you specify the exact configurations, exposure times and sequences of observations that ACS and the telescope should perform. To assemble your Phase II proposal, you should use the *ACS Instrument Handbook* in conjunction with the *Phase II Proposal Instructions*. The Instructions describe the exact rules and syntax that apply to the planning and scheduling of ACS observations and provide relevant observatory information.

---

## 1.4 The Help Desk at STScI

STScI maintains a Help Desk, the staff of which quickly provide answers on any HST-related topic, including questions regarding ACS and the proposal process. The Help Desk staff have access to all of the scientists and resources available at the Institute, and they maintain a database of answers so that frequently asked questions can be immediately answered. The Help Desk staff also provide STScI documentation, in either hardcopy or electronic form, including *Instrument Science Reports* and *Instrument Handbooks*. Questions sent to the Help Desk are answered within two working days. Usually, the Help Desk staff will reply with the answer to a question, but occasionally they will need more time to investigate the answer. In these cases, they will reply with an estimate of the time needed to reply with the full answer.

We ask that you please send *all* initial inquiries to the Help Desk. If your question requires an ACS Instrument Scientist to answer it, the Help Desk staff will put one in contact with you. By sending your request to the Help Desk, you are guaranteed that someone will provide you a timely response. To contact the Help Desk at STScI:

- **Send E-mail:** [help@stsci.edu](mailto:help@stsci.edu) (preferred)
- **Phone:** 1-410-338-1082  
Toll-free in the U.S.: 1-800-544-8125

The Space Telescope European Coordinating Facility (ST-ECF) also maintains a Help Desk. European users should generally contact the (ST-ECF) for help; all other users should contact STScI. To contact the ST-ECF Help Desk:

- **Send E-mail:** [stdesk@eso.org](mailto:stdesk@eso.org)

---

## 1.5 The ACS Web Site and Supporting Information

The ACS Branch at STScI maintains a World Wide Web (WWW) site, as part of STScI's web service. The address for the STScI ACS page is:


<http://www.stsci.edu/hst/acs>

The STScI ACS pages include sections that fall into the following categories:

- **Late Breaking News:** This is where new and important information is posted.

- **Document Archive:** Electronic versions of this Handbook will be maintained on the WWW site. In addition, more detailed technical information concerning the development, performance, testing, operation and calibration of ACS are contained in a series of ACS Instrument Science Reports (ISRs) and STScI Analysis Newsletters (STANs). These reports can be downloaded from the WWW pages or paper copies can be requested from the Help Desk.
- **Software Tools:** This section includes the Exposure Time Calculator (ETC), which can be used to predict exposure times for ACS observations.
- **Data Analysis:** Includes links to the locations of reference files and the CALACS tutorial.
- **Performance:** Information on the status of ACS and discussion of calibration strategies.
- **FAQs:** This section contains answers to the most Frequently Asked Questions.
- **Help:** This section tells you whom to contact when you need help.

Other information, not specific to ACS, can generally be accessed through the top-level STScI web page: <http://www.stsci.edu/>



## CHAPTER 2:

# Special Considerations for Cycle 14

In this chapter . . .

2.1 ACS is a Maturing Instrument / 11
2.2 SBC Scheduling Policies / 12
2.3 Prime and Parallel Observing with the SBC / 12
2.4 Policy for Auto-Parallel Observations / 14
2.5 Use of Available-but-Unsupported Capabilities / 14
2.6 Data Volume Constraints / 16
2.7 Charge Transfer Efficiency / 16
2.8 Two-gyro Guiding / 17
2.9 Status of STIS / 18

ACS was installed in HST as part of Servicing Mission 3B, on March 7, 2002. ACS operations have been smooth throughout the servicing mission orbital verification period after installation and throughout the first two cycles (11 and 12) of science observations. A complete Data Handbook is now available and calibrations and support are nearing a steady state.

---

## 2.1 ACS is a Maturing Instrument

ACS is still a relatively young instrument in comparison to others on HST, but its understanding has advanced well. At the time of Cycle 14

Handbook writing we have over two full years of combined science operations and calibration program execution and analysis from Cycles 11 and 12. Fortunately, operations, calibrations and science observations have continued to go well. Residual uncertainties from ground-based characterizations have been removed through a series of extensive on-orbit calibrations.

Instrument characteristics have for the most part remained stable with only minor or expected exceptions. An example of a minor exception is greater motion of the coronagraphic alignment than expected (see Section 5.2 discussion). An example of an expected change with time is the growth of Charge Transfer Efficiency losses for the CCDs (see Section 7.2 discussion).

The calibration state of the ACS will continue to evolve in the period prior to Cycle 14, but we are well beyond the period of rapid evolution in instrument calibration and characterization that applied two years ago. Most issues are now at a level still relevant for optimal science returns, but largely not useful at the Phase I proposing stage (e.g. sensitivity updates relevant for some filters may still occur at the  $\sim 1\%$  level). As always, we will endeavor to keep users informed on new developments through the ACS WWW site and the ACS STANs (Space Telescope Analysis Newsletters), issued on an occasional basis.

---

## 2.2 SBC Scheduling Policies

The STIS MAMA control electronics were found in orbit to be subject to resets due to cosmic-ray upsets, therefore STIS MAMAs are operated only during the contiguous orbits of each day which are free of the South Atlantic Anomaly (SAA). Even though the design of the ACS MAMA control electronics in the SBC was modified so that it would not be susceptible to cosmic-ray hits, the background count rate still exceeds the bright object limits for the SBC during SAA passage. Consequently, the SBC will in general only be scheduled for use during SAA-free orbits. As we expect the SBC usage to be relatively low compared to the CCD cameras, we do not expect this to pose a problem to users.

---

## 2.3 Prime and Parallel Observing with the SBC

As explained in greater detail in Section 7.5, the MAMA detector that ACS uses in the ultraviolet is subject to damage at high illumination rates. To protect the instrument, we have established limits on the maximum count rate at which the detector may be illuminated. These count-rate limits

translate into a set of configuration-dependent bright-object screening magnitudes. These are summarized in Table 7.8.

STScI will perform screening of all SBC exposures prior to scheduling. Targets not established as safe for the configuration in which they are being observed will not be scheduled. Observations that pass screening but are lost in orbit due to a bright-object violation will not be rescheduled. Observers are responsible for assuring that their observations do not violate the SBC count-rate limits. A detailed description of the SBC bright-object limits and the observers' responsibility is presented in Section 7.5.

To assure that STScI can adequately screen observations, special constraints are imposed on parallel observing with the SBC. In particular:

- No pure parallels are allowed using the SBC.
- Coordinated parallels are allowed with the SBC only if an exact spacecraft orientation (ORIENT) is requested and the RA and Dec. of the parallel field determined. Note that the specification of an exact ORIENT usually limits the scheduling of observations to a ~4–6 week period each year. The observer is responsible for assuring that observations do not violate the SBC count rate limits both for coordinated parallel SBC observations and for prime observations.
- SNAPSHOT observations with the SBC will not be allowed for Cycle 14.

Table 2.1 below summarizes the policy with respect to SBC observing in Cycle 13.

Table 2.1: Bright-Object Protection Policy for SBC Observations

Type of Observing	Policy
Prime	Allowed if target passes screening
Snapshots	Not allowed
Coordinated parallel	Allowed only if ORIENT is exactly specified and field passes screening
Pure parallel	Not allowed

Targets that are one magnitude or more fainter than the magnitude limits in the screening tables generally automatically pass screening. For a target that is within one magnitude of the screening limits, observers must provide a calibrated spectrum of the source at the intended observing wavelength. If such a spectrum is not available, the prospective GO must request an orbit in Phase I for a pre-qualification exposure, during which the target spectrum must be determined by observation in an allowed configuration (see Section 7.5 for more details).

Please also note that if you are proposing SBC target-of-opportunity observations, we ask you to provide an explanation in your Phase I proposal of how you will ensure that your target can be safely observed.

---

## 2.4 Policy for Auto-Parallel Observations

As described in Section 8.7, ACS is able to make simultaneous observations using the Wide-Field Channel and the High Resolution Channel. Such observations are added automatically by the scheduling system if doing so does not impact the primary exposures. However, since the WFC and HRC share the same filter wheel, the filter used in the “parallel” channel is determined by that selected for the “prime” detector; the observer does not have the capability to select the parallel filter independently. This means that the possibility and character of these “Auto-Parallel” observations are purely a result of the choices made by the proposer of the prime program. For this reason, the following policies will be in effect for Auto-Parallel observations:

- Auto-Parallel observations are the property of the PI of the program using the prime ACS detector.
- Auto-Parallel observations are not available for independent scheduling.
- There are some fairly severe timing constraints under which Auto-Parallel observations may be added. The scheduling system will add parallels only if it can do so without affecting the prime science.
- If WFC data are taken in parallel with prime HRC observations, the GAIN setting will be 2 (see Section 4.3), also for HRC parallels added to prime WFC exposures the GAIN will be 2.
- WFC Auto-parallel observations are subject to compression at a level that can occasionally result in some data loss. Such observations will not be repeated.

---

## 2.5 Use of Available-but-Unsupported Capabilities

We have established a set of core scientific capabilities for ACS which will be supported for Cycle 14 and are described fully in this Handbook. In addition there are a few capabilities with ACS, some of which are mentioned in this Handbook, for which limited access is available. These capabilities are “available-but-unsupported,” and in consultation with an ACS Instrument Scientist can be requested. These include a few apertures, limited interest optional parameters, some GAIN options, and filterless (CLEAR) operation. If you find that your science cannot be obtained using fully supported modes, or that it would be much better with use of these special cases, then you may wish to consider use of an unsupported mode.

Use of unsupported modes comes at a price, and they should be used only if the technical requirement and scientific justification are particularly compelling. The following caveats apply:

- Calibrations for available-but-unsupported modes will not be provided by STScI, it will be the observer's responsibility to obtain such as needed.
- STScI adopts a policy of shared risk with the observer for the use of these modes. Requests to repeat failed observations taken with unsupported capabilities will not be honored if the failure is related to use of this capability.
- User support from STScI will be more limited.

Cycle 14 Phase I proposals that include use of unsupported ACS capabilities must include the following:

- Justification of why supported modes don't suffice;
- A request for any observing time needed for calibration purposes;
- Justification for added risk of use in terms of scientific payback;
- Demonstration that the observers are able to analyze such data.

During the Phase II proposal submission process, use of available-but-unsupported modes requires formal approval from the ACS Branch at STScI. To request permission for use of an available-but-unsupported mode, please send a brief email to your Program Coordinator (PC) that addresses the above four points. The PC will relay the request to the contact scientist or relevant ACS instrument scientist, who will decide whether the use will be allowed. This procedure ensures that any potential technical problems have been taken into account. Note also that Archival research may be hindered by use of these modes. As a result, requests for use of unsupported modes which do not adequately address the above four points, or which will result in only marginal improvements in the quality of the data obtained, may be denied, even if the request was included in your approved Phase I proposal.

The current list of available-but-unsupported items are:

- Targets: BIAS
- Apertures: WFC RAMPs, WFC2-2K
- Optional parameters: SIZEAXIS1, SIZEAXIS2, CENTERAXIS1, CENTERAXIS2, COMPRESSION, AUTOIMAGE, AMP, FLASHEXP, WFC: GAIN=4,8, HRC: GAIN=1,8
- Spectral elements: CLEAR (both WFC and HRC)
- ACQ mode: optional parameter GAIN




---

*RAMP filters are fully supported with aperture WFC resulting in full field readouts. The WFC1-IRAMP, WFC1-MRAMP, WFC2-MRAMP and WFC2-ORAMP apertures (see Table 8.1) are available-but-unsupported.*

---

## 2.6 Data Volume Constraints

If ACS data are taken at the highest possible rate for more than a few orbits or in the CVZ, it is possible to accumulate data faster than it can be transmitted to the ground. High data volume proposals will be reviewed and on some occasions, users may be requested to break the proposal into different visits, consider using sub-arrays, or taking other steps to reduce data volume.

## 2.7 Charge Transfer Efficiency

Both the STIS and WFPC2 CCDs have shown a significant degradation in charge transfer efficiency (CTE) performance since their installation. The degradation is due to radiation damage of the silicon inducing the creation of traps that impede the clocking of the charge on the CCD. Since reading out the ACS WFC requires 2048 parallel transfers and 2048 serial transfers, it is not surprising that CTE effects have begun to manifest themselves in even the first years of ACS operation. For this reason, it is likely that some types of science, particularly those in which the source flux in each image is expected to be low ( $<0.1$  electrons/second) and compact, will be most effectively performed during the first few years of ACS operation.

Our initial expectations for growth of CTE for the Wide Field Camera have proven to be conservative. After multiple iterations of special programs designed to track the growth of CTE in time we have found that after 1 year of operation there was a loss of approximately 1-2% in the counts from a star with between 50 and 150 total electrons, a nominal sky background of 30 electrons, and with placement at row 1024 (center) in one of the WFC chips. After 2 years the growth rate appears to be linear, thus such a target would experience a loss of approximately 4-8% in the middle (early 2006) of Cycle 14. A target placed at the WFC aperture

reference point, near the maximum number of parallel shifts during readout, would have approximately twice the loss. Since the measurements to date extend only to 2 years post-launch of ACS, and the extrapolation to Cycle 14 is by a factor of two in baseline, these estimates must still be taken with an appropriate level of caution, however, the view now is that CTE is not developing as rapidly as previously expected, and is not yet a major driver affecting ACS science quality. Expected absolute errors after calibration of science data, at these low-loss levels, is expected to be of order 25% the relative loss.

As the CTE effects worsen in more remote future Cycles, users may want to consider using the post-flash capability (currently an “available-but-unsupported” mode) to add a background level to their images. This causes the Poisson noise from the background level to increase, and imposes a non-uniform background, but to-date only marginally improves the CTE performance of the detector. We do not recommend the use of the post-flash capability for any applications during Cycle 14, but we will continue to track this carefully and stand ready to revise this recommendation in a liberal way for future cycles. We are confident this is not yet the time to begin considering post-flash use. Please refer to Section 7.5 for more information on this topic.

---

## 2.8 Two-gyro Guiding

HST currently operates with three rate sensing gyros in the guiding control loop. At some point in the future additional gyroscopes on HST may fail, thus making it necessary to observe with only two gyroscopes instead of the usual contingent of three. This would have significant impacts on the scheduling of observations -- both the number of minutes available for observation per orbit, and the times of year when a given target can schedule, would be significantly reduced. It is also possible that the guiding would be less accurate -- there is a potential for a high-frequency (many Hz) pointing jitter to be superposed on the normal HST tracking, which would degrade the effective PSF. There is also some possibility that target positioning on the detectors would become less accurate. Tests of two-gyro guiding are planned for early 2005, where many of these impacts should become better defined. Additional tests would also be conducted in the event that gyro failures make two-gyro guiding necessary.



---

*Further discussion of how these impacts will affect the observatory and the instruments can be found in a separate Handbook, the HST Two-Gyro Handbook for Cycle 14. See the Two-Gyro Handbook for detailed information. All text in this ACS Handbook assumes three-gyro control.*

---

HST is expected to transfer into two-gyro mode at some point in the future; since gyro failures are unpredictable this event may occur as early as Cycle 14. Therefore proposers are requested to provide information on two-gyro observing on their programs; see the [Call for Proposals](#) for details.

---

## 2.9 Status of STIS

As this Handbook is being finished for press it seems likely that the Space Telescope Imaging Spectrograph suffered a failure that will prevent its use in Cycle 14. Wording in this Handbook still refers to STIS in the present tense; see the [Call for Proposals](#) and web links for updates.



PART II:

# User's Guide

---

The Chapters in this Part describe the basics of observing with ACS. Included are a description of the instrumental layout and basic operations, the imaging, spectroscopic, polarimetric and coronagraphic capabilities of ACS, the performance and limitations of its detectors, exposure-time calculations, and overhead and orbit-request determinations.

This part of the Handbook is all you need to plan your Phase I ACS Proposal.



# Introduction to ACS

In this chapter . . .

3.1 Instrument Capabilities / 21
3.2 Instrument Design / 22
3.3 Basic Instrument Operations / 28
3.4 Designing an ACS Observing Proposal / 29

In this Chapter we provide an overview of the capabilities and scientific applications of ACS. We describe the optical design and basic operation of the instrument, and provide a flow chart and discussion to help you design a technically feasible and scientifically optimized ACS observing proposal.

## 3.1 Instrument Capabilities

The ACS is a camera designed to provide HST with a deep, wide-field survey capability from the visible to near-IR, imaging from the near-UV to the near-IR with the PSF critically sampled at  $6300\text{\AA}$ , and solar blind far-UV imaging. The primary design goal, now verified, of the ACS Wide-Field Channel is to achieve a factor of 10 improvement in discovery efficiency, compared to WFPC2, where discovery efficiency is defined as the product of imaging area and instrument throughput.

ACS has three channels, each optimized for a specific goal:

- Wide Field Channel (WFC):  $202 \times 202$  arcsecond field of view from  $3700\text{--}11,000\text{\AA}$ , and peak efficiency of 48% (including the OTA). The plate scale of  $0.05$  arcsecond/pixel provides critical sampling at  $11,600\text{\AA}$ .

- High Resolution Channel (HRC):  $29 \times 26$  arcsecond field of view from 2000–11,000Å, and peak efficiency of 29%. The plate scale of 0.027 arcsecond/pixel provides critical sampling at 6300Å.
- Solar Blind Channel (SBC):  $35 \times 31$  arcsecond field of view from 1150–1700Å, and peak efficiency of 7.5%. The plate scale of 0.032 arcsecond/pixel provides a good compromise between resolution and field of view.

In addition to these three prime capabilities, ACS also provides:

- Grism spectroscopy: Low resolution ( $R \sim 100$ ) wide field spectroscopy from 5500–11,000Å available in both the WFC and the HRC.
- Objective prism spectroscopy: Low resolution ( $R \sim 100$  @ 2000Å) near-UV spectroscopy from 2000–4000Å available in the HRC.
- Objective prism spectroscopy: Low resolution ( $R \sim 100$  @ 1216Å) far-UV spectroscopy from 1150–1700Å available in the SBC.
- Coronagraphy: Aberrated beam coronagraphy in the HRC from 2000–11,000Å with 1.8 arcsecond and 3.0 arcsecond diameter occulting spots.
- Imaging Polarimetry: Polarimetric imaging in the HRC and WFC with relative polarization angles of  $0^\circ$ ,  $60^\circ$  and  $120^\circ$ .

Table 4.1, 4.2, and 4.3 provide a full list of filters and spectroscopic elements for each imaging channel.

ACS is a versatile instrument that can be applied to a broad range of scientific programs. The high sensitivity and wide field of the WFC in the visible and near-infrared will make it the instrument of choice for deep imaging programs in this wavelength region. The HRC, with its excellent spatial resolution, provides full sampling of the HST PSF at  $\lambda > 6000\text{Å}$  and can be used for high precision photometry in stellar population programs. The HRC coronagraph can be used for the detection of circumstellar disks and QSO host galaxies.

---

## 3.2 Instrument Design

In this section, we provide a high-level summary of the basic design and operation of ACS, concentrating on the information most relevant to the design of your HST observing proposal. Subsequent chapters provide more detailed information on specific aspects of the instrument's performance and the design of proposals.

### 3.2.1 Detectors

ACS uses one or more large-format detectors in each channel:

- The WFC detector, called ACS/WFC, employs a mosaic of two  $2048 \times 4096$  Scientific Imaging Technologies (SITe) CCDs, with  $\sim 0.05$  arcsecond pixels, covering a nominal  $202 \times 202$  arcsecond field of view (FOV), and a spectral response from  $\sim 3700$  to  $11,000 \text{ \AA}$ .
- The HRC detector, called ACS/HRC, is a  $1024 \times 1024$  SITe CCD, with  $\sim 0.028 \times 0.025$  arcsecond pixels, covering a nominal  $29 \times 26$  arcsecond field of view, and spectral response from  $\sim 2000$  to  $11,000 \text{ \AA}$ .
- The SBC detector, called the ACS/SBC, is a solar-blind CsI Multi-Anode Microchannel Array (MAMA), with  $1024 \times 1024$   $\sim 0.034 \times 0.030$  arcsecond pixels, and a nominal  $35 \times 31$  arcsecond FOV, with far-UV spectral response from  $1150$  to  $1700 \text{ \AA}$ .

#### The WFC & HRC CCDs

The ACS CCDs are thinned, backside-illuminated devices cooled by thermo-electric cooler (TEC) stacks and housed in sealed, evacuated dewars with fused silica windows. The spectral response of the WFC CCDs is optimized for imaging at visible to near-IR wavelengths, while the spectral response of the HRC CCD is optimized specifically for the near-UV. Both CCD cameras produce a time-integrated image in the ACCUM data-taking mode. As with all CCD detectors, there is noise (*readout noise*) and time (*read time*) associated with reading out the detector following an exposure. The minimum exposure time is  $0.1$  sec for HRC, and  $0.5$  sec for WFC, and the minimum time between successive identical exposures is  $45$  s (HRC) or  $135$  s (WFC) for full-frame and can be reduced to  $\sim 36$  s for subarray readouts. The dynamic range for a single exposure is ultimately limited by the depth of the CCD full well ( $\sim 85,000 \text{ e}^-$  for the WFC and  $155,000 \text{ e}^-$  for the HRC), which determines the total amount of charge that can accumulate in any one pixel during an exposure without saturation. Cosmic rays will affect all CCD exposures: CCD observations should be broken into multiple exposures whenever possible, to allow removal of cosmic rays in post-observation data processing; during Phase II you can use the CR-SPLIT optional parameter or dithering to do this (See Section 7.2.5).

#### The SBC MAMA

The SBC MAMA is a *photon-counting* detector which provides a two-dimensional ultraviolet capability. It can only be operated in ACCUM mode. The ACS MAMA detector is subject to both *scientific* and *absolute* brightness limits. At high local ( $\geq 50 \text{ counts sec}^{-1} \text{ pixel}^{-1}$ ) and global ( $> 285,000 \text{ counts sec}^{-1}$ ) illumination rates, counting becomes nonlinear in a way that is not correctable. At only slightly higher illumination rates, the

MAMA detectors are subject to damage. We have therefore defined absolute local and global count-rate limits, which translate to a set of configuration-dependent bright-object screening limits. Sources which violate the absolute count rate limits in a given configuration *cannot be observed in those configurations*, as discussed in Section 7.5.

### 3.2.2 ACS Optical Design

The ACS design incorporates two main optical channels: one for the WFC and one which is shared by the HRC and SBC. Each channel has independent corrective optics to compensate for HST's spherical aberration. The WFC has three optical elements, coated with silver, to optimize instrument throughput in the visible and in the near-IR. The silver coatings cut off at wavelengths shortward of 3700Å. The WFC has two filter wheels which it shares with the HRC, offering the possibility of internal WFC/HRC parallel observing for some filter combinations (Section 8.7). The optical design of the WFC is shown schematically in Figure 3.1. The HRC/SBC optical chain comprises three aluminized mirrors, overcoated with MgF<sub>2</sub> and is shown schematically in Figure 3.2. The HRC or SBC channels are selected by means of a plane fold mirror (M3 in Figure 3.3). The HRC is selected by inserting the fold mirror into the optical chain so that the beam is imaged onto the HRC detector through the WFC/HRC filter wheels. The SBC channel is selected by moving the fold mirror out of the beam to yield a two mirror optical chain which images through the SBC filter wheel onto the SBC detector. The aberrated beam coronagraph is accessed by inserting a mechanism into the HRC optical chain. This mechanism positions a substrate with two occulting spots at the aberrated telescope focal plane and an apodizer at the re-imaged exit pupil.

While there is no mechanical reason why the coronagraph could not be used with the SBC, for health and safety reasons **use of the coronagraph is forbidden with the SBC.**

Figure 3.1: ACS Optical Design: Wide Field Channel

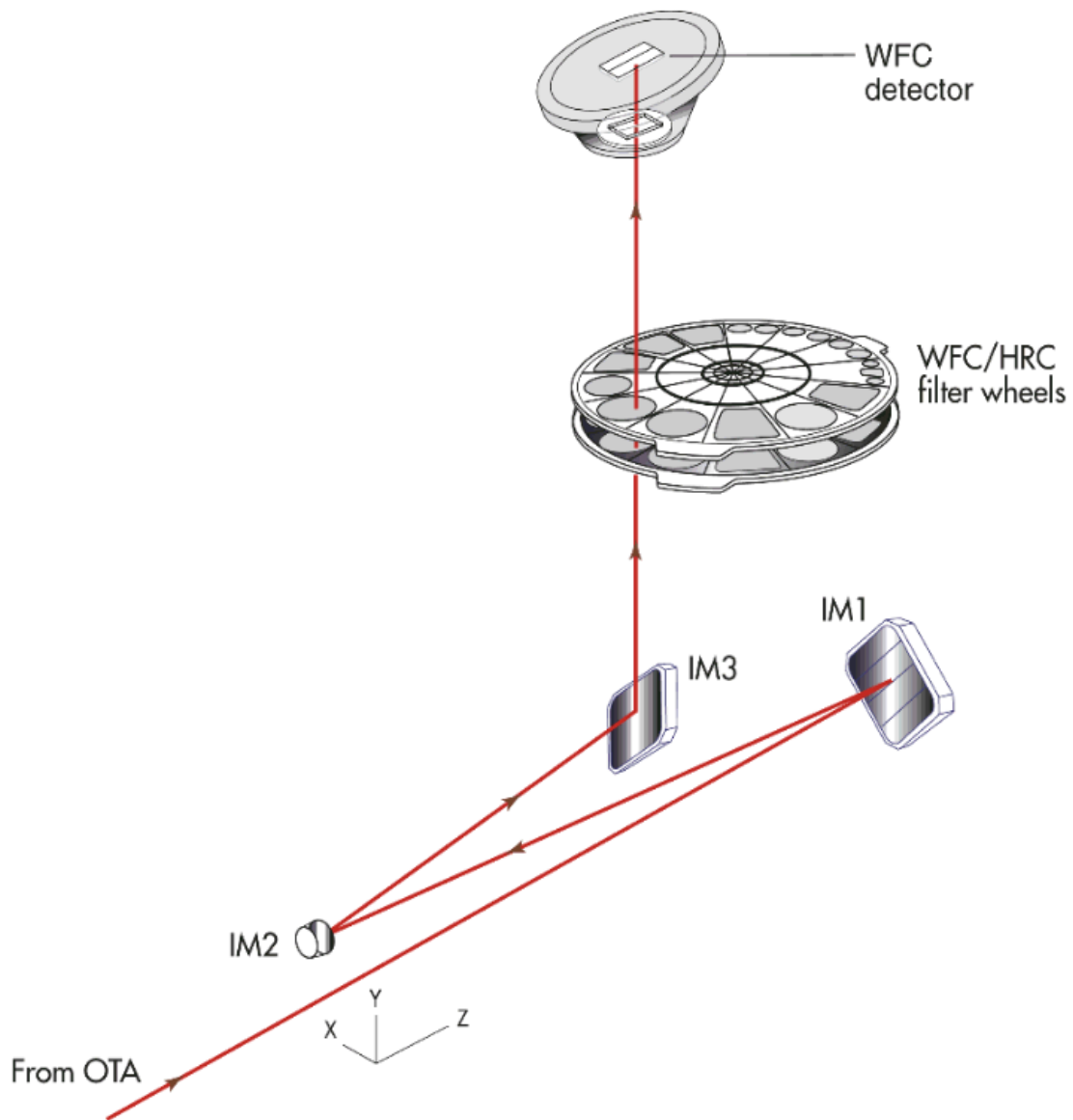
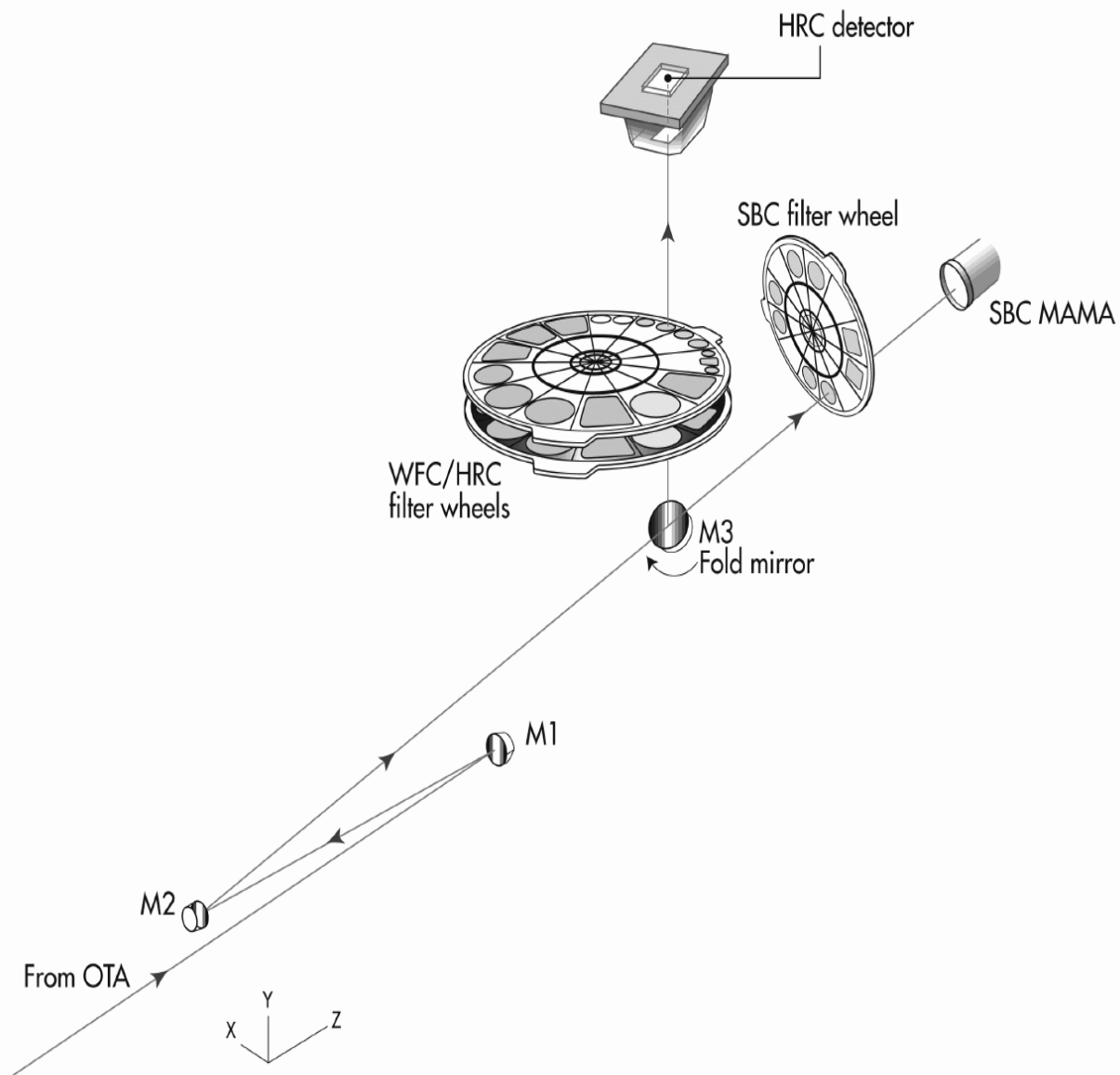


Figure 3.2: ACS Optical design: High Resolution/Solar Blind Channels



### Filter Wheels

ACS has three filter wheels: two shared by the WFC and HRC, and a separate wheel dedicated to the SBC. The WFC/HRC filter wheels contain the major filter sets summarized in Table 3.1. Each wheel also contains one clear WFC aperture and one clear HRC aperture (see Chapter 4). Parallel WFC and HRC observations are possible for some filter combinations and these are automatically added by APT in Phase II, unless the user disables this option via the PAREXP optional parameter, or if adding the parallel

observations cannot be done due to timing considerations. Note that since the filter wheels are shared it is not possible to independently select the filter for WFC and HRC parallel observations.

Table 3.1: ACS CCD Filters

Filter Type	Filter Description	Camera
Broadband	Sloan Digital Sky Survey (SDSS)	WFC/HRC
	B, V, Wide V, R, I	WFC/HRC
	Near-UV	HRC
Narrowband	H $\alpha$ (2%), [OIII] (2%), [NII] (1%)	WFC/HRC
	NeV (3440Å)	HRC
	Methane (8920Å)	HRC/[WFC <sup>1</sup> ]
Ramp filters	2% bandpass (3700-10700Å)	WFC/HRC
	9% bandpass (3700-10700Å)	WFC/HRC
Spectroscopic	Grism	WFC/HRC
	Prism	HRC
Polarizers	Visible (0°, 60°, 120°)	HRC/[WFC <sup>1</sup> ]
	Near-UV (0°, 60°, 120°)	HRC/[WFC <sup>1</sup> ]

1. Limited field of view (72" x 72") for these filters using WFC

The SBC filters are shown in Table 3.2.

Table 3.2: SBC Filters

Filter Type	Filter Description
Medium Band	Lyman-Alpha
Long pass	MgF <sub>2</sub> , CaF <sub>2</sub> , BaF <sub>2</sub> , Quartz, Fused Silica
Objective Prisms	LiF, CaF <sub>2</sub>

### Calibration-Lamp Systems

ACS has a calibration subsystem, consisting of tungsten lamps and a deuterium lamp for internally flat fielding each of the optical chains. The calibration subsystem illuminates a diffuser on the rear surface of the ACS aperture door, which must be closed for calibration exposures. Under normal circumstances, users are not allowed to use the internal calibration lamps.

In addition, a post-flash capability was added to the instrument to provide the means of mitigating the effects of Charge Transfer Efficiency (CTE) degradation. We do not expect to use this facility much in Cycle 14, (except for calibration and characterization) but in later years, as radiation damage of the CCDs causes the CTE to degrade, it is possible that some users will want to avail themselves of this facility. Since we are not yet at a

stage where use of post-flash is expected to be useful for any science observations, we do not provide an extensive discussion related to this.

---

## 3.3 Basic Instrument Operations

### 3.3.1 Target Acquisitions

For the majority of ACS observations target acquisition is simply a matter of defining the appropriate aperture for the observation. Once the telescope acquires its guide stars, your target will be within  $\sim 1\text{--}2$  arcseconds of the specified pointing. For observations with the ramp filters, one must specify the desired central wavelength for the observation. For the special case of coronagraphic observations, an onboard target acquisition will need to be specified. The nominal accuracy of the onboard target acquisition process is  $\sim 6$  mas, comparable to that achieved by STIS.

### 3.3.2 Typical ACS Observing Sequence

ACS is expected to be used primarily for deep, wide-field survey imaging. The important issues for observers to consider will be the “packaging” of their observations, i.e. how observations are CR-SPLIT to mitigate the impact of cosmic rays, whether sub-stepping or “dithering” of images is required for removal of hot pixels, and how, if necessary, to construct a mosaic pattern to map the target. HRC observations and narrowband observations with the WFC are more likely to be read-noise limited, requiring consideration of the optimum CR-SPLIT times. Observations with the MAMA detectors do not suffer from cosmic rays or read noise, but long integration times will often be needed to obtain sufficient signal-to-noise in the photon-starved ultraviolet.

A typical ACS observing sequence is expected to consist of a series of CR-SPLIT and dithered  $\sim 10\text{--}20$  minute exposures for each program filter. Coronagraphic observations will require an initial target acquisition observation to permit centering of the target under the occulter mask. Observers will generally not take their own calibration exposures. See Chapter 8 for more details of observing strategies.

### 3.3.3 Data Storage and Transfer

At the conclusion of each exposure, the science data is read out from the detector and placed in ACS’s internal buffer memory, where it is stored until it can be transferred to the HST solid state data recorder (and

thereafter to the ground). The internal buffer memory is large enough to hold one WFC image, or sixteen HRC or SBC images, and so the buffer will typically need to be dumped before or during the following WFC exposure. If the following exposure is longer than ~339 seconds, then the buffer dump from the proceeding exposure will be performed during integration (see Section 9.2 for a more complete discussion).

ACS's internal buffer stores the data in a 16 bit-per-pixel format. This structure imposes a maximum of 65,535 counts per pixel. For the MAMA detectors this maximum is equivalent to a limit on the total number of detected photons per pixel which can be accumulated in a single exposure. For the WFC and HRC, the 16 bit buffer format (and not the full well) limits the photons per pixel which can be accumulated without saturating in a single exposure when  $GAIN = 1$  for WFC, and  $GAIN \leq 2$  for the HRC is selected. See Chapters 7 and 8 for a detailed description of ACS instrument operations.

### 3.3.4 Parallel Operations

Parallel observations with the WFC and HRC are possible with ACS for certain filter combinations (See Section 8.7).

ACS can be used in parallel with any of the other science instruments on HST, within certain restrictions. Figure 3.3 shows the HST field of view following SM3B with ACS installed. Dimensions in this figure are approximate; accurate aperture positions can be found on STScI's Observatory web page under "Pointing"<sup>1</sup> or by using the Visual Target Tuner (VTT). The ACS grism and prism dispersion directions are approximately along the V2 axis. The policy for applying for parallel observing time is described in the *Call for Proposals*. We provide suggestions for designing parallel observations with ACS in Section 8.7. While the ACS CCDs can be used in parallel with another instrument on HST, subject to certain restrictions described in Section 8.7, there are significant restrictions on the use of the MAMA detectors in parallel – see Chapter 2.

---

## 3.4 Designing an ACS Observing Proposal

In this section, we describe the sequence of steps you will need to take when designing your ACS observing proposal. The process is an iterative one, as trade-offs are made between signal-to-noise ratio and the

---

1. Pointing web page: <http://www.stsci.edu/instruments/observatory/taps.html>

limitations of the instrument itself. The basic sequence of steps in defining an ACS observation are:

- Identify science requirements and select the basic ACS configuration to support those requirements.
- Estimate exposure time to achieve the required signal-to-noise ratio, determine GAIN selection, CR-SPLIT, dithering and mosaic strategy and check feasibility, including saturation and bright-object limits.
- Identify any additional target acquisition (coronagraph), and calibration exposures needed.
- Calculate the total number of orbits required, taking into account the overheads.

Figure 3.3: HST Field of View Following SM3B

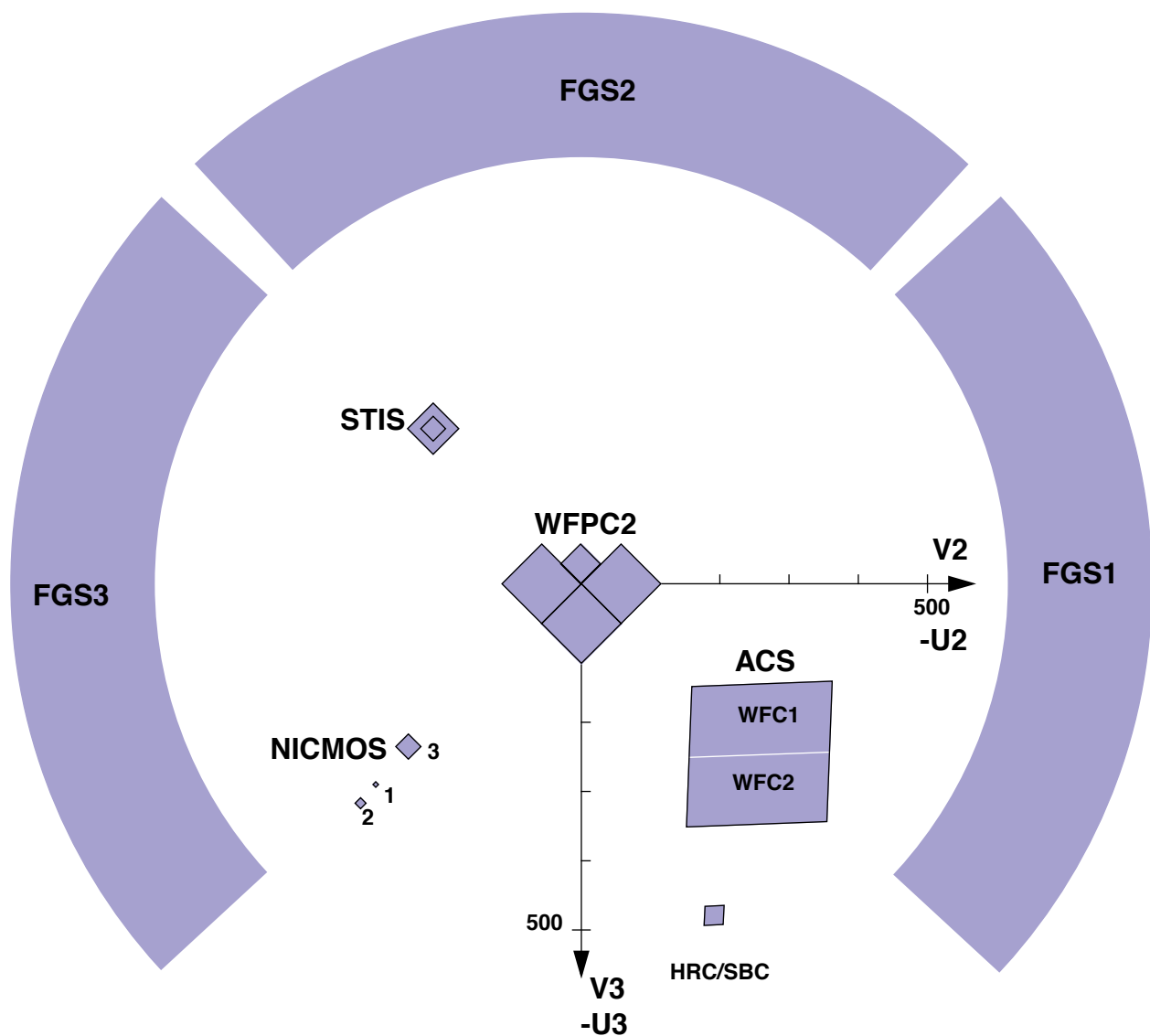
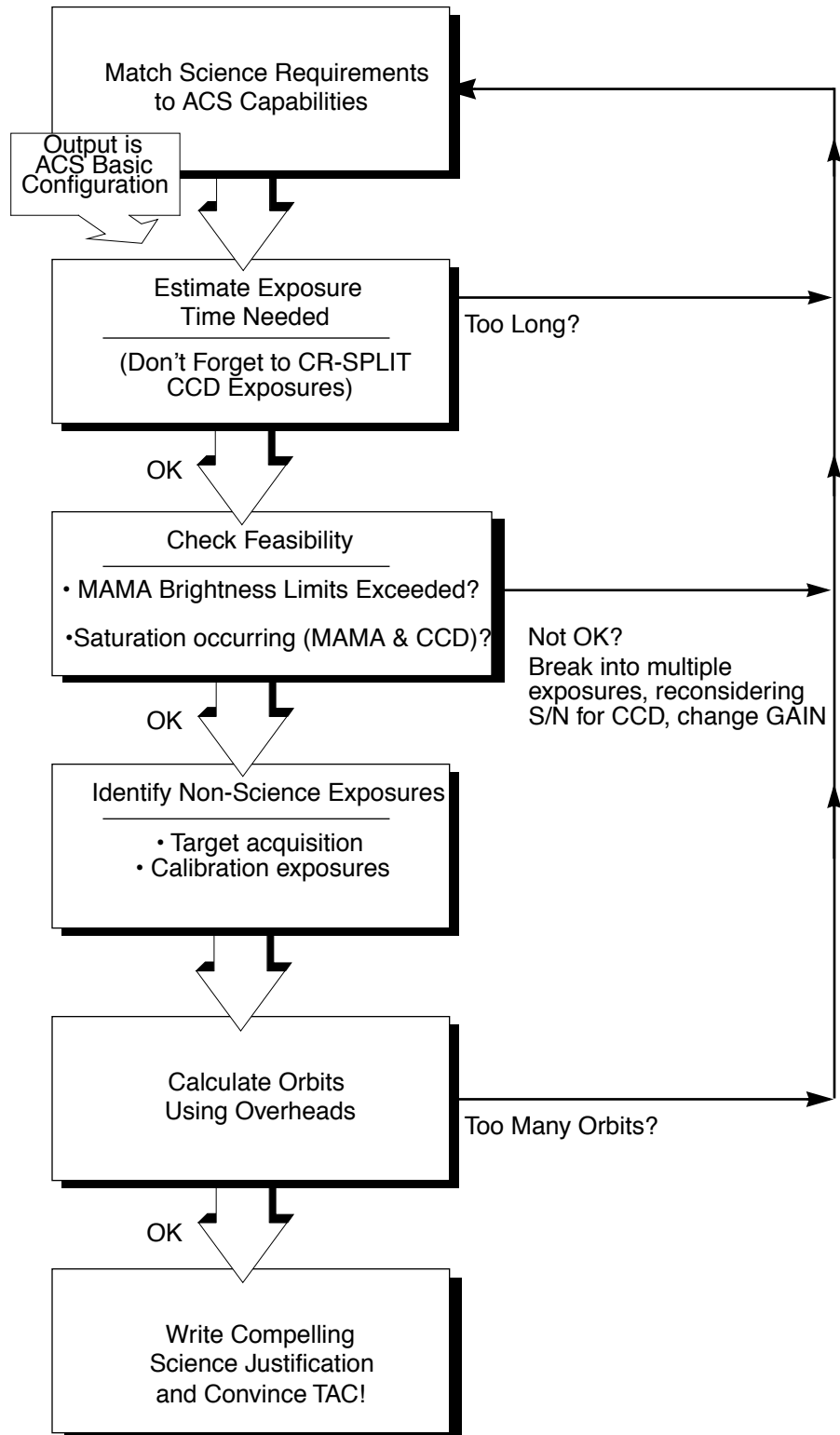


Figure 3.4: Defining an ACS Observation



### 3.4.1 Identify Science Requirements and Define ACS Configuration

First and foremost, of course, you must identify the science you wish to achieve with ACS. Basic decisions you will need to make are:

- Filter selection
- Nature of target

As you choose your science requirements and work to match them to the instrument's capabilities, keep in mind that those capabilities differ greatly depending on whether you are observing in the optical or near-UV with the CCD, or in the far-UV using the MAMA detector. Tradeoffs are described in Table 3.3.

Table 3.3: Science Decision Guide

Decision	Affects	Tradeoffs
Field of view	Camera Filter selection	WFC: 202 x 202 arcseconds HRC: 29 x 26 arcseconds SBC: 35 x 31 arcseconds
Spectral response	Camera Filter selection	WFC: 3700-11,000Å HRC: 2000-11,000Å SBC: 1150-1700Å
Spatial Resolution	Camera	WFC: ~50 milliarcsecond pixels HRC: ~27 milliarcsecond pixels SBC: ~32 milliarcsecond pixels
Filter Selection	Camera	WFC: broad, medium & narrow band, ramps HRC: Visible, UV, ramp middle sections
Spectroscopy	Camera Spatial resolution Field of View Wavelength range	Grism (G800L): WFC and HRC Prism (PR200L): HRC Prism (PR110L, PR130L): SBC
Polarimetry	Filters	UV polarizers combine with Wheel 2 filters VIS polarizers combine with Wheel 1 filters
Coronagraphy	Filter selection	Coronagraphic imaging available with HRC only

#### Imaging

For imaging observations, the base configuration is detector (Configuration), operating mode (MODE=ACCUM), and filter. Chapter 4 presents detailed information about each of ACS's imaging modes.

#### Special Uses

We refer you to Chapter 5 if you are interested in any of the following special uses of ACS: slitless spectroscopy, polarimetry and coronagraphy.

### 3.4.2 Determine Exposure Time and Check Feasibility

Once you have selected your basic ACS configuration, the next steps are to:

- Estimate the exposure time needed to achieve your required signal-to-noise ratio, given your source brightness. (You can use the ACS Exposure-Time Calculator for this, see also Chapter 6 and the plots in Chapter 10).
- For observations using the CCD detectors, assure that for pixels of interest, you do not exceed the per pixel saturation count limit of the CCD full well or the 16 bit word size at the GAIN setting you choose.
- For observations using the MAMA detector, assure that your observations do not exceed brightness (count-rate) limits.
- For observations using the MAMA detector, assure that for pixels of interest, your observations do not exceed the limit of 65,535 accumulated counts per pixel per exposure imposed by the ACS 16 bit buffer.

To determine your exposure-time requirements consult Chapter 6 where an explanation of how to calculate a signal-to-noise ratio and a description of the sky backgrounds are provided. To assess whether you are close to the brightness, signal-to-noise, and dynamic-range limitations of the detectors, refer to Chapter 7. For a consideration of observation strategies and calibration exposures, consult Chapter 8.

If you find that the exposure time needed to meet your signal-to-noise requirements is too great, or that you are constrained by the detector's brightness or dynamic-range limitations, you will need to adjust your base ACS configuration. Table 3.4 summarizes the options available to you and steps you may wish to take as you iterate to select an ACS configuration which is both suited to your science and is technically feasible.

Table 3.4: Science Feasibility Guide

Action	Outcome	Recourse
Estimate exposure time	If too long -> re-evaluate instrument configuration.	Consider use of an alternative filter.
Check full-well limit for CCD observations	If full well exceeded and you wish to avoid saturation-> reduce time per exposure.	Divide total exposure time into multiple, short exposures. <sup>1</sup> Consider use of different Gain.
Check bright-object limits for MAMA observations	If source is too bright -> re-evaluate instrument configuration.	Consider the use of an alternative filter or change detectors and wavelength regime.
Check 65,535 counts-per-pixel limit for MAMA observations	If limit exceeded -> reduce time per exposure.	Divide total exposure time into multiple, short exposures

1. Splitting CCD exposures affects the exposure time needed to achieve a given signal-to-noise ratio because of the read noise.

### 3.4.3 Identify Need for Additional Exposures

Having identified your desired sequence of *science* exposures, you need to determine what additional exposures you may require to achieve your scientific goals. Specifically:

- For coronagraphy, determine what target-acquisition exposure will be needed to center your target under the selected occulting mask.
- If the success of your science program requires calibration to a higher level of precision than is provided by STScI's calibration data, and if you are able to justify your ability to reach this level of calibration accuracy yourself, you will need to include the necessary calibration exposures in your program, including the orbits required for calibration in your total orbit request.

### 3.4.4 Determine Total Orbit Request

In this, the final step, you place all your exposures (science and non-science, alike) into orbits, including tabulated overheads, and determine the total number of orbits you require. Refer to Chapter 9 when performing this step. If you are observing a small target and find your total time request is significantly affected by data-transfer overheads (which will be the case *only* if you are taking many separate exposures under 339 seconds with the WFC), you can consider the use of CCD subarrays to lessen the data volume. Subarrays are described in Chapter 8 in sections “WFC CCD Subarrays” on page 159 and “HRC CCD Subarrays” on page 161 and in Section 9.2.1.

At this point, if you are happy with the total number of orbits required, you're done! If you are unhappy with the total number of orbits required, you can, of course, iterate, adjusting your instrument configuration, lessening your acquisition requirements, changing your target signal-to-noise or wavelength requirements, until you find a combination which allows you to achieve your science goals with ACS.

# CHAPTER 4:

# Imaging

## In this chapter . . .

4.1 Imaging Overview / 35
4.2 Which Instrument to Use? / 41
4.3 Caveats for ACS Imaging / 46
4.4 Wide Field Optical CCD Imaging / 49
4.5 High-Resolution Optical and UV Imaging / 51
4.6 Ultraviolet Imaging with the SBC / 53
4.7 ACS Point Spread Functions / 54
4.8 Two-Gyro Guiding / 62

In this Chapter we focus on the imaging capabilities of ACS. Each imaging mode is described in detail. Plots of throughput and comparisons to the capabilities of WFPC2 and STIS are also provided. Curves of sensitivity and exposure time to achieve a given signal-to-noise as a function of source luminosity or surface brightness are referenced in this chapter, but presented in Chapter 10. We note the existence of bright-object observing limits for SBC channel imaging; these are described in detail in Chapter 7, including tables of the SBC bright-object screening magnitudes as a function of mode and spectral type.

---

## 4.1 Imaging Overview

ACS can be used to obtain images through a variety of optical and ultraviolet filters. When the selected ACS camera is the WFC or the HRC, the appropriate filter in one of the two filter wheels is rotated into position and a clear aperture is automatically selected on the other filter wheel. For

SBC imaging the single filter wheel is rotated to the required position. A number of apertures are defined for each ACS camera. In general, these refer to different target positions on the detector.

Table 4.1 and Table 4.2 provide a complete summary of the filters available for imaging with each detector. Figures 4.1 through 4.5 show the filter transmission curves. In Figure 4.9 we show the integrated system throughputs.

The CCD filter wheels contain filters with two different sizes. Some filters (F435W, F475W, F502N, F550M, F555W, F606W, F625W, F658N, F660N, F775W, F814W, F850LP and G800L) are full-sized filters that can be used with both WFC and HRC. Others (F220W, F250W, F330W, F344N, F892N, POL0UV, POL60UV, POL120UV, POL0V, POL60V, POL120V, PR200L) are smaller, giving a full unvignetted field of view when used with the HRC, but a vignetted field of view of only 72"×72" when used with the WFC. Use of the small UV filters is not supported with the WFC due to the unpredictable behavior of the silver coatings shortward of 4000Å.

The Ramp Filters are designed to allow narrow or medium band imaging centered at an arbitrary wavelength. Each ramp filter is divided into three segments, of which only the middle segment may be used with the HRC. See “Ramp filters” on page 50 for more details on these filters.

Note that although the CLEAR filters are specified in the filter wheel tables, users do not need to specify these filters in their HST proposals; they are added automatically in conjunction with the desired filter in the complementary wheel. In the SBC filter wheel, every third slot (#1, 4, 7, 10) is blocked off, so that in the case of a bright object limit violation, it is only necessary to rotate the filter wheel to an adjacent slot to block the incoming light.

With either the WFC and HRC it is possible to select a filterless observation by specifying CLEAR (this is an “available-but-unsupported” filter) as the filter name, although the image will be of degraded quality. Rough wavelengths and widths when used with the WFC or HRC are listed in Table 4.1 under CLEAR entries. Use of CLEAR will provide slightly degraded PSFs with the HRC and seriously degraded PSFs for the WFC. More details on PSFs with use of CLEAR are provided in [ACS ISR 2003-03](#). Applications are expected to be rare, but a valid use could be astrometry of extremely faint targets with the HRC when color information is not required.

Table 4.1: ACS WFC/HRC Filters in Filter Wheel #1

Filter Name	Central Wavelength	Width (Å)	Description	Camera
CLEAR	6200	5200	Clear aperture	WFC/HRC
F555W	5346	1193	Johnson V	WFC/HRC
F775W	7764	1528	SDSS i	WFC/HRC
F625W	6318	1442	SDSS r	WFC/HRC
F550M	5580	547	Narrow V	WFC/HRC
F850LP	9445	1229	SDSS z	WFC/HRC
POL0UV	2000–6000	-	0° UV polarizer	HRC[/WFC]
POL60UV	2000–6000	-	60° UV polarizer	HRC[/WFC]
POL120UV	2000–6000	-	120° UV polarizer	HRC[/WFC]
F892N	8917	154	Methane (2%)	HRC[/WFC]
F606W	5907	2342	Broad V	WFC/HRC
F502N	5022	57	[OIII] (1%)	WFC/HRC
G800L	5800–11,000	-	Grism (R~100)	WFC/HRC
F658N	6584	78	H $\alpha$ (1%)	WFC/HRC
F475W	4760	1458	SDSS g	WFC/HRC

Table 4.2: ACS WFC/HRC Filters in Filter Wheel #2

Filter Name	Central Wavelength	Width (Å)	Description	Camera
CLEAR	6000	5200	Clear aperture	WFC/HRC
F660N	6602	40	[NII] (1%)	WFC/HRC
F814W	8333	2511	Broad I	WFC/HRC
FR388N	3710–4050	2%	[OII] Ramp—middle segment	WFC/HRC
FR423N	4050–4420	2%	[OII] Ramp—inner segment	WFC
FR462N	4420–4820	2%	[OII] Ramp—outer segment	WFC
F435W	4297	1038	Johnson B	WFC/HRC
FR656N	6270–6850	2%	H $\alpha$ Ramp—middle segment	WFC/HRC
FR716N	6850–7470	2%	H $\alpha$ Ramp—inner segment	WFC
FR782N	7470–8160	2%	H $\alpha$ Ramp—outer segment	WFC
POL0V	4000–8000	-	0° Visible Polarizer	HRC[/WFC]

Filter Name	Central Wavelength	Width (Å)	Description	Camera
F330W	3354	588	HRC U	HRC
POL60V	4000–8000	-	60° Visible Polarizer	HRC[/WFC]
F250W	2696	549	Near-UV broadband	HRC
POL120V	4000–8000	-	120° Visible Polarizer	HRC[/WFC]
PR200L	2000–4000	-	NUV Prism (R~100 @ 200 nm)	HRC
F344N	3434	60	Ne V (2%)	HRC
F220W	2228	485	Near-UV broadband	HRC
FR914M	7570–10,710	9%	Broad Ramp—middle segment	WFC/HRC
FR853N	8160–8910	2%	IR Ramp—inner segment	WFC
FR931N	8910–9720	2%	IR Ramp—outer segment	WFC
FR459M	3810–5370	9%	Broad Ramp—middle segment	WFC/HRC
FR647M	5370–7570	9%	Broad Ramp—inner segment	WFC
FR1016N	9720–10,610	2%	IR Ramp—outer segment	WFC
FR505N	4820–5270	2%	[OIII] Ramp—middle segment	WFC/HRC
FR551N	5270–5750	2%	[OIII] Ramp—inner segment	WFC
FR601N	5750–6270	2%	[OIII] Ramp—outer segment	WFC

Table 4.3: ACS SBC Filter Complement

Filter Name	Description
F115LP	MgF <sub>2</sub> (1150Å longpass)
F125LP	CaF <sub>2</sub> (1250Å longpass)
F140LP	BaF <sub>2</sub> (1400Å longpass)
F150LP	Crystal quartz (1500Å longpass)
F165LP	Fused Silica (1650Å longpass)
F122M	Ly- $\alpha$ ( $\lambda = 1200\text{\AA}$ , $\Delta\lambda = 60\text{\AA}$ )
PR110L	LiF Prism (R~100)
PR130L	CaF <sub>2</sub> Prism (R~100)

Figure 4.1: ACS Broad-band filters

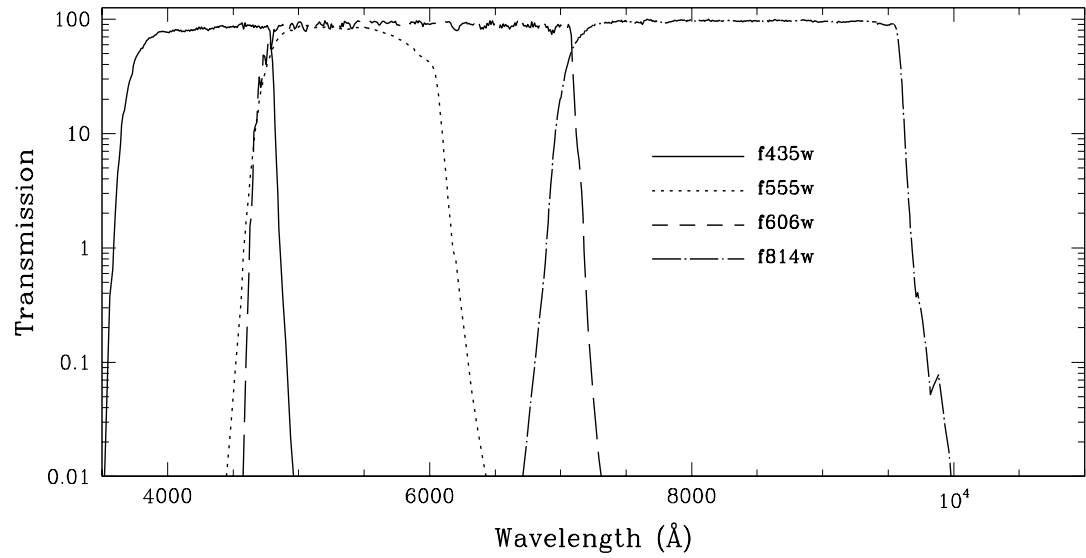


Figure 4.2: ACS SDSS filters

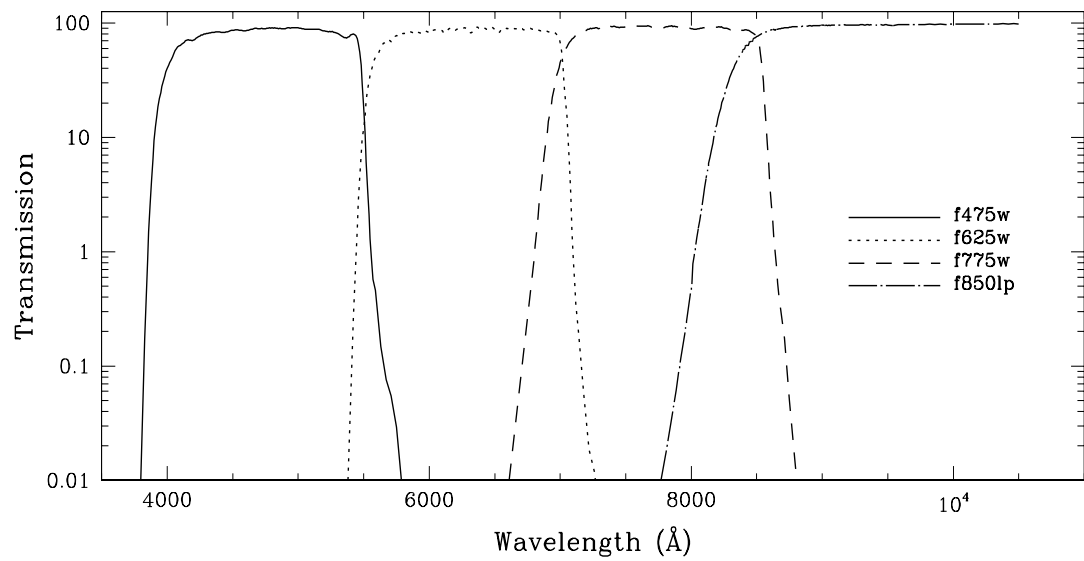


Figure 4.3: ACS UV and Medium-Band filters

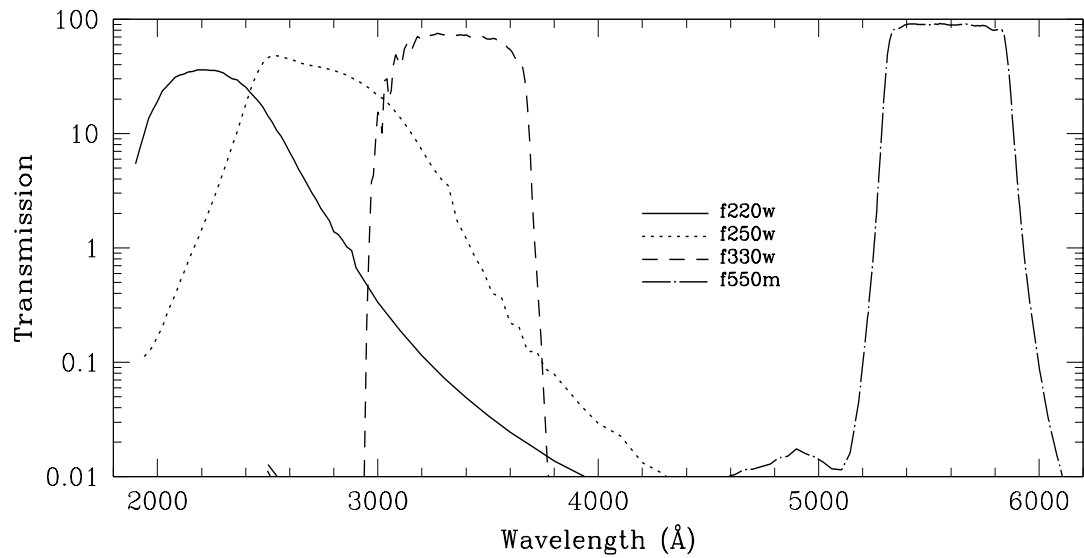


Figure 4.4: ACS Narrow-Band filters

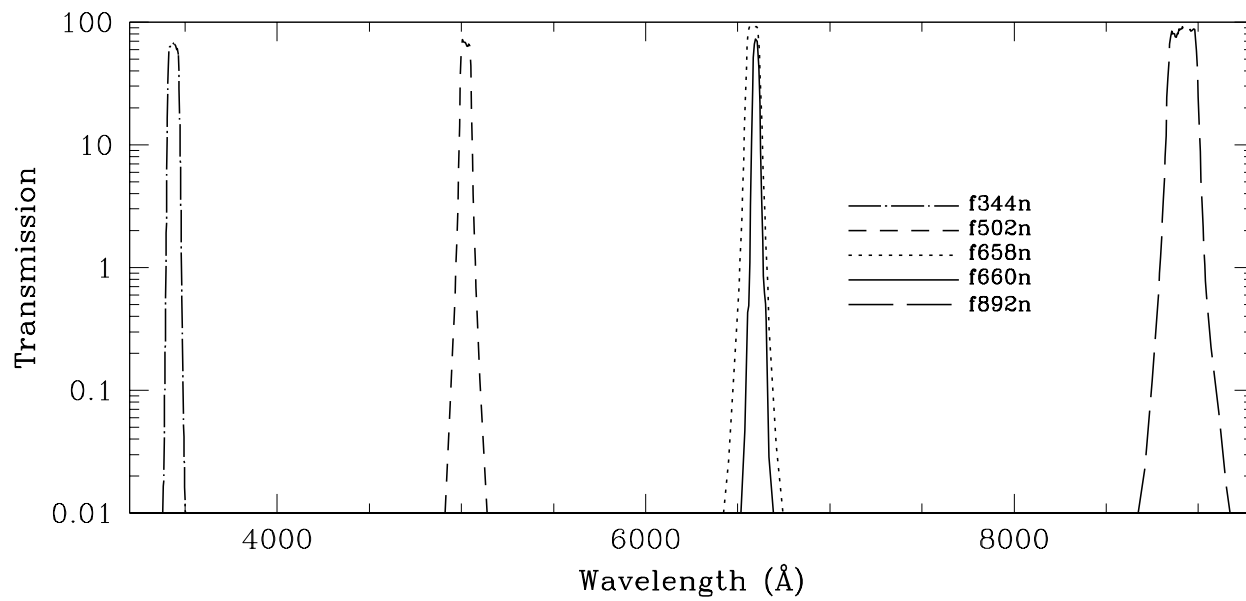
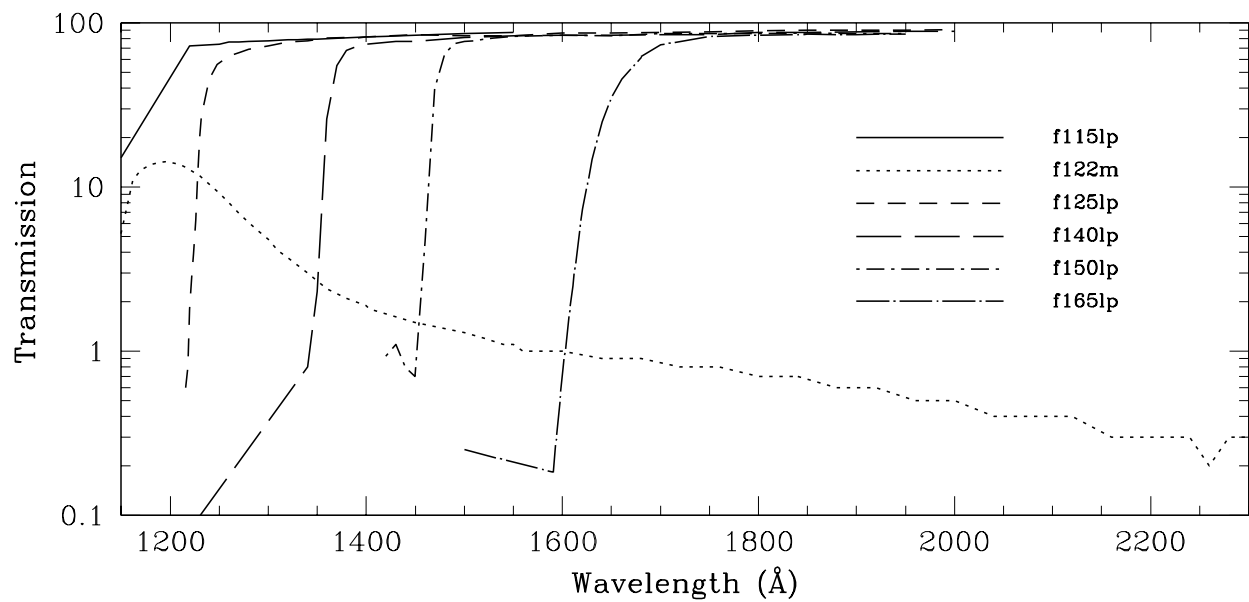


Figure 4.5: ACS SBC filters



## 4.2 Which Instrument to Use?

In this section, we compare briefly the performance of HST instruments with imaging and spectroscopic capability in the UV to near-IR spectral range. Important imaging parameters for all instruments are summarized in Table 4.4, followed by different sections where the ACS characteristics are compared to each other instrument.

Table 4.4: Characteristics of HST Imaging Instruments

Parameter	ACS		WFPC2	NICMOS	STIS	
<b>Wavelength range (Å)</b>	WFC HRC SBC	3700-11,000 2000-11,000 1150-1700	1150-11,000	8000-25,000	FUV-MAMA NUV-MAMA CCD	1150-1700 1700-3100 2000-11,000
<b>Detector(s)</b>	SITe CCDs, MAMA		Loral CCDs	HgCdTe	SITe CCD, MAMAs	
<b>Image format</b>	WFC HRC SBC	2×2048×4096 1024×1024 1024×1024	4×800×800	256×256 256×256 256×256	FUV-MAMA NUV-MAMA CCD	1024×1024 1024×1024 1024×1024
<b>FOV and pixel size</b>	WFC  HRC  SBC	202"×202" 0.05" /pix  29"×26" 0.027" /pix  35"×31" 0.032" /pix	150"×150" 0.1" /pixel  34"×34" 0.046" /pixel	11"×11" at 0.043" /pixel  19"×19" at 0.075" /pixel  51"×51" at 0.2" /pixel	FUV-MAMA  NUV-MAMA  CCD	25"×25" 0.024" /pix  25"×25" 0.024" /pix  51"×51" 0.05" /pix
<b>Read noise</b>	WFC HRC SBC	5.0 e <sup>-</sup> 4.7 e <sup>-</sup> 0 e <sup>-</sup>	5.5 e <sup>-</sup> 7.5 e <sup>-</sup>	30 e <sup>-</sup>	FUV-MAMA NUV-MAMA CCD	0 e <sup>-</sup> 0 e <sup>-</sup> 5.4 e <sup>-</sup>
<b>Dark current</b>	WFC HRC SBC	0.0032 e <sup>-</sup> /s/pix 0.0036 e <sup>-</sup> /s/pix 1.2×10 <sup>-5</sup> e <sup>-</sup> /s/pix	0.0076 e <sup>-</sup> /s/pix	<0.1 e <sup>-</sup> /s/pix	CCD NUV FUV.	0.0060 e <sup>-</sup> /s/pix 0.001 e <sup>-</sup> /s/pix 7×10 <sup>-6</sup> e <sup>-</sup> /s/pix
<b>Saturation</b>	WFC HRC	84,700 e <sup>-</sup> (gain 2) 155,000 e <sup>-</sup> (gain 4)	53,000 e <sup>-</sup> (gain 15)	200,000 e <sup>-</sup>		144,000 e <sup>-</sup> (gain 4)

### 4.2.1 Comparison of ACS and WFPC2

Advantages of each instrument may be summarized as follows:

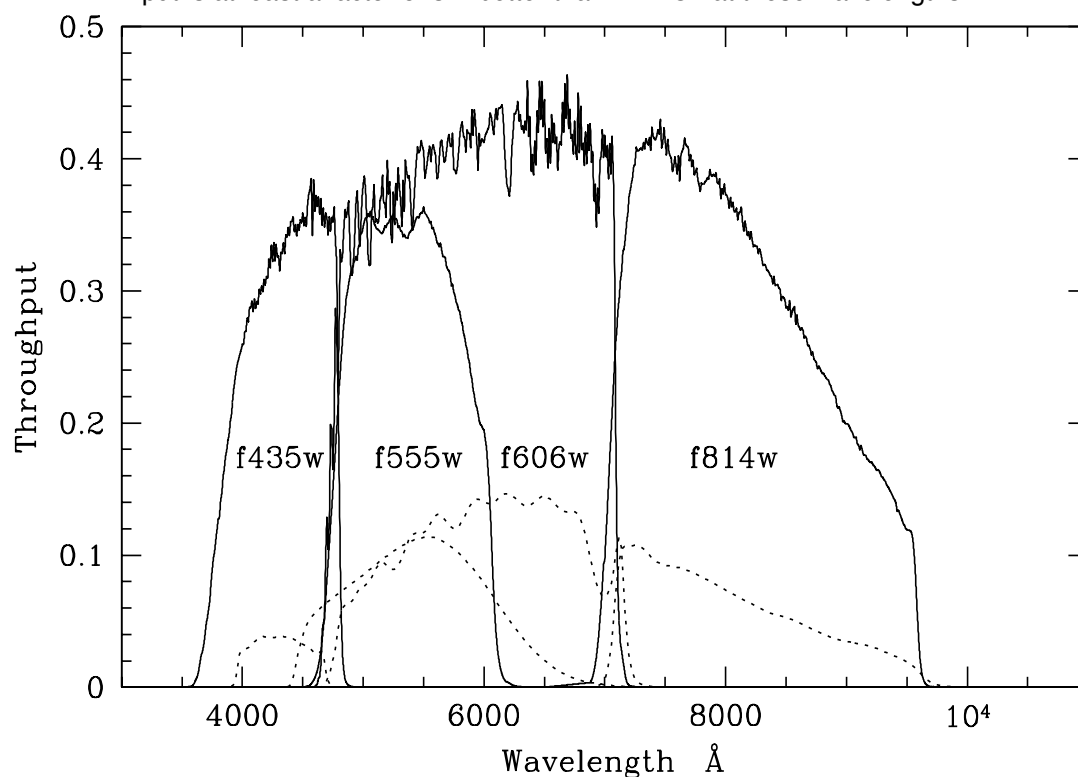
ACS advantages are:

- Wider field of view, 202"×202" vs. 150"×150" or less.
- Higher throughput at wavelengths >3700Å (see Figure 4.6).
- Better resolution: ACS/HRC offers 0.027" pixels vs. 0.046" on WFPC2 (PC).
- Better dynamic range: lower and well sampled read noise, larger sampled full well depth.
- Spectroscopic and coronagraphic observations are possible.
- ACS ramp filters have a higher throughput and FOV than those in WFPC2 (see Figures 4.6-4.9) and offer complete wavelength coverage from 3710Å to 10,710Å.
- Polarization observations on ACS can be made with 3 polarizer angles of 0°, 60°, 120° over the whole HRC FOV.
- For high contrast imaging, the WFPC2 PC has a higher scattered light floor than ACS HRC.
- ACS has more uniform PSFs over the entire field-of-view.
- ACS has better CTE and a lower dark current.

WFPC2 advantages are:

- Some special filters are available that are not found in ACS. These are the narrow filters (F343N, F375N (OII), F390N, F437N, F469N, F487N, F588N, F631N, F673N, F953N). ACS can do narrow-band imaging with the ramp filters, with a smaller FOV and has higher throughput and lower read noise.
- Wide-field UV observations are possible with the following filters: F122M, F160BW, F170W, F185W, F218W, F255W, F300W, F336W.

Figure 4.6: Comparison between the system efficiency (or throughput) of ACS WFC and WFPC2 for the filters: Johnson B, Johnson V, Broad V and Broad I. The solid lines are for ACS and the dotted lines for WFPC2. ACS total system throughput is at least a factor of 3-4 better than WFPC2 at these wavelengths.



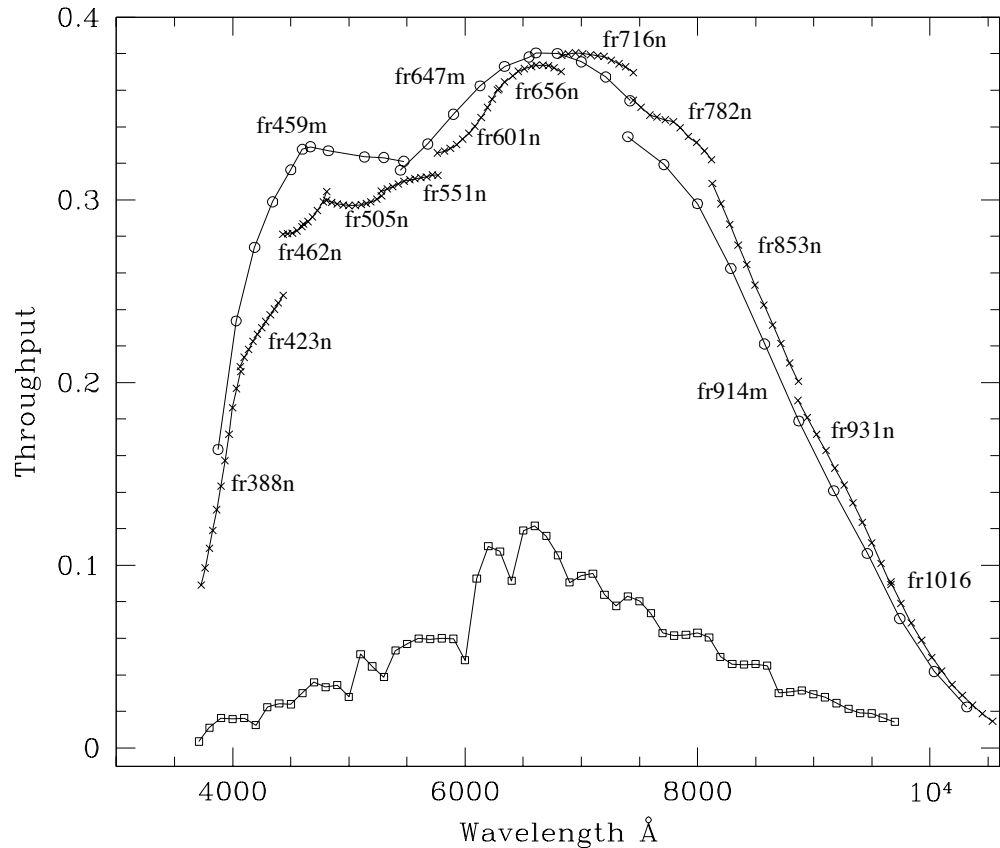
## 4.2.2 Comparison of ACS and NICMOS

ACS and NICMOS have a small overlap in imaging capability for filters at around 9000Å. At longer wavelengths NICMOS must be used; at shorter wavelengths either ACS, WFPC2 or STIS must be used. The following table compares the detection efficiency of ACS and NICMOS in the wavelength region where they both operate. Count rates for a  $V=20$  star of spectral class A1 are given for all filters at common wavelengths; the signal-to-noise (S/N) is also given for a 1 hour exposure of this same star using a 5x5 pixel aperture in each case.

Table 4.5: Near-IR capabilities of ACS compared to NICMOS

Instrument	Filter	Pivot Wavelength (Å)	FWHM (Å)	Count rate	S/N
ACS/WFC	F850LP	9054	1276	34.4	345
ACS/WFC	F892N	8915	172	3.6	107
NICMOS	F090M	9041	1318	13.9	162

Figure 4.7: Comparison between the ACS and WFPC2 ramp filters. The crosses and the open circles are for the ACS narrow and medium band ramps. The open squares are for the 4 WFPC2 ramps. For each of the ACS ramps the peak throughput that was calculated for eleven central wavelength values is plotted. For the WFPC2 ramps, the peak throughput calculated every 100Å within the field of view of any of the 4 chips and a 0° filter rotation angle (as mapped in Figs. 3.4 and 3.5 of the WFPC2 Instrument Handbook, version 3.0), is plotted.



### 4.2.3 Comparison of ACS and STIS

Both ACS and STIS are capable of imaging over the same wavelength range, between 1200Å and 11,000Å. At much longer wavelengths NICMOS must be used.

Advantages of each instrument may be summarized as follows:

ACS advantages are:

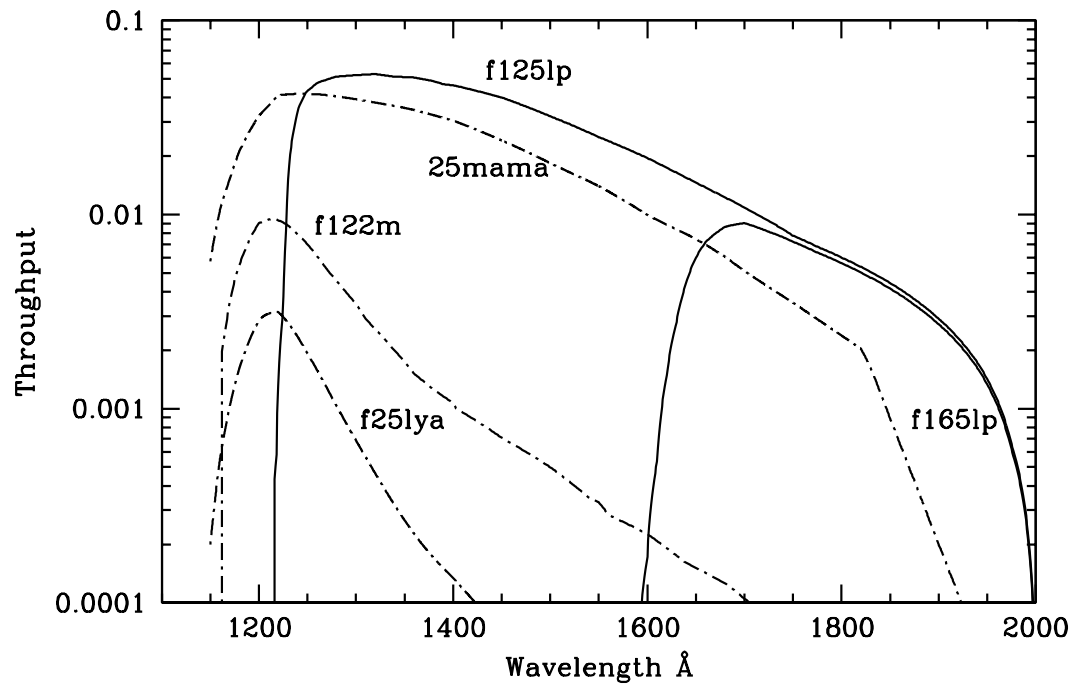
- Wider field-of-view at optical and near-infrared wavelengths, 202"×202" vs. 50"×50" or less.
- Greater selection of filters, including polarizers, are available.
- Higher sensitivity is possible.
- Better CTE and lower dark current.

STIS advantages are:

- MAMAs can be used in Time-Tag Mode.
- FUV-MAMA gives higher S/N than SBC due to the lower dark current.
- An OII filter centered at  $3727\text{\AA}$  is available that allows deep, high-resolution OII imaging.
- Narrow band filters at  $2800\text{\AA}$  and  $1900\text{\AA}$  allow imaging in MgII and CIII, respectively.
- Selectable aperture (slit) size for the MAMAs means that bright object concerns are lessened.

True to its name, ACS significantly enhances the imaging capabilities of HST. Due to the combination of sensitivity and field of view ACS has become the instrument of choice for UV/optical imaging on HST.

Figure 4.8: Comparison between the system efficiency of ACS SBC and STIS FUV-MAMA. For the ACS SBC the total system throughput for the f122m, f125lp and f165lp filters is plotted in the solid lines. For the STIS FUV-MAMA the system throughput for the Clear (25mama) and Lyman- $\alpha$  (f25lya) filters are given with the dashed lines.



## 4.3 Caveats for ACS Imaging

There are a few characteristics of ACS that should be taken into account when imaging with ACS:

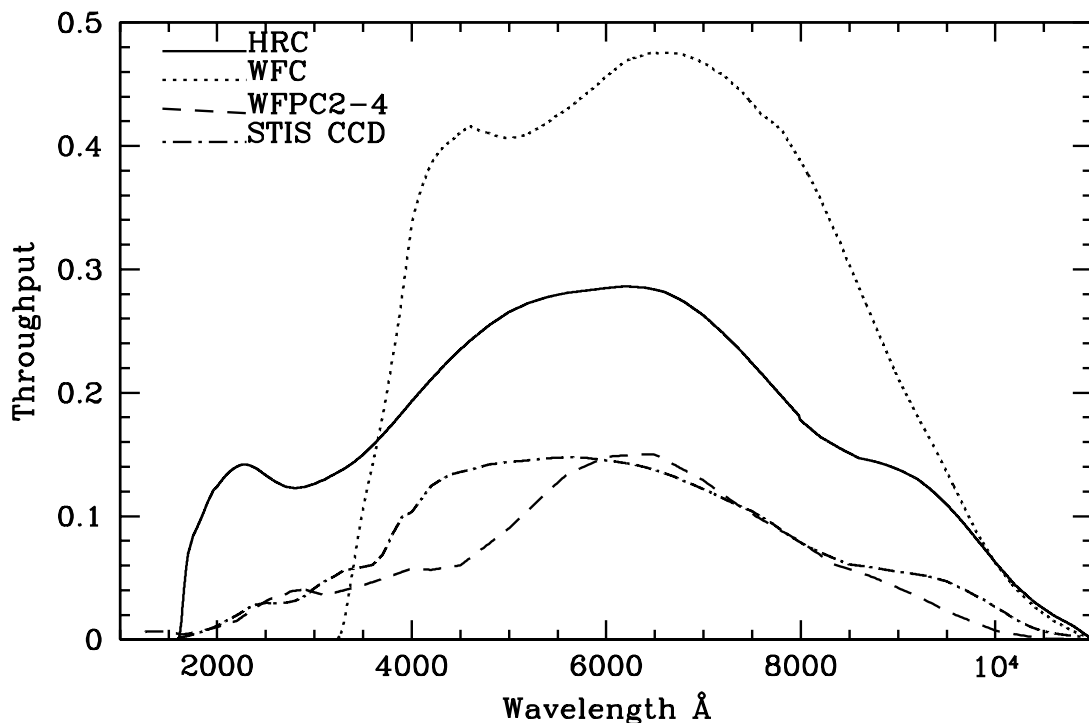
- The HRC and WFC filters are housed in two filter wheels shared by both cameras. As a consequence, when a filter is chosen for the primary camera the filter used in the parallel camera is not independently selectable (see Table 8.4).
- The ACS cameras are designed to be used with a single filter, and for this reason unfiltered imaging or imaging through two filters leads to significantly degraded imaging quality (particularly in the WFC) and is not normally used except for polarization observations, or bright target acquisitions with the HRC. The polarizer filters were designed with a zero optical thickness so that they can and should be used with another filter.
- The geometric distortion of the WFC is significant and causes the projected pixel area to vary by  $\pm 9\%$  over the field of view. This distortion affects both the photometric accuracy and the astrometric precision and must be accounted for when the required accuracy is better than 10%.
- The ratio of in-band vs. out-of-band transmission for the ACS CCD UV filters is similar to that of WFPC2, once the two detector QE curves are taken into account (the red leak on ACS F330W is very small). This implies that for imaging in the UV of intrinsically red objects the effect of filter red leaks needs to be calibrated.
- The cosmic ray fluxes for HRC and WFC are comparable, respectively, to those of the STIS CCD and WFPC2. As with these instruments typical imaging observations will need to be split or dithered for cosmic ray rejection.
- Hot pixels are a significant issue for WFC due to a lower than expected rate of removal through anneals. Section 7.2.6 provides further details and a recommendation that separate exposures with small dithers be considered as a means of helping to remove residual hot pixels.
- The large format of the WFC requires significantly more shifts to read out data than with STIS or WFPC2, therefore the impact of decreasing Charge Transfer Efficiency will be encountered earlier. Section 7.2.7 details current expectations, which for Cycle 14 are expected to remain modest.

- The default GAIN setting for WFC primary observations is  $\text{GAIN}=1$ . This allows for good sampling of the readout noise but it does not allow one to reach the full well counts of WFC. The readout noise for the WFC is still better than critically sampled at  $\text{GAIN}=2$ , which provides sampling of the full well depth as well (by contrast all WFPC2 results were obtained with a GAIN falling at least a factor of 3 short of critically sampling the readout noise). For HRC primary observations, the default gain is  $\text{GAIN}=2$ . For the HRC  $\text{GAIN}=4$  is needed to sample the detector full well depth, but this does result in modest undersampling of the readout noise. For HRC ACQ data, the default setting is  $\text{GAIN}=4$ . Users may select the GAIN they wish to use for their ACS observations by using the GAIN optional parameter in their Phase II proposal. However, not all GAIN settings are supported (see section 2.5).
- At wavelengths longward of  $\sim 8000\text{\AA}$ , internal scattering in the HRC CCD produces an extended PSF halo. This should affect only a minority of observations since at these wavelengths the WFC camera should normally be preferred. The WFC CCDs include a front-side metallization that eliminates the large angle, long wavelength halo problem for  $\lambda \lesssim 9000\text{\AA}$ . (For observations of red targets with the F850LP refer to Section 6.3.2).
- The ACS filter complement is not as rich as that in WFPC2. In particular, the Strömgren filter set and several narrow band filters available in WFPC2 (F375N, F390N, F437N, F469N, F487N, F588N, F631N, F656N, F673N, F953N) are not available on ACS. In general, these filters were not heavily used by the GO community. For most applications they can be replaced with the ACS medium and narrow ramps but it is conceivable that for some specialized applications the WFPC2 will still be preferred.

### 4.3.1 Throughputs and Limiting Magnitudes

In Figure 4.9 below, we show the throughput of the two unfiltered ACS CCD cameras: WFC and HRC. Superposed on this plot, we show the unfiltered WFPC2 (WF4) and the clear STIS throughputs. In Figure 4.8 the ACS SBC system throughput is compared to that of the STIS FUV-MAMA.

Figure 4.9: ACS CCD System Throughputs + OTA Versus those of STIS and WFPC2



### 4.3.2 Limiting Magnitudes

In Table 4.6, we give the V magnitude, in the Johnson-Cousins system, reached for an A0V star during a one-hour integration (CR-SPLIT=2) which produces a signal-to-noise ratio of 10 integrated over the number of pixels needed to encircle ~80% of the PSF flux. More precisely, for the WFC a boxsize of 5x5 pixels (0.2 arcsec) was used, for the HRC a 9x9 pixel boxsize (0.2 arcsec), and for the SBC a 15x15 pixel boxsize (0.5 arcsec). The last column gives the limiting magnitude assuming an optimally weighted PSF fit. The observations are assumed to take place in LOW-SKY conditions for the Zodiacal light and SHADOW of the Earthshine. Note that the assumed sky backgrounds are therefore much better than average conditions; these are best case limits.

Table 4.6: ACS limiting V magnitudes for A stars

ACS Camera	Filter	Magnitude	
		Aperture	PSF Fit
WFC	F606W	27.4	28.32
WFC	F814W	26.6	27.50
HRC	F330W	23.7	25.45
HRC	F606W	26.8	28.05
SBC	F125LP	23.7	24.53

### 4.3.3 Signal-To-Noise Ratios

In Chapter 10, we present, for each imaging mode, plots of exposure time versus magnitude to achieve a desired signal-to-noise ratio. These plots, which are referenced in the individual imaging-mode sections below, are useful for getting an idea of the exposure time you need to accomplish your scientific objectives. More accurate estimates will require the use of the ACS Exposure Time Calculator.

### 4.3.4 Saturation

Both CCD and SBC imaging observations are subject to saturation at high total accumulated counts per pixel: the CCDs, due either to the depth of the full well or to the 16 bit data format, and the SBC, due to the 16-bit format of the buffer memory (see Section 7.2.1 and Section 7.4.1). In Chapter 10, saturation levels as functions of source magnitude and exposure time are presented in the S/N plots for each imaging mode.

---

## 4.4 Wide Field Optical CCD Imaging

The Wide Field Channel of ACS was designed primarily for high throughput observations in the visible. The use of protected silver mirror coatings, the small number of reflections and the use of a red sensitive CCD have provided the high throughput required for this camera at the expense of a 3700 Å blue cutoff. The WFC detectors are two butted 2k by 4k thinned, backside-illuminated, SITe CCDs with a red optimized coating and long- $\lambda$  halo fix. The plate scale is 0.050 arcsecond per pixel which provides a good compromise between adequately sampling the PSF and a wide field of view. The WFC PSF is critically sampled at 11,600 Å and undersampled by a factor 3 at the blue end of the WFC sensitivity range (3700 Å). For well-dithered observations we expect that it will be possible to achieve a final reconstructed FWHM of 0.100-0.140 arcsec. Because the WFC PSF FWHM is largely dependent on the blurring caused by CCD charge diffusion, dithering will not be able to recover the full resolution of the optical system. See Section 8.2 for more discussion of how to use dithered observations to optimally sample the PSF.

The optical design of the camera introduces a two-component geometric distortion. The detectors themselves are at an angle with respect to the optical axis. This produces an 8% stretching of one pixel diagonal compared to the other. As a result WFC pixels project on the sky as rhombuses rather than squares. These effects are purely geometrical and are routinely corrected in the ACS data reduction pipeline. The second component of geometric distortion is more complex. This distortion causes

up to  $\pm 9\%$  variation in effective pixel area and needs to be taken into account when doing accurate photometry or astrometry as the effective area of the detector pixels varies nonlinearly with field position.

#### 4.4.1 Filter Set

##### WFPC2 and Johnson-Cousins filters

All of the most commonly used WFPC2 filters are included in the ACS filter set. In addition to a medium and a broad V band filter (F550M and F606W), there is a complete Johnson-Cousins *BVI* set (F435W, F555W, F814W).

##### Sloan Digital Sky Survey filters

The Sloan Digital Sky Survey (SDSS) *griz* filter set (F475W, F625W, F775W, F850LP) are designed to provide high throughput for the wavelengths of interest and excellent rejection of out-of-band wavelengths. They were designed to provide wide, non-overlapping filter bands that cover the entire range of CCD sensitivity from the blue to near-IR wavelengths.

##### Narrow Band filters

The H $\alpha$  (F658N), [OIII] (F502N), and [NII] (F660N) narrow band filters are full-size, and can be used with both WFC and HRC.

##### Ramp filters

ACS includes a complete set of ramp filters which provide full coverage of the WFC wavelength range at 2% and 9% bandwidth. Each ramp filter consists of 3 segments. The inner and outer filter segments can be used with the WFC only, while the central segments can be used by both WFC and HRC. Unlike the WFPC2 where the desired wavelength is achieved by offsetting the telescope, the wavelength of ACS ramps is selected by rotating the filter while the target is positioned in one of the pre-defined apertures. The monochromatic field of view of the ramp filters is approximately 40" by 80". Details of how to use the ramp filters are given in Section 8.5.2.

##### Polarizer filters

The WFC/HRC filter wheels contain polarizers with pass directions spaced by 60°, optimized for both the UV (POL0UV, POL60UV and POL120UV) and the visible (POL0V, POL60V and POL120V). All the polarizer filters are sized for the HRC field of view, so will induce vignetting when used with the WFC, where the FOV will be about 72" by 72". More information on the use of the polarizers is given in Chapter 5.

### Grism and Prism

The CCD channels also have a grism (G800L) for use with both WFC and HRC from 5500Å to 11,000Å, and a prism (PR200L) for use with the HRC from 1600Å to 3500Å. Again, these are described more fully in Chapter 5.

#### 4.4.2 Long Wavelength Halo Fix

The PSF of the STIS and HRC CCDs are characterized by a significant halo at long wavelengths which is due to photons crossing the CCD and being reflected back in random directions by the front side of the CCD. The problem becomes noticeable beyond 8000Å because only long wavelength photons can transverse the CCD without being absorbed. The so-called halo fix for the WFC consists of a metallization of the front side of the CCD which essentially reflects photons back to the original pixel.

Inflight calibrations observing stars with a broad color range, in particular very red stars, have shown that a significant halo does set in above 9000Å. A full discussion of this may be found in Gilliland & Riess, *2002 HST Calibration Workshop*, p61. In the F850LP filter, in particular, extremely red stars show a progressive loss of flux in small to moderate sized apertures as a function of color. This halo effect is only partially treated by the Exposure Time Calculator. Observers can use **synphot** (see Section 6.3.2) to most accurately calculate the photometry of red sources in the SDSS z-filter.

---

## 4.5 High-Resolution Optical and UV Imaging

The High Resolution Channel of ACS is the prime ACS camera for near-UV imaging. HRC provides high throughput in the blue and a better sampling of the PSF than either the WFC or other CCD cameras on HST. The HRC pixel size critically samples the PSF at 6300Å and is undersampled by a factor 3.0 at the blue end of its sensitivity range (2000Å). In this capability, the HRC functionally replaces the Faint Object Camera as the instrument able to critically sample the PSF in the V band. For this reason, although we expect that most of the usage of HRC will be for UV and blue imaging, HRC can also be convenient for imaging in the red when the PSF sampling is important. As an example, better PSF sampling is probably important for accurate stellar photometry in crowded fields and we expect that the photometric accuracy achievable by the HRC will be higher than that achievable with the WFC. Well-dithered observations with the HRC should lead to a reconstructed PSF FWHM of 0.03 arcsec at ~4000Å, increasing towards longer wavelengths. HRC also

includes a coronagraph that will be discussed in Chapter 5. The HRC CCD presents a long wavelength halo problem similar to the STIS CCD since the front-side metallization correcting the halo problem for the WFC CCDs was implemented only after the HRC CCD had been procured. Although most of the HRC imaging is likely to occur in the UV, users should be cautioned to take into account the effects of the long wavelength halo when using the HRC in combination with near-IR filters.

### 4.5.1 Filter Set

The HRC-specific filters are mostly UV and blue. The set includes UV and visible polarizers (discussed in Chapter 5), a prism (PR200L, discussed in Chapter 5), three medium-broad UV filters (F330W, F250W, and F220W) and two narrow band filters (F344N and F892N). Use of the UV filters with the WFC is not supported because of the uncertainty of the WFC silver coating transmission below 4000Å.

All broad, medium and narrow band WFC filters can be used with the HRC whenever a better PSF sampling is required. In general, where their sensitivity overlaps the throughput of WFC is higher than that of HRC. Only some of the WFC ramp filters can be used with the HRC since only the middle ramp segment overlaps with the HRC FOV. In particular, HRC can use the FR459M and FR914M broad ramps, and the FR505N [OIII], FR388N [OII] and FR656N (H $\alpha$ ) narrow ramps.

### 4.5.2 Multiple Electron Events

Like the STIS CCD but unlike WFPC2, the HRC CCD is directly sensitive to UV photons and for this reason is much more effective in detecting them. However, whenever a detector has non-negligible sensitivity over more than a factor two in wavelength, it becomes energetically possible for a UV photon to generate more than one electron, and so be counted more than once. This effect has indeed been seen in STIS and also during the ground testing of the HRC detector. The effect is only important shortward of 3200Å, and reaches a magnitude of approximately 1.7e<sup>-</sup>/photon at 2000Å. Multiple counting of photons has to be taken into account when estimating the detector QE and the noise level of a UV observation, since multiple photons cause a distortion in the Poisson distribution of electrons.

### 4.5.3 Red Leaks

When designing a UV filter, a high suppression of off-band transmission, particularly in the red, has to be traded with overall in-band transmission. The very high blue quantum efficiency of the HRC compared

to WFPC2 makes it possible to obtain an overall red leak suppression comparable to that of the WFPC2 while using much higher transmission filters. The ratio of in-band versus total flux is given in Table 4.7 for a few UV and blue HRC filters, where the cutoff point between in-band and out-of-band flux is defined as the filter's 1% transmission point. The same ratio is also listed for the equivalent filters in WFPC2. Clearly, red leaks are not a problem for F330W, F435W, and F475W. Red leaks are more important for F250W and F220W. In particular, accurate UV photometry of objects with the spectrum of an M star will require correction for the redleak in F250W and will be essentially impossible in F220W. For the latter filter a redleak correction will also be necessary for K and G types.

Table 4.7: In-band Flux as a Percentage of the Total Flux

	WFPC2 F218W	HRC F220W	WFPC2 F255W	HRC F250W	WFPC2 F300W	HRC F330W	WFPC2 F439W	HRC F435W	WFPC2 F450W	HRC F475W
O5V	99.8	99.8	99.6	99.7	99.9	99.9	99.9	99.9	99.9	99.9
B1V	99.7	99.7	99.6	99.7	99.9	99.9	99.9	99.9	99.9	99.9
A1V	99.4	99.1	99.2	99.3	99.2	99.9	99.9	99.9	99.9	99.9
F0V	98.5	97.8	98.8	99.0	98.8	99.9	99.9	99.9	99.9	99.9
G2V	92.5	90.2	97.4	98.4	97.4	99.9	99.9	99.9	99.8	99.9
K0V	71.7	69.6	95.0	97.3	95.0	99.9	99.9	99.9	99.8	99.9
M2V	0.03	2.5	45.5	71.9	45.4	99.9	99.9	99.9	99.6	99.9

## 4.6 Ultraviolet Imaging with the SBC

The Solar Blind Channel is the ACS camera optimized for far-UV imaging. The SBC uses the same optical train as the HRC and is comparable in performance to the FUV MAMA of STIS.

### 4.6.1 Filter Set

Like the STIS FUV MAMA, the SBC includes a Lyman  $\alpha$  narrow band filter (F122M), and a long pass quartz filter (F150LP). The STIS FUV clear and  $\text{SrF}_2$  filters are functionally replaced by the SBC  $\text{MgF}_2$  (F115LP) and  $\text{CaF}_2$  (F125LP) respectively. The SBC also includes two additional long pass filters not available in STIS (F140LP and F165LP) as well as prisms (discussed in Chapter 5).

### 4.6.2 Bright-Object Limits

The bright object limits are discussed in detail in Section 7.5.

### 4.6.3 Optical Performance

The optical performance of the SBC is comparable to that of the STIS FUV-MAMA. The use of the repeller wire increases the quantum efficiency of the detector by  $\sim 30\%$  or so, but adds a halo to the PSF.

### 4.6.4 Red Leaks

The visible light rejection of the SBC is excellent, but users should be aware that stars of solar type or later will have a significant fraction of the detected flux coming from outside the nominal wavelength range of the detector. Details are given below, in Table 4.8.

Table 4.8: Visible-Light Rejection of the SBC F115LP Imaging Mode

Stellar Type	Percentage of all Detected Photons which have $\lambda < 1800 \text{ \AA}$	Percentage of all Detected Photons which have $\lambda < 3000 \text{ \AA}$
O5	99.5	100
B1 V	99.4	100
A0 V	98.1	100
G0 V	72.7	99.8
K0 V	35.1	94.4

## 4.7 ACS Point Spread Functions

The ACS point spread function has been studied in ground test measurements, using models generated by the **TinyTIM** software of J. Krist and R. Hook and measured in on-orbit data. As with other HST instruments, the ACS point spread function is affected by both optical aberrations and geometric distortions. Also, point sources imaged with WFC and HRC experience blurring due to charge diffusion into adjacent pixels because of CCD subpixel variations, which reduces the limiting magnitudes that can be reached by WFC/HRC. The SBC PSF and the long-wavelength HRC PSF are additionally affected by a halo produced by the detectors themselves.

### 4.7.1 CCD Pixel Response Function

The sharpness of the CCD PSF is somewhat degraded by charge diffusion into adjacent pixels. The effect is usually described in terms of the pixel response function (PRF), which gives the distribution of flux from within the pixel into adjacent pixels. Charge diffusion results in  $\sim 0.5$  mag loss in the WFC limiting magnitude at short wavelengths (the worst case). At longer wavelengths and at all wavelengths for the HRC the reduction in the limiting magnitude is  $\sim 0.2$  mag or less. Due to variations in the CCD thickness, charge diffusion is not constant over the field of view. At different wavelengths, the CCD pixel response functions can be represented by the following kernels (for the center of the field):

$$K_{HRC} = \begin{bmatrix} 0.02 & 0.07 & 0.02 \\ 0.07 & 0.64 & 0.07 \\ 0.02 & 0.07 & 0.02 \end{bmatrix}, \quad K_{WFC} = \begin{bmatrix} 0.04 & 0.11 & 0.04 \\ 0.11 & 0.40 & 0.11 \\ 0.04 & 0.11 & 0.04 \end{bmatrix}$$

at  $\lambda = 4000\text{\AA}$ ,

$$K_{HRC} = \begin{bmatrix} 0.02 & 0.06 & 0.02 \\ 0.06 & 0.68 & 0.06 \\ 0.02 & 0.06 & 0.02 \end{bmatrix}, \quad K_{WFC} = \begin{bmatrix} 0.03 & 0.10 & 0.03 \\ 0.10 & 0.48 & 0.10 \\ 0.03 & 0.10 & 0.03 \end{bmatrix}$$

at  $\lambda = 5500\text{\AA}$ , and

$$K_{HRC} = \begin{bmatrix} 0.02 & 0.04 & 0.02 \\ 0.04 & 0.76 & 0.04 \\ 0.02 & 0.04 & 0.02 \end{bmatrix}, \quad K_{WFC} = \begin{bmatrix} 0.02 & 0.07 & 0.02 \\ 0.07 & 0.64 & 0.07 \\ 0.02 & 0.07 & 0.02 \end{bmatrix}$$

at  $\lambda = 8000\text{\AA}$ .

More details on ACS CCD charge diffusion are given in [ACS ISR 03-06](#).

### 4.7.2 Model PSFs

Table 4.9 and Table 4.10 give ACS model PSFs in the central  $5 \times 5$  pixel region in two wavelength bands (filters). Numbers listed are the fraction of the total energy received in each pixel. The models have been generated using **TinyTIM**, taking into account the HST optical aberrations and obscurations as well as the CCD pixel response function. Field dependent

geometrical distortions are included. The real PSF will also differ from the model because of the jitter in the HST pointing, HST focus variation (focus breathing), and other instrumental effects, some of which are briefly discussed below.

Table 4.9: Model ACS CCD PSFs

WFC model PSF, filter F435W					WFC model PSF, filter F814W				
0.00	0.01	0.01	0.01	0.00	0.01	0.01	0.02	0.01	0.01
0.01	0.04	0.07	0.05	0.02	0.01	0.03	0.07	0.03	0.02
0.02	0.08	0.17	0.08	0.02	0.02	0.07	0.18	0.07	0.02
0.01	0.04	0.08	0.04	0.01	0.01	0.03	0.07	0.03	0.01
0.00	0.01	0.02	0.01	0.00	0.01	0.02	0.02	0.01	0.00
HRC model PSF, filter F435W					HRC model PSF, filter F814W				
0.01	0.01	0.01	0.01	0.01	0.00	0.01	0.02	0.01	0.00
0.02	0.03	0.06	0.03	0.01	0.01	0.04	0.05	0.04	0.01
0.01	0.06	0.16	0.06	0.01	0.02	0.05	0.08	0.05	0.02
0.01	0.03	0.07	0.03	0.01	0.01	0.04	0.05	0.04	0.01
0.01	0.02	0.01	0.01	0.01	0.00	0.01	0.02	0.01	0.00

The SBC PSF is shown Figure 4.11.

Table 4.10: Model ACS SBC PSFs

SBC PSF at 120 nm					SBC PSF at 160 nm				
<0.01	0.01	0.01	0.01	<0.01	<0.01	<0.01	<0.01	<0.01	<0.01
0.01	0.02	0.03	0.02	0.01	<0.01	0.02	0.04	0.02	<0.01
0.01	0.03	0.15	0.03	0.01	<0.01	0.04	0.20	0.04	<0.01
0.01	0.02	0.03	0.02	0.01	<0.01	0.02	0.04	0.02	<0.01
<0.01	0.01	0.01	0.01	<0.01	<0.01	<0.01	<0.01	<0.01	<0.01

### 4.7.3 Encircled Energy

In general, the ACS channels encircled energy distribution has been found to be within the original instrument specifications. Figure 4.10 and Figure 4.11 show the ACS encircled energy curves derived from on-orbit images.

Figure 4.10: Encircled energy for the CCD channels

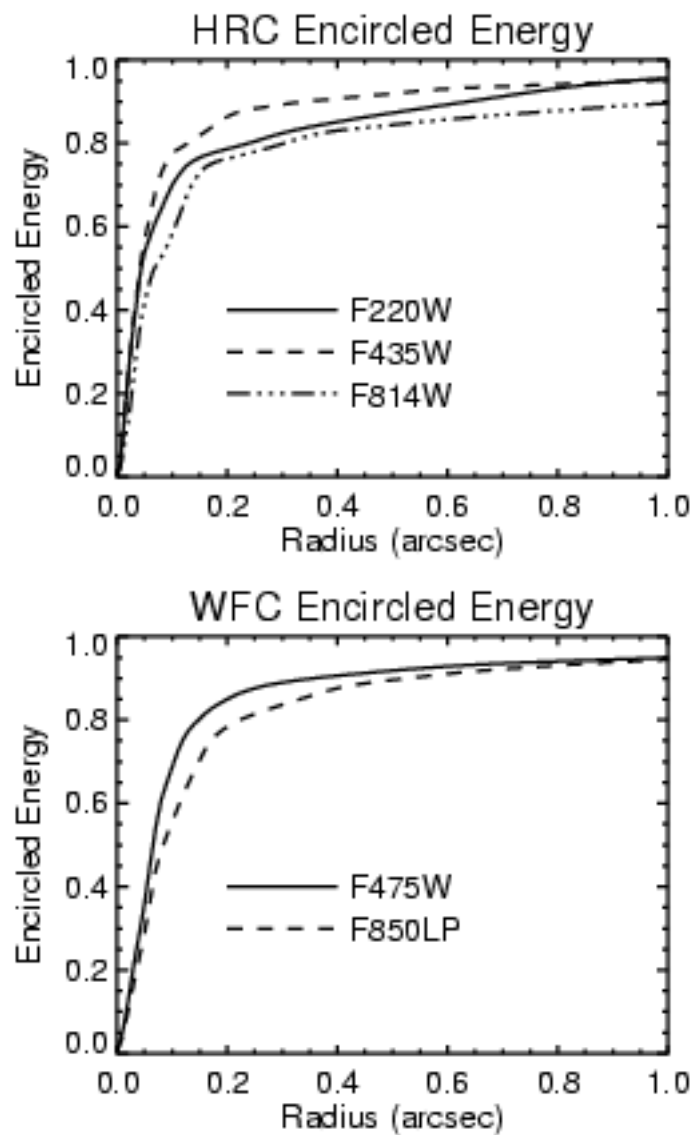
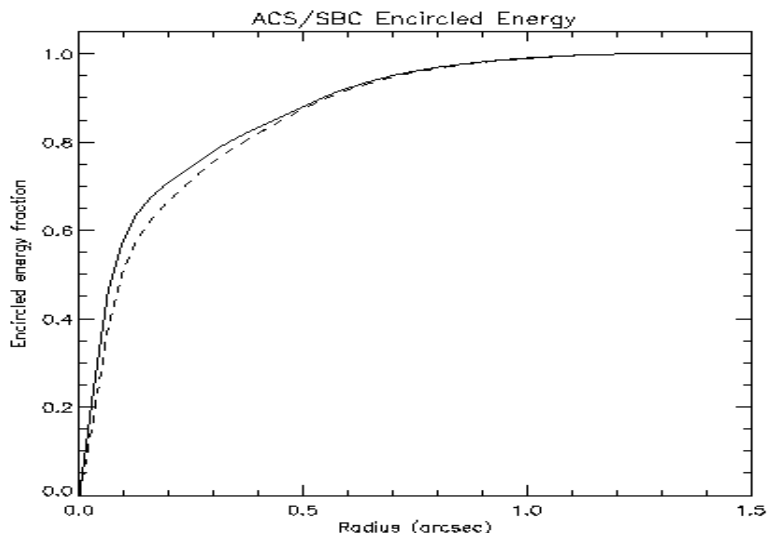


Figure 4.11: Encircled energy for the SBC



#### 4.7.4 Geometric Distortions

Geometric distortions produce a significant impact on the shape of the PSF in all three of the ACS channels, as can readily be seen in Figure 4.12 and Figure 4.13, which display WFC and HRC PSF images. The log stretch enhances the spider diffraction patterns, which the distortion renders non-perpendicular, and the outer Airy rings, which appear elliptical. The distortion owes primarily to the tilt of the focal surface to the chief ray at the large OTA field angles of the ACS apertures. The linear, field-independent, approximation for the WFC produces a difference in plate scale of about 8% between the two diagonals of the field and, in the HRC and SBC, about a 16.5% difference in scale between orthogonal directions rotated about 20 degrees from the aperture edges. Field-dependent distortions, measured as actual vs. predicted distances from field center, amount to about 2% peak in the WFC and about 1% in the HRC and SBC.

The distortions render the pixels, as projected on the sky, trapezoidal in shape and their area varies over the field by about 19% and 3.5% in the WFC and HRC/SBC, respectively. These variations have significant ramifications concerning appropriate techniques for flat-fielding and photometric calibration, especially when complicated by resampling in order to combine dithered image sets. A related issue is the manner in which the halation effects of the HRC and SBC detectors are removed and the treatment of spectra from the prisms and grism, which are not subject to the same distortion effects.

More details concerning geometric distortions in ACS can be found in “Distortion in the ACS” on page 248. A brief introduction to **CALACS** and **PyDrizzle** which apply corrections for geometric distortion is given in Chapter 12.

### 4.7.5 PSFs at Red Wavelengths and the UV

As previously noted, the CCDs used in the HRC and WFC suffer from a halo that is caused by very red photons passing through the device and being scattered back into the detector by the mounting substrate. This creates a large halo in HRC images beyond 7000 Å and WFC images past 10,000 Å. At 8000 Å in the HRC, the halo contains about 10% of the light. At 10,000 Å, it contains about 30% and increases the surface brightness of the PSF wings by over an order of magnitude; overwhelming the PSF diffraction rings and spikes.

Long wavelength photons that pass through the CCD can also be scattered by the electrode structure on the back side of the device. This creates two spikes that extend roughly parallel to the x-axis. These spikes are seen at wavelengths longer than 9500 Å in both the HRC and WFC (see Figure 4.14 and Figure 4.15).

In the UV the core of the PSF becomes rather asymmetrical due to midfrequency optical surface errors. In the SBC, a halo is created by charge migration at the microchannel plate surface. This effect, seen previously in STIS MAMA images, broadens the PSF core and redistributes a small portion of flux into a broad halo that can be approximated by a Gaussian with FWHM  $\sim 20$  pixels. The peak flux for a point source centered on a pixel is reduced by 30%-40% depending on wavelength.

The encircled energy curves presented in this handbook and incorporated into the ETC include all of the scattering effects discussed here.

### 4.7.6 Residual Aberrations

ACS provides excellent optical performance. Residual aberration levels at the center of the field are 1/30 wave (HRC) and 1/20 wave (WFC) RMS at 5500 Å (excluding defocus). Coma and astigmatism are minimized at the field center of each camera. The ACS PSF varies far less over the field of view than those of WFPC2 and STIS. WFPC2 especially suffers from a variable obscuration pattern that significantly alters the PSF structure depending on field position. Lacking the additional obscurations present in WFPC2, ACS PSF variations are instead due to changes in aberrations and charge diffusion.

At the extreme corners of the WFC field, increased astigmatism will slightly elongate the PSF core. The axis of elongation will rotate by 90 degrees if the system passes through focus due to breathing. This may affect ellipticity measurements of small galaxies with bright cores at the field edges. Focus variations in the WFC, which alter the amount of light in the peak, are largely due to detector surface height irregularities and amount to the equivalent of 5 microns of breathing (1/18 wave RMS). The

largest focus offset is along the gap between the two CCDs. Variations in the width of the PSF core are dominated by changes in CCD charge diffusion, which is dependent on the thickness of the detector (12-17 microns for the WFC). The PSF FWHM in F550M, for example, can vary by 20% over the field (0.10"-0.13").

The PSFs in the HRC and SBC are reasonably constant over their fields. The HRC FWHM is 0.060"-0.073" in F550M. More details on ACS PSF field variations are provided in [ACS ISR 03-06](#). The Tiny Tim PSF simulator includes field dependent aberrations and charge diffusion and may be used to estimate the impact of these variations.

Figure 4.12: ACS WFC PSF - F625W

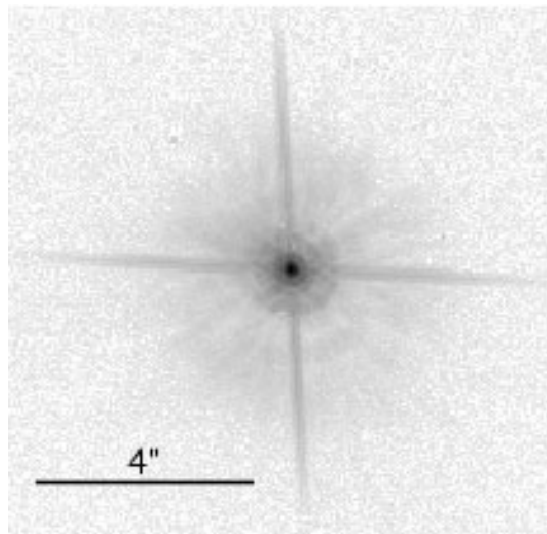


Figure 4.13: ACS HRC PSF - F625W

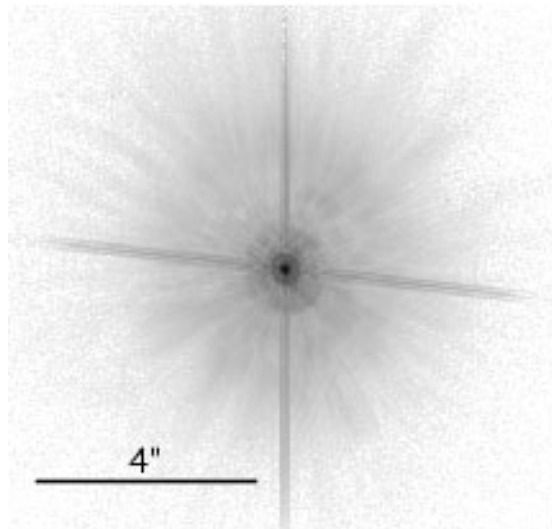


Figure 4.14: ACS WFC PSFs (10" x10"). FR914M images are saturated.

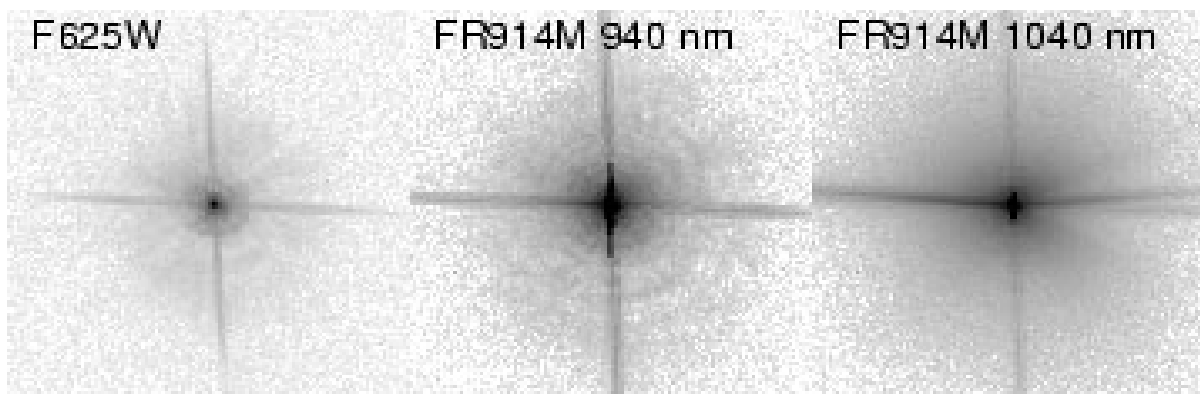
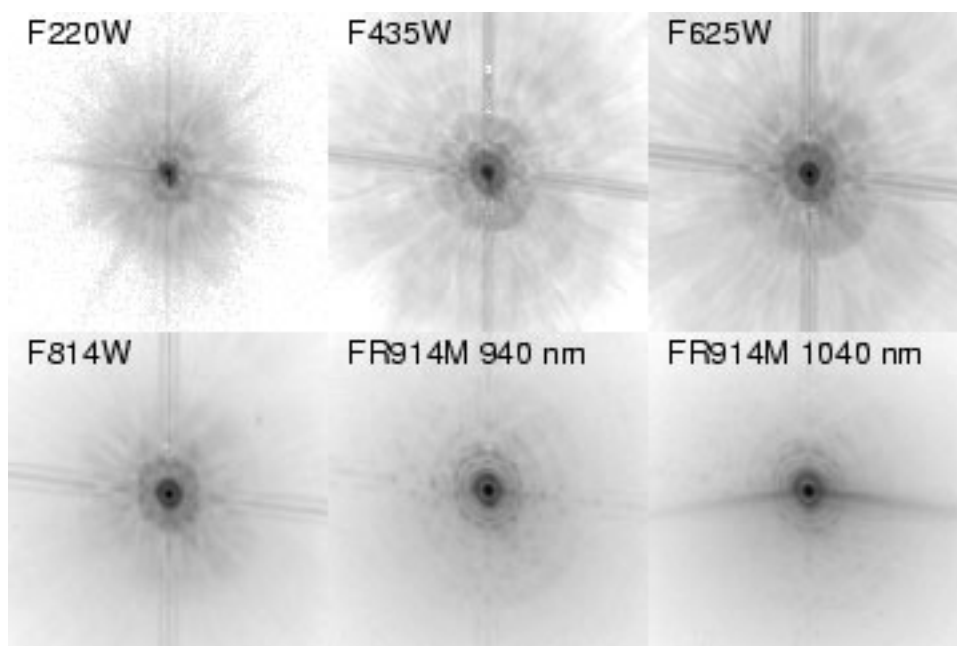


Figure 4.15: ACS HRC PSFs (3.25" x3.25")



---

## 4.8 Two-Gyro Guiding

At some future date HST may be operated with only two gyroscopes, hence causing additional spacecraft jitter and possible degradation of the effective PSF. Extensive tests of two-gyro guiding are planned in early 2005, where these impacts should become more clear.



---

*See the Two-Gyro Handbook for additional discussion of these effects..*

---

We anticipate that a two-gyro version of the ACS Exposure Time Calculator will be available to help assess these impacts.



CHAPTER 5:

# Polarimetry, Coronagraphy and Prism/Grism Spectroscopy

In this chapter. . .

5.1 Polarimetry / 63 5.2 Coronagraphy / 69 5.3 Grism/Prism Spectroscopy / 88
--

In this chapter we provide an overview of the special observing capabilities offered by ACS. These capabilities are optical and near-UV imaging polarimetry, coronagraphy with an aberrated beam coronagraph and low resolution ( $R \sim 100$ ) optical and near-UV spectroscopy.

---

## 5.1 Polarimetry

The Advanced Camera has a straightforward imaging polarimetric capability. Polarization observations require a minimum of three images taken using polarizing optics with different polarization characteristics in order to solve for the source polarization unknowns (polarization degree, position angle and total intensity). To do this, ACS offers two sets of polarizers, one optimized for the blue (POLUV) and the other for the red

(POLV). These polarizers can be used in combination with most of the ACS filters (see Table 5.2) allowing polarization data to be obtained in both the continuum and in line emission; and to perform rudimentary spectropolarimetry by using the polarizers in conjunction with the dispersing elements. (Due to the large number of possibilities in combination with ramp and dispersing elements, and heavy calibration overheads, observers wishing to use those modes should request additional calibration observations). For normal imaging polarization observations, the target remains essentially at rest on the detector with a suitable filter in beam, and an image is obtained with each of the appropriate polarizing elements in turn. The intensity changes between the resulting images provide the polarization information.

Each set of polarizers comprises three individual polarizing filters with relative position angles  $0^\circ$ ,  $60^\circ$  and  $120^\circ$ . The polarizers are designed as aplanatic optical elements and are coated with “Polacoat 105UV” for the blue optimized set and HN32 polaroid for the red set. The blue/near-UV optimized set is also effective all through the visible region, giving a useful operational range from approximately  $2000\text{\AA}$  to  $8500\text{\AA}$ . The second set is optimized for the visible region of the spectrum and is fully effective from  $4500\text{\AA}$  to about  $7500\text{\AA}$ .

The relative performance of the UV-optimized versus the visible optimized polarizers is shown in Figure 5.1. The visible polarizers clearly provide superior rejection for science in the  $4500\text{--}7500\text{\AA}$  bandpass, while the UV optimized polarizers deliver lower overall rejection across a wider range into the near-UV,  $2000\text{--}7500\text{\AA}$ . While performance of the polarizers begins to degrade at wavelengths longer than about  $7500\text{\AA}$ , useful observations should still be achievable to approximately  $8500\text{\AA}$  in the red. In this case, allowance for imperfect rejection of orthogonally polarized light should be made at the analysis stage.

A further caveat is that imperfections in the flat fields of the POLVIS polarizer set have been found which may limit the optimal field of view somewhat. Potential users are encouraged to check the STScI [ACS web](#) site for the latest information.

To first approximation, the ACS polarizers can be treated as three essentially perfect polarizers. The Stokes parameters (I, Q, U) in the most straightforward case of three images obtained with three perfect polarizers at  $60^\circ$  relative orientation, can be computed using simple arithmetic.

Using  $im1$ ,  $im2$ , and  $im3$  to represent the images taken through the polarizers POL0, POL60, and POL120 respectively, the Stokes parameters are as follows:

$$Q = \frac{2}{3}(2im1 - im2 - im3)$$

$$U = \frac{2}{\sqrt{3}}(im3 - im2)$$

$$I = \frac{2}{3}(im1 + im2 + im3)$$

These values can be converted to the degree of polarization  $P$  and the polarization angle  $\theta$ , measured counterclockwise from the  $x$  axis as follows:

$$P = \frac{\sqrt{Q^2 + U^2}}{I}$$

$$\theta = \frac{1}{2} \tan^{-1}(U/Q)$$

A more detailed analysis, including allowance for imperfections in the polarizers may be found in Sparks & Axon 1999 *PASP*, **111**, 1298. They find that the important parameter in experiment design is the product of expected polarization degree and signal-to-noise. A good approximation for the case of three perfect polarizers oriented at the optimal  $60^\circ$  relative position angles (as in ACS) is that the error on the polarization degree  $P$  (which lies in the range 0 for unpolarized to 1 for fully polarized) is just the inverse of the signal-to-noise per image. Specifically, they found

$$\log\left(\frac{\sigma_P}{P}\right) = -0.102 - 0.9898 \log(P \langle S/N \rangle_i)$$

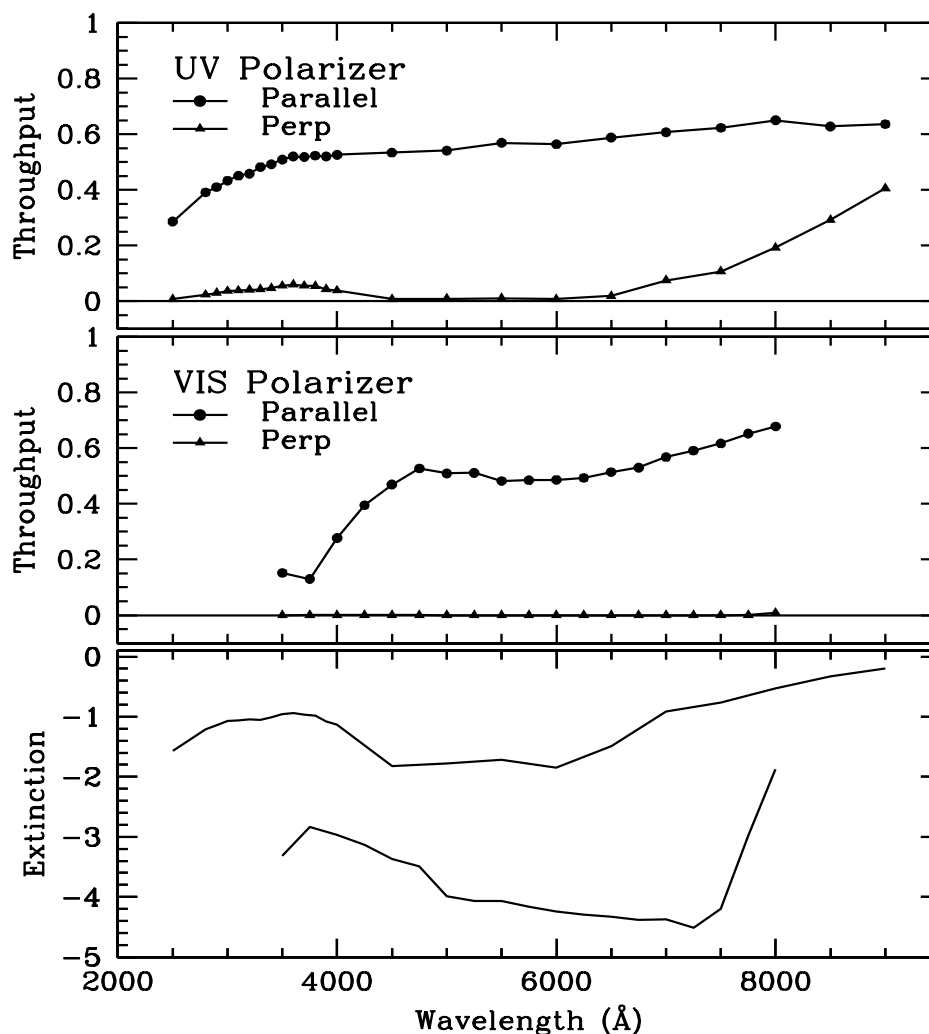
where  $\langle S/N \rangle_i$  is the signal to noise of the  $i^{\text{th}}$  image; and

$$\log \sigma_\theta = 1.514 - 1.068 \log(P \langle S/N \rangle_i)$$

The above discussion is for ideal polarizers with no instrumental polarization. Of course, the reality is that the polarizer filters, especially the UV polarizer, has significant leakage of cross-polarized light. And the instrumental polarization of the HRC ranges from a minimum of 4% in the red to 14% in the far-UV, while that of the WFC is  $\sim 2\%$  (see [ISR ACS](#)

2004-09). Other effects, such as phase retardance in the mirrors, may be significant as well. Please consult the ACS Data Handbook, STScI web pages, and ISRs for more detailed information.

Figure 5.1: Throughput and rejection of the ACS Polarizers. In the top two boxes, the upper curve is the parallel transmission, while the lower curve is the perpendicular transmission. The bottom panel shows the logarithm of the ratio of perpendicular to parallel transmission



The implementation of the ACS polarizers is designed for ease of use. The observer merely selects the camera (either HRC or WFC), the spectral filter, and then takes images stepping through the three filters of either the VIS set (POL0V, POL60V, POL120V) or the UV set (POL0UV, POL60UV, POL120UV). Once the camera and polarizer are specified, the scheduling system automatically generates slews to place the target in the optimal region of the field of view.

Since the ACS near-UV and visible filter complement is split between two filter wheels, there are restrictions on which filters the polarizer sets can be combined with. The choices available were determined by the

relative performance of the polarizers and the near-UV limitations of the WFC resulting from the silver mirror coatings.

The near-UV optimized polarizers are mounted on Filter Wheel 1 and may be crossed with the near-UV filter complement, which are mounted on Filter Wheel 2. The visible optimized polarizers are mounted on Filter Wheel 2 and can be crossed with filters on Filter Wheel 1, namely the primary broadband filters, and discrete narrowband filters  $H\alpha$ , [OII] and their continuum filters. Due to the calibration overhead required, it is not planned to support the use of ramp filters with either polarizer set. GOs are, therefore, required to include calibration observations, if they plan to use the ramp filters with the polarizers.

The polarizer sets are designed for use on the HRC where they offer a full unvignetted field of view,  $29\times 26$  arcsec with any of the allowable filter and coronagraph combinations including those ramps and spectroscopic elements that may also be used on the HRC (although see above re. additional calibrations).

The same allowable combinations, either UV or visible optimized, may also be used on the WFC where an unvignetted field of view of diameter 70 arcsec is obtained. This does not fill the field of view of the WFC due to the small size of the polarizing filters. However it does offer an area approximately five times larger than that obtained on the HRC. In order to avoid the gap between the WFC CCDs, and to optimize the readout noise and CTE effects, the scheduling system will automatically slew the target to roughly pixel (3096,1024) on the WFC1 CCD whenever the WFC aperture is selected in conjunction with one of the polarizers. Also, to reduce camera overhead times, only a  $2048\times 2048$  subimage centered on the target location will be readout from WFC1 (see Table 5.1).

Occasionally observers will ask to obtain non-polarized images at the same physical location on the detector as their polarized images. This is completely straight forward for the HRC; one merely takes the exposure without the polarizer filter. However, for the WFC it is more complicated because specifying WFC together with a polarizer automatically invokes a large slew, whereas no slew is performed when the polarizer filter is omitted. To obtain a non-polarizer image at the same physical detector location as the polarizer image in the WFC, one merely needs to specify the aperture as WFC1-2K instead of WFC (see Table 5.1).

Table 5.1: Examples of Polarizer and non-Polarizer Exposures in a Phase II Proposal

Aperture	Filters	Comment
HRC	F606W, POL0V	1024x1024 image centered at usual HRC aperture.
HRC	F606W, POL60V	Same but with POL60V.
HRC	F606W, POL120V	Same but with POL120V.
HRC	F606W	Non-polarizer image centered at same detector location as polarizer exposure.
WFC	F606W, POL0V	Target automatically placed at WFC1 pixel (3096,1024); 2048x2048 image.
WFC	F606W, POL60V	Same but with POL60V.
WFC	F606W, POL120V	Same but with POL120V.
WFC1-2K	F606W	Non-polarizer image at same detector location. Target at WFC1 pixel (3096,1024); 2048x2048 image.

Table 5.2: Filters that can be used in conjunction with the ACS Polarizers

Polarizer set	Filters	Filter Comments
POL0UV	F220W	HRC NUV short
POL60UV	F250W	HRC NUV long
POL120UV	F330W	HRC U
	F435W	Johnson B
	F814W	broad I
POL0V	F475W	SDSS g
POL60V	F606W	Johnson V
POL120V	F625W	SDSS r
	F658N	H $\alpha$
	F775W	SDSS i

The filters specified in Table 5.2 are those that we expect users to choose for their polarization observations. We will calibrate the most popular of these filters. Filter combinations not on this list will most probably not be calibrated, so potential users who have a strong need for such a polarizer/filter combination should include any necessary calibrations themselves.

We anticipate that the most accurate polarization observations will be obtained in the visible band (i.e., F606W) with the HRC and the visible polarizers. This mode has the advantages of a very high rejection of perpendicular polarization, and known mirror coatings with readily modeled properties. The WFC may be capable of similar accuracy to the HRC, however its proprietary mirror coatings will make modeling of the

polarization properties, and hence calibration, much more difficult (e.g., unknown phase retardance effects in the WFC IM3 mirror are a concern).

Polarimetry in the UV will be more challenging for a number of reasons. The UV polarizer has relatively poor rejection in the UV, and the instrumental polarization of the HRC, which is 4% - 7% in the visible, rises to 8% - 9% in the UV, and reaches 14% at 2200 Å (see [ACS ISR 04-09](#)). Far-UV polarimetry will be especially challenging since the polarizer properties were not well-characterized shortwards of 2800 Å, and appear to change rapidly with wavelength. Moreover, the low UV transmission of the UV polarizer, and the poor polarization rejection in the far-red, work together to exacerbate redleaks which are normally seen in the far-UV spectral filters.

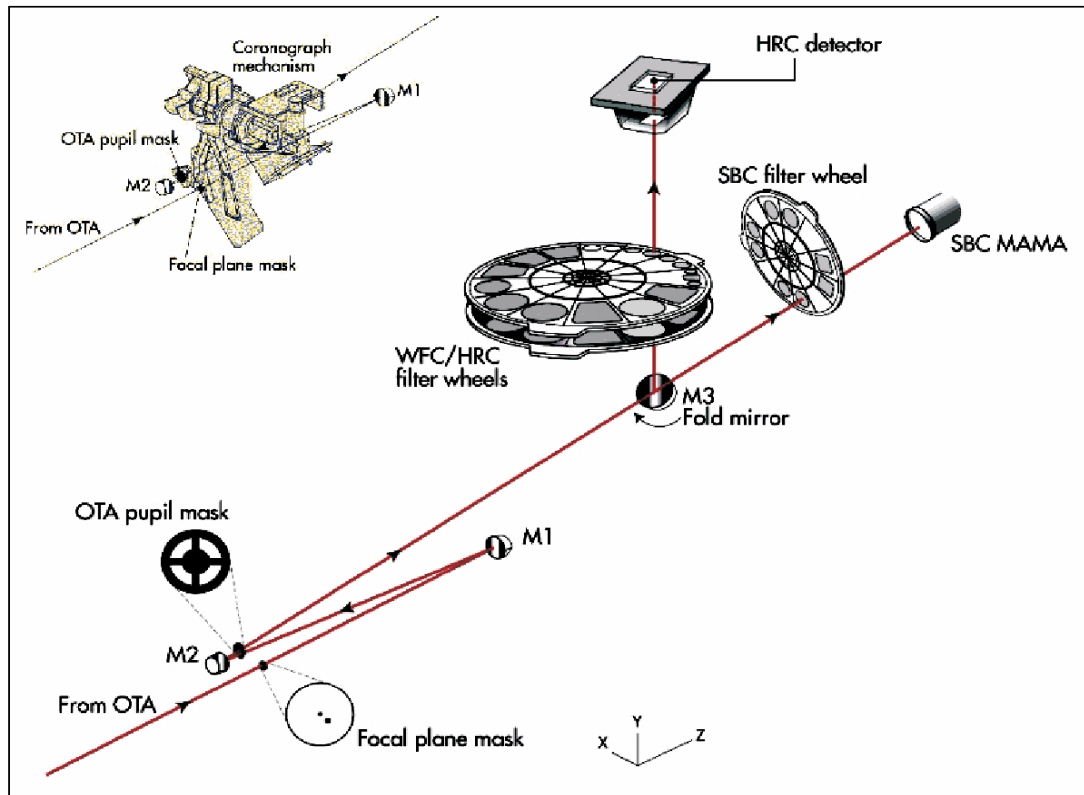
The polarizer filters contribute a weak geometric distortion which rises to about 0.3 pixel near the edges of the HRC field-of-view. This is caused by a weak positive lens in the polarizers, which is needed to maintain proper focus when multiple filters are in the beam. In addition, the visible polarizer has a weak ripple structure which is related to manufacture of its polaroid material; this contributes an additional  $\pm 0.3$  pixel distortion with a very complex structure (see [ACS ISR 04-10](#) and [ACS ISR 04-11](#)). All these geometric effects are correctable with the drizzle software, however, astrometry will likely be less accurate in the polarizers due to residual errors and imperfect corrections.

---

## 5.2 Coronagraphy

The ACS High Resolution Camera (HRC) has a user-selectable coronagraphic mode for the imaging of faint objects (circumstellar disks, substellar companions) near bright point sources (stars or luminous quasar nuclei). The coronagraph suppresses the diffracted light (diffraction spikes and rings) of the central source to below the level of the scattered light, most of which is caused by surface errors in the HST optics. The coronagraph was added after ACS construction began, at which point it was impossible to insert it into the aberration-corrected beam. Instead, the system is used in the aberrated beam, which is corrected after the coronagraph. While not as efficient as a corrected-beam coronagraph, especially for imaging close to the central source, it does provide a significant improvement to the high-contrast imaging capabilities of HST. Care must be taken, however, to design an observation plan that properly optimizes the coronagraph's capabilities and accounts for its limitations.

Figure 5.2: Schematic layout of the ACS HRC coronagraph. The upper left inset shows a schematic of the coronagraph mechanism that can be flipped in-and-out of the HRC optical path.



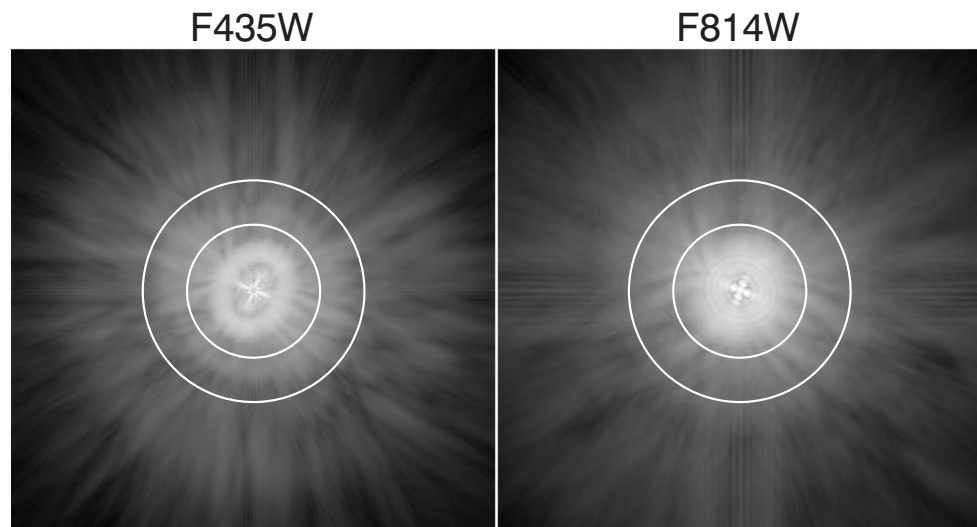
### 5.2.1 Coronagraph Design

A schematic layout of the ACS coronagraph is shown in Figure 5.2. The aberrated beam from the telescope first encounters one of two occulting spots. The beam continues to the M1 mirror, which forms an image of the HST entrance pupil on the M2 mirror, which corrects for the spherical aberration in the HST primary mirror. The coronagraph's Lyot stop is placed in front of M2. A fold mirror directs the beam onto the CCD detector. The field is 29'' by 26'' with a mean scale of 0.026''/pixel (geometric distortion results in effectively non-square pixels). The coronagraph can be used over the entire HRC wavelength range of  $\lambda=2000\text{-}10,000\text{\AA}$  using a variety of broad-to-narrowband filters.

The occulting spots are placed in the plane of the circle of least confusion, near where the unaberrated HST focal plane would be. At this location the balance of defocus and spherical aberration provides a good compromise between maximal occulted flux and minimal spot radius. The angular extent of the PSF in this plane necessitates larger spots than would be used in an unaberrated system (Figure 5.3). The ACS spots are solid (unapodized) metallic coatings deposited on a glass substrate (which

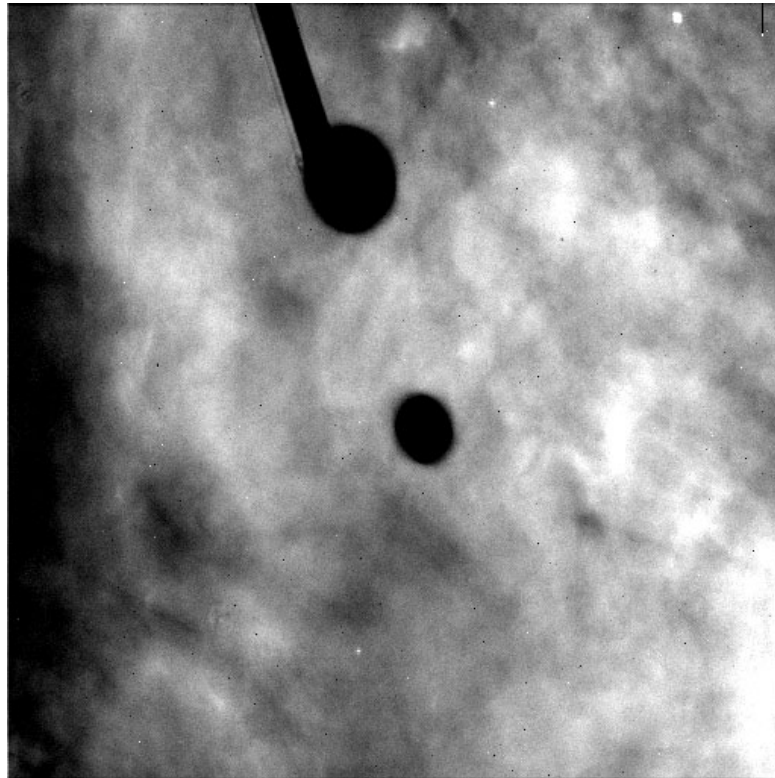
reduces throughput by 4.5%). The smaller spot is 1.8" in diameter and is at the center of the field. It is selected with the aperture CORON-1.8. A 3.0" diameter spot is near a corner (Figure 5.4) and is designated CORON-3.0. The smaller spot is used for the majority of the coronagraphic observations, as it allows imaging closer to the central source. The larger one may be used for very deep imaging of bright targets with less saturation around the spot edge than would occur with the smaller spot. Its position at the edge of the field also allows imaging of material out to 20" from the central source. The Lyot stop is located just in front of the M2 aberration correction mirror, where an image of the HST primary is formed. The stop is a thin metal mask that covers all of the diffracting edges in the HST system at the reimaged pupil (outer aperture, secondary mirror baffle, secondary mirror support vanes, and primary mirror support pads). The sizes of the stop and occulting spots were chosen to reduce the diffracted light below the level of the scattered light, which is unaltered by the coronagraph. The stop reduces the throughput by 48%, and it broadens the field PSF due to the smaller aperture and larger central obscuration relative to the beam diameter. The spots and Lyot stop are located on a panel attached to the ACS calibration door mechanism, which allows them to be flipped out of the beam when not in use. The inside surface of this door can be illuminated by a lamp to provide flat field calibration images for direct-mode imaging. However, the arrangement prevents the acquisition of internal flat fields in coronagraphic mode.

Figure 5.3: Computed point spread functions at the plane of the occulting spots through filters F435W and F814W. The elliptical, cross-shaped patterns in the cores are due to astigmatism at the off-axis location of the ACS aperture. It is corrected later by the ACS optics. The sizes of the two occulting spots ( $D=1.8''$  and  $3.0''$ ) are indicated. Logarithmic intensity scaled.



In addition to the combination of the occulting spots and Lyot stop that comprise the coronagraph, there is a 0.8" wide, 5" long occulting finger (OCCULT-0.8) permanently located at the window of the CCD dewar. It does not provide any suppression of diffracted light because it occurs after the Lyot stop. It was to be used to image closer to stars than is possible with the occulting spots while preventing saturation of the detector. However, because the finger is located some distance from the image plane, there is significant vignetting around its edges, reducing its effectiveness. Originally aligned to cover the central portion of the 3.0" spot, shifting of the spots relative to the beam during launch now places the finger along that spot's edge. Because of vignetting and the sensitivity of the PSF wings to the centering of the star, unocculted, saturated observations of sources will likely be more effective than using the occulting finger.

Figure 5.4: Region of the Orion Nebula observed with the coronagraph in filter F606W. The silhouettes of the occulters can be seen superposed against the background nebulosity. The 1.8" spot is located at the center and the 3.0" spot towards the top. The finger is aligned along one edge of the larger spot. This image has not been geometrically corrected, so the spots appear elliptical.



### 5.2.2 Acquisition Procedure and Pointing Accuracy

The central source must be placed precisely behind the occulting spot to ensure the proper suppression of the diffracted light. The absolute pointing

accuracy of HST is about 1", too crude to ensure accurate positioning. An on-board acquisition procedure, borrowed from the STIS coronagraph, is used to provide better alignment. The observer must request an acquisition image immediately before using the coronagraph and must specify a combination of filter and exposure time that provides an unsaturated image of the source. An acquisition image is taken by specifying HRC-ACQ as the aperture and ACQ as the opmode in APT.

Beginning in Cycle 12, acquisition images are taken with the coronagraphic masks inserted. The star is imaged within a predefined 200 x 200 pixel (5"x5") subarray near the small occulting spot. Two identical exposures are taken, each of the length specified by the observer (rather than each being half the length specified, as they would be for a conventional CR-SPLIT). From these two images, the on-board computer selects the minimum value for each pixel as a crude way of rejecting cosmic rays. The result is then smoothed with a 3x3 pixel box and the maximum pixel in the subarray is identified. The center-of-mass centroid is then computed for the unsmoothed image within a 5x5 pixel box centered on this pixel. Based on this position, the telescope is then slewed to place the star behind the occulting spot.

Because the coronagraphic masks are in place during acquisition, throughput is decreased by 52% relative to a non-coronagraphic observation. Also, the PSF is broader than in the normal imaging mode due to the larger obscurations in the Lyot stop, resulting in a lower relative peak pixel value (see Section 5.2.6). Care must be taken to select a combination of exposure time and filter that will prevent saturation of the star while providing enough flux to provide a good centroid measurement. A peak pixel flux of 2000 e<sup>-</sup> should be considered the minimum while 50K e<sup>-</sup> is a safe maximum (the HRC saturation limit is ~140K e<sup>-</sup>). Narrowband filters can be used, but for the brightest targets crossed filters are required. Allowable filter combinations for acquisitions are F220W+F606W, F220W+F550M, and F220W+F502N, in order of decreasing throughput. Be warned that the calibration of these filter combinations is poor, so estimated count rates from SYNPHOT or the APT ETC should be considered to be a factor of two off (either high or low).

Initial results from multiple on-orbit observations indicate that the combined acquisition and slew errors are on the order of ±0.25 pixels (±6 mas). While small, these shifts necessitate the use of subpixel registration techniques to subtract one coronagraphic PSF from another (Section 5.2.5). The position of the spots relative to the detector also varies over time. This further alters the PSF, resulting in subtraction residuals.

### 5.2.3 Vignetting and Flat Fields

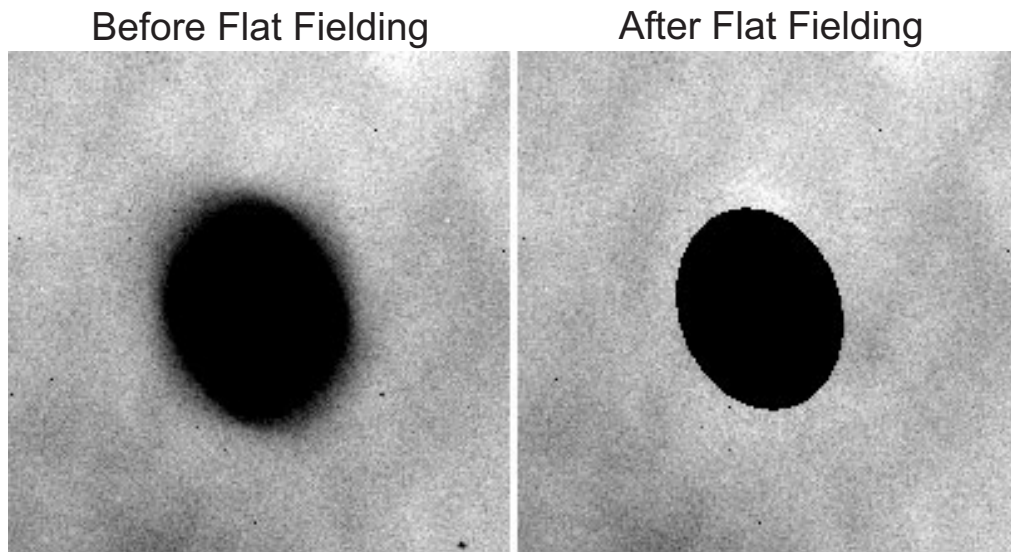
ACS coronagraphic flat fields are different from the standard flats due to the presence of the occulting spots and alteration of the field vignetting caused by the Lyot stop. The large angular extent of the aberrated PSF results in vignetting beyond one arcsecond of the spot edge (Figure 5.4), which can be corrected by dividing the image by the spot pattern (Figure 5.5). Unfortunately, the spots move over time relative to the other flat field

features (see Section 5.2.7). To account for this, separate flat fields have been derived that contain just the spot patterns (spot flats) and the remaining features (P-flats). For a full discussion see [ACS ISR 04-16](#).

The ACS pipeline will divide images by the P-flat. P-flats specific to the coronagraph have been derived from either ground-based or on-orbit data for filters F330W, F435W, F475W, F606W, and F814W. Other filters use the normal flats, which may cause some small-scale errors around dust diffraction patterns. As of the time of writing, the pipeline does not divide the images by spot flats, which must be manually applied by the observer as described in the ACS Data Handbook. Spot flats for the filters listed above are available for download from the ACS reference files web page. For other filters, the available spot flat closest in wavelength should be used. The spot flat must be shifted by an amount listed on the reference files page to account for motions of the occulting spots.

Because coronagraphic P-flats and spot flats exist only for the few filters listed above, observers are encouraged to use those filters. It is unlikely that flat fields for other filters will be available in the future.

Figure 5.5: (Left) Region of the Orion Nebula around the D=1.8" spot. The spot edge appears blurred due to vignetting. The image has not been geometrically corrected. (Right) The same region after the image has been corrected by dividing the flat field. The interior of the spot has been masked.

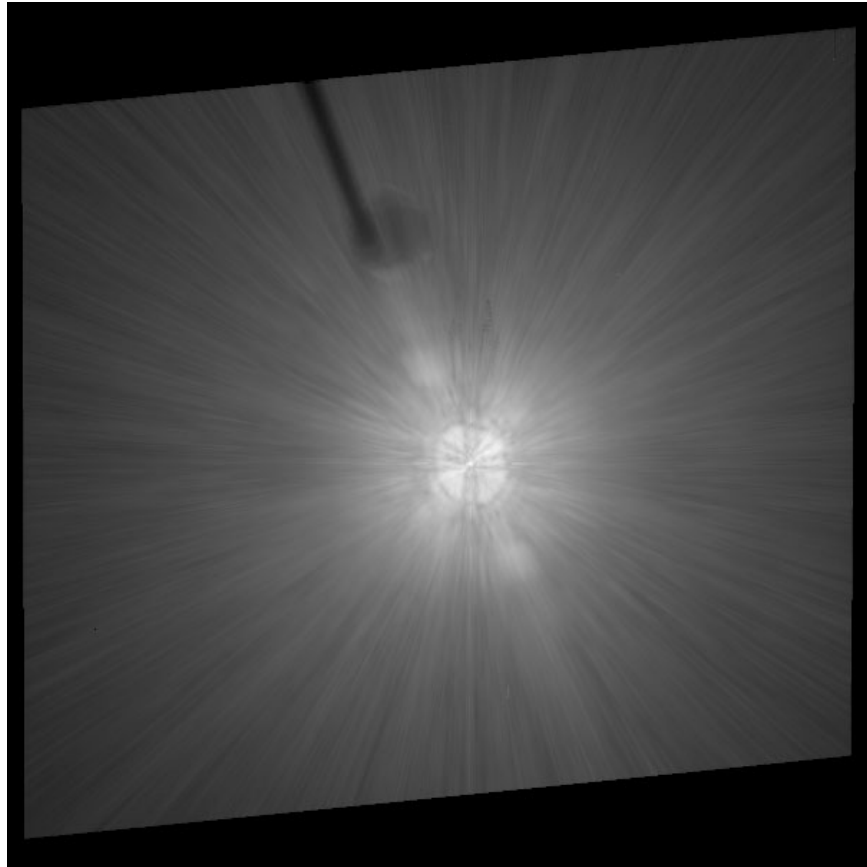


### 5.2.4 Coronagraphic Performance

Early in Cycle 11, coronagraphic performance verification images were taken of the V=0 star Arcturus (Figures 5.6 & 5.7). This star has an angular diameter of 25 mas and is thus unresolved by the coronagraph. The coronagraphic image of a star is quite unusual. Rather than appearing as a dark hole surrounded by residual light, as would be the case in an

aberration-free coronagraph, the interior of the spot is filled with a diminished and somewhat distorted image of the central source. This is due to correction by the M2 mirror of aberrated light from the star that is not blocked by the spot. The small spot is filled with light, while the large one is relatively dark. Broad, ring-like structures surround the spots, extending their apparent radii by about  $0.5''$ . These are due to diffraction in the wings of the aberrated PSF by the occulting spot itself. A consequence of these features is that stars may saturate the interior and edges of the spot within a short time. Within the small spot, the brightest pixels can become saturated in less than one second for a  $V=0.0$  star, while pixels at edge of the larger spot will saturate in about 14 seconds.

Figure 5.6: Geometrically corrected ( $29''$  across) image of Arcturus observed in F814W behind the  $1.8''$  spot. This is a composite of short, medium, and long (280s) exposures. The “bar” can be seen extending from the upper left to lower right. The shadows of the occulting finger and large spot can be seen against the scattered light background. Logarithmic intensity scale.



The measured radial surface brightness profiles (Figure 5.8) show that the coronagraph is well aligned and operating as expected. The light diffracted by the HST obscurations is suppressed below the level of the scattered light – there are no prominent diffraction spikes, rings, or ghosts beyond the immediate proximity of the spots. At longer wavelengths ( $\lambda > 600$  nm) the diffraction spikes appear about as bright as the residual scattered light (at longer wavelengths, the diffraction pattern is larger and

therefore not as well suppressed by the coronagraph). The spikes are more prominent in images with the large spot than the small one. This can be explained by the fact that the Lyot stop is not located exactly in the pupil plane but is instead slightly ahead of it, so the beam can “walk” around the stop depending on the field angle of the object. Because the large spot is at the edge of the field, the beam is slightly shifted, allowing more diffracted light to pass around the mask edges.

The residual background is dominated by radial streaks that are caused primarily by scattering from zonal surface errors in the HST mirrors. This halo increases in brightness and decreases in size towards shorter wavelengths. One unexpected feature is a diagonal streak or “bar” seen in both direct and occulted star images. It is about 5x brighter than the mean azimuthal surface brightness in the coronagraphic images. This structure was not seen in the ground-test images and is likely due to scattering introduced by the HST optics. There appears to be a corresponding feature in STIS as well.

Figure 5.7: Regions around the occulting spots in different filters. The occulting finger can be seen in the 3” spot images. Logarithmic intensity scaled.

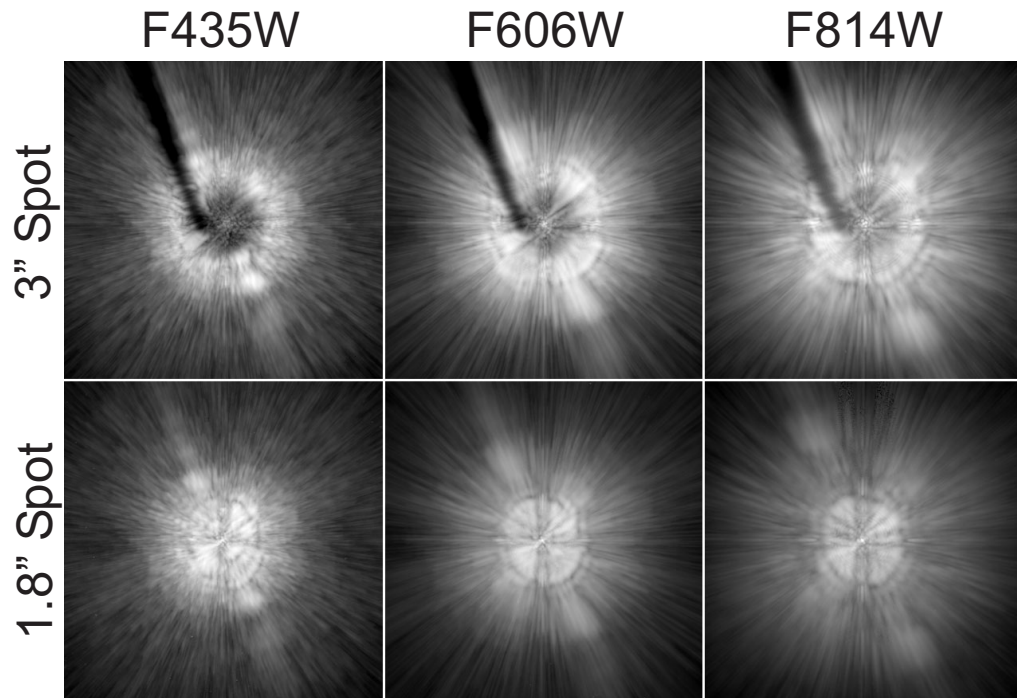
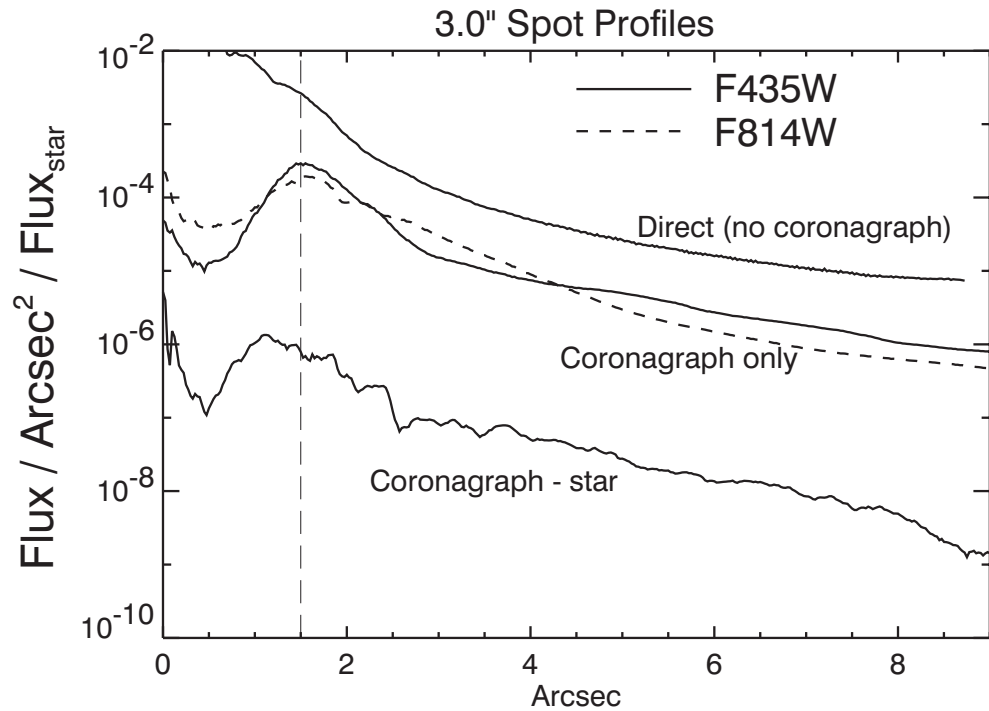
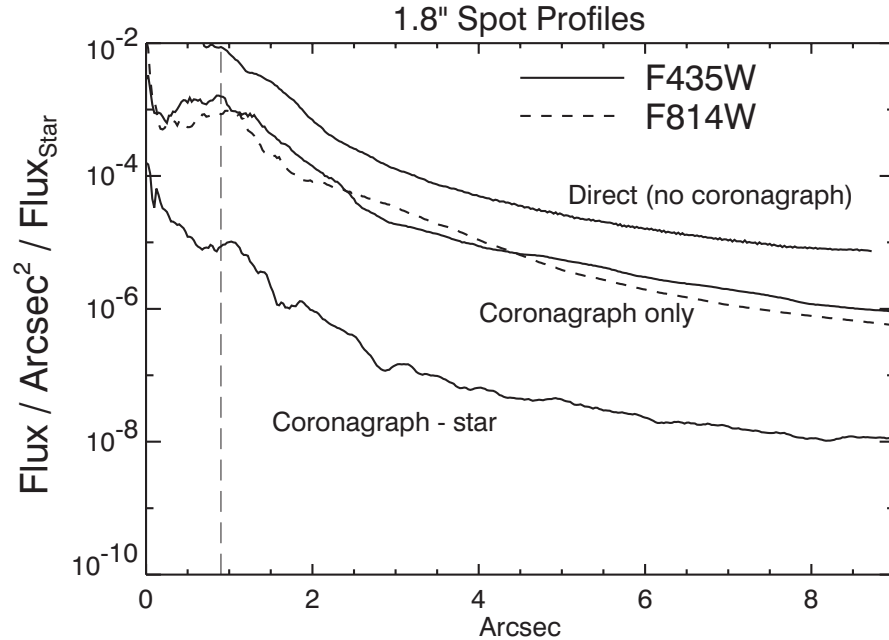


Figure 5.8: Surface brightness plots derived by computing the median value at each radius. The brightness units are relative to the total flux of the star. The direct profile is predicted; the coronagraphic profiles are measured from on-orbit images of Arcturus. “Coronagraph-star” shows the absolute median residual level from the subtraction of images of the same star observed in separate visits.



### 5.2.5 Residual Light Subtraction

While the coronagraph suppresses the diffracted light from the central star, the scattered light still overwhelms faint, nearby sources. It is possible to subtract most of the remaining halo using an image of another occulted star. PSF subtraction has been successfully used with images taken by other HST cameras, with and without a coronagraph. The quality of the subtraction depends critically on how well the target and reference PSFs match.

As mentioned above, for any pair of target and reference PSF observations there is likely to be a difference of 5-20 mas between the positions of the stars. Because the scattered light background is largely insensitive to small errors in star-to-spot alignment (it is produced before the coronagraph), most of it can be subtracted if the two stars are precisely registered and normalized. Due to the numerous sharp, thin streaks that form the scattered light background, subtraction quality is visually sensitive to registration errors as small as 0.03 pixels (0.75 mas). To achieve this level of accuracy, the reference PSF may be iteratively shifted and subtracted from the target until an offset is found where the streaks are minimized. This method relies on the judgment of the observer, as any circumstellar material could unexpectedly bias a registration optimization algorithm. A higher-order sampling method, such as cubic convolution interpolation, should be used to shift the reference PSF by subpixel amounts; simpler schemes such as bilinear interpolation degrade the fine PSF structure too much to provide good subtractions.

Normalization errors as small as 1-4% between the target and reference stars may also create significant residuals. However, derivation of the normalization factors from direct photometry is often not possible. Bright, unocculted stars will be saturated in medium or broadband filters at the shortest exposure time (0.1 sec). An indirect method uses the ratio of saturated pixels in unocculted images (the accuracy will improve with greater numbers of saturated pixels). A last-ditch effort would rely on the judgment of the observer to iteratively subtract the PSFs while varying the normalization factor.

In addition to registration offsets, positional differences can alter the diffraction patterns near the spots' edges. The shape and intensity of these rings are very sensitive to the location of the star relative to the spot. They cannot be subtracted by simply adjusting the registration or normalization. These errors are especially frustrating because they increase the diameter of the central region where the data are unreliable. The only solution to this problem is to observe the target and reference PSF star in adjacent orbits without flipping the masks out of the beam between objects.

Color differences between the target and reference PSF can be controlled by choosing an appropriate reference star. As wavelength increases, the speckles that make up the streaks in the halo move away from the center while their intensity decreases (Figure 5.7). The diffraction

rings near the spots' edges will expand as well. These effects can be seen in images through wideband filters – a red star will appear to have a slightly larger PSF than a blue one. Thus, an M-type star should be subtracted using a similarly red star – an A-type would result in significant residuals. Even the small color difference between A0V and B8V stars, for example, may be enough to introduce bothersome errors (Figure 5.9).

A focus change can also alter the distribution of light in the PSF. The telescope focus changes over time scales of minutes to months. Within an orbit, the separation between the primary and secondary mirrors varies on average by  $3\text{ }\mu\text{m}$  (resulting in  $1/28$  wave RMS of defocus @  $\lambda=0.5\text{ }\mu\text{m}$ ) – an effect called *breathing*. This is caused by the occultation of the telescope's field of view by the warm Earth, which typically occurs during half of each 96-minute orbit. This heats HST's interior structure, which expands. After occultation the telescope gradually shrinks. Large changes in the pointing attitude relative to the Sun can also introduce  $3\text{--}10\text{ }\mu\text{m}$  of expansion, which decays back to normal over several orbits. The main result of these small focus changes is the redistribution of light in the wings (Figure 5.10).

Figure 5.9: Predicted absolute mean subtraction residual levels for cases where the target and reference stars have color mismatches. The brightness units are relative to the total flux of the target star.

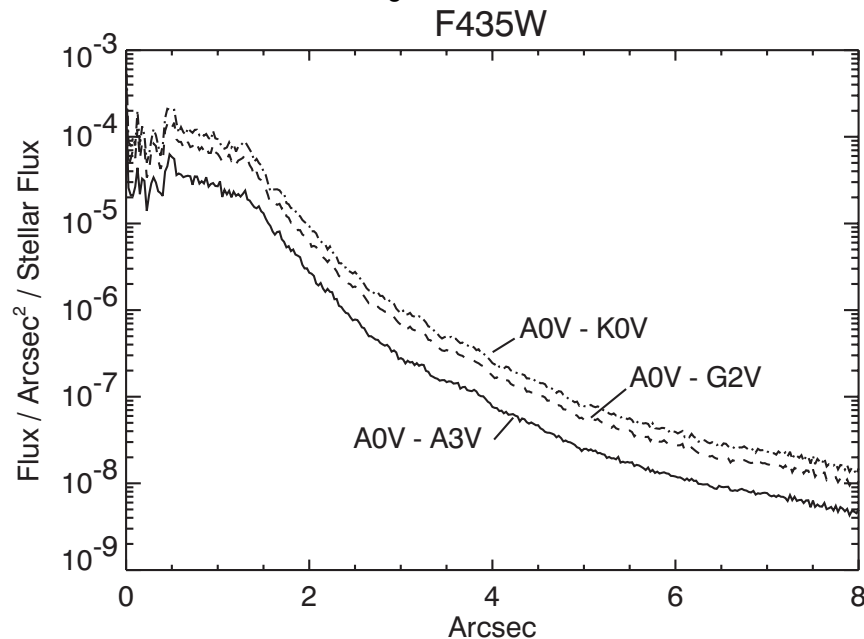
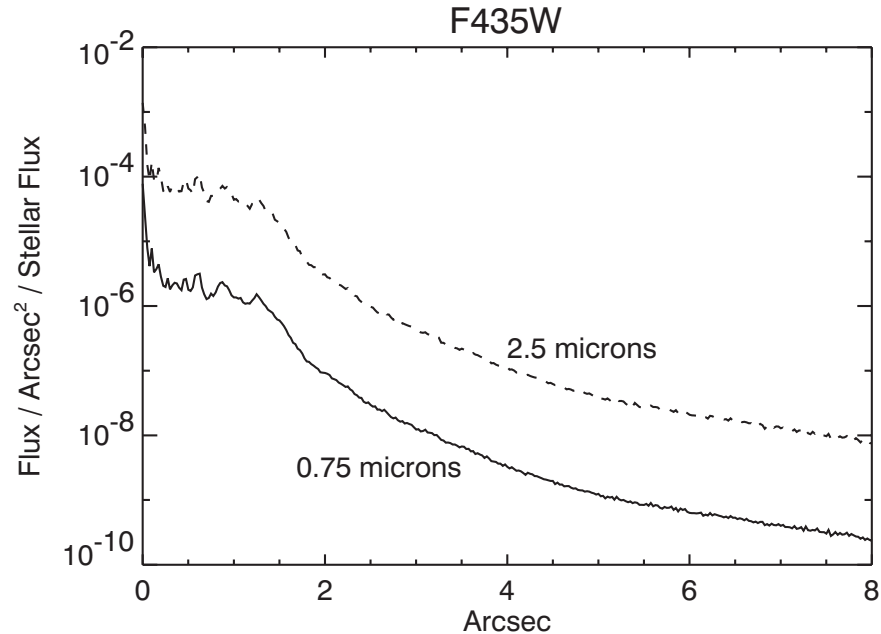


Figure 5.10: Predicted absolute mean subtraction residual levels for cases where the target and reference stars are imaged at different breathing-induced focus positions. The offset (0.75 or 2.5  $\mu\text{m}$ ) from perfect focus (0  $\mu\text{m}$ ) is indicated with respect to the change in the primary-secondary mirror separation (the typical breathing amplitude is 3-4  $\mu\text{m}$  within an orbit). The brightness units are relative to the total flux of the target star.

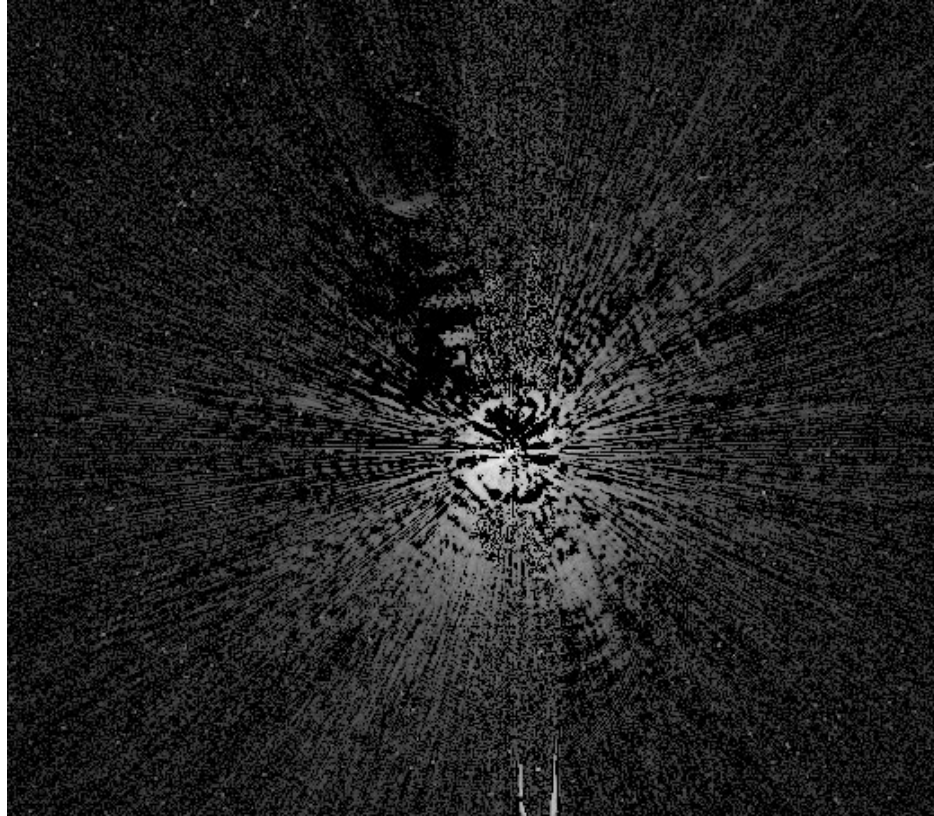


Plots of the azimuthal median radial profiles after PSF subtraction are shown in Figure 5.8. In these cases, images of Arcturus were subtracted from others of itself taken a day later. The images were registered as previously described. Combined with PSF subtraction, the coronagraph reduces the median background level by 250-2500x, depending on the radius and filter. An example of a PSF subtraction is shown in Figure 5.11. The mean of the residuals is not zero. Because of PSF mismatches, one image will typically be slightly brighter than the other over a portion of the field (such as shown in Figure 5.12). The pixel-to-pixel residuals can be more than 10x greater than the median level (Figure 5.13). Note that these profiles would be worse if there were color differences between the target and reference PSFs.

One way to get around both the color and normalization problems is to take images of the central source at different orientations and subtract one from the other (*roll subtraction*). This can be done by either requesting a roll of the telescope about the optical axis (up to 30° total) between orbits or by revisiting the object at a later date when the default orientation of the telescope is different. This technique only works when the nearby object of interest is not azimuthally extended. It is the best method for detecting point source companions or imaging strictly edge-on disks (e.g. Beta Pictoris). This method can also be used to reduce the pixel-to-pixel variations in the subtraction residuals by rotating and co-adding the images

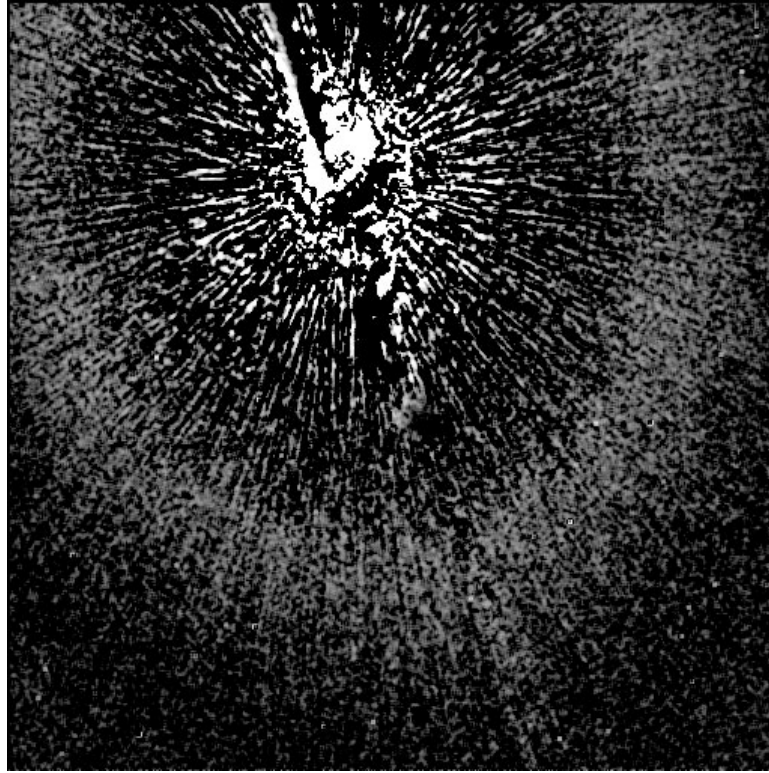
taken at different orientations (this works for extended sources if another PSF star is used). Ideally, the subtraction errors will decrease as the square root of the number of orientations.

Figure 5.11: Residual errors from the subtraction of one image of Arcturus from another taken in a different visit (filter=F435W, D=1.8" spot). The image is 29" across and has not been geometrically corrected. Logarithmic intensity scaled.



The large sizes of the occulting spots severely limit how close to the central source one can image. It may be useful to combine coronagraphic imaging with direct observations of the target, allowing the central columns to saturate (additional observations at other rolls would help). PSF subtraction can then be used to remove the diffracted and scattered light.

Figure 5.12: Subtraction of Arcturus from another image of itself taken during another visit using the large ( $D=3.0''$ ) spot and F435W filter. The image has been rebinned, smoothed, and stretched to reveal very low level residuals. The broad ring at about  $13''$  from the star is a residual from some unknown source – perhaps it represents a zonal redistribution of light due to focus differences (breathing) between the two images. The surface brightness of this ring is  $20.5 \text{ mag arcsec}^{-2}$  fainter than the star. The diameter, brightness, and thickness of this ring may vary with breathing and filter. The image has not been geometrically corrected.



### 5.2.6 The Off-Spot PSF

Objects that are observed in the coronagraphic mode but that are not placed behind an occulting mask have a PSF that is defined by the Lyot stop. Because the stop effectively reduces the diameter of the telescope and introduces larger obscurations, this PSF is wider than normal, with more power in the wings and diffraction spikes (Figure 5.14). In addition, the stop and spot substrate reduce the throughput by 52.5%. In F814W, this PSF has a peak pixel containing 4.3% of the total (reduced) flux and a sharpness (including CCD charge diffusion effects) of 0.010 (compare these to 7.7% and 0.026, respectively, for the normal HRC PSF). In F435W the peak is 11% and the sharpness is 0.025 (compared to 17% and 0.051 for the normal F435W PSF). Observers need to take the reduced throughput and sharpness into account when determining detection limits for planned observations. Tiny Tim can be used to compute off-spot PSFs.

Figure 5.13: Plots of the azimuthal RMS subtraction residual levels at each radius for the large (3") spot. The flux units are counts per pixel relative to the total unocculted flux from the central source. These plots were derived from Arcturus-Arcturus subtractions represent the best results one is likely to achieve. The undistorted HRC scale assumed here is 25 mas/pixel.

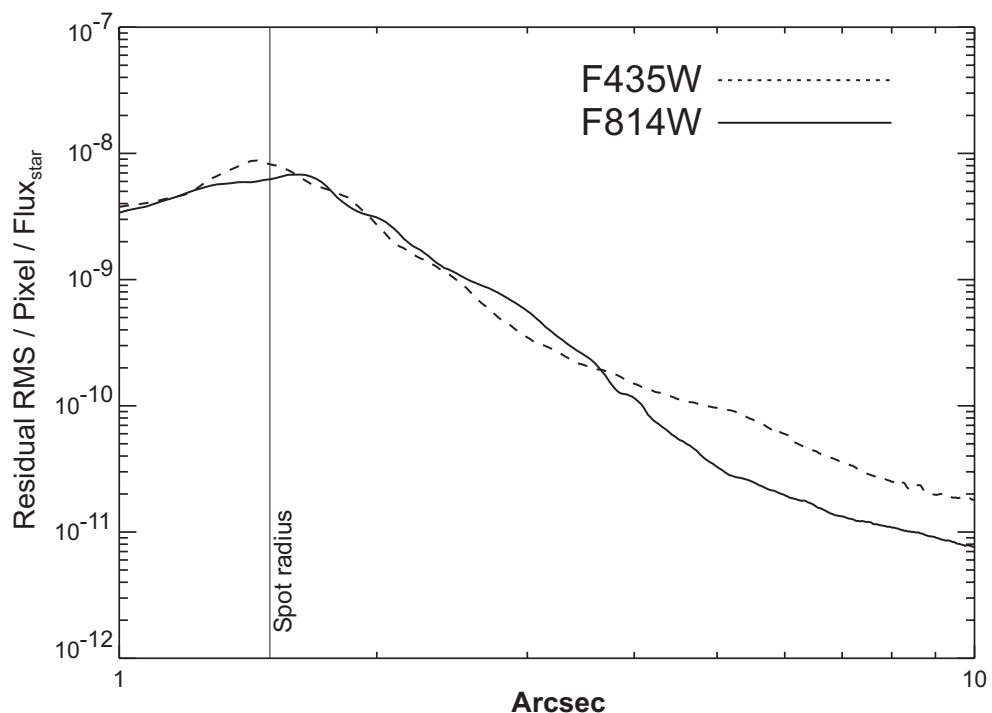
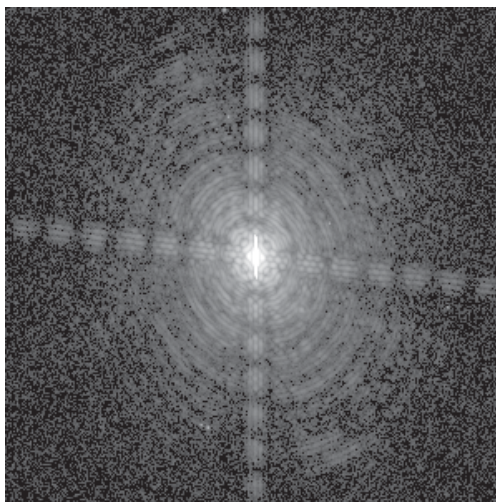


Figure 5.14: Image of Arcturus taken in coronagraphic mode with the star placed outside of the spot. The coronagraphic field PSF has more pronounced diffraction features (rings and spikes) than the normal HRC PSF due to the effectively larger obscurations introduced by the Lyot stop. The central portion of this image is saturated. It was taken through a narrowband filter (F660N) and is not geometrically corrected



### 5.2.7 Occulting Spot Motions

Monitoring of the occulting spot positions using earth flats shows that they move over weekly, and even daily, time scales in an unpredictable manner. The cause of this motion is unknown. Their locations typically vary by  $\sim 0.3$  pixel (8 mas) over the span of one week, but on occasion they have shifted by 1-5 pixels over 1-3 weeks. While inserted in the beam, however, they remain stable to better than  $\pm 0.1$  pixel, and when cycled within an orbit they return to the same position within  $\pm 0.25$  pixel.

The uncertainties in the locations lead to star-to-spot registration errors. After the acquisition exposure the star is moved to the predefined aperture position of the spot, which is measured on the ground from on-orbit flats and may be out of date. Due to the layout of ACS, it is not possible to determine the spot location automatically before a coronagraphic observation, as can be done for NICMOS. Also, unlike STIS, the star cannot be dithered around until the stellar flux within the occulter is minimized.

Star-to-spot registration errors affect coronagraphic imaging. If the star is significantly offset from the spot center ( $>3$  pixels), then one side of the spot interior and edge will be brighter than expected and may possibly saturate much earlier than predicted. A large offset will also slightly degrade the coronagraphic suppression of the diffraction pattern. Most importantly, even slight changes in the spot position will alter the residual diffraction pattern, introducing mismatches between the target and reference PSFs that may result in large subtraction residuals. This means that an observer cannot rely on reference PSFs taken in other programs or at different times.

To reduce the impact of spot motion, observers using the ACS coronagraph are required to obtain a reference PSF in an orbit immediately before or after their science observation. A single reference PSF can be used for two science targets if all three objects can be observed in adjacent orbits and are of similar color (note that it is difficult to schedule more than five consecutive orbits). Otherwise, if multiple science targets are observed, each one will require a reference PSF. The additional reference PSF orbit(s) must be included in the Phase 1 proposal.

As of Cycle 13, STScI is using a procedure to update the coronagraphic spot positions shortly before a proposal executes to provide better registration. Currently, it takes more than three weeks to revise the official aperture location of a spot, which means that its actual position at the time of a science observation could be off by pixels. In this new procedure, the last measured offset of the spot from its defined aperture location is uploaded to HST a few orbits before a coronagraphic observation executes. By including a USE OFFSET special requirement for each coronagraphic exposure after an acquisition, the target will be shifted by the appropriate amount. The spots are measured weekly from earth flats, so this method provides more up-to-date positions than relying on the aperture location.

This procedure adds approximately 40 seconds to each visit. This procedure is required for all coronagraphic observations. More details will be provided on the STScI [ACS web](#) site and in Phase II proposal instructions.

## 5.2.8 Planning ACS Coronagraphic Observations

### Exposure Time Estimation

The estimation of exposure time for coronagraphic observations is similar to direct-mode time calculations, except that the additional background contribution from the central source's PSF has to be accounted for. Generally, most coronagraphic observations are limited by the central source's PSF wings. The APT Exposure Time Calculator includes a coronagraphic mode for estimating exposure times. We will now demonstrate how exposure times for coronagraphic observations can be determined using the web-based version of the ACS Exposure Time Calculator. The following steps are required:

- Determine which occulting mask to use
- Calculate the count rate for the target
- Calculate the count rate for the central source
- Calculate the background contribution from the surface brightness of the central source's PSF wings at the location of the target.
- Verify that background+target does not saturate at this location in exposure time  $t_{\text{exp}}$  (or use exposure times of increasing length)
- Calculate the signal-to-noise ratio  $\Sigma$ , given by:

$$\Sigma = \frac{Ct}{\sqrt{Ct + N_{\text{pix}}(B_{\text{sky}} + B_{\text{det}} + B_{\text{PSF}})t + N_{\text{pix}}N_{\text{read}}R^2}}$$

Where:

- $C$  = the signal from the astronomical target in electrons  $\text{sec}^{-1}$  from the CCD.
- $N_{\text{pix}}$  = the total number of detector pixels integrated over to achieve  $C$ .
- $B_{\text{sky}}$  = the sky background in counts  $\text{sec}^{-1} \text{ pixel}^{-1}$ .
- $B_{\text{det}}$  = the detector dark current in counts  $\text{sec}^{-1} \text{ pixel}^{-1}$ .
- $B_{\text{PSF}}$  = the background in counts  $\text{sec}^{-1} \text{ pixel}^{-1}$  from the wings of the central source's PSF at the same distance from the central source as the target.

- $N_{\text{read}}$  = the number of CCD readouts.
- $t$  = the integration time in seconds.
- $R$  is the readout noise of the HRC CCD =  $4.7e^-$ .

In order to illustrate a calculation we shall consider the case where we are trying to determine the S/N achieved in detecting a M6V star with a V magnitude of 20.5 at a distance of 4.25 arcsec from a F0V star with a V magnitude of 6, for an exposure time of 1000 seconds with the F435W filter. Using the ACS Exposure Time Calculator and considering the case for the 3.0" occulting mask:

- Target count rate =  $5.9 e^-/\text{sec}$  for a  $5 \times 5$  aperture (including 47.5% throughput of coronagraph)  
Sky count rate =  $0.003 e^-/\text{sec/pixel}$   
Detector dark rate =  $0.0036 e^-/\text{sec/pixel}$
- Central star count rate =  $3.3 \times 10^7 e^-/\text{sec}$  for a  $101 \times 101$  aperture ( $101 \times 101$  aperture used to estimate total integrated flux)
- At a distance 4.25 arcsec from the central star, from Figure 5.8, the fraction of flux per  $0.026'' \times 0.026''$  pixel in the PSF wings is  $5 \times 10^{-9}$ .  
 $B_{\text{PSF}} = 3.3 \times 10^7 * 5 \times 10^{-9} = 0.165 e^-/\text{sec/pixel}$
- Using the equation above we find the signal to noise for a 1000 sec exposure is 57. Note that a M6V star with a V magnitude of 20.5 observed with the HRC in isolation would yield a S/N of 129.

### Observing sequence for point source companions

The best way to detect faint stellar or substellar companions is to use roll subtraction to avoid color differences between the target and reference PSFs. This also provides duplicate observations that make it easier to verify true companions from noise. It is best to roll the telescope between visits and repeat the image sequence in a new orbit. This way, you can better match the breathing cycle of the telescope than if you rolled the telescope in the middle of an orbital visibility window. You can force this to happen by selecting both orientation and time-sequencing constraints in the visit special requirements. Remember that the coronagraphic field PSF is somewhat broader than the normal HRC PSF, which may influence your assumed signal-to-noise ratio. Off-spot PSF models can be generated with the Tiny Tim PSF software. You can estimate the residual background noise level using Figure 5.13.

Suggested point-source companion observing sequence:

1. Obtain an acquisition image
2. Execute image sequence.
3. Request telescope roll offset (use **ORIENT  $\theta_1$  TO  $\theta_2$  FROM  $n$**  special requirement in visit).
4. Obtain another acquisition.
5. Repeat image sequence.
6. Repeat 3-5 as necessary.

### **Observing sequence for extended sources (e.g. circumstellar disks and AGN host galaxies)**

When imaging extended objects, the remaining scattered light must be subtracted using a reference star image, which should match the color of your target as closely as possible. To reduce the impact of noise in the subtracted images, it helps if the reference PSF is bright enough to provide higher signal-to-noise ratios in the wings, than that of the target source. If possible, select a reference star that is nearby ( $<20^\circ$ ) and request that it be observed immediately before or after the target source. This reduces the chance that there will be large focus differences between the two visits. In order to better discriminate between subtraction artifacts and real structure, it may also help to obtain images of the target at two or more orientations of the telescope (there is no need to get reference PSF images at different rolls). You can estimate the residual background noise level using Figure 5.13.

Suggested extended source observing sequence:

1. Obtain direct images of the science target in each filter to derive normalization factors
2. Obtain an acquisition image of the science target.
3. Take image sequence of science target.
4. Request a new telescope orientation.
5. Repeat steps 2-3.
6. In a new visit immediately after the science observation, point at the reference star.
7. Obtain an acquisition image of reference star.
8. Take image sequence of reference star.
9. Obtain direct images of the reference star in each filter to derive normalization factors.

Note that the order of the observations places direct imaging before or after coronagraphic imaging. This reduces cycling of the coronagraphic

mechanism. Because the occulting spots are large, you may wish to image closer to the source using additional direct observations without the coronagraph. Multiple roll angles are necessary in this case because portions of the inner region will be affected by saturated columns and diffraction spikes. Direct observations of the reference star will be required as well to subtract both the diffracted and scattered light. Color and focus mismatches between the target and reference PSFs will be even more important in the direct imaging mode than with the coronagraph because the diffracted light is not suppressed. However, there are no mismatches caused by star-spot alignment to worry about.

### 5.2.9 Choice of Filters for Coronagraphic Observations

All of the HRC filters are available for coronagraphic observations. However, there are only a few that have been used in the past in this mode, and can be considered well-characterized. These are F435W, F475W, F606W, and F814W. The first three have produced good results and can be considered “safe” choices.

Filter F814W has been problematic, however. Because the PSF is larger at red wavelengths than blue, less of the light from the central star is blocked by the occulting spot. This makes the residual PSF more sensitive to spot shifts and misalignments of the star behind the spot. Mismatches between target and reference PSF star-to-spot alignments may cause significant subtraction residuals. Also, F814W images suffer from the red halo, which still affects coronagraphic observations because the central spot is filled with light that will be scattered to large radii. Color differences between the target and reference PSF stars will thus cause differences in the halo pattern, altering the local background level in unpredictable ways. If multicolor images are needed, it may be safer to choose F435W and F606W rather than F606W and F814W, for instance. Of course, for red objects it may not be feasible to choose a blue filter due to low flux levels, in which case F814W must be used.

---

## 5.3 Grism/Prism Spectroscopy

The ACS filter wheels include four dispersing elements for low resolution slitless spectrometry over the field of view of the three ACS channels. One grism (G800L) provides low resolution spectra over the 5500-11,000Å range for both the WFC and HRC; a prism (PR200L) in the HRC covers the range 1600 to beyond 3900Å; in the SBC a LiF prism covers the wavelength range 1150 to ~1800Å (PR110L) and a CaF<sub>2</sub> prism is useful over the 1250 to ~1800Å range (PR130L). Table 5.3 summarizes the essential features of the four ACS dispersers in the five available modes.

The grism provides first order spectra with dispersion almost linear with wavelength but with second order overlap beyond about 10,000Å; the prisms however have non-linear dispersion with maximum resolution at shorter wavelengths but much lower resolution at longer wavelengths. The two-pixel resolution is listed for each grism or prism at a selected wavelength in Table 5.3. The pixel scale for the prism spectra is given at the selected wavelength. The tilt of the spectra to the detector X axis (close to the spacecraft V2 axis) is also listed.

Table 5.3: Optical Parameters of ACS Dispersers

Disperser	Channel	Wavelength range (Å)	Resolution	Å/pixel	Tilt <sup>1</sup> (deg)
G800L	WFC	1st order: 5500-11000	100@8000Å	39.8 <sup>2</sup>	-2
G800L	WFC	2nd order: 5000-9500	200@8000Å	20.7 <sup>2</sup>	-2
G800L	HRC	1st order: 5500-11000	140@8000Å	23.9 <sup>3</sup>	-38
G800L	HRC	2nd order: 5500-9500	280@8000Å	12.0 <sup>3</sup>	-38
PR200L	HRC	1600-3900	59@2500Å	21.3	-1
PR110L	SBC	1150-1800	79@1500Å	9.5	0
PR130L	SBC	1250-1800	96@1500Å	7.8	0

1. Tilt with respect to the positive X-axis of the data frame.

2. The dispersion varies over the field by +/- 11%; the tabulated value refers to the field center.

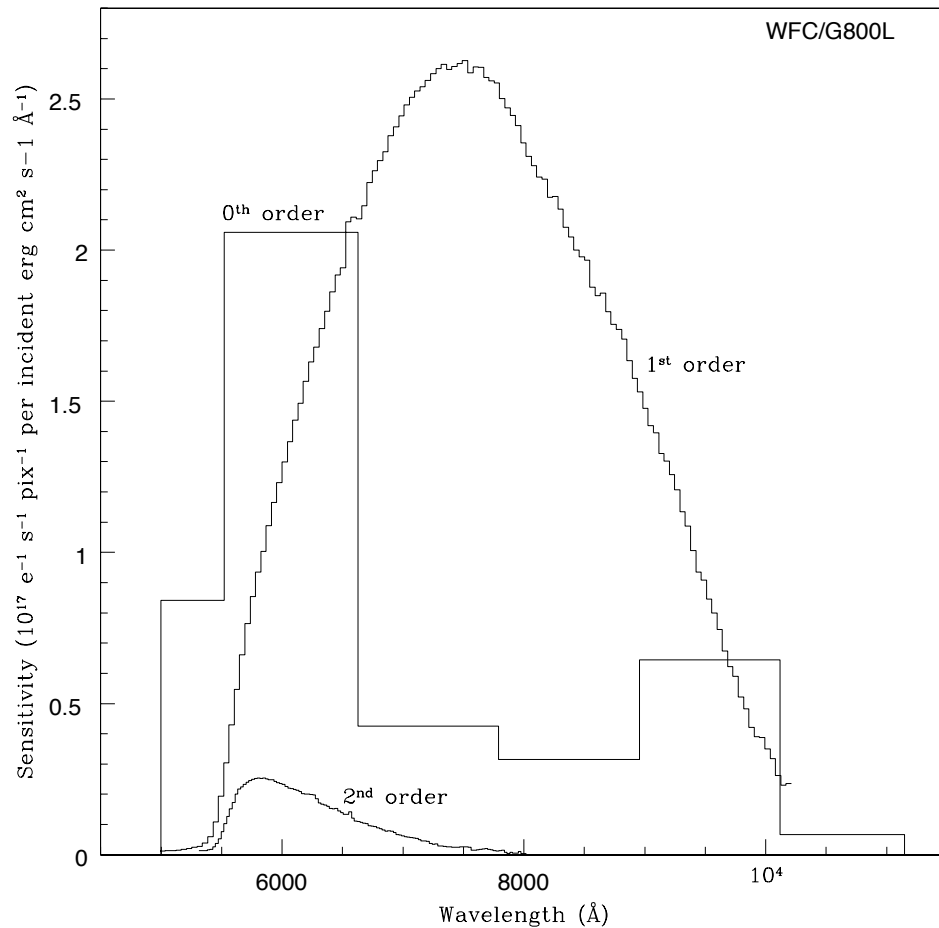
3. The dispersion varies over the field by +/- 2%; the tabulated value refers to the field center.

### 5.3.1 WFC G800L

The G800L grism and the WFC provide two-pixel resolution from 69 (at 5500Å) to 138 (at 11,000Å) for first order spectra over the whole accessible field of 202x202". Table 5.3 lists the linear dispersion, but a second order dispersion solution provides a better fit. Figure 5.15 shows the wavelength extent and sensitivity for the zeroth, first, and second order spectra when used with the WFC; Figure 5.16 shows the same plot in pixel extent. The 0 position refers to the position of the direct image and the pixel size is 0.05". Note that there is contamination of the 1st order spectrum above 10,000Å by the second order. The total power in the zeroth order is 2.5% of that in the first order, so locating the zeroth order may not

be an effective method of measuring the wavelengths of weak spectra. The default method will be to obtain a matched direct image-grism pair. There is also sensitivity of about a percent of first order in the third and fourth orders and about half a percent in the negative orders. The full extent the spectrum of a bright source (orders -2, -1, 0, 1, 2 and 3) covers is 1200 pix (60"). Figure 5.17 shows the full spectrum extent for a 60s exposure of the white dwarf GD153 ( $V=13.35$ ) with the individual orders indicated. When observing bright objects, the signal in fainter orders may be mistaken for separate spectra of faint sources and in crowded fields many orders from different objects can overlap. The wavelength solution is field dependent on account of the tilt of the grism to the optical axis and the linear dispersion varies by  $\pm 11\%$  from center to corner. This field dependence has been calibrated to allow wavelength determination to better than 0.5 pixels over the whole field.

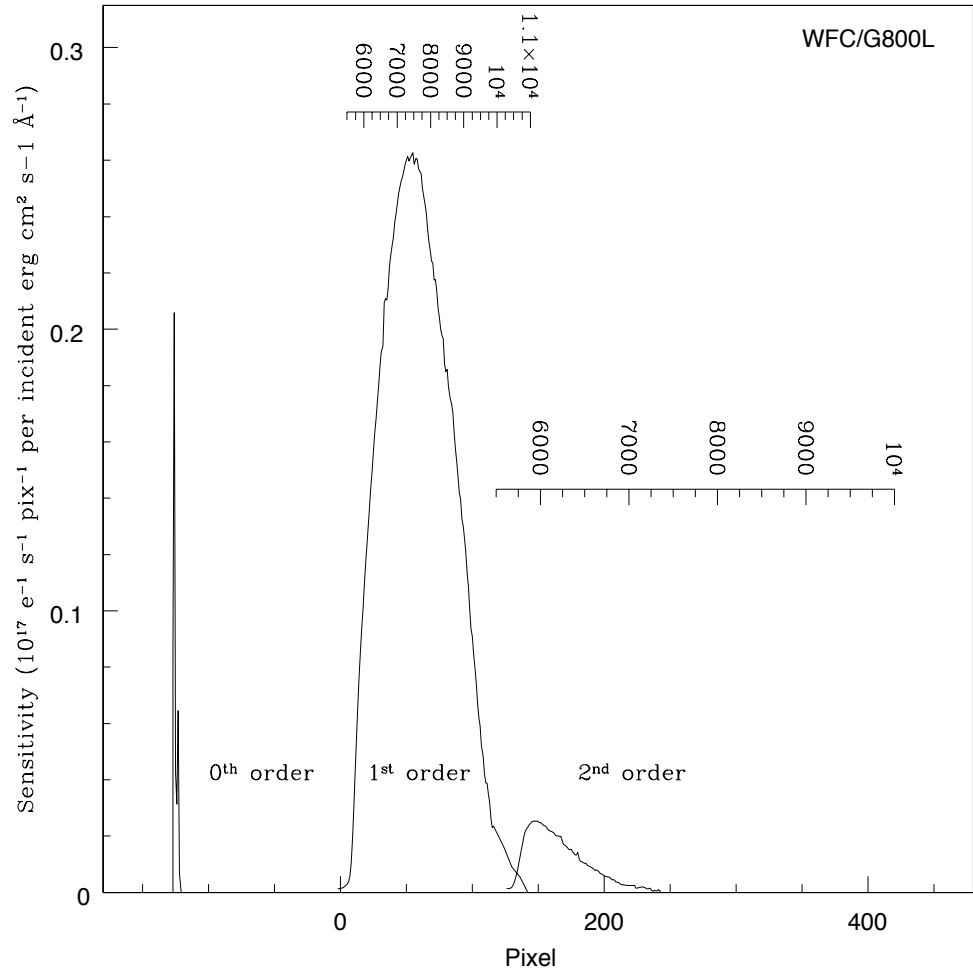
Figure 5.15: Sensitivity versus wavelength for WFC G800L



### 5.3.2 HRC G800L

When used with the HRC, the G800L grism provides higher spatial resolution ( $0.028''$ ) pixels than the WFC and also higher spectral resolution. However, the spectra are tilted at  $-38$  degrees to the detector X axis. Figure 5.18 shows the wavelength extent and sensitivity in the zero, first and second orders, with the pixel extent shown in Figure 5.19. Figure 5.20 shows the observed spectrum of the standard star GD153. Again there is contamination of the first order spectrum by the second order beyond  $9500\text{\AA}$ . The total extent of the spectrum (orders -1 and +2) in Figure 5.20 covers about 70% of the 1024 detector pixels. In addition, a much greater number of spectra will be formed by objects situated outside the HRC direct image, or will have their spectra truncated by the chip edges, than for the WFC. The variation of the grism dispersion over the HRC field is about  $\pm 2\%$  from center to corner and has been calibrated.

Figure 5.16: Sensitivity versus pixel position for WFC G800L



### 5.3.3 HRC PR200L

The maximum pixel resolution of the prism is  $5.3\text{\AA}$  at  $1800\text{\AA}$ . At  $3500\text{\AA}$ , the dispersion drops to  $91\text{\AA}/\text{pix}$  and is  $515\text{\AA}/\text{pix}$  at  $5000\text{\AA}$ . The result is a bunching up of the spectrum to long wavelengths with about 8 pixels spanning  $1500\text{\AA}$ . For bright objects, this effect can lead to blooming of the HRC CCD from filled wells; the overfilled pixels bleed in the detector Y direction, and would thus affect other spectra. Figure 5.21 shows the sensitivity versus wavelength for PR200L and the wavelength extent of the pixels is indicated. The variation of the dispersion across the detector for PR200L amounts to about  $\pm 3\%$ . The angle of the prism causes a large deviation between the position of the direct object and the region of the dispersed spectrum. The pixel numbers on Figure 5.21 indicate the size of the offset from the direct image. On account of the size of this offset, special apertures have been defined in the observation scheduling system so that the spectrum of the target centered on the direct image occurs near the center of the field in the prism image.

Figure 5.17: Full Dispersed Spectrum for White Dwarf GD153 with WFC/G800L. The numbers indicate the different grism orders.

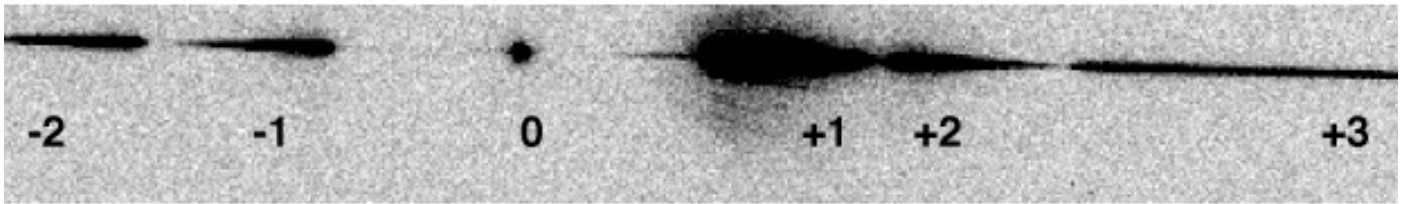
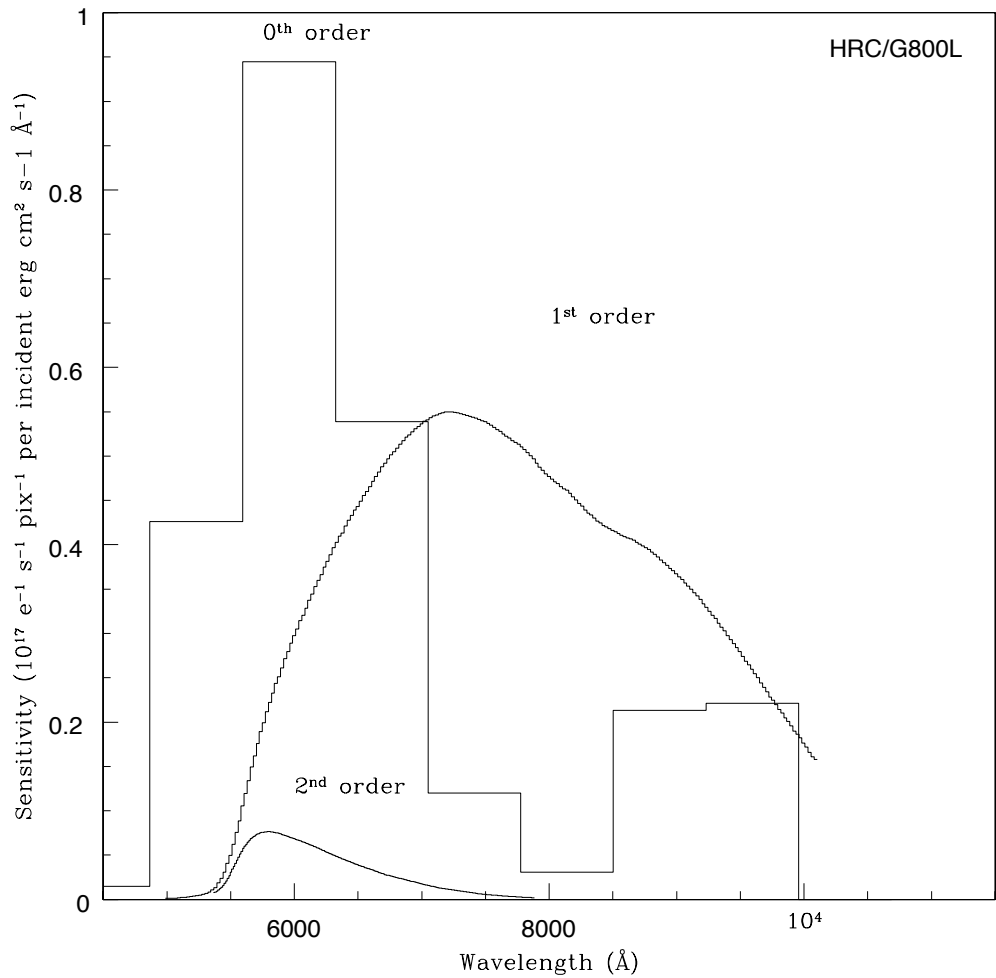


Figure 5.18: Sensitivity versus wavelength for HRC G800L



### 5.3.4 SBC PR110L

The PR110L prism is sensitive to below  $1200\text{\AA}$  and includes the geo-coronal Lyman-alpha line, so it is subject to high background. The dispersion at Lyman-alpha is  $2.6\text{\AA}$  per pixel. Figure 5.22 shows the sensitivity with wavelength and the wavelength width of the pixels. The long wavelength cut-off of the CsI MAMA detector at  $\sim 1800\text{\AA}$  occurs before the long wavelength build-up of flux; the dispersion at  $1800\text{\AA}$  is  $21.6\text{\AA}/\text{pixel}$ . However the detected counts at the long wavelength edge must be within the MAMA Bright Object Protection Limits (see Section 7.5). These limits must include the contribution of the geo-coronal Lyman-alpha flux per SBC pixel. The numbers in Figure 5.22 show the offset of the spectrum from the direct image.

### 5.3.5 SBC PR130L

The short wavelength cut-off of the PR130L prism at  $1250\text{\AA}$  excludes the geocoronal Lyman-alpha line, making it the disperser of choice for faint object detection in the  $1250\text{-}1800\text{\AA}$  window. The dispersion varies from  $1.65\text{\AA}$  at  $1250\text{\AA}$  to  $20.2\text{\AA}$  at  $1800\text{\AA}$ . Figure 5.23 shows the sensitivity versus wavelength and the pixel widths in angstroms. Bright Object Protection (BOP) considerations similar to the case of PR110L also apply to the use of this prism, except that the background count rate is lower (see Section 7.5).

Figure 5.19: Sensitivity versus pixel position for HRC G800L

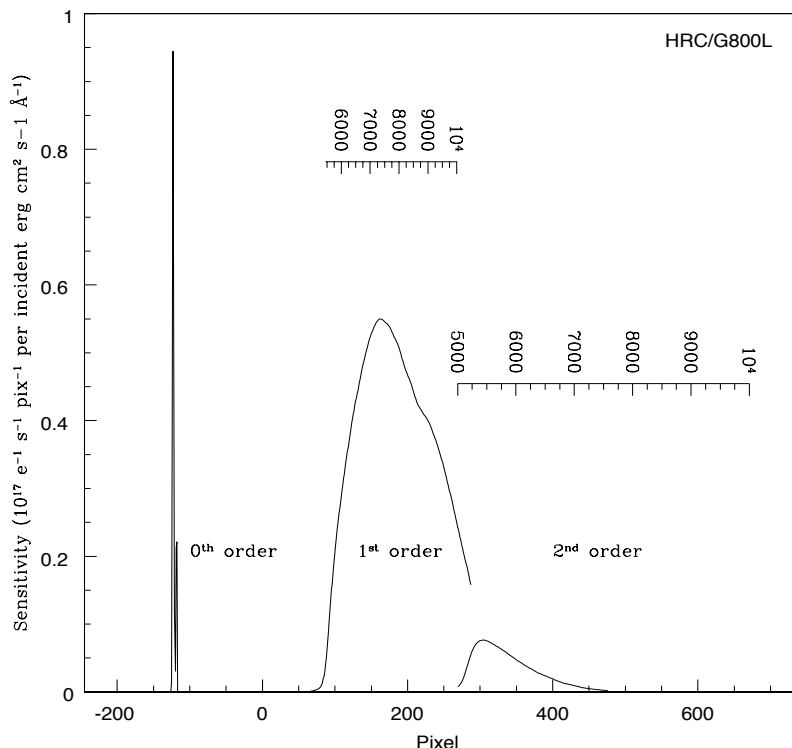
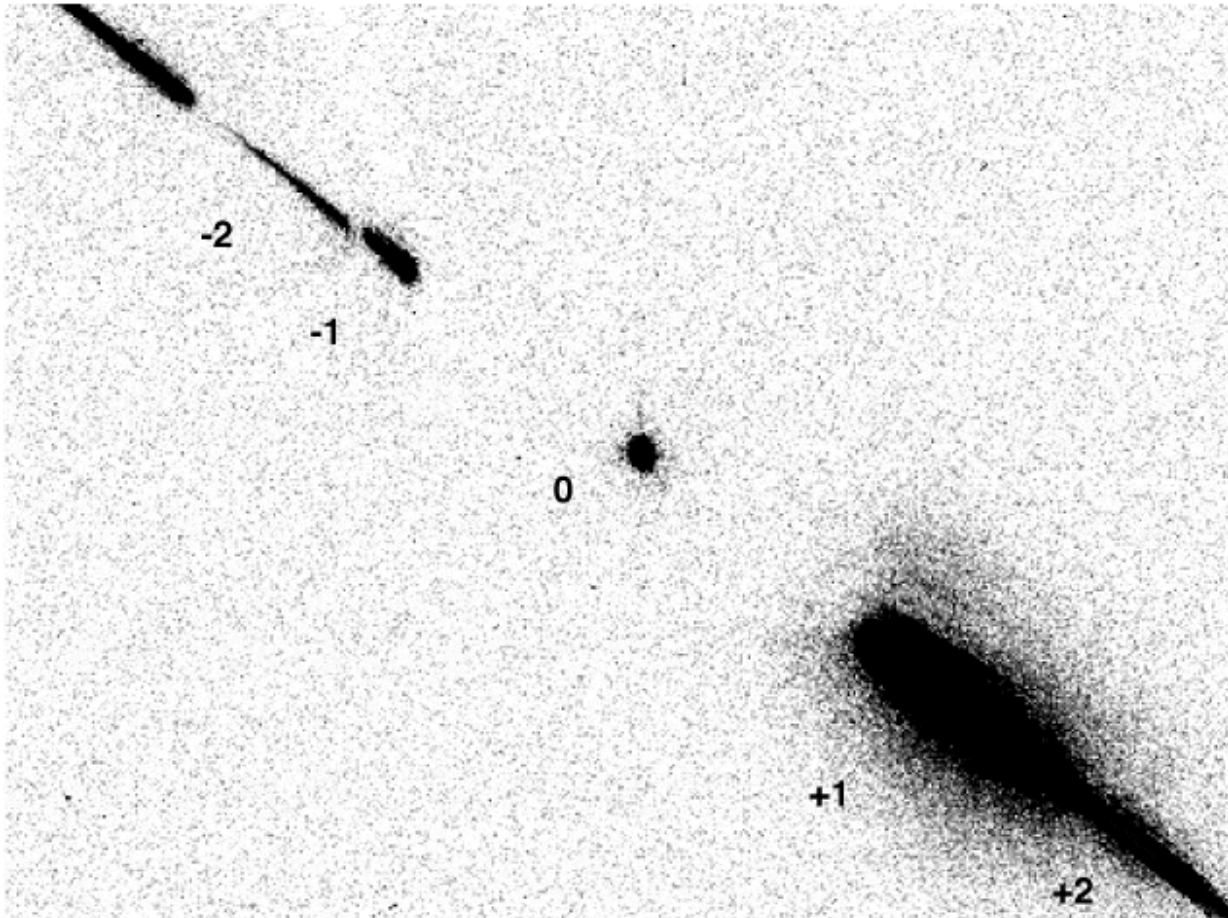


Figure 5.20: Full Dispersed Spectrum of White Dwarf GD153 with HRC/G800L. The numbers indicate the different grism orders.

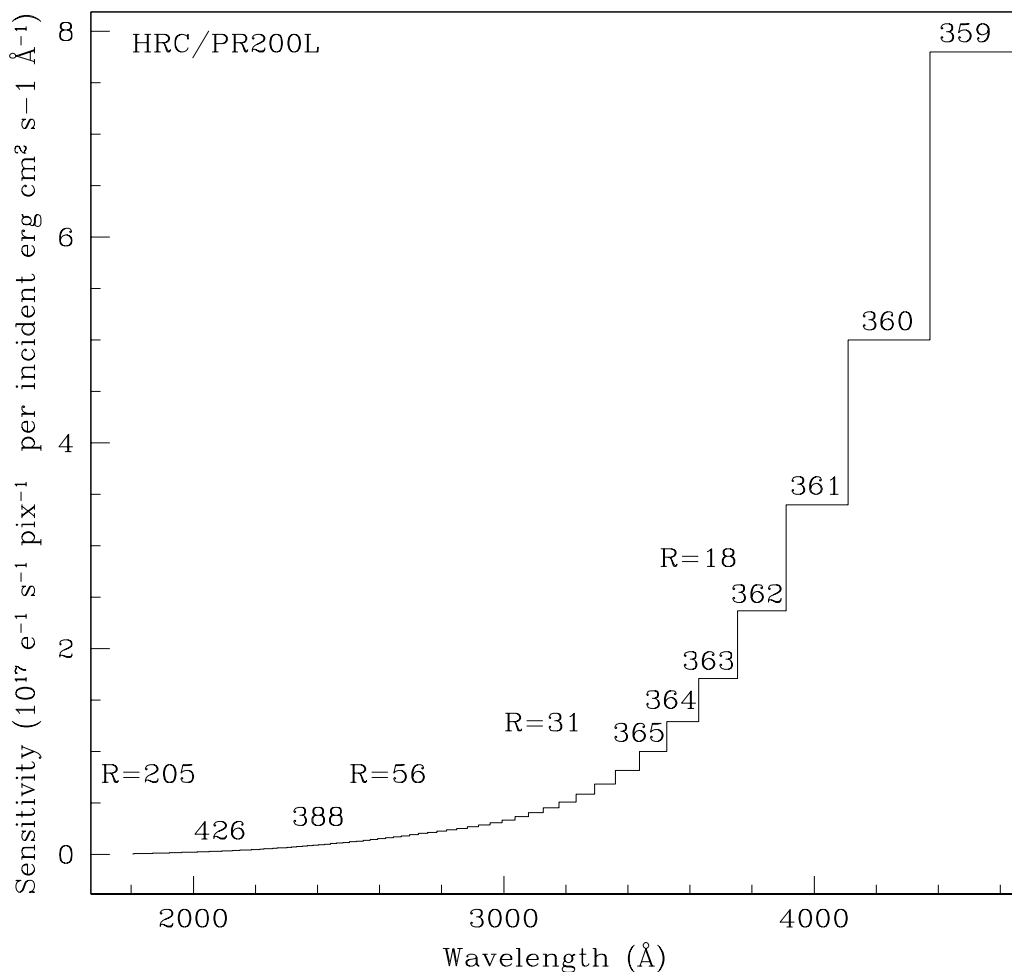


### 5.3.6 Observation Strategy

The default observing mode for all ACS WFC grism and HRC grism and prism modes is to obtain a direct image of the field followed by a dispersed grism/prism image. This combination will then allow the wavelength calibration of the individual target spectra by reference to the corresponding target on the direct image. The direct image will be added by default to the dispersed image by the scheduling system (AUTOIMAGE=YES). For the WFC and HRC G800L spectra, an F606W exposure will be employed and, for the HRC PR200L prism an F330W image will be applied. The companion direct image can be switched off by AUTOIMAGE=NO, allowing, for example, a separate direct image in a different filter to be specified if desired. For the SBC, the default mode will be to obtain spectra without an accompanying direct image on account of the need for Bright Object Protection (BOP), see Section 7.5. The user can separately specify a direct image to accompany the prism image, which

should be scheduled immediately before or after the prism image in the same orbit. The direct image must also of course pass the BOP check.

Figure 5.21: Sensitivity versus wavelength for HRC/PR200L, numbers in figure show offset in pixels from direct image.



All exposures with the SBC prisms must fall within the Bright Object Protection limits. In the case of spectra, the most important determination is that the flux at the longest wavelength must not exceed 50 counts/s/pix. Table 5.4 lists for the PR110L and PR130L prisms, the observed magnitudes of stars of various spectral types whose spectra are expected to just exceed this BOP limit.

Table 5.4: BOP limits for SBC Prism spectra

Spectral Type	PR110L	PR130L
O5V	15.8	15.6
A1V	11.0	10.9
G2V	2.9	2.9

Figure 5.22: Sensitivity versus wavelength for SBC PR110L, numbers in figure show offset from direct image.

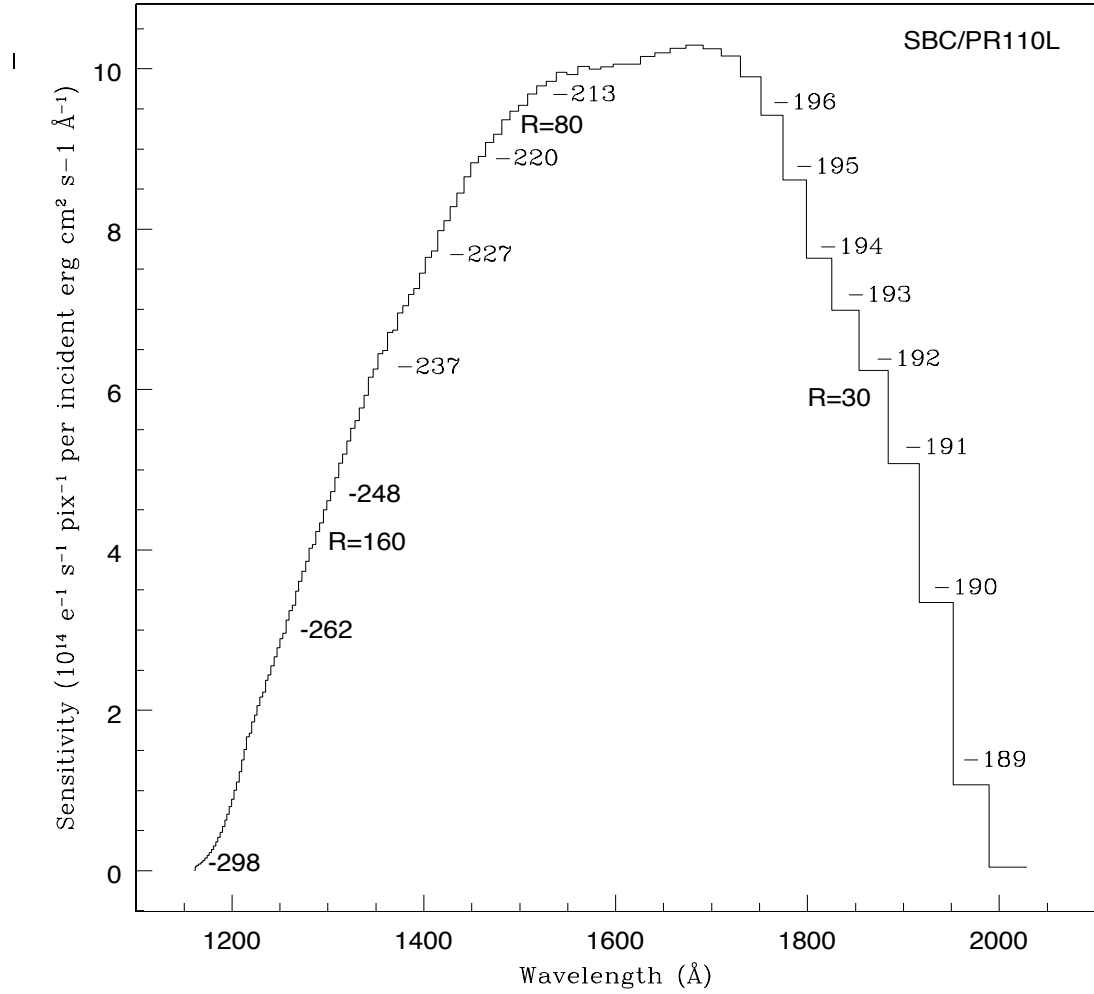


Table 5.5 lists the V detection limits for the ACS grism/prism modes for various spectral types without reddening. An exposure time of 1 hour was assumed with LOW Zodiacal background and a signal-to-noise of 5 per resolution element. For the WFC and HRC exposures, a CR-SPLIT of two was used and GAIN=1.

Table 5.5: V detection limits for the ACS Grism/Prism modes

Mode	V limit for a given spectral type			Wavelength of reference (Å)
	O5V	A1V	K4V	
WFC/G800L	24.4	24.6	25.5	7000
HRC/G800L	23.6	23.8	24.6	7000
HRC/PR200L	26.0	23.7	19.5	3000
SBC/PR110L	23.8	19.6	1.9	1700
SBC/PR130L	24.6	20.4	2.6	1700

Figure 5.15 through Figure 5.23 can be used to compute the detected count rate in the various orders of the grisms and prisms given the flux of the source spectra. Chapter 6 provides details of the calculations. Depending on the wavelength region, the background must also be taken into account in computing the signal-to-noise ratio. The background at each pixel consists of the sum of all the dispersed light in all the orders from the background source. For complex fields, the background consists of the dispersed spectrum of the unresolved sources; for crowded fields, overlap in the spectral direction and confusion in the direction perpendicular to the dispersion may limit the utility of the spectra.

The ACS Exposure Time Calculator supports all the available spectroscopic modes of the ACS and is available for more extensive calculations at [http://apt.stsci.edu/webetc/acs/acs\\_spec\\_etc.jsp](http://apt.stsci.edu/webetc/acs/acs_spec_etc.jsp). The current version employs the on-orbit determinations of the dispersion solution and sensitivity determination where available.

For more detailed simulations of ACS spectra, an image-spectral simulator, called **SLIM**, is available. This tool allows synthetic target fields to be constructed and dispersed images from spectrum templates to be formed. **SLIM** can simulate spectra for all the ACS spectral modes. The simulator runs under Python and an executable version is available at: <http://www.stecf.org/software/SLIM/SLIM10/index.html>. Version 1.0 uses a Gaussian PSF but this has been found to be an adequate representation to the **Tiny Tim** model of the ACS PSF. A detailed description of the tool and examples of its use are given by Pirzkal et al. (ACS ISR 01-03).

### 5.3.7 Extraction and Calibration of Spectra

Since there is no slit in the ACS, the Point Spread Function of the target modulates the spectral resolution. In the case of extended sources it is the extension of the target in the direction of dispersion which sets the achievable resolution. Simulations show that for elliptical sources, the

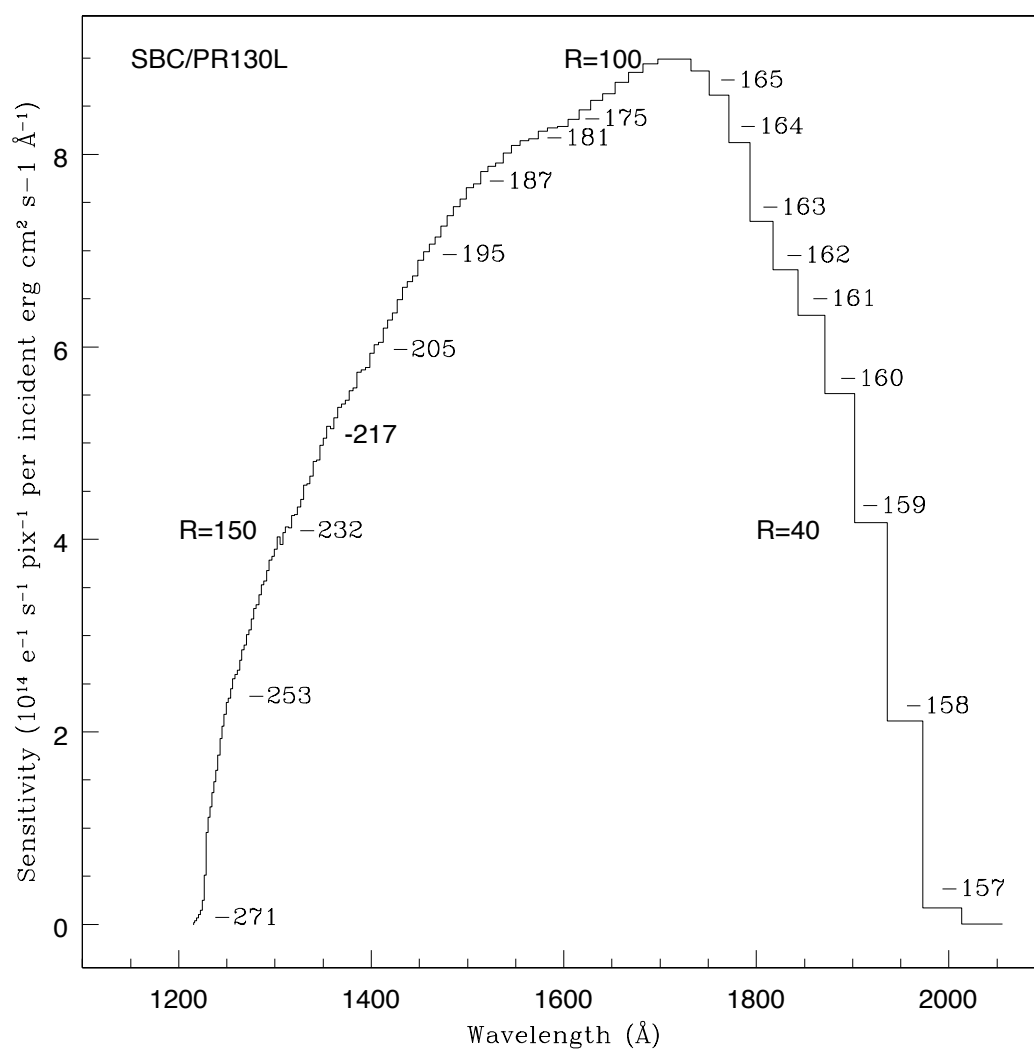
spectral resolution depends on the orientation of the long axis of the target to the dispersion direction and is described in more detail in Pasquali et al. (2001) <http://www.stsci.edu/hst/acs/documents/isrs/isr0102.pdf>. The dispersion of the gratings and prisms is well characterized, but for the wavelength zero point it is important to know the position of the target in the direct image. For the gratings, the zeroth order will generally be too weak to reliably set the wavelength zero point. Given the typical spacecraft jitter, wavelength zero points to  $\pm 0.4$  pixels should be routinely achievable using the direct image taken just before or after the slitless spectrum image. Some improvement is possible in zero point assignment if the HST jitter files are employed to determine exactly the offsets between the direct and grism images.

The jitter information can be used to obtain more accurate coordinates for the center of the FOV. These in turn allow one to determine better relative offsets between the direct and the spectroscopic images.

The wavelength extent of each pixel for the WFC and HRC G800L modes in the red is small enough that fringing modulates the spectra. For the HRC, the peak-to-peak fringe amplitude is about 30% at 9500Å, similar to STIS, and is about 25% for the WFC chips. In practice, when observing point sources, and even more so when observing extended objects, the amount of detectable fringing is significantly reduced by the smoothing effect that the PSF together with the intrinsic object size have on the spectrum in the dispersion direction. Moreover, application of an optical model for the CCD fringing can allow the fringe amplitude per pixel to be reduced to below 4% peak-to-peak.

An extraction software package, **aXe**, is available to extract, wavelength calibrate, flat field and flux calibrate ACS grism and prism spectra. Full details can be found at: <http://www.stecf.org/software/aXe/>. The package is also available in STSDAS.

Figure 5.23: Sensitivity versus wavelength for SBC/PR130L



# Exposure-Time Calculations

In this chapter. . .

6.1 Overview / 101
6.2 Determining Count Rates from Sensitivities / 102
6.3 Computing Exposure Times / 108
6.4 Detector and Sky Backgrounds / 111
6.5 Extinction Correction / 117
6.6 Exposure-Time Examples / 118
6.7 Tabular Sky Backgrounds / 122

---

## 6.1 Overview

In this chapter, we explain how to use sensitivities and throughputs to determine the expected count rate from your source and how to calculate exposure times to achieve a given signal-to-noise ratio for your ACS observations taking various background contributions into account. At the end of this chapter in “Exposure-Time Examples”, you will find examples to guide you through specific cases.

### 6.1.1 The ACS Exposure Time Calculator

The ACS Exposure-Time Calculator (ETC) is available to help with proposal preparation at:

[http://www.stsci.edu/hst/acs/software/etcs/ETC\\_page.html](http://www.stsci.edu/hst/acs/software/etcs/ETC_page.html).

This ETC calculates count rates for given source and background parameters, and signal-to-noise ratios for a given exposure time, or count

rates and exposure time for a given signal-to-noise ratio for imaging, spectroscopic and coronagraphic observations. A variety of apertures are now available, both circular and square, allowing the user to either select a radius in arcseconds or a size in pixels. The current default are a 0.2 arcsec radius for both the WFC and the HRC and a 0.5 arcsec radius for SBC observations, which enclose approximately 80% of the PSF flux. Square and circular apertures are available between 0.1 and 2.0 arcsec. For extended sources the S/N calculation is based on counts summed over one resolution element of 2x2 pixels, as the source size is assumed to be larger than the ACS resolution. A calibrated spectrum of your source can be provided directly to the Exposure-Time Calculator. The ETC also determines peak per-pixel count rates and total count rates to aid in feasibility assessment. Warnings appear if the source exceeds the local or global brightness limits for SBC observations (see Section 7.5). The ETC has online help for its execution and interpretation of results. Alternatively, users can use **synphot** to calculate count rates and the wavelength distribution of detected counts.

---

## 6.2 Determining Count Rates from Sensitivities

In this Chapter, specific formulae appropriate for imaging and spectroscopic modes are provided to calculate the expected count rates and the signal-to-noise ratio from the flux distribution of a source. The formulae are given in terms of sensitivities, but we also provide transformation equations between the throughput ( $QT$ ) and sensitivity ( $S$ ) for imaging and spectroscopic modes.

Throughputs are presented in graphical form as a function of wavelength for the prisms and for the imaging modes in Chapter 10. Given your source characteristics and the sensitivity of the ACS configuration, calculating the expected count rate over a given number of pixels is straightforward, since the ACS PSF is well characterized. The additional required information is the encircled energy fraction ( $\epsilon_f$ ) in the peak pixel, the plate scale, and the dispersions of the gratings and prisms. This information is summarized in Tables 6.1 to 6.3.

Table 6.1: Useful Quantities for the ACS WFC

Filter	Pivot $\lambda$ (Å)	$\int Q_{\lambda} T_{\lambda} d\lambda/\lambda$	AB mag zero point	$\int S_{\lambda} d\lambda$	encircled energy	Flux in central pixel	Background sky rate
F435W	4317.4	0.0744	25.67	3.18E18	0.85	0.22	0.0284
F475W	4744.3	0.1070	26.07	5.53E18	0.86	0.21	0.0609
F502N	5023.0	0.0032	22.27	1.88E17	0.86	0.21	0.0020
F550M	5581.2	0.0362	24.89	2.59E18	0.85	0.22	0.0280
F555W	5359.6	0.0775	25.72	5.11E18	0.86	0.21	0.0545
F606W	5917.7	0.1573	26.49	1.26E19	0.85	0.22	0.1358
F625W	6310.5	0.0915	25.90	8.37E18	0.85	0.22	0.0825
F658N	6583.9	0.0050	22.75	5.00E17	0.85	0.22	0.0045
F660N	6599.4	0.0019	21.67	1.87E17	0.85	0.22	0.0017
F775W	7693.0	0.0731	25.65	9.93E18	0.85	0.20	0.0780
F814W	8059.8	0.0948	25.94	1.41E19	0.83	0.19	0.1044
F850LP	9054.8	0.0352	24.86	6.63E18	0.73	0.14	0.0415
F892N	8914.9	0.0036	22.37	6.48E17	0.77	0.15	0.0039
G800L	7480.7	0.1591	26.50	2.04E19	0.86	0.17	0.1526
CLEAR	6269.8	0.3833	27.45	3.46E19	----	0.10	0.3580

Table 6.2: Useful Quantities for the ACS HRC

Filter	Pivot $\lambda$ (Å)	$\int Q_{\lambda} T_{\lambda} d\lambda/\lambda$	AB mag zero point	$\int S_{\lambda} d\lambda$	encircled energy	Flux in central pixel	Background sky rate
F220W	2255.3	0.0106	23.55	1.23E17	0.79	0.17	0.0001
F250W	2715.8	0.0123	23.72	2.09E17	0.82	0.16	0.0003
F330W	3362.7	0.0172	24.08	4.47E17	0.84	0.16	0.0006
F344N	3433.7	0.0017	21.59	4.67E16	0.84	0.16	0.0001
F435W	4311.0	0.0436	25.09	1.86E18	0.86	0.17	0.0043
F475W	4775.7	0.0650	25.53	3.40E18	0.85	0.17	0.0120
F502N	5022.9	0.0021	21.82	1.24E17	0.85	0.17	0.0003
F550M	5579.8	0.0234	24.42	1.67E18	0.85	0.15	0.0048
F555W	5356.0	0.0503	25.25	3.31E18	0.85	0.16	0.0099
F606W	5888.0	0.0983	25.98	7.82E18	0.85	0.14	0.0238
F625W	6295.5	0.0557	25.36	5.07E18	0.84	0.13	0.0148

Filter	Pivot $\lambda$ (Å)	$\int Q_{\lambda} T_{\lambda} d\lambda/\lambda$	AB mag zero point	$\int S_{\lambda} d\lambda$	encircled energy	Flux in central pixel	Background sky rate
F658N	6583.7	0.0030	22.18	2.98E17	0.83	0.13	0.0008
F660N	6599.1	0.0011	21.11	1.11E17	0.83	0.13	0.0003
F775W	7665.1	0.0380	24.94	5.13E18	0.78	0.11	0.0111
F814W	8115.3	0.0521	25.29	7.88E18	0.76	0.10	0.0161
F850LP	9145.2	0.0228	24.39	4.37E18	0.68	0.08	0.0075
F892N	8916.1	0.0022	21.87	4.09E17	0.73	0.09	0.0007
G800L	7506.4	0.0924	25.91	1.20E19	0.81	0.07	0.0250
PR200L	5650.2	0.2756	27.10	2.02E19	0.80	0.16	0.0624
CLEAR	5472.0	0.3205	27.26	2.20E19	----	0.12	0.0683

Table 6.3: Useful Quantities for the ACS SBC

Filter	Pivot $\lambda$ (Å)	$\int Q_{\lambda} T_{\lambda} d\lambda/\lambda$	AB mag zero point	$\int S_{\lambda} d\lambda$	encircled energy	Flux in central pixel	Background sky rate
F115LP	1406.1	0.0147	23.92	6.70E16	0.83	0.11	0.0238
F122M	1273.8	0.0010	20.95	3.56E15	0.82	0.09	0.0042
F125LP	1437.5	0.0122	23.71	5.80E16	0.83	0.12	0.0027
F140LP	1527.0	0.0069	23.09	3.68E16	0.84	0.13	0.0000
F150LP	1610.7	0.0038	22.45	2.27E16	0.84	0.14	0.0000
F165LP	1757.9	0.0010	21.02	7.29E15	0.85	0.16	0.0000
PR110L	1429.4	0.0120	23.69	5.62E16	0.86	0.26	0.0129
PR130L	1438.8	0.0120	23.68	5.66E16	0.87	0.28	0.0027

In each Table, the following quantities are listed:

- The pivot wavelength, a source-independent measure of the characteristic wavelength of the bandpass, defined such that it is the same if the input spectrum is in units of  $F_{\lambda}$  or  $F_{\nu}$ :

$$\lambda_p = \sqrt{\frac{\int Q(\lambda) T(\lambda) d\lambda}{\int Q(\lambda) T(\lambda) ((d\lambda)/\lambda)}}$$

- The integral  $\int Q_{\lambda} T_{\lambda} d\lambda/\lambda$ , used to determine the count rate when given the astronomical magnitude of the source.

- The ABmag zero point, defined as the AB magnitude of a source with a constant  $F_\nu$  that gives 1 count/sec with the specified configuration.
- The sensitivity integral, defined as the count rate that would be observed from a constant  $F_\lambda$  source with flux  $1 \text{ erg cm}^{-2} \text{ s}^{-1} \text{ \AA}^{-1}$ .
- The encircled energy, defined as the fraction of PSF flux enclosed in the default photometry aperture 0.2" for the WFC and HRC and 0.5" for the SBC. These correspond approximately to 5×5, 9×9 and 15×15 boxsizes respectively.
- The fraction of PSF flux in the central pixel, useful for determining the peak count rate to check for overflow or bright object protection possibilities.
- The sky background count rate, which is the count rate that would be measured with average zodiacal background, and average earthshine. It does not include the contribution from the detectors, tabulated separately in Table 6.5.

Here, we describe how to determine two quantities:

1. The counts  $\text{sec}^{-1}$  ( $C$ ) from your source over some selected area of  $N_{\text{pix}}$  pixels, where a signal of an electron on a CCD is equivalent to one count.
2. The peak counts  $\text{sec}^{-1} \text{ pixel}^{-1}$  ( $P_{cr}$ ) from your source, which is useful for avoiding saturated CCD exposures and for assuring that SBC observations do not exceed the bright-object limits.

We consider the cases of point sources and diffuse sources separately in each of the imaging and spectroscopy sections following.

## 6.2.1 Imaging

### Point Source

For a point source, the count rate,  $C$ , can be expressed as the integral over the bandpass of the filter:

$$C = A \int F_\lambda \frac{\lambda}{hc} Q_\lambda T_\lambda \epsilon_f d\lambda = \int F_\lambda S_\lambda \epsilon_f d\lambda$$

Where:

- $A$  is the area of the unobstructed 2.4 meter telescope (i.e., 45,239  $\text{cm}^2$ )
- $F_\lambda$  is the flux from the astronomical source in  $\text{erg sec}^{-1} \text{ cm}^{-2} \text{ \AA}^{-1}$
- $h$  is Planck's constant
- $c$  is the speed of light

- The factor  $\lambda/hc$  converts ergs to photons.
- $Q_\lambda T_\lambda$  is the system fractional throughput, i.e. the probability of detecting a count per incident photon, including losses due to obstructions of the full 2.4 m OTA aperture. It is specified this way to separate out the instrument sensitivity  $Q_\lambda$  and the filter transmission  $T_\lambda$ .
- $\epsilon_f$  = the fraction of the point source energy encircled within  $N_{pix}$  pixels.
- $S_\lambda$  is the total imaging point source sensitivity with units of counts  $\text{sec}^{-1} \text{\AA}^{-1}$  per incident  $\text{erg sec}^{-1} \text{cm}^{-2} \text{\AA}^{-1}$ .

The peak counts  $\text{sec}^{-1} \text{pixel}^{-1}$  from the point source, is given by:

$$C_{peak} = \int F_\lambda S_\lambda \epsilon_f(1) d\lambda$$

Where:

- $F_\lambda$ , and  $S_\lambda$  are as above.
- $\epsilon_f(1)$  is the fraction of energy encircled within the peak pixel.

Again, the integral is over the bandpass.

If the flux from your source can be approximated by a flat continuum ( $F_\lambda = \text{constant}$ ) and  $\epsilon_f$  is roughly constant over the bandpass, then:

$$C = F_\lambda \epsilon_f \int S_\lambda d\lambda$$

We can now define an equivalent bandpass of the filter ( $B_\lambda$ ) such that:

$$\int S_\lambda d\lambda = S_{peak} B_\lambda$$

Where:

- $S_{peak}$  is the peak sensitivity.
- $B_\lambda$  is the effective bandpass of the filter.

The count rate from the source can now be written as:

$$C = F_\lambda \epsilon_f S_{peak} B_\lambda$$

In Tables 6.1–6.3, we give the value of  $\int S_\lambda d\lambda$  for each of the filters. Alternatively, we can write the equation in terms of V magnitudes:

$$C = 2.5 \times 10^{11} \epsilon_f \left( \int Q T d\lambda / \lambda \right) \times 10^{-0.4(V + AB_v)}$$

where V is the visual magnitude of the source, the quantity under the integral sign is the mean sensitivity of the detector+filter combination and is tabulated in Tables 6.1–6.3, and  $AB_v$  is the filter-dependent correction for the deviation of the source spectrum from a constant  $F_v$  spectrum. This

latter quantity is tabulated for several different astronomical spectra in Tables 10.1 to 10.3 in Chapter 10.

### Diffuse Source

For a diffuse source, the count rate,  $C$ , per pixel, due to the astronomical source can be expressed as:

$$C = \int I_{\lambda} S_{\lambda} m_x m_y d\lambda$$

Where:

- $I_{\lambda}$  = the surface brightness of the astronomical source, in  $\text{erg sec}^{-1} \text{cm}^{-2} \text{\AA}^{-1} \text{arcsec}^{-2}$ .
- $S_{\lambda}$  as above.
- $m_x$  and  $m_y$  are the plate scales along orthogonal axes.

### Emission Line Source

For a source where the flux is dominated by a single emission line, the count rate can be calculated from the equation

$$C = 2.23 \times 10^{12} \cdot (QT)_{\lambda} \cdot F(\lambda) \cdot \lambda$$

where  $C$  is the observed count rate in counts/sec,  $(QT)$  is the system throughput at the wavelength of the emission line,  $F(\lambda)$  is the emission line flux in units of  $\text{erg cm}^{-2} \text{s}^{-1}$ , and  $\lambda$  is the wavelength of the emission line in Angstroms.  $(QT)_{\lambda}$  can be determined by inspection of the plots in Chapter 10. See Section 6.6.4 for an example of emission-line imaging using ACS.

## 6.2.2 Spectroscopy

### Point Source

For a point source spectrum with a **continuum flux distribution**, the count rate,  $C$ , is per pixel in the dispersion direction and is integrated over a fixed extraction height  $N_{spix}$  in the spatial direction perpendicular to the dispersion:

$$C = F_{\lambda} S'_{\lambda} \epsilon'_{Nspix} = F_{\lambda} A \frac{\lambda}{hc} T_{\lambda} \epsilon'_{Nspix} d$$

Where:

- $S'_{\lambda}$  is the total point source sensitivity in units of  $\text{counts sec}^{-1}$  per incident  $\text{erg sec}^{-1} \text{cm}^{-2} \text{\AA}^{-1}$ ; and  $S_{\lambda} = S'_{\lambda} \cdot d$
- $d$  is the dispersion in  $\text{\AA}/\text{pix}$ .

- $\epsilon'_{N_{spix}}$  is the fraction of the point source energy within  $N_{spix}$  in the spatial direction.
- the other quantities are defined above.

For an **unresolved emission line** at  $\lambda = L$  with a flux of  $F_L$  in  $\text{erg sec}^{-1} \text{cm}^{-2}$  the total counts recorded over the  $N_{spix}$  extraction height is:

$$C = F_\lambda S'_\lambda / d$$

These counts will be distributed over pixels in the wavelength direction according to the instrumental line spread function.

In contrast to the case of imaging, sensitivity  $S_\lambda$ , the spectroscopic point source sensitivity calibration ( $S_\lambda \times \epsilon_{N_{spix}}$ ) for a default extraction height of  $N_{spix}$  is measured directly from observations of stellar flux standards after insertion of ACS into HST. Therefore, the accuracy in laboratory determinations of  $T_\lambda$  for the ACS prisms and grisms is NOT crucial to the final accuracy of their sensitivity calibrations.

The peak counts  $\text{sec}^{-1} \text{pixel}^{-1}$  from the point source, is given by:

$$P_{cr} = \epsilon'_f(1) F_\lambda S'_\lambda$$

Where:

- $\epsilon'_f(1)$  is the fraction of energy contained within the peak pixel.
- the other quantities are as above.

## 6.3 Computing Exposure Times

To derive the exposure time to achieve a given signal-to-noise ratio, or to derive the signal-to-noise ratio in a given exposure time, there are four principal ingredients:

- Expected counts  $C$  from your source over some area.
- The area (in pixels) over which those counts are received ( $N_{pix}$ ).
- Sky background ( $B_{sky}$ ) in counts  $\text{pixel}^{-1} \text{sec}^{-1}$ .
- The detector background, or dark, ( $B_{det}$ ) in counts  $\text{sec}^{-1} \text{pixel}^{-1}$  and the read noise ( $R$ ) in counts of the CCD.
- Section 6.4 provides the information for determining the sky-plus-detector background.

### 6.3.1 Calculating Exposure Times for a Given Signal-to-Noise

The signal-to-noise ratio,  $\Sigma$  is given by:

$$\Sigma = \frac{Ct}{\sqrt{Ct + N_{pix}(B_{sky} + B_{det})t + N_{pix}N_{read}R^2}}$$

Where:

- $C$  = the signal from the astronomical source in counts  $\text{sec}^{-1}$ , or electrons  $\text{sec}^{-1}$  from the CCD. The actual output signal from a CCD is  $C/G$  where  $G$  is the gain. You must remember to multiply by  $G$  to compute photon events in the raw CCD images.
- $G$  = the gain is always 1 for the SBC and  $\sim 1, 2, 4$  or  $8$  for the CCDs, depending on GAIN.
- $N_{pix}$  = the total number of detector pixels integrated over to achieve  $C$ .
- $B_{sky}$  = the sky background in counts  $\text{sec}^{-1} \text{ pixel}^{-1}$ .
- $B_{det}$  = the detector dark current in counts  $\text{sec}^{-1} \text{ pixel}^{-1}$ .
- $R$  = the read noise in electrons; = 0 for SBC observations, 5.0 and 4.7 for WFC and HRC respectively
- $N_{read}$  = the number of CCD readouts.
- $t$  = the integration time in seconds.

This equation assumes the optimistic (and often realistic) condition that the background zero point level under the object is sufficiently well known (and subtracted) to not significantly contribute; in crowded fields this may not be true.

Observers using the CCD normally take sufficiently long integrations that the CCD read noise is not important. This condition is met when:

$$Ct + N_{pix}(B_{sky} + B_{det})t > 2N_{pix}N_{read}R^2$$

For the CCD in the regime where read noise is not important and for all SBC observations, the integration time to reach a signal-to-noise ratio  $\Sigma$ , is given by:

$$t = \frac{\Sigma^2 [C + N_{pix}(B_{sky} + B_{det})]}{C^2}$$

If your source count rate is much brighter than the sky plus detector backgrounds, then this expression reduces further to:

$$t = \frac{\Sigma^2}{C}$$

i.e. the usual result for Poisson statistics of  $\Sigma = \sqrt{\text{total counts}}$ .

More generally, the required integration time to reach a signal to noise ratio  $\Sigma$  is given by:

$$t = \frac{\Sigma^2 [C + N_{pix}(B_{sky} + B_{det})] + \sqrt{\Sigma^4 [C + N_{pix}(B_{sky} + B_{det})]^2 + 4\Sigma^2 C^2 [N_{pix} N_{read} R^2]}}{2C^2}$$

### 6.3.2 Exposure Time Estimates for Red Targets in F850LP

At wavelengths greater than 7500Å (HRC) and about 9000Å (WFC) ACS CCD observations are affected by a red halo due to light scattered off the CCD substrate. An increasing fraction of the light as a function of wavelength is scattered from the center of the PSF into the wings. This problem affects particularly the very broad z-band F850LP filter, for which the encircled energy depends on the underlying spectral energy distribution the most. In the currently available ETC, the treatment of such an effect has been ameliorated but not solved. The encircled energy fraction is calculated at the effective wavelength which takes into account the source spectral distribution. This fraction is then multiplied by the source counts. (The effective wavelength is the weighted average of the system throughput AND source flux distribution integrated over wavelength). However, this does not account for the variation in enclosed energy with wavelength.

As a consequence, in order to obtain correct estimated count rates for red targets, observers are advised to use the **Synphot** package in IRAF/STSDAS for which the proper integration of encircled energy over wavelength has now been incorporated. To quantify this new **Synphot** capability, we compare ETC results with **Synphot** for a set of different spectral energy distributions and the observation mode WFC/F850LP. In Table 6.4, the spectral type is listed in the first column. The fraction of light with respect to the total integrated to infinity is listed in the other two columns, for the ETC and **Synphot** calculations respectively. These values are derived for a 0.2 arcsec aperture for the ETC calculations and **Synphot**.

Table 6.4: Encircled Energy Comparison for WFC/F850LP

Sp. Type	APT ETC	Synphot
O	0.76	0.74
M	0.71	0.7
L	0.69	0.68
T	0.61	0.6

The ETC results are off by 3% (O star), 2% (M star), 2% (L star), and 1% (T star). If this small effect is relevant to particular observations, then the Synphot software package can be used. To learn how to use the synphot tool, we refer to the instructions provided in the April 2003 STAN, <http://www.stsci.edu/hst/acs/documents/newsletters/stan0302.html>, and in ACS ISR 2003-08.

### 6.3.3 Two-Gyro Guiding

At some future date HST may be operated with only two gyroscopes, hence causing additional spacecraft jitter and degradation of the effective PSF. This could potentially degrade the signal-to-noise ratio for point sources.




---

*See the Two-Gyro Handbook for detailed information.*

---

We anticipate that a two-gyro version of the ACS Exposure Time Calculator will be available to help assess these impacts.

---

## 6.4 Detector and Sky Backgrounds

When calculating expected signal-to-noise ratios or exposure times, the background from the sky and the background from the detector must be taken into account.

### 6.4.1 Detector Backgrounds

Table 6.5 shows the read-noise and dark-current characteristics of the detectors. See Table 7.3 for further details including variations by amplifier and GAIN for the CCDs.

Table 6.5: Detector Backgrounds

	WFC	HRC	SBC
Read noise (electrons pix <sup>-1</sup> )	~5	~4.7	0
Dark current (electrons sec <sup>-1</sup> pix <sup>-1</sup> )	3.2×10 <sup>-3</sup>	3.6×10 <sup>-3</sup>	1.2×10 <sup>-5</sup>

### 6.4.2 Sky Background

The sources of sky background which will affect ACS observations include:

- Earth shine (ES).
- Zodiacal light (ZL).
- Geocoronal emission (GC).

The background in counts sec<sup>-1</sup> pixel<sup>-1</sup> for **imaging observations** can be computed as:

$$B_{sky} = \int I_{\lambda} S_{\lambda} m_x m_y d\lambda$$

Where:

- $I_{\lambda}$  is the surface brightness of the sky background, in erg sec<sup>-1</sup> cm<sup>-2</sup> Å<sup>-1</sup> arcsec<sup>-2</sup>.
- $S_{\lambda}$  is the point source sensitivity for the imaging mode.
- $m_x$  and  $m_y$  are the plate scales along orthogonal axes.

The image of the sky through a disperser is not uniform, since some wavelengths fall off the detector for regions of sky near the edge of the field of view (FOV). Since the ACS grism spectra are of order 200 pixels long, the regions of lower sky will be strips at the long and short wavelength edges of the FOV. The maximum width of the strips from where the signal starts to decline to the edge, where the signal is down by roughly 2x, is about half the total length of a spectrum of a point source, i.e. roughly 100 pixels in the case of a sky background with a **continuum** of wavelengths. In the case of the HRC, the sky for the dispersed mode will not have the low background strips, since the FOV is not masked to the detector size. These small strips of lower sky background in the SBC and the WFC are ignored in the following formulae. Furthermore in the SBC and the WFC, since the spectra do not lie along the direction of the anamorphic distortion,

the plate scales of  $m_x$  and  $m_y$  above must be replaced by the plate scales  $m_s$  and  $m_\lambda$  in the orthogonal spatial and dispersion directions, respectively. Interior to the strips, a point on the detector sees a region of sky over the full wavelength coverage of the disperser. Thus, for **spectroscopic observations**:

$$B_{sky}^\lambda = \int I_\lambda S'_\lambda m_s m_\lambda d\lambda$$

For a **monochromatic** sky emission line at  $\lambda = L$  like Lyman- $\alpha$ , which will dominate the background through the LiF prism:

$$B_{sky}^L = I_L S'_\lambda m_s m_\lambda / d$$

where

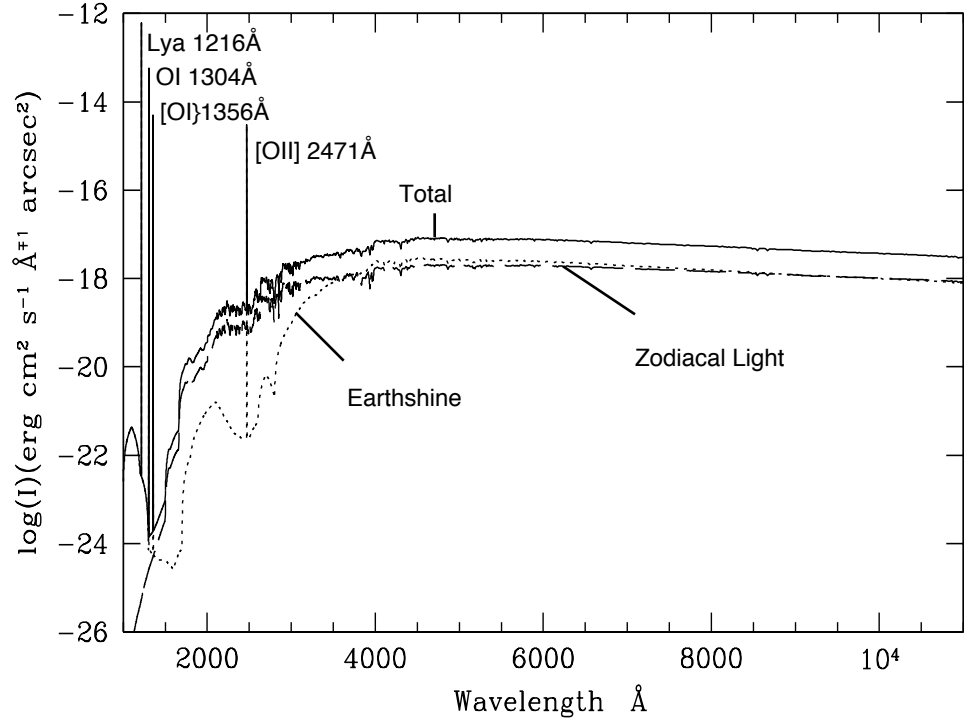
- $I_L$  is the monochromatic intensity of a line at wavelength  $L$  in  $\text{erg sec}^{-1} \text{cm}^{-2} \text{arcsec}^{-2}$ .

The total sky background is:

$$B_{sky} = B_{sky}^\lambda + B_{sky}^L$$

Figure 6.1 and Table 6.8 show “high” sky background intensity as a function of wavelength, identifying the separate components which contribute to the background. The “shadow” and “average” values of the Earthshine contribution in the ACS Exposure Time Calculator correspond, respectively, to 0 and 50% of the “high” values in Figure 6.1 and Table 6.8. For the zodiacal sky background, the values in Figure 6.1 and Table 6.8 correspond to the high value of  $m_V = 22.1$  from Table 6.6, while the “low” and “average” zodiacal light is scaled to  $m_V = 23.3$  and 22.7, respectively.

Figure 6.1: High Sky Background Intensity as a Function of Wavelength. The zodiacal contribution (ZL) is at ecliptic latitude and longitude of 30,180 degrees, and corresponds to  $m_v = 22.7$  per square arcsec. The Earthshine (ES) is for a target which is 24 degrees from the limb of the sunlit Earth. Use Figure 6.2 to estimate background contributions at other angles. The daytime geo-coronal line intensities are in  $\text{erg cm}^{-2} \text{s}^{-1} \text{arcsec}^{-2}$  (see Table 6.7).



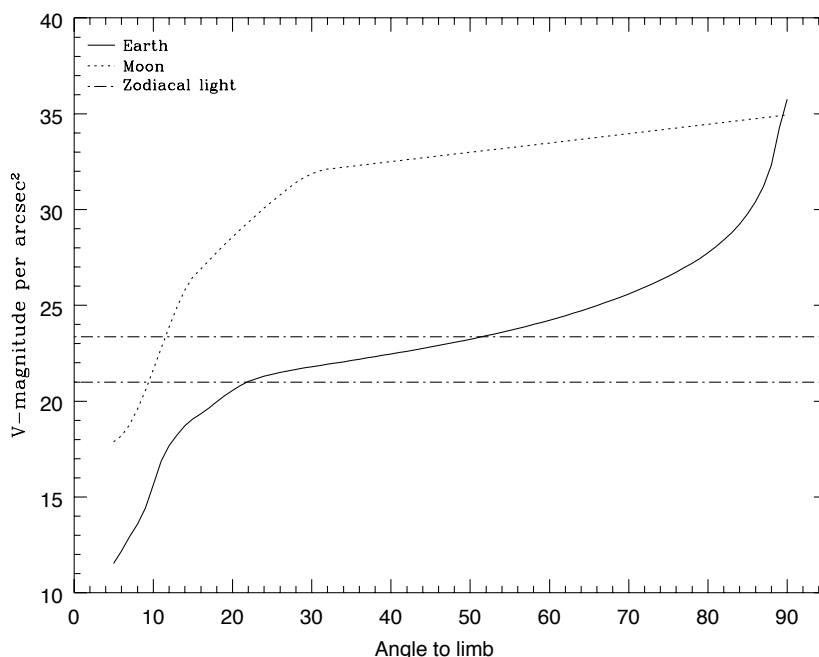
### Background Variations and LOW-SKY

In the ultraviolet, the background contains bright airglow lines, which vary from day to night and as a function of HST orbital position. The airglow lines may be the dominant sky contributions in the UV both for imaging-mode and spectroscopic observations. Away from the airglow lines, at wavelengths shortward of  $\sim 3000 \text{Å}$ , the background is dominated by zodiacal light, where the small area of sky that corresponds to a pixel of the high resolution HST instrumentation usually produces a signal that is much lower than the intrinsic detector background. The contribution of zodiacal light does not vary dramatically with time and varies by only a factor of about three throughout most of the sky. Table 6.6 gives the variation of the zodiacal background as a function of ecliptic latitude and longitude. For a target near ecliptic coordinates of (50,0) or (-50,0), the zodiacal light is relatively bright at  $m_v = 20.9$ , i.e. about 9 times the faintest values of  $m_v = 23.3$ . Deep imaging applications must carefully consider expected sky values!

On the other hand, Earthshine varies strongly depending on the angle between the target and the bright Earth limb. The variation of the Earthshine as a function of limb angle from the sunlit Earth is shown in Figure 6.2. The Figure also shows the contribution of the moon, which is

typically much smaller than the zodiacal contribution, for which the upper and lower limits are shown. For reference, the limb angle is approximately  $24^\circ$  when the HST is aligned toward its orbit pole (i.e., the center of the CVZ). The Earthshine contribution shown in Figure 6.1 and Table 6.8 corresponds to this position.

Figure 6.2: Background Contributions in V Magnitude per arcsec<sup>2</sup> due to the zodiacal light, Moon, and the Sunlit Earth as a Function of Angle Between the Target and the Limb of the Earth or Moon. The two zodiacal light lines show the extremes of possible values.



For observations taken longward of  $3500\text{\AA}$ , the Earthshine dominates the background at small ( $<22^\circ$ ) limb angles. In fact, the background increases exponentially for limb angles  $<22^\circ$ . The background near the bright limb can also vary by a factor of  $\sim 2$  on timescales as short as two minutes, which suggests that the background from Earthshine also depends upon the reflectivity of the terrain over which HST passes during the course of an exposure. Details of the sky background as it affects ACS, as well as STIS, are discussed by Shaw, et al. (STIS ISR 98-21). The impact of Earthshine on ACS observations is discussed by Biretta, et al., (ACS ISR 03-05).

Table 6.6: Approximate Zodiacal Sky Background as a Function of ecliptic latitude and ecliptic longitude (in V magnitudes per square arcsec)

Ecliptic Longitude (deg)	Ecliptic Latitude (deg)			
	0	30	60	90
180	22.1	22.7	23.2	23.3
145	22.4	22.9	23.3	23.3
110	22.3	22.9	23.3	23.3
50	20.9	22.2	22.9	23.3

Observations of the faintest objects may need the special requirement **LOW-SKY** in the Phase II observing program. **LOW-SKY** observations are scheduled during the part of the year when the zodiacal background light is no more than 30% greater than the minimum possible zodiacal light for the given sky position. **LOW-SKY** in the Phase II scheduling also invokes the restriction that exposures will be taken only at angles greater than 40 degrees from the bright Earth limb to minimize Earthshine and the UV airglow lines. The **LOW-SKY** special requirement limits the times at which targets within 60 degrees of the ecliptic plane will schedule, and limits visibility to about 48 minutes per orbit. The use of **LOW-SKY** must be requested and justified in the Phase I Proposal.

The ETC provides the user with the flexibility to separately adjust both the zodiacal (low, average, high) and Earthshine (shadow, average, high) sky background components in order to determine if planning for use of **LOW-SKY** is advisable for a given program. However, the absolute sky levels that can be specified in the ETC may not be achievable for a given target; e.g., as shown in Table 6.6 the zodiacal background minimum for an ecliptic target is  $m_v = 22.4$  which is still brighter than both the low and average options with the ETC. By contrast, a target near the ecliptic pole would always have a zodiacal=low background in the ETC. The user is cautioned to carefully consider sky levels as the backgrounds obtained in HST observations can cover significant ranges.

### Geocoronal Emission and Shadow

Background due to geocoronal emission originates mainly from hydrogen and oxygen atoms in the exosphere of the Earth. The emission is concentrated in the four lines listed in Table 6.7. The brightest line is Lyman- $\alpha$  at 1216Å. The strength of the Lyman- $\alpha$  line varies between about 2 and ~30 kilo-Rayleighs (i.e., between  $6.1 \times 10^{-14}$  and  $6.1 \times 10^{-13}$  erg  $\text{sec}^{-1} \text{cm}^{-2} \text{arcsec}^{-2}$  where 1 Rayleigh =  $10^6$  photons  $\text{sec}^{-1} \text{cm}^{-2}$  per  $4\pi$  steradian) depending on the position of HST with respect to the day-night terminator and the position of the target relative to the Earth limb. The next strongest line is the OI line at 1304Å, which rarely exceeds 10% of

Lyman- $\alpha$ . The typical strength of the OI 1304Å line is about 1 kilo-Rayleighs (which corresponds to about  $2.85 \times 10^{-14} \text{ erg sec}^{-1} \text{ cm}^{-2} \text{ arcsec}^{-2}$ ) on the daylight side and about 75 times fainter on the night side of the HST orbit. OI 1356 Å and OI 2471 Å lines may appear in observations on the daylight side of the orbit, but these lines are  $\sim 10$  times weaker than the OI 1304 Å line. The width of the lines also vary with temperature, the line widths given in Table 6.7 are representative values assuming a temperature of 2000 K.

Except for the brightest objects (e.g. planets), a filter or prism mode which does not transmit at Lyman- $\alpha$  should be employed. To minimize geocoronal emission the special requirement SHADOW can be requested. Exposures using this special requirement are limited to roughly 25 minutes per orbit, exclusive of the guide-star acquisition (or reacquisition) and can be scheduled only during a small percentage of the year. SHADOW reduces the contribution from the geocoronal emission lines by roughly a factor of ten while the continuum Earthshine is set to zero. SHADOW requirements must be included and justified in your Phase I proposal (see the *Call for Proposals*).

Table 6.7: Geocoronal emission lines

Wavelength (Å)	ID	Line Width (Å)	Intensity			
			Day		Night	
			kilo- Rayleighs	$\text{erg s}^{-1} \text{ cm}^{-2} \text{ arcsec}^{-2}$	kilo- Rayleighs	$\text{erg s}^{-1} \text{ cm}^{-2} \text{ arcsec}^{-2}$
1216	Ly- $\alpha$	0.04	$\sim 20$	$6.1 \times 10^{-13}$	2	$6.1 \times 10^{-14}$
1304	OI	0.013	$\sim 2$	$5.7 \times 10^{-14}$	0.013	$3.8 \times 10^{-16}$
1356	OI	0.013	$\sim 0.2$	$\sim 5 \times 10^{-15}$	$\sim 0.001$	$\sim 3 \times 10^{-17}$
2471	OI	0.023	$< 0.2$	$< 3 \times 10^{-15}$	$< 0.001$	$< 1.5 \times 10^{-17}$

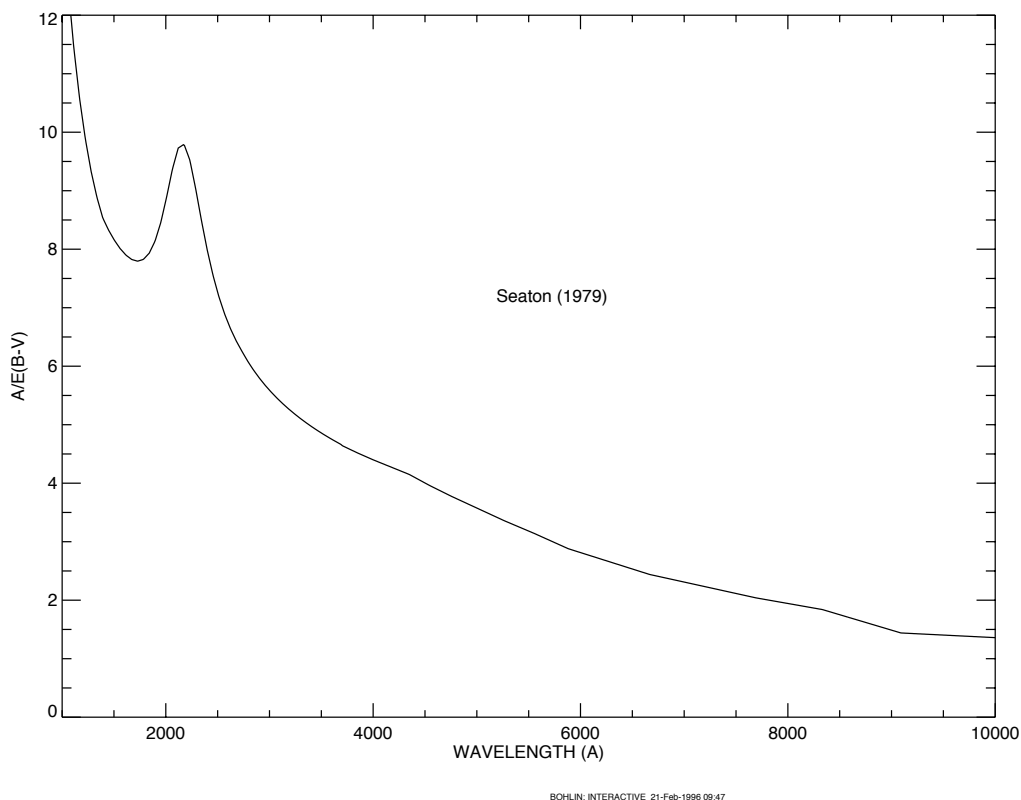
## 6.5 Extinction Correction

Extinction can dramatically reduce the counts expected from your source, particularly in the ultraviolet. Figure 6.3 shows the average  $A_V / E(B - V)$  values for our galaxy, taken from (Seaton, *MNRAS*, **187**, 73P, 1979). Large variations about the average are observed (Witt, Bohlin, Stecher, *ApJ*, **279**, 698, 1984).

Extinction curves have a strong metallicity dependence, particularly in the UV wavelengths. Sample extinction curves can be seen in Koornneef and Code, *ApJ*, **247**, 860 1981 (LMC); Bouchet et al., *A&A*, **149**, 330 1985

(SMC); and Calzetti, Kinney and Storchi-Bergmann, *ApJ*, **429**, 582, 1994, and references therein. At lower metallicities, the 2200Å bump which is so prominent in the galactic extinction curve disappears; and  $A_V / E(B - V)$  may increase monotonically at UV wavelengths.

Figure 6.3: Extinction versus Wavelength



## 6.6 Exposure-Time Examples

In the following you will find a set of examples for the three different channels and for different types of sources. The examples were chosen in order to present typical objects for the three channels and also to present interesting cases as they may arise with the use of ACS.



*At some future date HST may be operated with only two gyros, hence causing additional spacecraft jitter and degradation of the effective PSF. See the Two-Gyro Handbook for detailed information. All text in this ACS Handbook assumes three-gyro control.*

### 6.6.1 Example 1: WFC Imaging a Faint Point Source

What is the exposure time needed to obtain a signal to noise of 10 for a point source of spectral type F2V, normalized to  $V=26.5$ , when using the WFC, F555W filter? Assume a GAIN of 1 and a photometry box size of  $11 \times 11$  pixels, and average sky values.

The ACS Exposure Time Calculator (ETC) gives a total exposure time of 4410 sec to obtain this S/N in a single exposure. Since such an exposure would be riddled with cosmic rays and essentially useless, it is necessary to specify how many exposures to split the observation into. ACS WFC observations generally should be split if the exposure time is larger than about 5 minutes, but for multi-orbit observations, splitting into 2 exposures per orbit is generally sufficient.

For a typical object visibility of 53 minutes, after applying the requisite overheads, there is time for two 1200 sec exposures per orbit. The required exposure time can thus be reached in 4 exposures, but re-running the ETC using CR-SPLIT=4 raises the required exposure time to 5303 sec (because of the extra noise introduced by the four extra readouts). To achieve the required exposure time would require CR-SPLIT=5, or three orbits.

Using the pencil and paper method, Table 6.1 gives the integral  $Q_T d\lambda/\lambda$  as 0.0775, and the  $AB_V$  correction term can be retrieved from Table 10.1 as 0.040. According to Figure 4.10, a circular aperture of radius 0.3 arcsec (which has an area of 116 pixels, close to the 121 pixel box specified) encloses about 90% of the light from a star. The count rate is then  $2.5 \times 10^{11} * 0.0775 * 0.9 * 10^{-0.4(26.5+0.040)} = 0.423$  counts/sec, which agrees with the ETC-returned value of 0.42. The exposure time can then be found by using the equation

$$t = \frac{\Sigma^2 [C + N_{pix}(B_{sky} + B_{det})]}{C^2}$$

to give  $t=4172$  sec, which is close to the ETC-derived value of 4410s. We have inserted the background rate from Table 6.1 ( $B_{sky}=0.055$ ) and Table 6.5 ( $B_{det}=0.0032$ ) and assumed that the noise on the background is much greater than the readout noise.

Note that this can be greatly shortened by specifying a smaller analysis box (for example,  $5 \times 5$ ) and using LOW-SKY. Dropping the aperture size to  $5 \times 5$  at average sky which still encloses 81% of the light requires 1532 sec. Including both the smaller  $5 \times 5$  box and LOW-SKY (Zodiacal=LOW, Earthshine=AVERAGE) using the ETC gives the required exposure time as only 1306 sec (using CR-SPLIT=1), or 1540 sec with CR-SPLIT=2. The LOW-SKY visibility per orbit is 47 minutes, which allows a total on-target exposure time of 2000 sec in one orbit with CR-SPLIT=2.

Note also that the count rate from WFPC2 would be 0.167 electrons/sec, a factor of 2.5 lower.

### 6.6.2 Example 2: SBC Objective Prism Spectrum of a UV Spectrophotometric Standard Star

What is the peak count rate using the PR110L prism in the SBC for the HST standard star HS2027+0651 ( $V=16.9$ ) that was used for the STIS prism calibration (this spectrum is not in the ETC list, therefore we quote below the flux which could be found by dearchiving the STIS spectrum)?

The sensitivity peaks in the 1500-1600 Å region. To find the count rate at 1537 Å, inspection of Figure 5.22 gives the sensitivity of  $9.9 \times 10^{14}$  counts/sec per erg/cm<sup>2</sup>/s/Å. Multiplying by the stellar flux of  $5.3587 \times 10^{-14}$  gives 53.0 counts/sec, summed in the cross dispersion direction. For the fraction of light in the central pixel  $\epsilon=0.31$ , the brightest pixel at 1437.6 Å is 17.6 counts/sec/pixel, well below the bright object limit.

The SBC has no readout noise, and the dark current rate is negligible, while the main sky contribution for PR110L is from Lyman- $\alpha$ . For daytime Ly- $\alpha$  intensity of  $20kR=6.1 \times 10^{-13}$  erg cm<sup>-2</sup> s<sup>-1</sup> arcsec<sup>-2</sup>,  $S'=1.7 \times 10^{14}$  and  $d$ , the dispersion in Å/pixel, is 2.58. Therefore, the background count rate is  $6.1 \times 10^{-13} * 1.7 \times 10^{14} * 0.032^2 / 2.58 = 0.041$  counts/sec/pixel. This value varies somewhat over the field, as the plate scale varies from the nominal 0.032 arcsec/pixel. For faint source spectroscopy, it is better to use PR130L, which is on a CaF<sub>2</sub> substrate to block Ly- $\alpha$ .

### 6.6.3 Example 3: WFC VIS Polarimetry of the Jet of M87

What signal to noise ratio is reached in three one orbit exposures (~2400s each) for M87, when using the WFC, F555W for one orbit each in the three VIS polarizers? Gain is 2, box size is 5x5 pixels, CR-SPLIT=2 and average sky.

If the M87 jet region has  $\mu_V=17$  mag/square arcsec, using the ETC with a flat continuum spectral distribution and an exposure time of 2400s (CR-SPLIT=2), gives  $S/N=131.6$  for an observation with each VIS polarizer filter (which is an average of the polarizer at the 3 available position angles 0°, 60° and 120°). If the polarization  $P$  is 20%, then  $P*S/N = 26.3$ , so using

$$\log\left(\frac{\sigma_P}{P}\right) = -0.102 - 0.9898 \log(P \langle S/N \rangle_i)$$

from Chapter 5,  $\sigma_P/P = 0.031$ , or  $\sigma_P=6.2 \times 10^{-3}$ , which is the error on the fractional polarization. The error on the position angle should be  $\sim 1.0^\circ$  using the formula, again from Chapter 5, of

$$\log \sigma_\theta = 1.514 - 1.068 \log(P \langle S/N \rangle_i)$$

### 6.6.4 Example 4: SBC imaging of Jupiter's Aurora at Lyman-alpha

What signal to noise ratio is reached in a one orbit exposure (2000 sec) observing Jupiter's aurora in Ly- $\alpha$  using the SBC and F122M filter?

The equation from the Section, "Emission Line Source," on page 107 can be used to calculate the expected count rate. The aurora is variable, up to  $\sim 100\text{kR}$ . The value of (QT) for the SBC+F122M filter at  $1216\text{\AA}$  is 0.0009, from inspection of Figure 10.106 on page 238. For a surface brightness of  $40\text{kR} = 1.22 \times 10^{-12} \text{ erg cm}^{-2} \text{ s}^{-1} \text{ arcsec}^{-2}$  (See "Geocoronal Emission and Shadow" on page 116. for conversion), the total counts per pixel are given by the following calculation:

$$2.23 \times 10^{12} \times 0.0009 \times 1.22 \times 10^{-12} \times 1216 \times (0.032)^2 \times 2000 = 61.0.$$

The background contributions are the detector dark of  $1.2 \times 10^{-5}$  counts/pixel/sec (which can be ignored in this case) and a sky background which is dominated by geocoronal Lyman- $\alpha$ . During the daytime, the geocoronal background is  $20\text{kR}$ , or 30.5 counts, while at night the background drops to one tenth of this, or 3.05 counts.

Finally, we calculate the signal to noise ratio  $\Sigma$  for a  $2 \times 2$  pixel resolution element: in the daytime,  $\Sigma = 61.0 \cdot 4 / \sqrt{(61.0 + 30.5) \cdot 4} = 12.7$ , while at night,  $\Sigma = 61.0 \cdot 4 / \sqrt{(61.0 + 3.05) \cdot 4} = 15.2$

### 6.6.5 Example 5: Chronographic imaging of the Beta-Pictoris Disk

In the final example we shall consider the case where we are trying to determine the S/N achieved on the Beta Pictoris disk, assuming a disk surface brightness of  $R$  magnitude of  $16 \text{ arcsec}^{-2}$  at a distance of 6 arcsec from the central star with a  $V$  magnitude of 3.9, for an exposure time of 1000 seconds with an F435W filter. Assume that the star and disk have an A5V-type spectrum. Using the ACS Exposure Time Calculator and considering the case for the  $3.0''$  occulting mask:

- Disk count rate =  $4.98 \text{ e}^-/\text{sec}$  for a  $2 \times 2$  aperture (including 47.5% throughput of coronagraph) Sky count rate =  $0.010 \text{ e}^-/\text{sec/pixel}$ , Detector dark rate =  $0.015 \text{ e}^-/\text{sec/pixel}$
- In 1000s, this gives  $4,980 \text{ e}^-/2 \times 2$  aperture in the disk region.
- Central star count rate =  $3.63 \times 10^8 \text{ e}^-/\text{sec}$  for a  $101 \times 101$  aperture ( $101 \times 101$  aperture used to estimate total integrated flux)
- At a distance 6 arcsec from the central star, the fraction of flux per square arcsec in the PSF wings is  $2.6 \times 10^{-6}$ .  
 $B_{\text{PSF}} = 3.63 \times 10^{11} \times 2.6 \times 10^{-6} = 943.8 \text{ e}^-$  per square arcsec. The counts collected in 4 pixels are  $4 \times 0.027^2 \times (943.8) = 2.752$ .
- The S/N in a  $2 \times 2$  box is then  $4980 / \sqrt{4980 + 2.8} \approx 70.5$ .

## 6.7 Tabular Sky Backgrounds

We provide a table of the “high” sky background numbers as plotted in Figure 6.1. See the text and the caption in Figure 6.1 for more details. These high sky values are defined as the earthshine at  $38^\circ$  from the limb and the high zodiacal light of  $m_V = 22.1$  mag arcsec $^{-2}$ .

Table 6.8: High Sky Backgrounds

Wavelength	Earthshine	Zodiacal Light	Total Background
$\text{\AA}$	$\frac{\text{erg sec}^{-1}}{\text{cm}^{-2}\text{\AA}^{-1} \text{ arcsec}^{-2}}$	$\frac{\text{erg sec}^{-1}}{\text{cm}^{-2}\text{\AA}^{-1} \text{ arcsec}^{-2}}$	$\frac{\text{erg sec}^{-1}}{\text{cm}^{-2}\text{\AA}^{-1} \text{ arcsec}^{-2}}$
1000.	2.41E-23	1.26E-28	2.41E-23
1100.	4.38E-22	1.02E-26	4.38E-22
1200.	4.01E-23	1.05E-25	4.02E-23
1400.	4.29E-25	2.50E-24	2.93E-24
1500.	4.16E-25	9.12E-24	9.54E-24
1600.	2.55E-25	2.30E-22	2.30E-22
1700.	7.89E-23	7.06E-21	7.14E-21
1800.	9.33E-23	1.50E-20	1.51E-20
1900.	4.39E-22	2.20E-20	2.24E-20
2000.	1.01E-21	3.49E-20	3.59E-20
2100.	1.60E-21	1.21E-19	1.23E-19
2200.	7.49E-22	2.16E-19	2.17E-19
2300.	3.32E-22	1.75E-19	1.75E-19
2400.	2.50E-22	1.79E-19	1.79E-19
2500.	2.39E-22	2.47E-19	2.47E-19
2600.	5.62E-22	2.93E-19	2.94E-19
2700.	6.77E-21	9.95E-19	1.00E-18
2800.	2.03E-21	2.82E-19	2.91E-19
2900.	4.32E-20	2.04E-18	2.08E-18
3000.	9.34E-20	1.20E-18	1.29E-18
3100.	2.07E-19	1.46E-18	1.67E-18
3200.	3.60E-19	2.25E-18	2.61E-18
3400.	6.40E-19	2.81E-18	3.45E-18

Table 6.8: High Sky Backgrounds (Continued)

Wavelength	Earthshine	Zodiacal Light	Total Background
Å	$\frac{\text{erg sec}^{-1}}{\text{cm}^{-2}\text{Å}^{-1}\text{arcsec}^{-2}}$	$\frac{\text{erg sec}^{-1}}{\text{cm}^{-2}\text{Å}^{-1}\text{arcsec}^{-2}}$	$\frac{\text{erg sec}^{-1}}{\text{cm}^{-2}\text{Å}^{-1}\text{arcsec}^{-2}}$
3500.	8.20E-19	2.73E-18	3.55E-18
3600.	1.06E-18	2.68E-18	3.74E-18
3700.	1.22E-18	3.25E-18	4.47E-18
3800.	1.23E-18	3.05E-18	4.28E-18
3900.	1.52E-18	3.27E-18	4.79E-18
4000.	2.38E-18	4.54E-18	6.92E-18
4250.	2.33E-18	4.48E-18	6.81E-18
4500.	2.78E-18	5.32E-18	8.10E-18
5000.	2.55E-18	4.92E-18	7.47E-18
5250.	2.69E-18	5.28E-18	7.97E-18
5500.	2.56E-18	5.20E-18	7.76E-18
5750.	2.56E-18	5.33E-18	7.89E-18
6000.	2.40E-18	5.11E-18	7.51E-18
6250.	2.27E-18	4.94E-18	7.21E-18
6500.	2.20E-18	4.88E-18	7.08E-18
6750.	2.07E-18	4.69E-18	6.76E-18
7000.	1.90E-18	4.40E-18	6.30E-18
7250.	1.85E-18	4.34E-18	6.19E-18
7500.	1.73E-18	4.13E-18	5.86E-18
7750.	1.63E-18	3.95E-18	5.58E-18
8000.	1.57E-18	3.85E-18	5.42E-18
8250.	1.48E-18	3.68E-18	5.16E-18
8500.	1.37E-18	3.46E-18	4.83E-18
8750.	1.31E-18	3.36E-18	4.67E-18



# Feasibility and Detector Performance

In this chapter. ..

7.1 The CCDs / 125
7.2 CCD Operations and Limitations / 131
7.3 The SBC MAMA / 142
7.4 SBC Operations and Limitations / 145
7.5 SBC Bright-Object Limits / 149

ACS employs two fundamentally different types of detectors: CCDs for use from the near UV to the near IR, and a Multi-Anode Microchannel Array detector, known as a MAMA, for use in the ultraviolet. The CCD and the MAMA detectors are used in different ways and impose their own unique limitations on the feasibility of observations performed with them. In this chapter we present the properties of the ACS detectors, describe how to use them to optimize scientific programs, and list the steps you should take to ensure the feasibility of your observations.

---

## 7.1 The CCDs

### 7.1.1 Detector Properties

#### WFC Properties

The WFC/CCD consists of two 2048×4096 charge-coupled devices that are sensitive from the near UV to the near IR. They are thinned,

backside-illuminated devices manufactured by Scientific Imaging Technologies (SITE). They are butted together along their long dimension to create an effective  $4096 \times 4096$  array with a gap corresponding to approximately 50 pixels between the chips.

As with STIS, the CCD camera design incorporates a warm dewar window, designed to prevent buildup of contaminants on the window, which were found to cause a loss of UV throughput for the WFPC2 CCDs. A summary of the ACS/CCDs' performance is given in Table 7.1. The performance values on read noise and dark current are valid as of June 2004.

Table 7.1: ACS CCD Detector Performance Characteristics

Characteristic	WFC Performance	HRC Performance
Architecture	Thinned, backside illuminated anti-reflection coated multi-phase pinned	Thinned, backside illuminated anti-reflection coated multi-phase pinned
Wavelength range	3700–11000 Å	2000–11000 Å
Pixel format	2 butted 2048×4096	1024×1024
Field of view	202×202 arcsec	29×26 arcsec
Pixel size	15×15 $\mu\text{m}$	21×21 $\mu\text{m}$
Pixel plate scale	0.05 arcsec	0.027 arcsec
Quantum efficiency	~77% @ 4000 Å ~83% @ 6000 Å ~67% @ 8000 Å	~33% @ 2500 Å 69% @ 6000 Å ~53% @ 8000 Å
Dark count	$\sim 0.0032 \text{ e}^- \text{ sec}^{-1} \text{ pix}^{-1}$	$0.0036 \text{ e}^- \text{ sec}^{-1} \text{ pix}^{-1}$
Read noise	$\sim 5 \text{ e}^- \text{ rms}$	$\sim 4.7 \text{ e}^- \text{ rms}$
Full well	$\sim 84700 \text{ e}^-$	$\sim 155000 \text{ e}^-$
Gain (max. 65, 535 DN)	1, 2, 4 and 8 $\text{e}^-/\text{dn}$	1, 2, 4 and 8 $\text{e}^-/\text{dn}$

## HRC

The HRC CCD is a flight-spare STIS 1024×1024 CCD also manufactured by SITE. It is also a thinned, backside-illuminated device, but is coated using a process developed by SITE to provide good quantum efficiency in the near-ultraviolet. The performance characteristics and specifications are given in Table 7.1

## 7.1.2 CCD Spectral Response

### WFC

The spectral response of the unfiltered WFC camera is shown in Figure 4.9. This figure illustrates the excellent quantum efficiency in the visible and near infrared part of the spectrum, along with the violet cutoff imposed by the silver coatings on the optical elements.

### HRC

The HRC spectral response is also shown in Figure 4.9. As well as excellent quantum efficiency in the visible and near-infrared part of the spectrum, the sensitivity in the near ultraviolet is improved over that of the STIS CCD by means of the coating.

## 7.1.3 Quantum Efficiency Hysteresis

Based on current data, the ACS CCDs do not suffer from Quantum Efficiency Hysteresis (QEH)—that is, the CCD responds in the same way to light levels over its whole dynamic range, irrespective of the previous illumination level.

## 7.1.4 CCD Long-Wavelength Fringing

Like most CCDs, the ACS CCDs exhibit fringing in the red, longward of  $\sim 7500\text{\AA}$ . The amplitude of the fringes is a strong function of wavelength and spectral resolution.

The fringe pattern can be corrected by rectification with an appropriate flat field. The fringe pattern is a convolution of the contours of constant distance between the front and back surfaces of the CCD and the wavelength of the light on a particular part of the CCD. The fringe pattern has been shown to be very stable in similar devices, as long as the wavelength of light on a particular part of the CCD stays constant. In practice, this means that the fringe pattern is dependent on the spectrum of the light incident on the detector, with the sensitivity to the source spectrum a function of the bandwidth of the filter.

## 7.1.5 Optical Performance

Testing of the WFC and HRC optics and detectors, following fine alignment activities on-orbit, has shown that the optical quality objectives of the cameras are met. The encircled energy values obtained from observations made in SMOV are given in Table 7.2.

Table 7.2: Encircled energy measurements for the ACS channels

Channel	Encircled Energy	
	Center of Field	Edge of Field
WFC at 632.8nm in 0.25 arcsec diameter	80.0%	79.4%
HRC at 632.8nm in 0.25 arcsec diameter	81.8%	81.6%
SBC at 121.6nm in 0.10 arcsec diameter	28%	---

### 7.1.6 Readout Format

#### WFC

Each CCD chip is read out as a  $4144 \times 2068$  array, including physical and virtual overscans. This is made up of 24 columns of physical overscan, 4096 columns of pixel data and then 24 further columns of physical overscan. Each column consists of 2048 rows of pixel data followed by 20 rows of virtual overscan. The orientation of the chip is such that for the grism spectra, the dispersed images have wavelength increasing from left to right in the positive x-direction.

#### HRC

The HRC chip is read out as a  $1062 \times 1044$  array, including physical and virtual overscans. There are 19 columns of physical overscan, followed by 1024 columns of pixel data and then 19 more columns of physical overscan. Each column consists of 1024 rows of pixel data followed by 20 rows of virtual overscan. As with WFC, the orientation of the chip was chosen so that grism images have wavelength increasing from left to right.

### 7.1.7 Analog-To-Digital Conversion

Electrons which accumulate in the CCD wells are read out and converted to data numbers (DN) by the analog-to-digital converter (ADC). The ADC output is a 16-bit number, producing a maximum of 65,535 DN in one pixel.

The CCDs are capable of operating at gains of 1, 2, 4 or 8  $e^-/\text{DN}$ . In principle, use of a lower gain value can increase the dynamic range of faint source observations by reducing the quantization noise; however, in practice this improvement is not significant. Table 7.3 shows the actual gain levels and readout noise in electrons for the 4 WFC amps and the default C amp used for the HRC.

Table 7.3: CCD Gain and Readout Noise

Chip	Amp	Gain=1		Gain=2		Gain=4	
		Gain	Noise	Gain	Noise	Gain	Noise
WFC1	A	1.000	5.57	2.002	5.84	4.01	---
WFC1	B	0.972	4.70	1.945	4.98	3.90	---
WFC2	C	1.011	5.18	2.028	5.35	4.07	---
WFC2	D	1.018	4.80	1.994	5.27	4.00	---
HRC	C	1.163	4.46	2.216	4.80	4.235	5.86

For the WFC, gain factors of 1 and 2 are fully supported, and so are gain values of 2 and 4 for the HRC. The remaining two gain factors for each camera are available but unsupported, i.e. users of the latter modes must plan their own calibration. It is worth noticing that, for the WFC, the readout noise associated with GAIN=2 is on average only 0.28 e<sup>-</sup> higher per amplifier than that of GAIN=1. The noise increase brought about by the use of GAIN=2 is equivalent to that produced by adding a mere 1.7 e<sup>-</sup> of noise in quadrature to the noise of the GAIN=1 configuration: when the number of detected photons is larger than 3, the Poisson noise alone on the combination of source and sky would exceed this level. Thus, in terms of readout noise, the advantage of using GAIN=1 is minimal, whereas by adopting the higher gain value one would extend by 0.32 magnitude the ability of doing accurate photometry before saturation, would increase the number of bright unsaturated sources to provide cross-image registration and, for point sources, could perform photometry several magnitudes beyond saturation in some cases. Further information about gain values can be found in [ACS ISR 2002-03](#) and [ACS ISR 04-01](#).

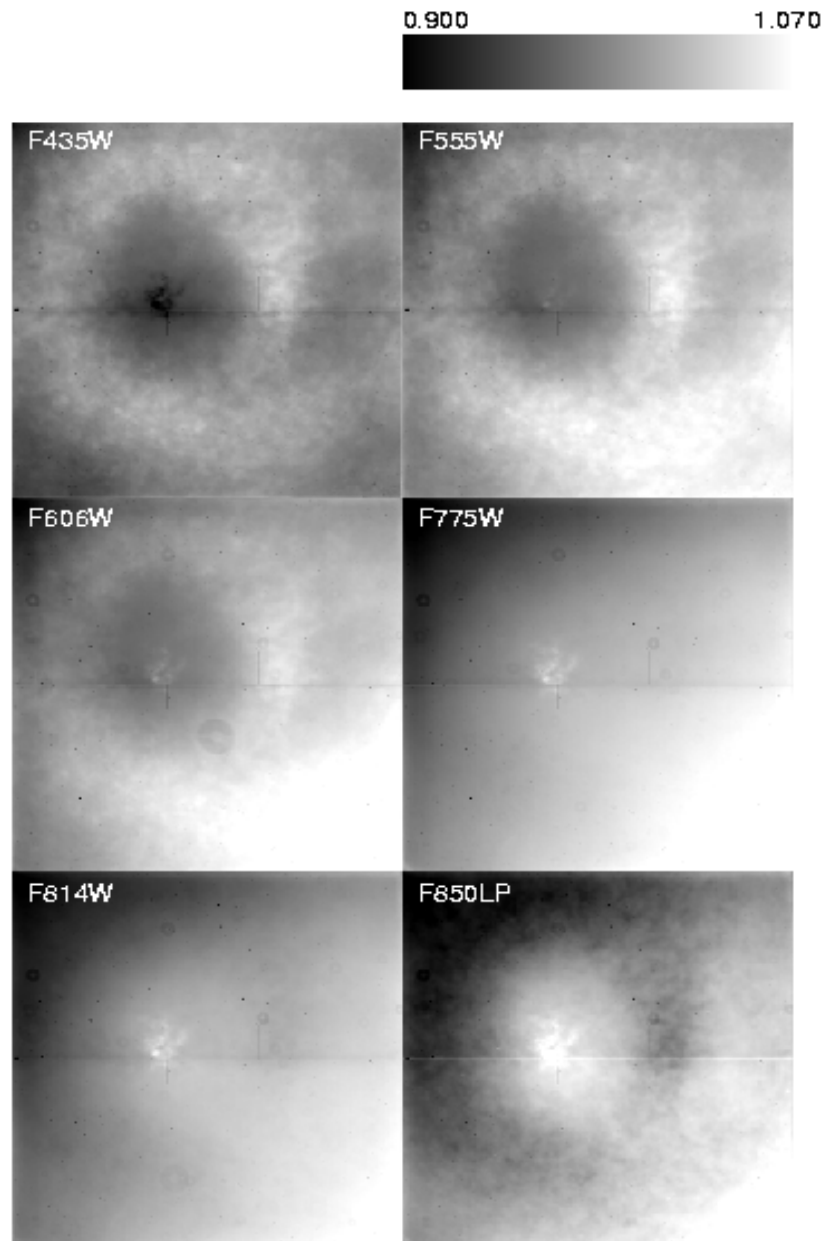
## 7.1.8 Flat Fields

### WFC

The flat fields for the WFC now combine information from two sources. Ground-based flats were obtained for all filters at S/N of ~300 per pixel. To refine the low-frequency domain of the ground flats, in-flight observations of a rich stellar field with large scale dithers have been analyzed (see [ACS ISR 2002-08](#)). The required L-flat correction is a corner-to-corner gradient of 10-18%, dependent on wavelength. The resulting flat field supports photometry to ~1% over the full WFC field of view.

Figure 7.1 shows the corrected WFC ground flats for several broadband filters, **note that on the sky a gap of 50 pixels exist between the top and bottom halves that is not shown here**. The central donut-like structure is wavelength dependent, where pixels in the central region are less sensitive than surrounding pixels in the blue F435W filter, for example, and more sensitive in the red F850LP filter. For further discussion of WFC flat fields, see ACS ISRs [2001-11](#) and [2002-04](#).

Figure 7.1: WFC Flat Field



## HRC

As for the WFC, the HRC ground flats were refined using in-flight observations of a rich stellar field with large scale dithers to determine the low-frequency domain of the flat fields. The correction required for the visible filters is a corner-to-corner gradient of 6-12%, dependent on wavelength. For the NUV filters, flats were taken in-flight using observations of the bright earth (see [ACS ISR 2003-02](#)) and include both the pixel-to-pixel and low-frequency structure of the detector response.

The current HRC flat fields have S/N  $\sim 300$  per pixel and support photometry to  $\sim 1\%$  over the full HRC field of view. Figure 7.2 shows the corrected HRC ground flats, derived for 6 broadband optical filters. The donut-like structure seen in the WFC response is not found in the HRC flats. For further discussion of HRC flat fields, see ACS ISRs [2001-11](#) and [2002-04](#).

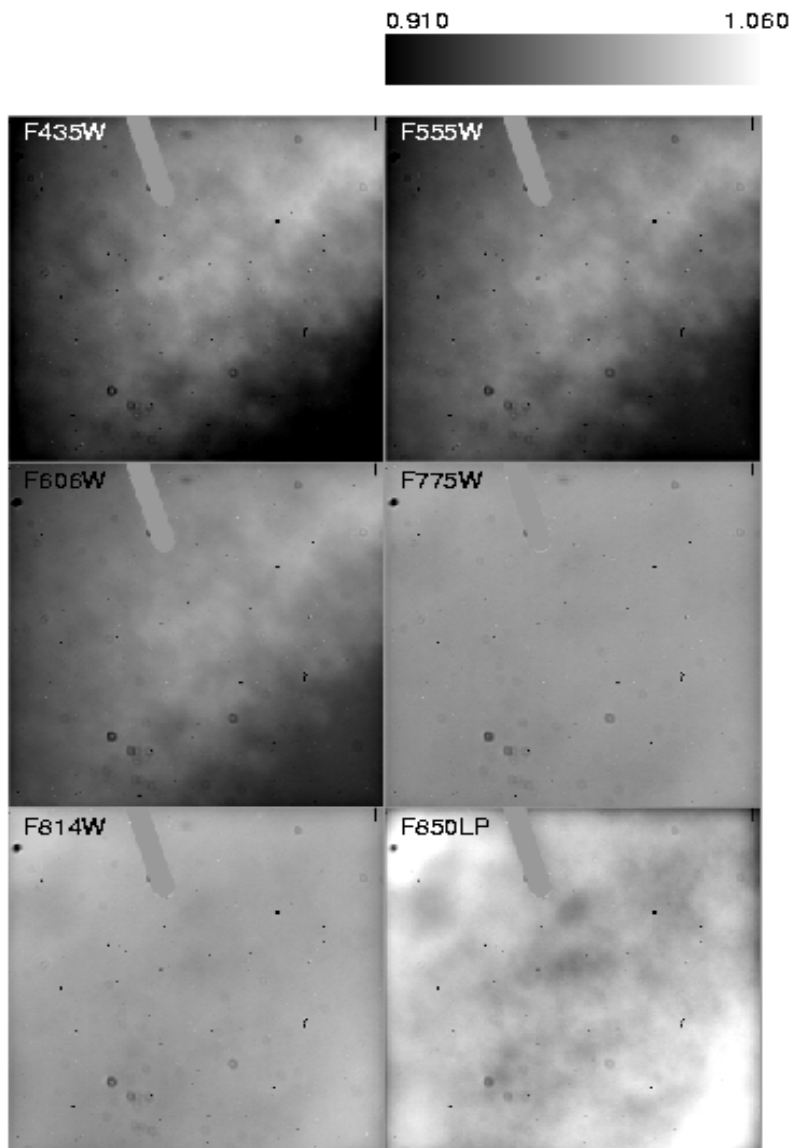
---

## 7.2 CCD Operations and Limitations

### 7.2.1 CCD Saturation: the CCD Full Well

The full well capacity for the ACS CCDs is given in Table 7.1 as 84,700  $e^-$  for the WFC and 155,000  $e^-$  for the HRC. This is somewhat dependent on the position on the chip. If the CCD is over-exposed, blooming will occur. This happens when a pixel becomes full, so excess charge flows into the next pixels along the column. However, extreme overexposure is not believed to cause any long-term damage to the CCDs, so there are no bright object limits for the ACS CCDs. When using  $GAIN = 2$  on the WFC and  $GAIN = 4$  on the HRC, it has been shown that the detector response remains linear to well under 1% up to the point when the central pixel reaches the full well depth. On-orbit tests have demonstrated that when using aperture photometry and summing over the pixels bled into, linearity to  $\leq 1\%$  holds even for cases in which the central pixel has received up to 10 times the full well depth (see [ACS ISR 04-01](#) for details).

Figure 7.2: HRC Flat Field



### 7.2.2 CCD Shutter Effects

The ACS camera includes a very high-speed shutter, so that even the shortest exposure times are not significantly affected by the finite traversal time of the shutter blades. On-orbit testing reported in [ACS ISR 2003-03](#), has verified that shutter shading corrections are not necessary to support 1% photometry on either the HRC or WFC. A total of 4 exposure times were found to be in error by up to 4.1%, e.g. the nominal 0.1s HRC exposure is really 0.1041s (updates for reference files have now been made to use the correct values in pipeline processing). No significant differences were found between exposure times controlled by the two shutters (A and

B), with the possible exception of non-repeatability up to  $\sim 1\%$  on the WFC for exposures in the 0.7 - 2.0 sec range. The HRC provides excellent shutter time repeatability.

### 7.2.3 Readnoise

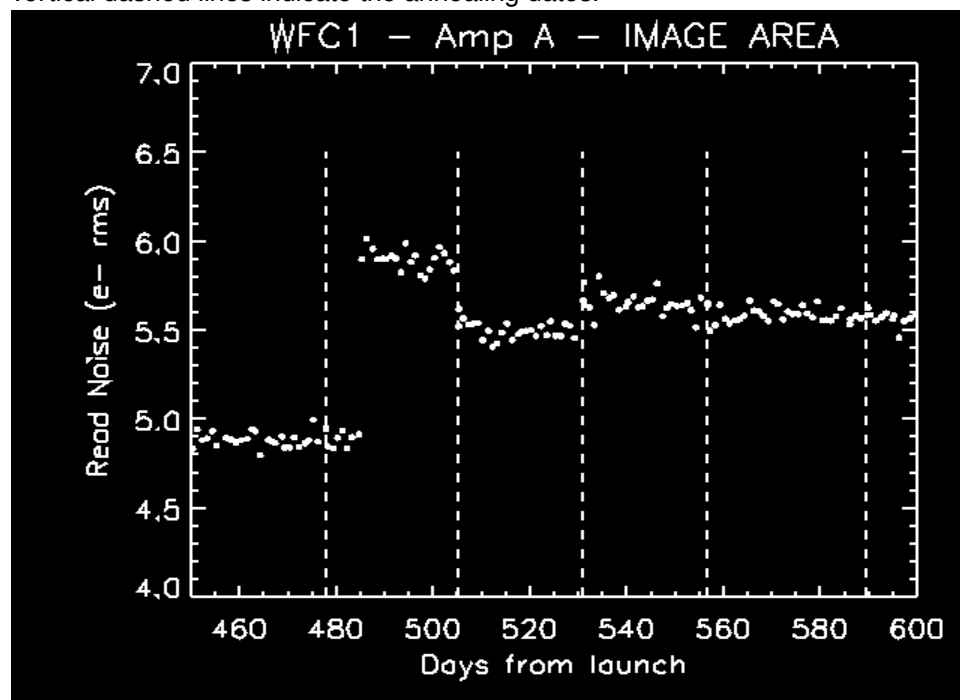
#### WFC

We measured the read noise level in the active area and overscan regions for all the amplifiers at the default gain settings. In general the read noise has been constant with time. On June 29, 2003, just after a transit through the South Atlantic Anomaly (SAA) the readnoise in Amp A changed from  $\sim 4.9$  to  $\sim 5.9$   $e^-$  rms.

Although the telemetry did not show any anomaly in any component of the camera, it is likely that the read noise jump was due to some sort of radiation damage. Amp A is the only amplifier that showed this anomaly. The amplitude of the variation ( $\sim 1$   $e^-$ ) was the same for GAIN 1 and 2. After the following anneal date the readnoise dropped to  $\sim 5.5$  and it remained constant for 27 days. After the following two anneal cycles the read noise reached stability at  $\sim 5.6$   $e^-$  rms, approximately  $0.7$   $e^-$  higher than before the change and it has remained constant since then. Figure 7.3 shows the read noise in the image area for amplifier A during the “instability” period. The readnoise of all the other amplifiers have been very stable since launch with post-launch figures almost unchanged from the pre-launch measurements made during ground testing.

Even with a slightly higher read noise in Amp A most of the WFC broadband science observations are sky limited while narrowband observations are primarily read noise limited.

Figure 7.3: Readnoise Jump in WFC Amp A (occurred on June 29, 2003). The vertical dashed lines indicate the annealing dates.



### HRC

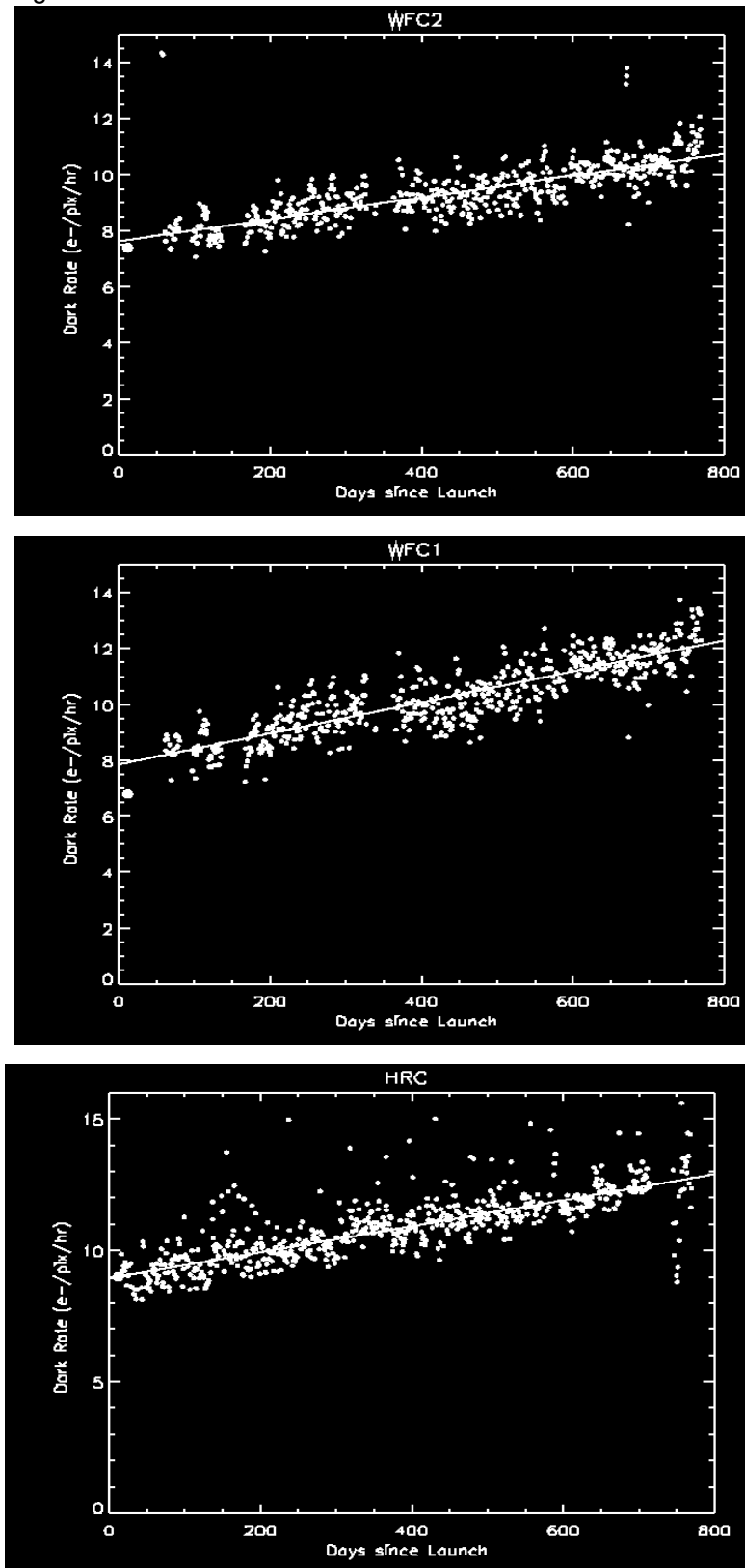
The read noise is monitored only for the default readout amplifier C at the default gain setting (2 e<sup>-</sup>/DN). No variations have been observed with time. The read noise measured in the image area (4.80 +/- 0.12) is in agreement with the readnoise figure measured in the two overscan regions and it is comparable to the pre-flight value of 4.74 e<sup>-</sup>.

## 7.2.4 Dark Current

The dark current of CCDs operated in a radiative environment is predicted to increase with time. Ground testing of WFC devices, radiated with a cumulative fluence equivalent to 2.5 and 5 years of on-orbit exposure, predicted a linear growth of ~1.5 e<sup>-</sup>/pix/hr/yr. During the testing the WFC CCDs were operated at ~81 C, about 5 degrees cooler than the operating temperature.

The dark current in ACS CCDs is monitored four days per week with the acquisition of four 1000 seconds dark frames (totaling 16 images per week). Dark frames are used to create reference files for the calibration of scientific images and to track and catalog hot pixels as they evolve. The four daily frames are combined together to remove cosmic rays and to extract hot pixel information for any specific day. The dark reference files are generated by combining two weeks of daily darks in order to reduce the statistical noise. The hot pixel information for a specific day are then added to the combined bi-weekly dark. In order to study the evolution of the dark current with time we calculate the modal dark current value in the cosmic-ray free daily darks. As expected, the dark current increases with time (Figure 7.4). The observed rate of dark current linear growth are 1.4 and 2 e<sup>-</sup>/pix/hr/yr for WFC1 and WFC2 respectively and 1.8 for the HRC CCD. These rates are in general agreement with the ground testing prediction.

Figure 7.4: Dark rate trend with time for the ACS CCDs



### 7.2.5 Cosmic Rays

Initial studies have been made of the characteristics of cosmic ray impacts on the two ACS imaging cameras, HRC and WFC. The fraction of pixels affected by cosmic rays varies from 1.5% to 3% during a 1000 second exposure for both cameras, similar to what was seen on WFPC2 and STIS. This number provides the basis for assessing the risk that the target(s) in any set of exposures will be compromised. The affected fraction is the same for the WFC and HRC despite their factor of two difference in pixel areas because the census of affected pixels is dominated by charge diffusion, not direct impacts. Observers seeking rare or serendipitous objects as well as transients may require that every single WFC pixel in at least one exposure among a set of exposures is free from cosmic ray impacts. For the CR fractions of 1.5% to 3% in 1000 sec, a single  $\sim 2400$  sec orbit must be broken into 4 exposures (4 CR splits of 500 to 600 sec each) to reduce the number of uncleanable pixels to 1 or less. (It is also recommended that users dither these exposures to remove hot pixels as well.)

The flux deposited on the CCD from an individual cosmic ray does not depend on the energy of the cosmic ray but rather the length it travels in the silicon substrate. The electron deposition due to individual cosmic rays has a well defined cut-off with negligible events of less than 500 electrons and a median of  $\sim 1000$  electrons (see Figure 7.5 and Figure 7.6).

Figure 7.5: Electron deposition by cosmic rays on WFC.

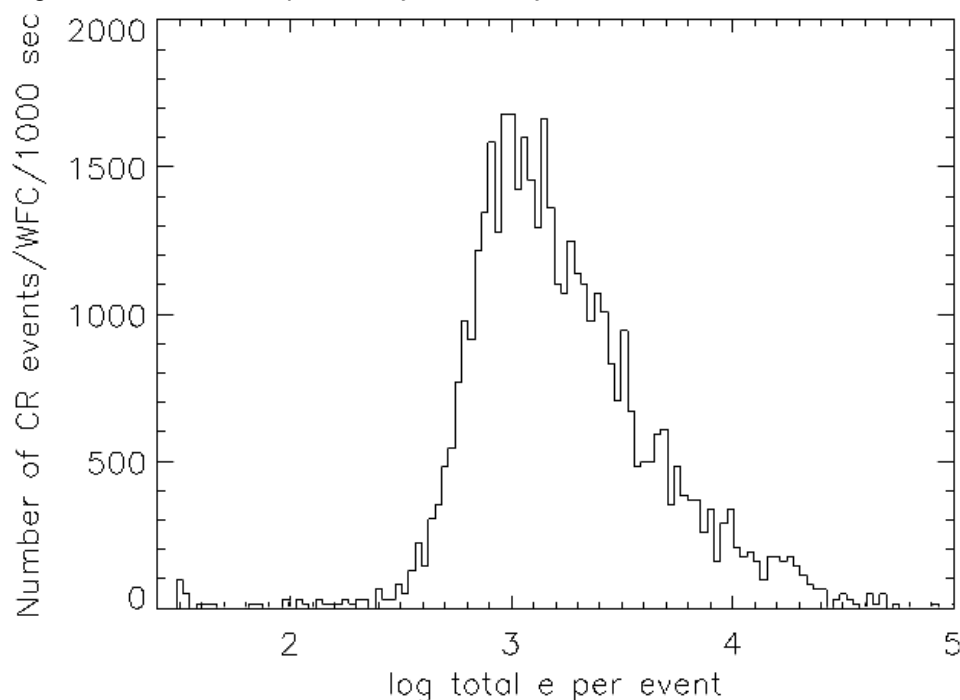
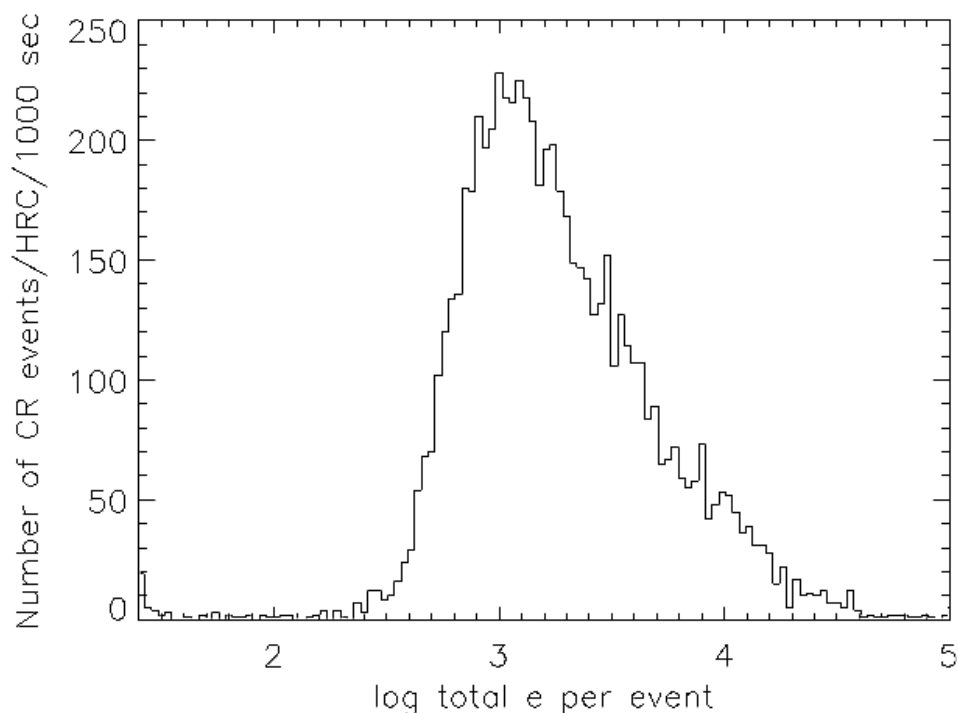


Figure 7.6: Electron deposition of Cosmic Rays on HRC.



The distribution of the number of pixels affected by a single cosmic ray is strongly peaked at 4 to 5 pixels. Although a few events are seen which encompass only one pixel, examination of these events indicate that at least some and maybe all of these sources are actually transient hot pixels or unstable pixels which can appear hot in one exposure (with no charge diffusion) and normal in the next. Such pixels are very rare but do exist. There is a long tail in the direction towards increasing numbers of attached pixels.

Distributions of sizes and anisotropies can be useful for distinguishing cosmic rays from astrophysical sources in a single image. The size distribution for both chips peaks near 0.4 pixels as a standard deviation (or 0.9 pixels as a FWHM). This is much narrower than for a PSF and is thus a useful discriminant between unresolved sources and cosmic rays.

## 7.2.6 Hot Pixels

The dark current and the “hot” pixels on the ACS CCDs have been studied throughout SMOV and Cycle 11. The hot pixels appear similar to those seen on previous CCDs flown on HST and are likely caused by radiation damage.

The dark current distribution is well described by a Gaussian with a center at  $0.0022 \text{ e}^-/\text{sec}$  and rms of  $0.0029 \text{ e}^-/\text{sec}$  for the WFC, and  $0.0025 \text{ e}^-/\text{sec}$  and rms of  $0.0015 \text{ e}^-/\text{sec}$  for the HRC. As expected from experience with earlier HST cameras, very significant tails in these distributions are

seen from much “warmer” or “hotter” pixels. We have chosen a conservative limit of  $0.04 \text{ e}^-/\text{sec}$  for WFC and  $0.08 \text{ e}^-/\text{sec}$  for HRC as a threshold above which we consider a pixel to be “hot” and not part of the normal distribution of pixel dark current. Figure 7.7 and Figure 7.8 show the daily growth of these hot pixels. For WFC we find a growth rate of approximately 1200 new hot pixels per day with dark current greater than  $0.04 \text{ e}^-/\text{sec}$ . For HRC the number of new hot pixels per day above the threshold is approximately 90. Because the distribution of dark current in hot pixels is strongly peaked near the threshold, the specific number of such pixels is necessarily a strong function of the chosen threshold. During the HST safing events marked in Table 7.7 and Table 7.8, the ACS thermo-electric coolers (TECs) were not operating. This warming reduced the number of hot pixels, as if an anneal had occurred.

Figure 7.7: Hot Pixel Trends for WFC.

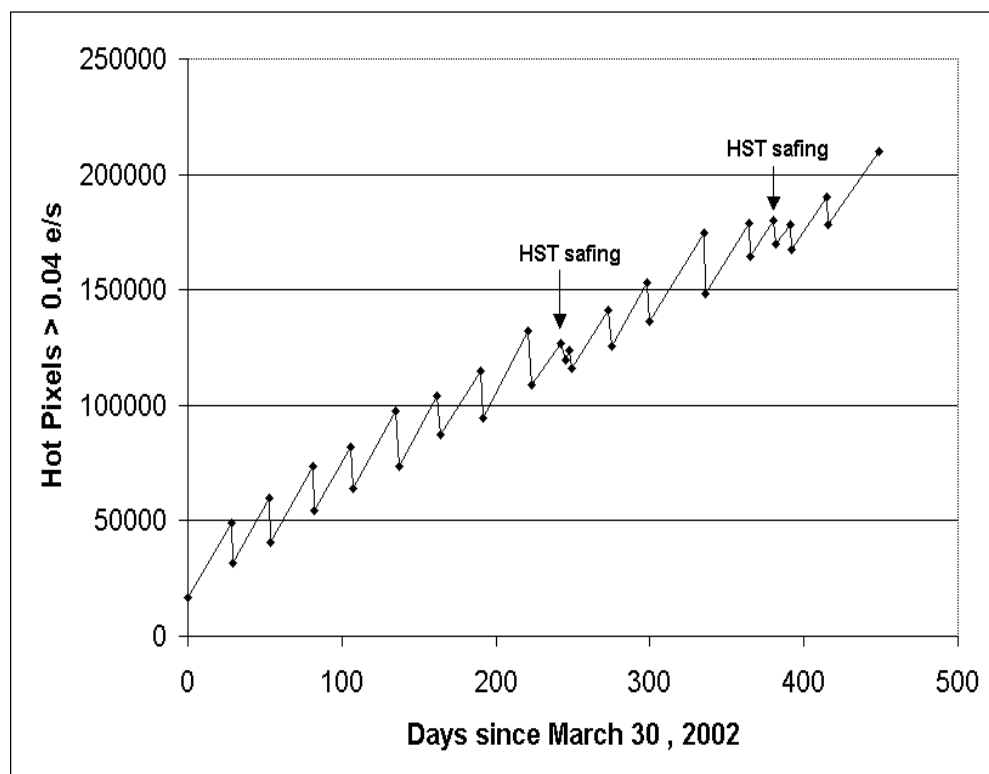
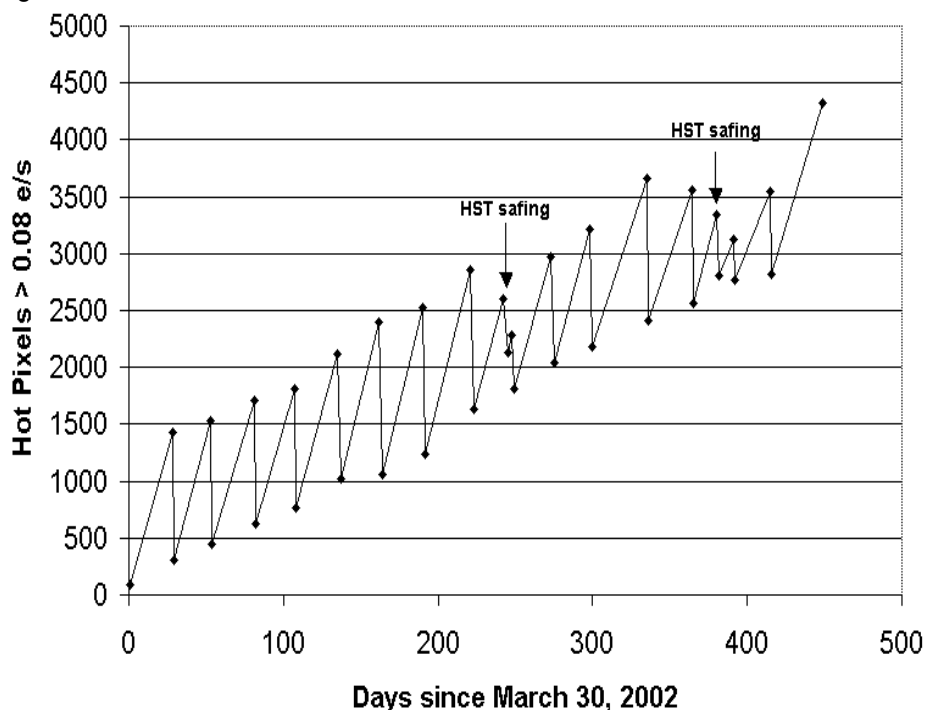


Figure 7.8: Hot Pixel Trends for HRC.



The monthly anneals on HRC heal on average 80-85% of new hot pixels, similar to what is seen with WFPC2 and STIS. The anneals on WFC heal only ~60% of hot pixels, leading to a growing population of permanent hot pixels. About 1% of the WFC FOV is covered by permanent hot pixels each year. While the standard CR-SPLIT approach allows for cosmic-ray subtraction, without additional dithering it will not eliminate hot pixels in post-observation processing. Hence, we recommend that observers who would have otherwise used a simple CR-SPLIT now use some form of dithering instead. For example, a simple ACS-WFC-DITHER-LINE pattern has been developed, based on integer pixel offsets, which shifts the image by 2 pixels in X and 2 in Y along the direction that minimizes the effects of scale variation across the detector. The specific parameter values for this pattern are given in Section 8.4.3 of the [Phase II Proposal Instructions](#). However, any form of dithering providing a displacement of at least a few pixels can be used to simultaneously remove the effects of cosmic ray hits and hot pixels in post-observation processing.

Subtraction of a superdark frame from a science image during pipeline calibration can remove the dark current from hot pixels just as it does for normal pixels. However, hot pixels are often orders of magnitude noisier than normal pixels, which in many cases limits their ability to provide useful measurements of flux. In rare cases (but not without precedents), hot pixels can spontaneously “heal”, a circumstance which could create false positive detections in some science programs.

## 7.2.7 Charge Transfer Efficiency

Charge Transfer Efficiency (CTE) is a measure of how effective the CCD is at moving charge from one pixel location to the next when reading out the chip. A perfect CCD would be able to transfer 100% of the charge as the charge is shunted across the chip and out through the serial register. In practice, small traps in the silicon lattice are able to compromise this process by holding on to electrons, releasing them at a significantly later time (seconds rather than microseconds). For large charge packets (several thousands of electrons), losing a few electrons along the way is not a serious problem, but for smaller ( $\sim 100$  electrons or less) signals, it can have a substantial effect.

CTE is typically measured as a pixel transfer efficiency, and would be 1 for a perfect CCD. The CTE numbers for the ACS CCDs at the time of installation are given in Table 7.4. While the numbers look impressive, remember that reading out the WFC CCD requires 2048 parallel and 2048 serial transfers, so that almost 2% of the charge from a pixel in the corner opposite the readout amplifier is lost.

Table 7.4: Charge Transfer Efficiency measurements for the ACS CCDs at installation time (Fe55 test at 1620 e<sup>-</sup>)

Chip	Parallel	Serial
WFC1	0.999995	0.999999
WFC2	0.999995	0.999999
HRC	0.999983	0.999994

Also, the CTE numbers are significantly different for images where the pixels have a low intensity compared to those where the intensity is high.

Both the WFPC2 and STIS CCDs have been found to suffer from a significant degradation in CTE since their installation in 1993 and 1997, respectively. More details can be found in the latest versions of the *WFPC2 Instrument Handbook* and the *STIS Instrument Handbook*.

At the end of Cycle 11 we performed the first on-orbit calibration of the photometric losses due to imperfect CTE on ACS HRC and WFC. We utilized images of 47 Tucanae from a CTE calibration program to measure the dependence of stellar photometry on the number of parallel and serial transfers. The results are described in Riess et al. ([ACS ISR 2003-09](#)) and are summarized here. For WFC, significant photometric losses are apparent for stars undergoing numerous parallel transfers (y-direction) and are  $\sim 1$ -2% for typical observing parameters rising to  $\sim 10$ % in worst cases (faint stars, low background). The size of the photometric loss appears to have a strong power-law dependence on the stellar flux, as seen for other CCD's flown on HST.

The dependence on background is significant but there is little advantage to increasing the background intentionally (e.g., by post-flashing) due to the added shot noise. No losses are apparent for WFC due to serial transfer (x-direction). For HRC, significant photometric losses also arise from parallel transfer ( $\sim 1\%$  for typical observations,  $\sim 5\%$  for worst case) but are not seen for serial transfer. Correction formulae are presented in [ACS ISR 04-06](#) to correct photometric losses as a function of a source's position, flux, background, time, and aperture size. Figure 7.9 shows the predicted photometric losses for the WFC due to imperfect parallel CTE as a function of time. These curves require extreme extrapolation and should be used for planning purposes only. Four specific science applications are shown as examples: the measure of the faint end of M31's CMD (GO 9453), the measurement of high-redshift supernovae (GO 9528), the measurement of any PSF whose brightness is the zeropoint (i.e.,  $1 \text{ e}^-/\text{sec}$ ) and a 20th mag star in a narrow band.

Figure 7.9: Projected CTE losses (and equivalently, the size of corrections) for example, science applications described in Table 7.5. The precision of measurements is not limited by the size of the loss but rather its uncertainty. As a rule of thumb we suggest that the ultimate limit of precision will be  $\sim 25\%$  of the loss after correction.

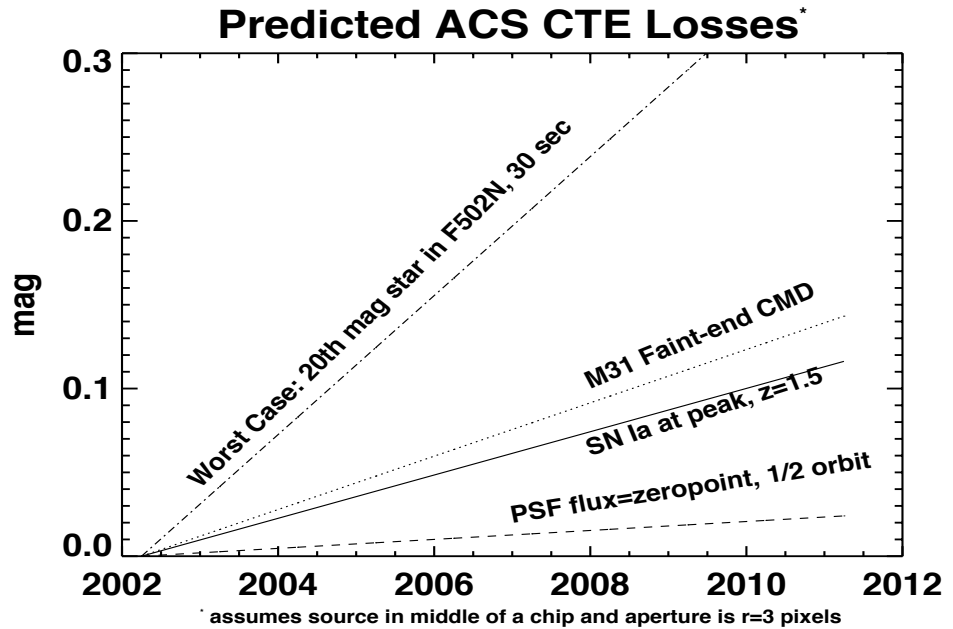


Table 7.5: Example Science Applications and their Assumed Parameters

Science Application	Source Flux ( $\text{e}^-$ )	Sky ( $\text{e}^-$ )
SN Ia at peak $z=1.5$	100	30
M31 faint-end of CMD	40	100
PSF, $1 \text{ e}^-/\text{sec}$ , 1/2 orbit	1000	40
F502N, 30 sec, 20th mag star	258	0.1

When observing a single target significantly smaller than a single detector, it is possible to place it near an amplifier to reduce the impact of imperfect CTE. Although we do not believe this is necessary for Cycle 14, it is easy to accomplish by judicious choice of aperture and target position or by utilizing POS TARG commands (however be aware that such large POS TARGs are not advisable because they change the fractional pixel shifts of dither patterns due to the geometric distortion of ACS). An alternative means to achieve the placement of a target near the amplifier is by using some of the subarray apertures. For example, WFC1-512 (target will have 256 transfers in X and Y), WFC1-1K and WFC1-2K place the target near the B amplifier (or WFC2-2K for the C amplifier).

### 7.2.8 UV Light and the HRC CCD

In the optical, each photon generates a single electron. However, in the near UV, shortward of  $\sim 3200\text{\AA}$  there is a finite probability of creating more than one electron per UV photon (see Christensen, O., *J. App. Phys.* **47**, 689, 1976). At room temperature the theoretical quantum yield, i.e., the number of electrons generated for a photon of energy  $E > 3.5\text{ eV}$  ( $\sim 3500\text{\AA}$ ) is  $N_e = E(\text{eV})/3.65$ . The HRC CCDs quantum efficiency curve has not been corrected for this effect. The interested reader may wish to see Chapter 6 of the *STIS Instrument Handbook* for details on Signal-to-Noise treatment.

---

## 7.3 The SBC MAMA

### 7.3.1 MAMA Properties

The ACS MAMA detector is the STIS flight spare STF7 and provides coverage from 1150 to  $1700\text{\AA}$ . The MAMA detector is a photon-counting device which processes events serially. The ACS MAMA only operates in the accumulate (ACCUM) mode in which a time-integrated image is produced. Unlike the STIS MAMAs, the ACS does not offer the high-resolution ( $2048 \times 2048$ ) mode or the time-tagged data acquisition. The primary benefits afforded by the STIS and ACS MAMAs, in comparison with previous HST UV spectroscopic detectors such as those of the GHRS and FOS, are high spatial resolution, two-dimensional imaging over a relatively large field of view, and low background for point sources.

Figure 7.10: Design of the SBC MAMA

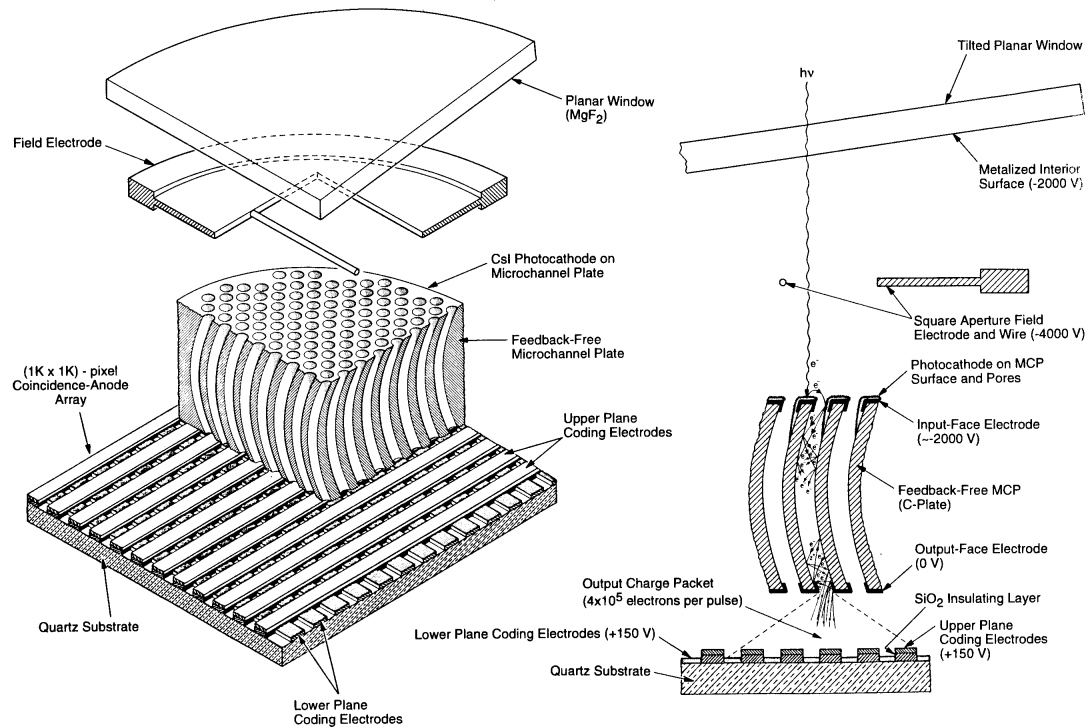


Figure 7.10 illustrates the design of the MAMA which has an opaque CsI photocathode deposited directly on the face of the curved microchannel plate (MCP). Target photons strike the photocathode, liberating single photoelectrons which pass into the microchannel plate (MCP). There they are multiplied to a pulse of  $\sim 4 \times 10^5$  electrons. The pulse is recorded by an anode array behind the photocathode and detected by the MAMA electronics which process it, rejecting false pulses and determining the origin of the photon event on the detector.

The field electrode, or *repeller wire*, repels electrons emitted away from the microchannel plate back into the channels. This provides an increase in quantum efficiency of the detector at the price of an increase in the detector PSF halo. The repeller wire voltage is always on for SBC observations.

Table 7.6: SBC Detector Performance Characteristics

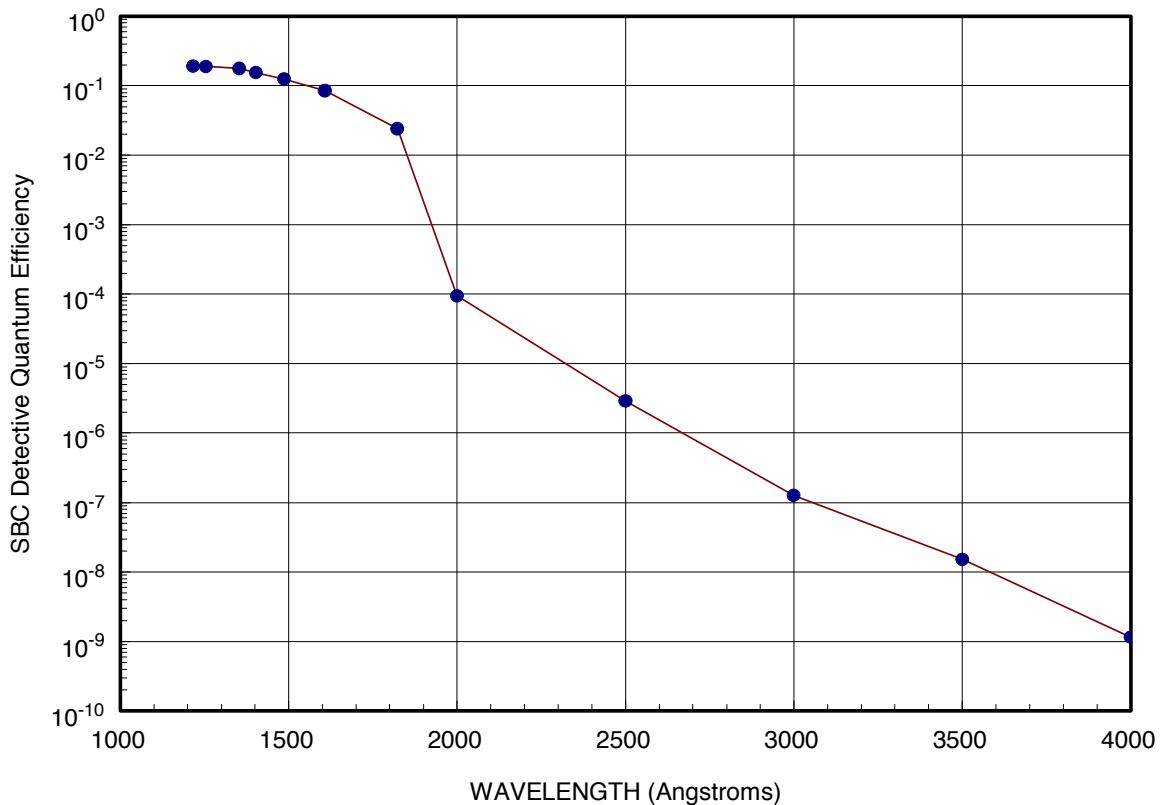
Characteristic	SBC MAMA Performance
Photocathode	CsI
Wavelength range	1150–1700Å
Pixel format	1024×1024
Pixel size	25×25 μm
Plate scale	0.034×0.030 arcseconds/pixel
Field of view	34.6 x 30.8 arcseconds
Quantum efficiency	19.2% @ 1216Å
Dark count	$1.2 \times 10^{-5}$ counts sec <sup>-1</sup> pix <sup>-1</sup>
Global count-rate linearity limit <sup>1</sup>	360,000 counts sec <sup>-1</sup>
Local count-rate linearity limit	~350 counts sec <sup>-1</sup> pix <sup>-1</sup>
Visible light DQE	< $1.2 \times 10^{-9}$ above 400 nm

1. Rate at which counting shows 10% deviation from linearity. These count rates are well above the bright-object screening limits.

### 7.3.2 SBC Spectral Response

The spectral response of the unfiltered SBC is illustrated in Figure 7.11. The peak photocathode response occurs at Lyman- $\alpha$ . Its spectral response is defined by the cutoff of the MgF<sub>2</sub> window at 1150Å at short wavelengths, and by the relatively steep decline of the CsI photocathode at long wavelengths. Out-of-band QE at longer wavelengths (>4000Å) is <10<sup>-8</sup> yielding excellent solar-blind performance.

Figure 7.11: ACS SBC Detective Quantum Efficiency



### 7.3.3 Optical Performance

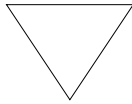
The SBC exhibits low-level extended wings in the detector point-spread function (PSF). Sample MAMA detector PSF profiles are shown in Figure 7.12.

## 7.4 SBC Operations and Limitations

### 7.4.1 MAMA Overflowing the 16 Bit Buffer

The MAMA is a photon-counting detector: as each photon is recorded, it is placed into buffer memory. The buffer memory stores values as 16-bit integers; hence the maximum number it can accommodate is 65,535 counts per pixel in a given ACCUM mode observation. When accumulated counts per pixel exceed this number, the values will wrap. As an example, if you are counting at  $25 \text{ counts sec}^{-1} \text{ pixel}^{-1}$ , you will reach the MAMA “accumulation” limit in  $\sim 44$  minutes.

One can keep accumulated counts per pixel below this value by breaking individual exposures into multiple identical exposures, each of which is short enough that fewer than 65,535 counts are accumulated per pixel. There is no read noise for MAMA observations, so no penalty is paid in lost signal-to-noise ratio when exposures are split. There is only a small overhead for each MAMA exposure (see Section 9.2).

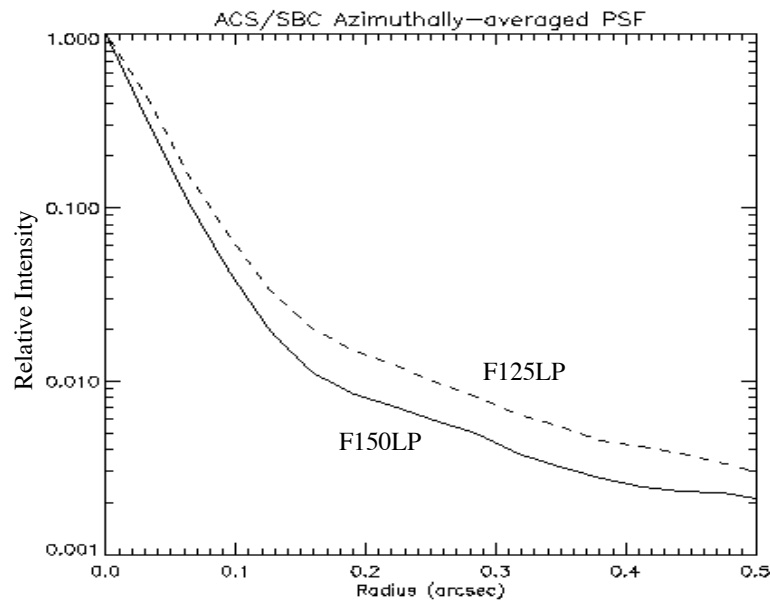



---

***Keep the accumulated counts per SBC pixel below 65,535, by breaking single exposures into multiple exposures, as needed.***

---

Figure 7.12: MAMA Point Spread Function



### 7.4.2 MAMA Darks

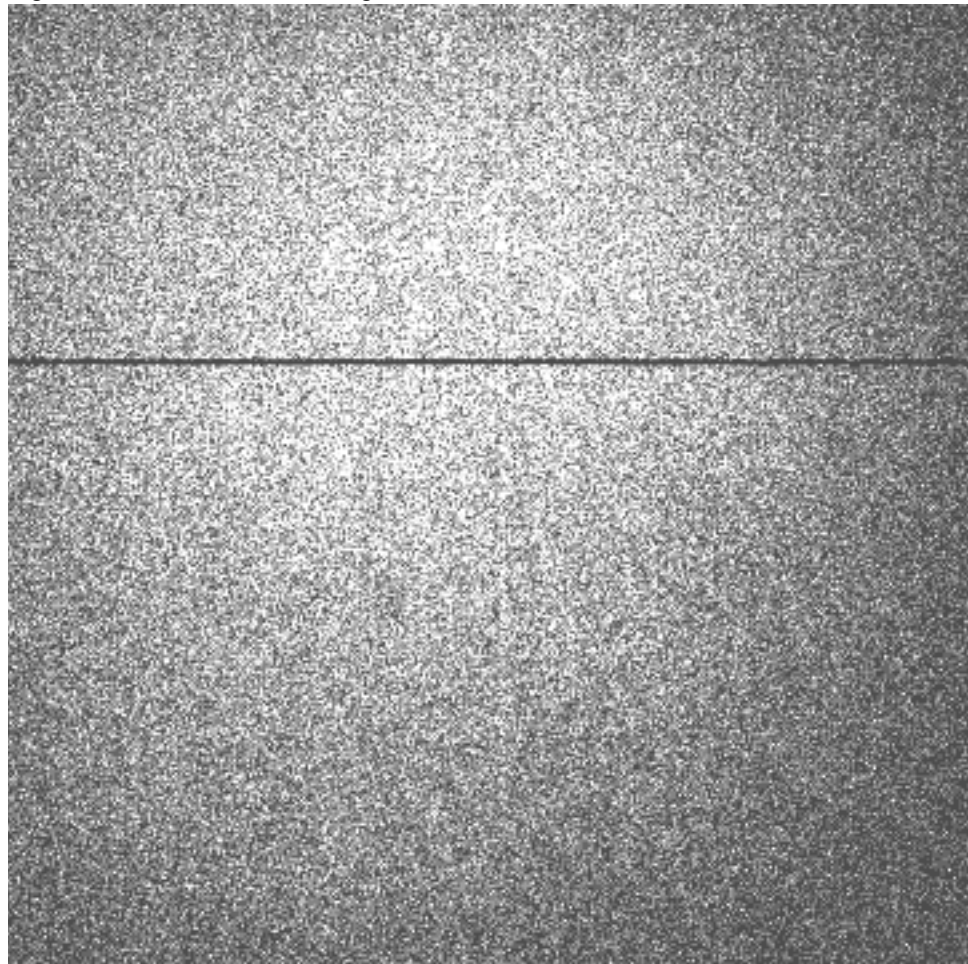
MAMA detectors have intrinsically low dark currents. Ground test measurements of the ACS MAMA showed count rates in the range of  $10^{-5}$  to  $10^{-4}$  counts per pixel per second as the temperature varied from 28 to 35°C degrees. The count rate increased by about 30% for one degree increase in temperature. In-flight measurements, taken weekly throughout June and July 2002, show count rates between  $8 \times 10^{-6}$  and  $10^{-5}$ . These measurements were taken as soon as the MAMA was turned on and were therefore at the lower end of the temperature range. A 10 hour observation in SMOV, long enough for nominal temperatures to be reached yield a dark current of  $1.2 \times 10^{-5}$  counts per second per pixel. Monthly monitoring throughout cycle 11 shows the in-flight dark current to be about  $9 \times 10^{-6}$

counts per second per pixel. For typical SBC operations, in which the detector is turned on for less than two hours, a dark image collected at lower temperatures is more suitable and will replace the current calibration image. This has a mean dark rate of  $10^{-5}$  counts per second per pixel.

The ACS MAMA has a broken anode which disables the seven rows 599 to 605. There are three dark spots, smaller than 50 microns at positions (334,977), (578,964) and (960,851) and two bright spots at (55,281) and (645,102) with rates which fluctuate but are always less than 3 counts per second.

An example of the dark current variation across the detector can be seen in Figure 7.13 below.

Figure 7.13: MAMA Dark Image



### 7.4.3 SBC Signal-to-Noise Ratio Limitations

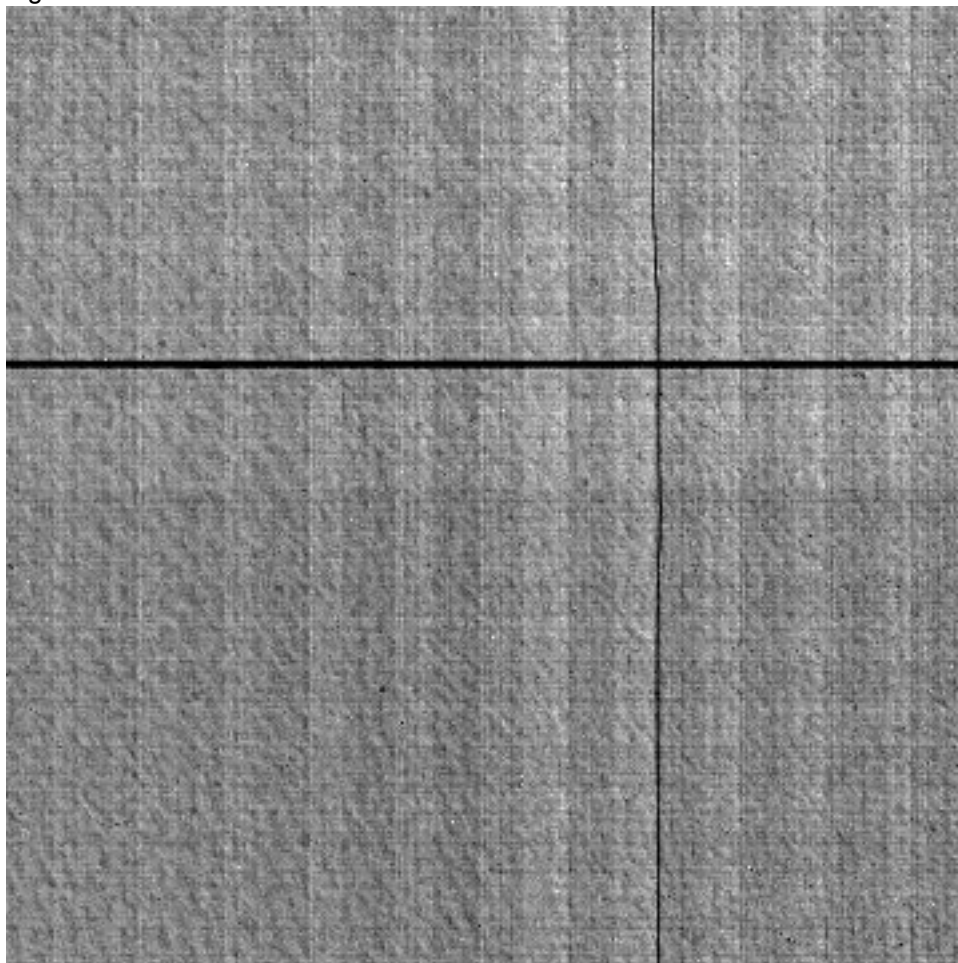
MAMA detectors are capable of delivering signal-to-noise ratios on the order of 100:1 per resolution element ( $2 \times 2$  pixels) or even higher. Tests in

orbit have demonstrated that such high S/N is possible with STIS (Kaiser et al., *PASP*, **110**, 978; Gilliland, STIS ISR 98-16.)

For targets observed at a fixed position on the detector, the signal-to-noise ratio is limited by systematic uncertainties in the small-scale spatial and spectral response of the detector. The MAMA flats show a fixed pattern that is a combination of several effects including beating between the MCP array and the anode pixel array, variations in the charge-cloud structure at the anode, and low-level capacitive cross-coupling between the fine anode elements. Intrinsic pixel-to-pixel variations are of order 6% but are stable to <1%.

#### 7.4.4 SBC Flatfield

Figure 7.14: Mama Flat Field



High S/N SBC flat fields were taken on the ground. In-flight observations of a UV-bright stellar field with large scale dithers will be used to refine the low frequency structure of the SBC flats. The ground flat in Figure 7.14 illustrates several features. The low frequency response is

extremely uniform except for a change of response that can be seen in the four image quadrants. The rows 601 to 605, disabled due to the broken anode, are clearly displayed as is the shadow of the repeller wire running vertically near column 577. A regular fixed “tartan” pattern is visible showing the effect of the discrete anodes. For further discussion of SBC flat fields, see [ACS ISR 1999-02](#).

### 7.4.5 SBC Nonlinearity

#### Global

The MAMA detector begins to experience nonlinearity (photon impact rate not equal to photon count rate) at global (across the entire detector) count rates of 200,000 counts  $\text{sec}^{-1}$ . The nonlinearity reaches 10% at 360,000 counts  $\text{sec}^{-1}$  and can be corrected for in post-observation data processing at the price of a loss of photometric reliability. Additionally, the MAMA detector plus processing software are not able to count reliably at rates exceeding 285,000 count  $\text{sec}^{-1}$ . For this reason and to protect the detectors, observations beyond this rate are not allowed (see Section 7.5).

#### Local

The MAMA detector remains linear to better than 1% up to  $\sim 22$  counts  $\text{sec}^{-1} \text{ pixel}^{-1}$ . At higher rates, they experience local (at a given pixel) nonlinearity. The nonlinearity effect is image dependent—that is, the nonlinearity observed at a given pixel depends on the photon rate affecting neighboring pixels. This property makes it impossible to correct reliably for the local nonlinearity in post-observation data processing. In addition, MAMA detectors are subject to damage at high local count rates (see Section 7.5).

---

## 7.5 SBC Bright-Object Limits

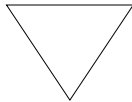
STScI has responsibility to ensure that the MAMA detectors are not damaged through over-illumination. Consequently, we have developed procedures and rules to protect the MAMA. We ask all potential users to share in this responsibility by reading and taking note of the information in this section and designing observing programs which operate in the safe regime for these detectors.

### 7.5.1 Overview

The SBC detector is subject to catastrophic damage at high global and local count rates and cannot be used to observe sources which exceed the

defined safety limits. The potential detector damage mechanisms include over-extraction of charge from the microchannel plates causing permanent reduction of response, and ion feedback from the microchannel plates causing damage to the photocathode and release of gas which can overpressure the tube.

To safeguard the detector, checks of the global (over the whole detector) and local (per pixel) illumination rates are automatically performed in flight for all SBC exposures. The *global illumination rate* is monitored continuously; if the global rate approaches the level where the detector can be damaged, the high voltage on the detector is automatically turned off. This event can result in the loss of all observations scheduled to be taken with that detector for the remainder of the calendar (~1 week). The *peak local illumination rate* is measured over the SBC field at the start of each new exposure. If the local rate approaches the damage level, the SBC filter wheel will be used to block the light, since there is no “shutter”. Also, all subsequent SBC exposures (in the obset) will be lost until a new filter is requested.




---

*Sources that would over-illuminate the SBC detector cannot be observed. It is the responsibility of the observer to avoid specifying observations that exceed the limits described below.*

---

### 7.5.2 Observational Limits

To ensure the safety of the SBC detector and the robustness of the observing timeline, we have established observational limits on the incident count rates. Observations which exceed the allowed limits will not be scheduled. The allowed limits are given in Table 7.7, which includes separate limits for nonvariable and irregularly-variable sources. The global limits for irregular variable sources are a factor 2.5 more conservative than for sources with predictable fluxes. Predictable variables are treated as nonvariable for this purpose. Examples of sources whose variability is predictable are Cepheids or eclipsing binaries. Irregularly variable sources are, for instance, cataclysmic variables or AGN.

Table 7.7: Absolute SBC Count-Rate Limits for Nonvariable and Variable Objects

Target	Limit Type	Mode	Screening Limit
Nonvariable	Global	All modes	200,000 counts sec <sup>-1</sup>
Nonvariable	Local	Imaging	50 counts sec <sup>-1</sup> pix <sup>-1</sup>
Irregularly Variable <sup>1</sup>	Global	All modes	80,000 counts sec <sup>-1</sup>
Irregularly Variable <sup>1</sup>	Local	Imaging	50 counts sec <sup>-1</sup> pix <sup>-1</sup>

1. Applies to the phase when the target is brightest.

Table 7.8: Limiting V-band Magnitudes for SBC observations in various filters

Spectral type	log T <sub>eff</sub>	f122m	f115lp	f125lp	f140lp	f150lp	f165lp	pr110l	pr130l
O5V	4.648	17.1	20.2	20.0	19.5	19.0	17.6	16.8	16.5
B1V	4.405	16.2	19.4	19.2	18.7	18.1	16.9	16.0	15.7
B3V	4.271	15.3	18.6	18.5	18.0	17.4	16.2	15.2	15.0
B5V	4.188	14.5	18.0	17.9	17.5	16.9	15.7	14.6	14.4
B8V	4.077	12.9	16.9	16.8	16.5	16.0	14.8	13.7	13.5
A1V	3.965	10.4	14.9	14.9	14.8	14.5	13.5	12.1	12.0
A3V	3.940	9.2	14.0	14.0	13.9	13.9	13.2	11.5	11.3
A5V	3.914	7.8	12.9	12.9	12.9	12.9	12.5	10.9	10.8
F0V	3.857	6.8	12.0	12.0	11.9	11.9	11.8	10.2	10.2
F2V	3.838	6.0	11.2	11.2	11.2	11.2	11.1	9.5	9.5
F5V	3.809	4.1	9.4	9.4	9.4	9.4	9.3	7.9	7.8
F8V	3.792	2.9	8.2	8.2	8.2	8.1	8.1	6.7	7.7
G2V	3.768	1.3	6.7	6.7	6.6	6.6	6.5	5.1	5.0
G5V	3.760	0.8	6.2	6.2	6.1	6.1	6.0	4.6	4.5
G8V	3.746	1.9	5.7	5.8	5.4	4.9	4.0	3.7	3.4
K0V	3.720	1.9	5.7	5.8	5.4	4.9	4.0	3.7	3.4
Double <sup>1</sup>	---	14.4	17.5	17.3	16.8	16.3	14.9	14.1	13.8
AG Peg <sup>2</sup>	---	13.9	17.0	16.8	16.4	16.0	14.3	13.4	13.1

1. System made of a main sequence late-type star with an O5V star contributing 20% to the total light in the V band. In the UV, the O5 component dominates and sets the same limiting magnitude for companion types A-M. A one magnitude safety factor has been added, as for the O5V case.

2. Star with a flux distribution like AG Peg.

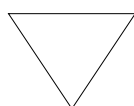
### 7.5.3 How Do You Determine if You Violate a Bright Object Limit?

As a first step, you can check your source V magnitude and peak flux against the bright-object screening magnitudes in Table 7.8 for your chosen observing configuration. In many cases, your source properties will be much fainter than these limits, and you need not worry further.

However, if you are near these limits (within 1 magnitude or a factor of 2.5 of the flux limits), then you need to carefully consider whether your source will be observable in that configuration. Remember the limits in these tables assume zero extinction. Thus you will want to correct the limits appropriately for your source's reddening and the aperture throughput.

You can use the information presented in Section 6.2 to calculate your peak and global count rates. Perhaps better, you can use the ACS Exposure-Time Calculator to calculate the expected count rate from your source. It has available to it a host of template stellar spectrograms. If you have a spectrum of your source (e.g., from IUE, FOS, or GHRS) you can also input it directly to the calculator. The calculator will evaluate the global and per pixel count rates and will warn you if your exposure exceeds the absolute bright-object limits. We recommend you use the ACS exposure time calculator if you are in *any doubt* that your exposure may exceed the bright-object MAMA limits.

### 7.5.4 Policy and Observers' Responsibility in Phase I and Phase II




---

***It is the observers' responsibility to ensure that their observations do not exceed the bright-object count limits stated in Table 7.7.***

---

It is your responsibility to ensure that you have checked your planned observations against the brightness limits prior to proposing for Phase I. If your proposal is accepted and we, or you, subsequently determine (in Phase II), that your source violates the absolute limits, then you will either have to change the target, if allowed, or lose the granted observing time. We encourage you to include a justification in your Phase I proposal if your target is within 1 magnitude of the bright-object limits for your observing configuration. For SBC target-of-opportunity proposals, please provide in your Phase I proposal an explanation of how you will ensure your target can be safely observed.

STScI will screen all ACS observations that use the MAMA detector to ensure that they do not exceed the bright-object limits. In Phase II, you will

be required to provide sufficient information to allow screening to be performed.

Here we describe the required information you must provide.

### **Prism Spectroscopy**

To allow screening of your target in Phase II for spectroscopic MAMA observations you must provide the following for your target (i.e., for all sources which will illuminate the detector during your observations):

- V magnitude.
- Expected source flux at observing wavelength.
- Spectral type (one of the types in the screening tables).
- E(B-V).
- B-V color.

If you wish to observe a target which comes within one magnitude (or a factor of 2.5 in flux) of the limits in the spectroscopic bright-object screening table (Table 7.8) for your configuration, after correction for reddening, but which you believe will not exceed the absolute limits in Table 7.7 and so should be observable, you must provide auxiliary information to justify your request. Specifically:

- You must provide an existing UV spectrum (e.g., obtained with IUE, FOS, GHRS, STIS or GALEX) of the star which proves that neither the global nor the local absolute limits will be exceeded.

### **Imaging**

The SBC imaging bright-object screening magnitudes are very stringent, ranging from  $V = 15$  to  $V = 20.5$  for the different imaging apertures, and apply to all sources imaged onto the MAMA detector (i.e., not just the intended target of interest). Table 7.8 can be used to determine if the target of interest is above the bright-object limit. Starting in Cycle 8, STScI has been using the second-generation Guide-Star Catalog (GSC II) to perform imaging screening for objects in the field of view other than the target itself. The GSC II contains measurements from photometrically calibrated photographic plates with color information for magnitudes down to at least  $V = 22$  mag. This information will be used to support bright-object checking for fixed and for moving targets (major planets). STScI will make a best effort to perform the imaging screening using GSC II. However, observers should be prepared for the possibility that under exceptional circumstances GSC II may be insufficient. For instance, fields close to the Galactic plane may be too crowded to obtain reliable photometry. If for any reason the screening cannot be done with GSC II, the observer is responsible for providing the required photometry. In the case of moving targets, STScI will identify “safe” fields, and the observations will be scheduled accordingly. Observers will be updated on

the status of their observations by their Program Coordinators. We anticipate that bright-object considerations will not have a significant effect on the scheduling of such observations.

### **Policy on Observations Which Fail Because they Exceed Bright-Object Limits**

If your source passes screening, but causes the automatic flight checking to shutter your exposures or shut down the detector voltage causing the loss of your observing time, *then that lost time will not be returned to you*; it is the observer's responsibility to ensure that observations do not exceed the bright-object limits.

## **7.5.5 What To Do If Your Source is Too Bright for Your Chosen Configuration?**

If your source is too bright, there may be no way of performing the observation with the SBC. The SBC has no neutral-density filters and only low resolution prism dispersing modes. The options open to you if your source count rate is too high in a given configuration include:

- Change configurations totally to observe a different portion of the spectrum of your target (e.g., switching to the CCD).
- Attempt to locate an equivalent but less bright target.

## **7.5.6 Bright-Object Protection for Solar System Observations**

Observations of planets with ACS require particularly careful planning due to the very stringent overlight limits of the SBC. In principle Table 7.7 and Table 7.8 can be used to determine if a particular observation of a solar-system target exceeds the safety limit. In practice the simplest and most straightforward method of checking the bright object limits for a particular observation is to use the ACS Exposure-Time Calculator. With a user-supplied input spectrum, or assumptions about the spectral energy distribution of the target, the ETC will determine whether a specified observation violates any bright object limits.

Generally speaking, for small ( $< \sim 0.5$ – $1$  arcsec) solar-system objects the local count rate limit is the more restrictive constraint, while for large objects ( $> \sim 1$ – $2$  arcsec) the global limit is much more restrictive.

As a first approximation, small solar system targets can be regarded as point sources with a solar (G2V) spectrum, and if the V magnitude is known, Figure 7.7 and Table 7.8 can be used to estimate whether an observation with a particular ACS prism or filter is near the bright-object limits. V magnitudes for the most common solar-system targets (all planets

and satellites, and the principal minor planets) can be found in the *Astronomical Almanac*. This approximation should provide a conservative estimate, particularly for the local limit, because it is equivalent to assuming that all the flux from the target falls on a single pixel, which is an overestimate, and because the albedos of solar-system objects in the UV are almost always significantly less than their values in the visible part of the spectrum (meaning that the flux of the object will be less than that of the assumed solar spectrum at UV wavelengths where the bright-object limits apply). A very conservative estimate of the global count rate can be obtained by estimating the peak (local) count rate assuming all the flux falls on one pixel, and then multiplying by the number of pixels subtended by the target. If these simple estimates produce numbers near the bright-object limits, more sophisticated estimates may be required to provide assurance that the object is not too bright to observe in a particular configuration.

For large solar-system targets, checking of the bright-object limits is most conveniently done by converting the integrated V magnitude ( $V_0$ , which can be found in the *Astronomical Almanac*) to V magnitude/arcsec<sup>2</sup> as follows:

$$V/(\text{arcsec}^2) = V_0 - 2.5 \log(1/\text{area})$$

where *area* is the area of the target in arcsec<sup>2</sup>. This  $V / \text{arcsec}^2$  and the diameter of the target in arcsec can then be input into the ETC (choose the Kurucz model G2 V spectrum for the spectral energy distribution) to test whether the bright-object limits can be satisfied.



# Observing Techniques

In this chapter . . .

8.1 Operating Modes / 157
8.2 Patterns and Dithering / 162
8.3 A Road Map for Optimizing Observations / 165
8.4 CCD Gain Selection / 168
8.5 ACS Apertures / 169
8.6 Fixing Orientation on the Sky / 177
8.7 Parallel Observations / 181
8.8 Two-Gyro Guiding / 186

In this Chapter we describe how to carry out observations with the ACS. We include a description of the operating modes, some suggestions on how to split exposures for cosmic ray rejection and a description of the use of subarrays and dithering patterns.

---

## 8.1 Operating Modes

ACS supports two types of operating modes:

- ACCUM for each of the cameras. This is the standard data taking mode and it is the one most generally used by observers.
- ACQ (acquisition). This is the mode used to acquire a target for coronagraphic observations. ACQ is only available on the HRC.

### 8.1.1 WFC ACCUM Mode

In this mode the WFC CCD accumulates signal during the exposure in response to photons. The charge is read out at the end of the exposure and translated by the A-to-D converter into a 16 bit data number (DN, ranging from 0 to 65,535). The number of electrons per DN can be specified by the user as the GAIN value. The full well of the WFC CCD is about 85,000 electrons and consequently all GAIN values larger than 1 will allow the observer to count up to the full well capacity. For GAIN=1 only 75% of full well capacity is reached when the DN value saturates at 65,535. The read-out noise of the WFC CCD is about 5 electrons rms and thus it is critically sampled even at GAIN=2. WFC can make use of a user-transparent, lossless, on-board compression algorithm, the benefits of which will be discussed in the context of parallel observations. The algorithm is more effective with higher GAIN values, i.e. when the noise is undersampled.

A total of nine supported apertures are accessible to WFC users. WFC1-FIX and WFC2-FIX select the geometric centers of the two WFC camera chips. The WFCENTER corresponds to the geometric center of the combined WFC field and will be useful for facilitating mosaics and obtaining observations at multiple orientations. WFC, WFC1 and WFC2 are approximately located near the field of view center and the centers of chips 1 and 2, respectively. Their locations were chosen to be free of detector blemishes and hot pixels and they are the preferred apertures for typical observations. See Section 8.5 for more details about ACS apertures, including the subarray apertures.

Usually each CCD is read from two amplifiers to minimize Charge Transfer Efficiency (CTE) problems and minimize read-out time. As a result the two 2k by 2k portions in a single chip may have slightly different read-out noise. The WFC chips have both physical and virtual overscan which can be used to estimate the bias level and the read-out noise on each single image.

The ACS internal buffer can only store a single full frame WFC image. When this image is compressed, and depending on the compression factor, the buffer can store a number of additional HRC and SBC images. As a consequence of the implementation of the compression strategy, under no circumstance can more than one full frame WFC image be stored in the buffer. Note also that the adopted policy is not to compress primary WFC observations. The present flight software does not allow reading an ACS frame directly into the HST on-board recorder. Images have to be first stored in the internal buffer. When more than one WFC image is obtained during an orbit a buffer dump must occur during the visibility period so as to create space in the buffer for a new WFC image. If each exposure is longer than approximately 339 seconds, buffer dumps can occur during the integration of the following image with no impact on observing efficiency. Conversely, short, full frame, integrations with the WFC during the same

orbit will cause buffer dumps to be interleaved with observations and will negatively affect the observing efficiency. See Chapter 9, *Overheads and Orbit-Time Determination*, for more details about ACS overheads.

### WFC CCD Subarrays

It is possible to read-out only a portion of a detector thus obtaining a subarray which has a smaller size than the full frame. Subarrays are mostly useful to reduce the data volume, to store more frames in the internal buffer (thus avoiding the efficiency loss due to buffer dumps), or to read only the relevant portion of the detector when imaging with ramp filters or with HRC filters (which produce a vignetted field of view on WFC). WFC subarrays have some limitations:

1. they can be specified only on a single WFC chip;
2. they may have physical but no virtual overscan;
3. they cannot include the CCD edge (i.e. the maximum subarray size is 4140 by 2046); and
4. they are read through a single amplifier and may take longer to read-out than a full-frame image, depending on size and location.

Users can utilize WFC subarrays either by using a supported pre-defined subarray (which is recommended) or by defining their own general subarrays. For supported subarrays, the dark, flat and bias frames used for calibration will simply be extracted from available full-frame images. Tests have shown that this does not degrade the quality of the dark, flat-field or bias corrections, as compared to full-frame data. However, this is true only for subarrays that fall entirely within a single amplifier quadrant (true for all the supported subarrays). Users who define general subarrays that cross amplifier boundaries (not advised) must request their own subarray bias images and these will typically be scheduled during the following occultation. In some special cases where a general subarray is cleverly defined so as to include a physical overscan region, no separate bias frames are needed.

Pre-defined subarrays are the appropriate choice for observing a small target; when lessening the data volume is desired. These supported subarrays for WFC are invoked by using the named apertures WFC1-1K, WFC1-2K, and WFC1-512. On WFC1, at the amplifier B corner there are square apertures WFC1-512, WFC1-1K, and WFC1-2K with light collecting areas being squares with sides of length 512, 1024 and 2048 pixels. A 2048 pixel aperture is available at the amplifier D corner of WFC2 called WFC2-2K, but is available-but-unsupported. These all incorporate 22 columns of the physical overscan pixels. These have been chosen bearing in mind that as charge transfer efficiency degrades with radiation damage to the detectors, there is an advantage in being close to

the readout amplifier. The reference pixel and extent of the subarrays are listed in Table 8.1.

To define a general subarray, the available-but-unsupported parameters `SIZEAXIS1`, `SIZEAXIS2`, `CENTERAXIS1`, and `CENTERAXIS2` can be used. More practical information about defining subarrays can be found at <http://www.stsci.edu/hst/acs/faqs/subarrays.html>. When polarizers or the small HRC filter F892N is used with the WFC, the aperture WFC must be selected and a subarray is forced by the system. If the user chooses to use a polarizer with a ramp filter, then they may select an available-but-unsupported ramp aperture but a subarray is still read out.

### Ramp Filters

Unlike WFPC2, ACS ramp filter observations at different wavelengths are obtained at the same location on the CCD, thus simplifying data processing in, e.g., continuum subtraction of emission line data. In practice the observer specifies a ramp filter and a central wavelength; the filter wheel is automatically rotated to place the central wavelength at the reference point of the relevant aperture. The different ramp apertures and their reference points on the WFC chip are shown in Table 8.1 and Figure 8.3. To select the desired wavelength, the ramp filter is rotated to move the appropriate part of the filter over the specified pointing. Observations with different ramp filters do not generally occur at the same pointing. The precise location where a given observation will be performed can be found from Table 8.1 where for each ramp filter we list the fiducial pointing for the inner IRAMP, middle MRAMP, and outer ORAMP filter segment. The inner segment corresponds to the WFC1 chip, while the outer to the WFC2 chip. The middle segment can be used with either of the WFC chips but is used by default with WFC1. For any ramp filter observation three ramp filters will end up in the FOV even though the target is properly positioned only for the requested one. Or, if desired, the user can define a general subarray to readout only a portion of the chip. Table 4.1 and Table 4.2 can be used to determine the remaining two ramp filters which can be of interest for serendipitous observations. While all fifteen ramp filters can be used with the WFC, over specified regions of the WFC1 and WFC2 chips, only the five middle ramp filters are available with the HRC and they cover the region over the HRC chip defined by the HRC aperture (Table 8.2).

## 8.1.2 HRC ACCUM Mode

In this mode the HRC CCD accumulates signal during the exposure in response to photons. The charge is read out at the end of the exposure and translated by the A-to-D converter into a 16 bit data number (DN, ranging from 0 to 65,535). The number of electrons per DN can be specified by the user as the `GAIN` value. The full well of the HRC CCD is about 155,000 electrons. As a consequence, in order not to overflow the 16-bit pixel word

size, one needs to use  $GAIN=4$ . In many applications  $GAIN=2$  is adequate since it still allows critical sampling of the read-out noise of HRC (about 4.7 electrons rms) and for this reason it has been chosen as the default  $GAIN$  ratio. For typical HRC observations the observer should specify the HRC aperture which is approximately located at the center of the field of view in a location free of detector blemishes and hot pixels. The HRC-FIX aperture is located at the geometric center of the field-of-view. Additional apertures are used for coronagraphic observations - see Table 8.3 for more details of HRC apertures.

Up to 16 HRC images can be stored in the ACS buffer. Alternatively, HRC images can share the buffer with some SBC images and/or a single compressed WFC image. The number of HRC images will depend in the latter case on the WFC compression factor.

### **HRC CCD Subarrays**

Similarly to the WFC, a subarray is obtained when only a portion of the detector is read-out and transmitted to the ground. Generally the smaller size of the HRC CCD reduces the usefulness of subarrays. However, subarrays are used during on-board coronagraphic target acquisition which is similar to the STIS target acquisition and cannot be changed. A square subarray of 512x512 pixels in the C Amp readout corner, and a 512 pixel square aperture centered on the 1.8" coronagraphic spot are available. In addition, on an available-but-unsupported basis, nearly arbitrary sizes and locations for subarrays can be specified. When coupling use of subarrays with PATTERNS or POS TARGS the issue arises of whether to keep the subarray fixed in pixel space or have it track and stay centered on the target. With PATTERNS, the subarray stays fixed in pixel space. When using (Phase II terminology) POS TARGS, the observer can decide which mode to adopt.

### **8.1.3 SBC ACCUM Mode**

The SBC ACCUM mode accumulates photons into a 1024 by 1024 array, 16 bits per pixel. At the end of the exposure the data are sent to the onboard recorder via the internal ACS memory buffer. The high-res mode used in the STIS MAMAs is not available for the SBC. Note that ACCUM is the only mode available for SBC observations since the Time Tag mode of STIS is also not available on ACS. The minimum SBC exposure time is 0.1 seconds and the maximum 1.0 hours. The minimum time between SBC exposures is 40 seconds. Note that the SBC, like the STIS MAMAs, has no read-out noise. As a consequence there is no scientific driver for longer exposure times apart from the small overhead between successive images, described in Section 9.2.

Up to 17 SBC images can be stored in the internal buffer. SBC images can also share the buffer with HRC images and/or a single, compressed WFC image.

### 8.1.4 HRC ACQ Mode

The HRC target acquisition mode is used to place a target under the occulting finger or the coronagraphic mask. Observations through two (non-polarizer) filters are allowed in ACQ images to cut down the flux to acceptable levels for very bright targets. Due to the optical design of HRC the simultaneous use of two filters leads to a degraded imaging quality which is however still acceptable for a successful target acquisition. The ACS IDT has identified a number of filter combinations that effectively act as neutral density filters and allow the observer to acquire a very bright target that would otherwise saturate the CCD. These filter pairs are F220W+F606W, F220W+F550M and F220W+F502N in order of decreasing transmission. A more complete description of the Target Acquisition procedure is given in Section 5.2.2.

---

## 8.2 Patterns and Dithering

A number of different patterns are available for ACS to support dithered observations, i.e., observations where the pointing is shifted between frames. The size of the offsets can be very different depending on the purpose of offsetting the pointing between exposures. In particular, it is useful to distinguish between *mosaicing* and *dithering*. Mosaicing is done with the aim of increasing the area covered by a particular set of exposures, while providing a seamless joining of contiguous frames. Dithering is done for a variety of goals, namely

- better removal of detector blemishes
- straightforward removal of hot pixels
- improving the PSF sampling
- improving the photometric accuracy by averaging over flat fielding errors
- obtaining a contiguous field of view for the WFC.

Patterns have been defined to allow ACS users to easily carry out both mosaicing and dithering. Using patterns allows exposures to be automatically associated in **CALACS** pipeline processing with the following restrictions: only pattern exposures obtained within a single visit and those patterns where the cumulative offset is under the  $\sim 100$  arcsec

guide star limitation can be associated. For the latter, these patterns include the dither patterns for all three cameras, the HRC and SBC mosaic patterns and the 2-point ACS-WFC-MOSAIC-LINE pattern. All patterns designed with POS TARGs will not be associated. These are described in detail on the ACS Dither web page: <http://www.stsci.edu/hst/acs/proposing/dither>.

The plate scale for the WFC varies by about  $\pm 5\%$ , and so a one pixel dither near the center will be 0.95 or 1.05 pixels near the corners. For this reason, dither patterns should strike a balance between being large enough to reject detector artifacts, and being as compact as possible to maintain the integrity of the pattern over the entire field-of-view. Large displacements will have varying sub-pixel properties across the image.

In addition to the plate scale variation associated with the significant ACS geometric distortion, there can also be a temporal variation of overall image alignment. Some CR-SPLIT images taken during SMOV testing, in which the two components were separated by the scheduling system across orbital occultations (about one hour gap), showed registration differences of about 0.5 pixels corner-to-corner. Thus for programs that wish to combine multiple images to create oversampled images at the resolution ACS is capable of providing, the user may need to allow for the general problem of combining distorted, misregistered images. A variety of tools are being made available within STSDAS and **pyraf** to assist with these tasks including PyDrizzle and Multidrizzle. See the ACS Drizzle Web page and the ACS Data Handbook at:

<http://www.stsci.edu/hst/acs/analysis/drizzle>

### 8.2.1 How to Obtain Dithered Data

Whenever possible, observers should make use of the pre-defined mosaic and dither patterns. For WFC exposures requiring a contiguous field of view, offsets by 2.5 arcsec or more are required to cover the interchip gap. The STSDAS **Multidrizzle** package is the recommended software package for processing dithered observations. It includes tools for rejecting CR affected pixels from data sets with a single image at each pointing so that CR-SPLITting observations at each pointing is not necessary. **Multidrizzle** enhances and simplifies the functionality of the STSDAS dither package. The following are suggestions on the optimal number of exposures for a dithered data set:

- A minimum of 3 images are required to cover the WFC interchip gap (so that in the interchip region, the data allow for cosmic ray rejection).
- At least 2 images are always required for CR rejection. If dithering is performed it is not necessary to do a CR-SPLIT as well.

- For exposures filling one orbit the recommended minimum number of images for a good CR rejection is 3 for small dithers not bridging the gap and 4 for dithers bridging the gap.
- Programs attempting to optimize the PSF sampling are advised to use a 4 point box pattern.

Given the relatively low read-out noise and the high throughput of the WFC, broad-band optical images longer than about 500 seconds will be background limited.

## 8.2.2 Supported Patterns

As with the other instruments, a suite of carefully designed ACS dither and mosaic “convenience patterns” is available for Phase II proposers. The goals of these patterns are to accomplish the removal of detector features (including the WFC interchip gap), and provide sub-pixel PSF sampling (optimized for the number of dither points). Both `Line` and `Box` patterns are available for each detector, with designation `DITHER` or `MOSAIC` depending on the intended purpose of the pattern. Default parameters are available for these convenience patterns, although observers may override these and specify their own patterns if desired. Detailed description of the use of these patterns and the syntax to employ in developing a Phase II proposal may be found in the Phase II Proposal Instructions, and on the ACS Dither web page: <http://www.stsci.edu/hst/acs/proposing/dither>.

## 8.2.3 How to Combine Dithered Observations

Because of the nonlinear geometric distortion of ACS, a shift by an integer number of pixels at the chip center will not, in general, correlate to an integer shift at the edge. Therefore, simple shift-and-add schemes are inadequate for the proper combination of ACS dither exposures for all but the smallest shifts (e.g., the 2x2 “hot pixel” dither pattern). In the case of WFC the effect can be very significant since a shift by 50 pixels, as required to bridge the interchip gap, will be different by 2.5 pixels at the edge of the CCD, causing stars in different exposures not to be aligned across the FOV when a simple shift is applied to the images.

The STSDAS **dither** package contains tools which can be used to effectively combine dithered ACS images. These include the low-level IRAF tasks such as `drizzle` itself but also high-level (Python) scripts which automate the process to a large degree. These require that the user be running the Pyraf environment rather than the IRAF “`cl`”. For typical dithered ACS data the user will be able to use `MultiDrizzle` to combine datasets and simultaneously flag and ignore cosmic rays and other defects during the combination process. `MultiDrizzle` and `PyDrizzle`, which it uses

as an interface layer to drizzle and other tools, are described in detail in the Data Handbook.

The quality of final images which can be obtained from well dithered datasets is limited by the optical PSF, the pixel size and charge diffusion effects and any broadening introduced by the combination process. Appropriate dither patterns and careful combination allow the last of these factors to be kept to a minimum. Rules of thumb which may be used to estimate the final PSF width are given in Fruchter & Hook 2002, PASP, 114, 144.

### 8.2.4 How to Determine the Offsets

Within a single visit the commanded relative positions and the positions that are actually achieved are in very good agreement, often to better than  $0''.01$ . Thus within one visit the commanded offsets are usually a very good starting point for image combination. On occasion the guide star acquisition leads to a false lock. In this case, the commanded position can be incorrect even by  $0''.5$  or more. The jitter files allow the observer to track such false locks since they also contain information on the rms of the pointing, on the guide star separation and on the guide star separation rms. During false locks one or more of these indicators are normally anomalous. Across different visits the mismatch between commanded and achieved offsets can instead be significant. In these cases the offsets derived from the jitter files are better than the commanded ones, although they are only good to about  $0''.02$  rms. For accurate combination of images the recommended strategy is to derive the offsets from cross-correlation of the images themselves, or by using matched object catalogues derived from the images. The **dither** package includes software to carry out such cross-correlations.

---

## 8.3 A Road Map for Optimizing Observations

Dithering and CR-SPLITting more than the minimum recommended values tends to yield higher quality images with fewer residual detector defects, hot pixels or CR signatures in the final combined image. In cases where hot pixels are of particular concern, dithering may be especially useful for simultaneous removal of hot pixels and cosmic rays. Unfortunately, splitting a given exposure time into several exposures reduces its signal-to-noise when the image is read-out noise limited. WFC images taken through the broad band filters and longer than about 500 seconds are background limited, while shorter exposures and narrow band images are read-out noise limited for all practical exposure times. Thus, the optimal number of CR-splits and dithering positions is a result of a

trade-off between completeness of the hot pixel elimination, CR-rejection, final image quality, and optimal S/N. A schematic flow chart of this trade-off is given in Figure 8.1. The main steps in this, possibly iterative, process are the following:

1. determine the exposure time required to achieve the desired S/N
2. determine the maximum number of acceptable residual CR in the final combined image. This number depends critically on the scientific objective since, for example, a survey of distant galaxies or a globular cluster color magnitude diagram, a few residual CR will not compromise the scientific output of the observations. In contrast, a search for an optical counterpart of some radio or gamma ray selected object even one residual CR would not be acceptable over the region of interest. In this latter case, since we expect about 5 percent (range of ~4-7%) of the pixels to be affected by CR hits during a one orbit exposure on the WFC, the requirement that no pixel in the final image is affected by CR hits would force one to use at least 4 CR-SPLITS. For an experiment in which the number of allowed false alarms is zero, e.g. a search for cosmological supernovae, observers may wish to consider using a number of CR-SPLITS at least twice the number required to formally avoid coincidences. Note also that given the large number of pixels in the WFC even a few thousand residual CR hits would correspond to only a small fraction of the total number of pixels. In general, the number of pixels affected by coincident CR hits for a given total exposure time and number of CR-SPLITS  $N$  will be:

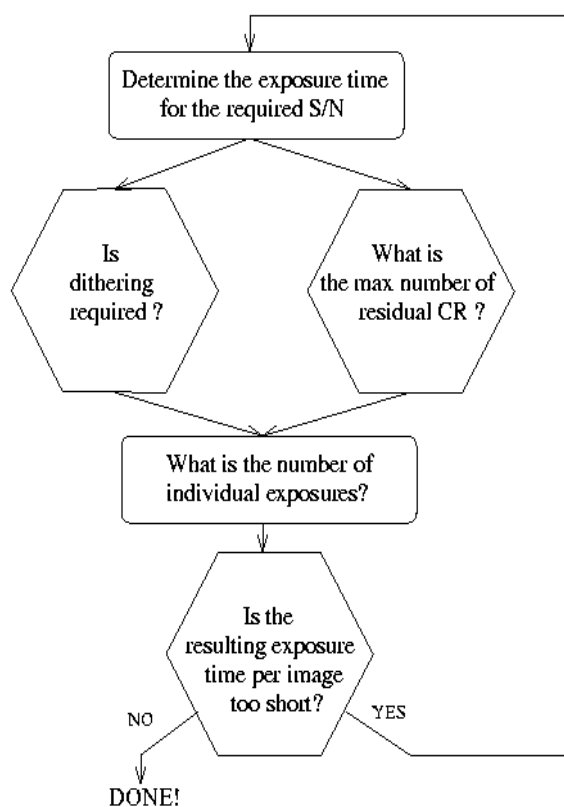
$$\left(0.05 \times \frac{\text{ExposureTime}}{2400s \times N}\right)^N \times 4096^2$$

3. determine whether dithering is required. CR-SPLITS of course have no effect on hot pixels which form due to CCD radiation damage and which persist for ~weeks or indefinitely. If such features would critically affect the science, then dithering is required to remove them. For some imaging programs the spatial resolution provided by the WFC and the presence of some detector defects and hot pixels in the final image are acceptable. For such observations dithering would not be required and one would simply split the exposure time for CR hit correction. For observations where several orbits worth of data are obtained with each filter the best strategy is to observe using a sub-pixel dither pattern *without* obtaining multiple images at each position. Since each CR hit will now influence more than one output pixel the requirement on the number of separate exposures is more stringent than in the simple CR-SPLIT case, but when 10 or more images (and a fast CPU with a lot of memory) are available one will obtain both a high image quality and a negligible number of residual

CR hits. If the total exposure time with each filter is short, one will have to compromise between S/N and image quality. In general, dithering with sub-pixel steps increases the number of individual exposures required to eliminate CR hits. Given that the geometric distortion of WFC makes any dithering step non-integer somewhere in the field of view (unless the dither steps are very small,  $<2$  pixels), the size of the high image quality field of view also comes into play. If the high quality area is small, one may make do with integer pixel dithers. In this case a few CR-SPLITS may be obtained at each dithering position and the combined images may then be combined together using **drizzle** or **MultiDrizzle**. On the edges of the field the CR-rejection quality will be lower than in the field center. A minimum number of 4 images for a two position dither and 8 for a four position dither is then required.

4. once the required number of individual exposures has been established on the basis of CR rejection and dithering requirements, the observer will need to verify whether the resulting read-out noise affects the achieved S/N.

Figure 8.1: Schematic flow-chart of the CR-split vs. dithering vs. S/N trade-off.



## 8.4 CCD Gain Selection

As quantified in Table 7.3 both the WFC and HRC CCDs have selectable gain values near 1, 2, 4, and 8 electrons per digital number. Various factors should influence the gain selected in Phase II for your science program: level of support and calibrations provided, influence of associated readout noise on data quality, dynamic range on the bright end, and for the WFC in limited applications data compressibility.

### 8.4.1 WFC Gain

GAINS 1 and 2 are fully supported for the WFC, since GAIN=1 provides the smallest readout noise, while GAIN=2 (or above) is needed to sample the available full well depth. It is the goal, now closely achieved, to provide equal calibration support for data taken in these two supported gains, although more calibration data will be taken in the default GAIN=1 setting. Calibration support will not be provided for the “available-but-unsupported” GAIN=4 and 8 settings; users proposing their use should provide special justification and discussion of calibrations to be used. Note that WFC auto-parallel data is taken with GAIN=2.

While the readout noise is lower at GAIN=1, the advantage over GAIN=2 ( $< 0.3$  e<sup>-</sup> extra rms) is modest. GAIN=2 has the offsetting advantage of completely sampling the full well depth of nearly 85,000 e<sup>-</sup> thus providing a  $> 0.3$  magnitude dynamic range extension before saturation is reached. The latter could be advantageous even for programs in which the prime targets are very faint, if serendipitous objects in the field of view can be used to support image-to-image registration solutions as needed for optimal dithered image combinations. Furthermore, charge is conserved even beyond filling the full well depth, for point sources at GAIN=2 it is possible to obtain valid aperture photometry several magnitudes beyond saturation by summing over all pixels bled into. Both GAINS 1 and 2 provide better than critical sampling of the readout noise supporting robust background sky-level determination even at low values. Recent evidence also suggests that a minor electronic cross-talk feature is relatively less pronounced with GAIN=2, then the default GAIN=1.

The large pixel count for WFC can create data rate problems if images are acquired as quickly as possible over multiple orbits. The available-but-unsupported mode COMPRESSION is more effective when the noise is undersampled which could result in special circumstances for which the GAIN values of 4 or 8 are preferred.

### 8.4.2 HRC Gain

GAINS 2 and 4 are fully supported for the HRC, and analogous to the supported WFC values provide a low readout noise case and a GAIN that provides sampling of the physical full well depth.

GAIN = 4 on the HRC, which is needed if high dynamic range on the bright end is desired, does not provide critical sampling of the readout noise. Not only is the readout noise penalty in going from GAIN = 2 to 4 non-trivial, but background estimation will be less robust without critical noise sampling. As with WFC, when the full well depth is sampled with GAIN = 4 the detector response remains accurately linear up to and even well beyond saturation. Compression is not an issue for the small HRC images, therefore rationales for use of the unsupported GAIN = 8 are not anticipated. GAIN = 1 is available-but-unsupported, but the very modest improvement of readout noise in comparison to GAIN = 2 ( $< 0.2$  e- higher rms) seems unlikely to present compelling need for its use.

---

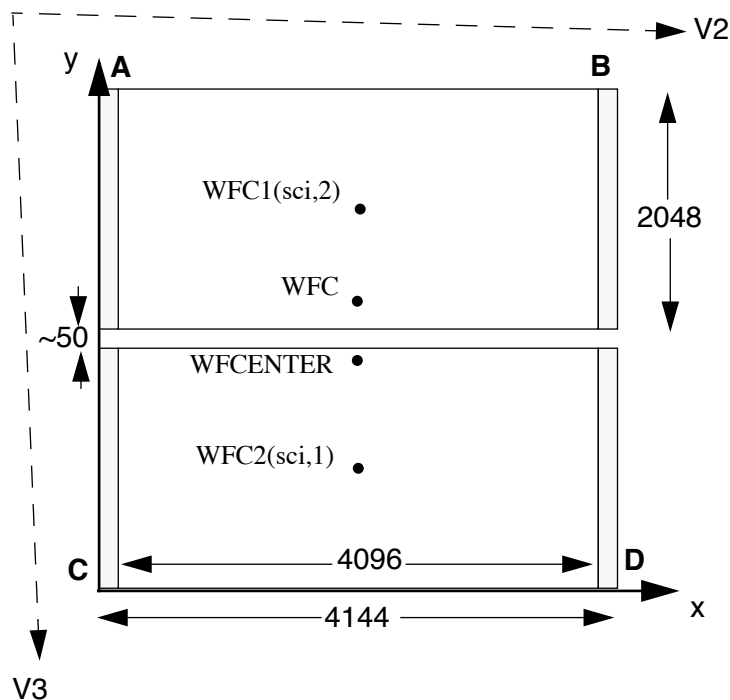
## 8.5 ACS Apertures

As discussed in Section 3.2, the ACS consists of three cameras: the WFC, the HRC and the SBC. The WFC is constructed of two CCDs each nominally 2048 by 4096 pixels, with their long sides adjacent to form a roughly square array, 4096 pixels on a side. The HRC CCD and the SBC MAMA detectors are each 1024 pixels square.

### 8.5.1 WFC Apertures

The active image area of each WFC detector is 4096 by 2048. The mean scale is 0.049 arcsec/pixel and the combined detectors cover an approximately square area of 202 arcseconds on a side. In establishing reference pixel positions we have to consider the overscan pixel areas which extend 24 pixels beyond the edges in the long direction. So each CCD must be regarded as a 4144 by 2048 pixel area. The gap between the two CCDs is equivalent to 50 pixels. In Figure 8.2 the letters A, B, C and D show the corner locations of the four readout amps.

Figure 8.2: WFC Aperture Definitions



We define apertures named WFC1 and WFC2 which represent the two CCDs, with their reference points at the geometric center of each chip, at pixel positions (2072,1024). If the appearance of new hot pixels makes these apertures undesirable, we will define new reference positions nearby. However, we keep two other apertures named WFC1-FIX and WFC2-FIX at the original central locations. For extended sources, choosing new positions may not be of any advantage and it may be more effective to use these fixed positions.

The aperture WFC encompasses both detectors and has its reference point near the overall center but about 10 arcsec away from the interchip gap. This has been chosen to be position (2072,200) on the WFC1 CCD. Again, this is the initial selection for the aperture named WFC which might be shifted later, but the reference point for WFC-FIX will remain at this value. Selection of WFC1, WFC2 or WFC only changes the pixel where the target will be positioned. In all three cases data is normally delivered in a file containing two imsets, one for each detector. See Section 11.1 for details of the ACS data format. Reading out a subarray, which consists of part of only one of the chips, is done only if requested.

WFCENTER is similar to WFC, but is placed at the center of the combined WFC full field. The center is defined as the average of the four corners in the distortion corrected space. Because of the scale variation this does not appear at the center in pixel space, but rather is on WFC2 about 20 pixels from the edge. Selection of WFCENTER can be of use in obtaining

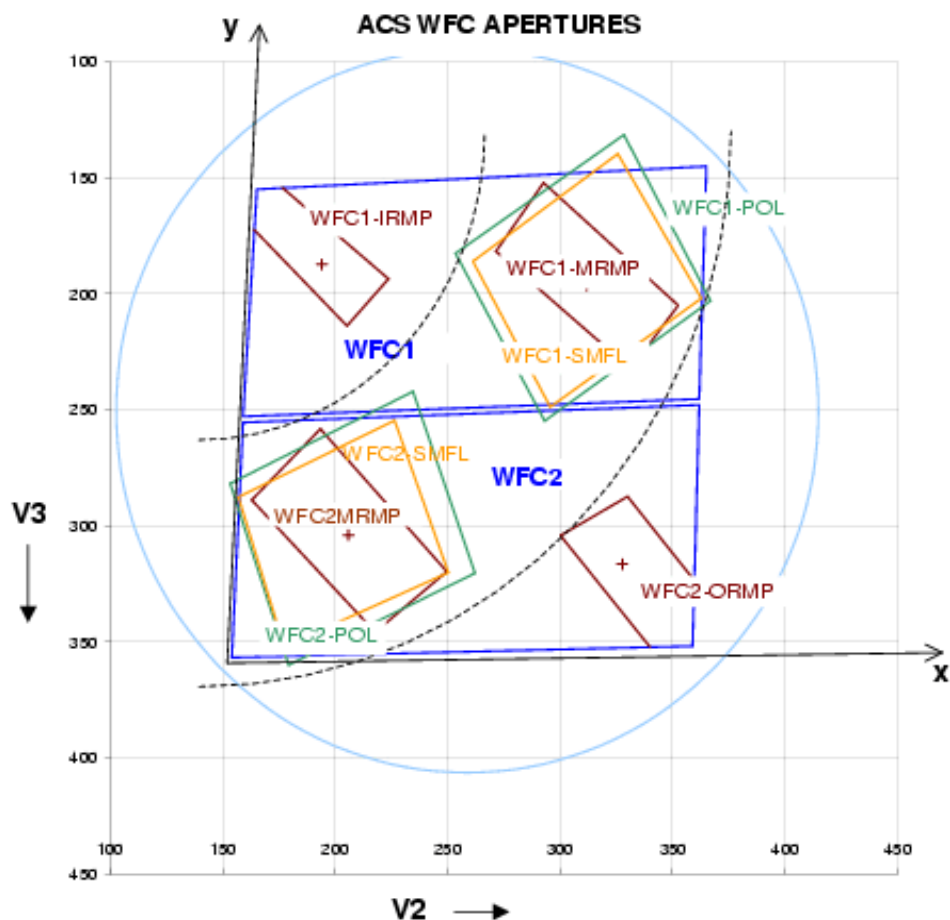
observations with maximum overlap at unique orientations and for mosaics.

For sets of observations which take place over a substantial part of a year, the telescope roll limitations will require measurements to be taken over most of the angular range. On sky, the WFC aperture is roughly square and it is natural to design observations in steps of 90 degrees to consistently cover the same area. There will be some region at the edges not covered at all four orientations. However, a square area of side 194.8 arcseconds centered on WFCENTER, and with edges parallel to the V2 and V3 axes, is overlapped at all four positions. In designing a mosaic which combines observations at 90 degree steps, a translation of about 190 arcseconds between pointings would provide continuous coverage.

### 8.5.2 Ramp Filter Apertures

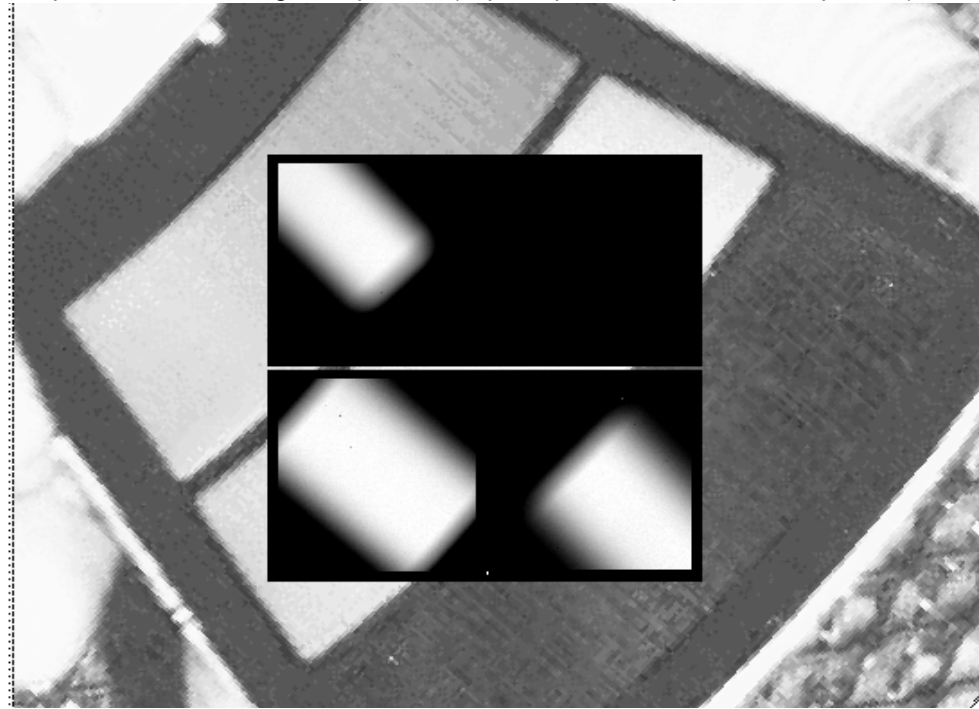
Each ramp filter consists of three segments that can be rotated across the WFC field of view as indicated in Figure 8.3. The IRAMP filter can only be placed on WFC1 in a location which will define the aperture *WFC1-IRAMP* and the ORAMP only on WFC2 creating the aperture *WFC2-ORAMP*. The MRAMP filter can lie on WFC1 or WFC2 with corresponding apertures *WFC1-MRAMP* and *WFC2-MRAMP*. The approximate aperture locations are indicated in Figure 8.3, while actual data obtained during ground calibrations are overlayed on an image of a ramp filter in Figure 8.4. Operationally, a fixed reference point will be defined for each detector and filter combination. Then the ramp filter will be rotated to place the required wavelength at the reference position.

Figure 8.3: Schematic WFC apertures and Ramp Filters - Shown are the approximate active areas defined by the filters. The actual readout areas are the quadrants for the polarizers and small (HRC) filters and the full chip for the ramp filters.



The reference positions for all defined apertures are given in Table 8.1 in pixels and in the telescope V2,V3 reference frame, where values are measured in arcseconds. The values given here are based on in-flight calibration results. The x and y axis angles are measured in degrees from the V3 axis towards the V2 axis. This is in the same sense as measuring from North to East on the sky. The “extent” of the ramp filter apertures given in Table 8.1 are the FWHM of the monochromatic patches (visible in Figure 8.4) measured from a small sample of ground calibration data. To use a ramp filter in a Phase II program, specify the filter name and the wavelength, and choose aperture “WFC”. The scheduling software will then automatically rotate the filter to the appropriate wavelength, and point at the reference point of the aperture that is associated with the chosen filter (e.g., WFC2-ORAMP, if an ORAMP filter has been chosen). The specific aperture names WFC1-IRAMP, WFC2-ORAMP, WFC1-MRAMP and WFC2-MRAMP should not generally be listed explicitly in a Phase II program, but they are accessible as “available-but-unsupported” choices (see Section 2.5).

Figure 8.4: Monochromatic patches in ground calibration data showing actual aperture sizes through ramp filters (superimposed on photo of ramp filters).



### 8.5.3 The Small Filter Apertures

When a filter designed for the HRC is used on the WFC, it only covers a small area on either WFC1 or WFC2. The projected filter position may be placed on either chip by selection of the filter wheel setting. Figure 8.3 shows how the filter projection may be placed so as to avoid the borders of the chips. The apertures `WFC1_SMFL` and `WFC2_SMFL` are defined for this purpose and are automatically assigned when a WFC observation is proposed using an HRC filter. Reference positions at or near the center of these apertures are defined so that a target may be placed in the region covered by the chosen filter.

The axis angles given in Table 8.1 do not refer to the edges of the apertures as drawn, but rather to the orientation of the x and y axes at the WFC reference pixel. These angles vary slightly with position due to geometric distortion.

For the polarizers and F892n used with WFC, the default will be to read out a subarray. The subarray will be a rectangular area with sides parallel to the detector edges which encompasses the indicated filtered areas. For ramp filters the default will be to readout the entire WFC detector, unless a polarizer is used with the ramp filter, in which case a subarray is readout. Users cannot override the small filter subarrays.

Table 8.1: WFC Aperture Parameters

Aperture Name readout area	Extent (arcsec)	Reference pixel	Reference V2,V3 (arcsec)	x-axis angle (degrees from V3 through V2)	y-axis angle
WFC 4096 × 4096	202 × 202	(2072,200) <i>on WFC1</i>	(259,239)	92.2	177.5
WFCENTER 4096 × 4096	202 × 202	(2114,2029) <i>on WFC2</i>	(261,252)	92.1	177.5
WFC1 4096 × 4096	202 × 202	(2072, 1024)	(261,198)	92.5	177.4
WFC1-FIX 4096 × 4096	202 × 202	(2072, 1024)	(261,198)	92.5	177.4
WFC2 4096 × 4096	202 × 202	(2072, 1024)	(257,302)	91.7	177.8
WFC2-FIX 4096 × 4096	202 × 202	(2072, 1024)	(257,302)	91.7	177.8
WFC1-IRAMP 4096 × 4096	25 × 65	(680,1325)	(194,187)	93.1	176.6
WFC1-MRAMP 4096 × 4096	35 × 80	(3096,1024)	(312,196)	92.2	177.8
WFC2-MRAMP 4096 × 4096	40 × 80	(1048,1024)	(206,304)	91.9	177.5
WFC2-ORAMP 4096 × 4096	35 × 65	(3494,708)	(328,316)	91.4	178.2
WFC1-SMFL 2048 × 2048	70 × 80	(3096,1024)	(312,196)	92.2	177.8
WFC2-SMFL 2048 × 2048	70 × 80	(1048,1024)	(206,304)	91.9	177.5
WFC1-POL0UV 2048 × 2048	90 × 80	(3096,1024)	(312,196)	92.1	177.8
WFC1-POL0V 2048 × 2048	90 × 80	(3096,1024)	(312,196)	92.2	177.8
WFC2-POL0UV 2048 × 2048	90 × 80	(1048,1024)	(206,304)	91.9	177.5
WFC2-POL0V 2048 × 2048	90 × 80	(1048,1024)	(206,304)	91.9	177.5
WFC1-512 512 × 512	25 × 25	(3864,1792)	(352,158)	92.1	178.0
WFC1-1K 1024 × 1024	50 × 50	(3608,1536)	(338,170)	92.1	177.9
WFC1-2K 2048 × 2048	101 × 101	(3096,1024)	(312,196)	92.2	177.8
WFC2-2K 2048 × 2048	101 × 101	(1048,1024)	(206,304)	91.9	177.5

### 8.5.4 Polarizer Apertures

Apertures have been provided for use with the polarizer sets similar to the SMFL apertures. These apertures are selected automatically when a polarizing spectral element is used, and a single WFC chip quadrant readout is obtained. The aperture parameters given in Table 8.1 are valid for all three polarizing filters in each polarizer set, UV or visible, to the stated significant figures.

### 8.5.5 HRC Apertures

The HRC has an area of 1062 by 1024 including 19 physical overscan pixels at each end in the x direction. The active area is 1024 by 1024 pixels. The mean scales along the x and y directions are 0.028 and 0.025 arcseconds/pixel, thus providing a field of view of about 29 by 26 arcseconds in extent. The anisotropy and variation of scales is discussed in a later section of this handbook. The reference point for the aperture labelled HRC-FIX, and initially for HRC, is at the geometric center, (531,512). As with the WFC apertures, there may be reason to move the HRC reference point later.

The HRC is equipped with two coronagraphic spots, nominally 1.8 and 3.0 arcseconds in diameter and a coronagraphic finger, 0.8 arcseconds in width. Apertures HRC-CORON1.8, HRC-CORON3.0 and HRC-OCCULT0.8 are defined to correspond to these features. In addition we define a target acquisition aperture, HRC-ACQ designed for acquiring targets which are subsequently automatically placed behind a coronagraphic spot or the occultation finger. The positions of the coronagraphic spots have been found to fluctuate. Observations will need to incorporate a USE OFFSET special requirement to allow current values to be inserted at the time of the observation (see the Phase II Proposal Instructions).

A substantial region masked out by the occulting finger can be present in the HRC data (Figure 8.5). The occulting finger is not retractable -- it will be in every HRC exposure. However as with any other detector feature or artifact, the "lost" data can be recovered by combining exposures which were suitably shifted with respect to each other. A dither pattern, ACS-HRC-DITHER-LINE has been defined for this purpose and spans the area flagged for the HRC occulting finger (~1.6 arcsec or ~56 pixels wide), with an extra ~0.3 arcsec or ~10 pixels of overlap. More details can be found in the Phase II Instructions Handbook.

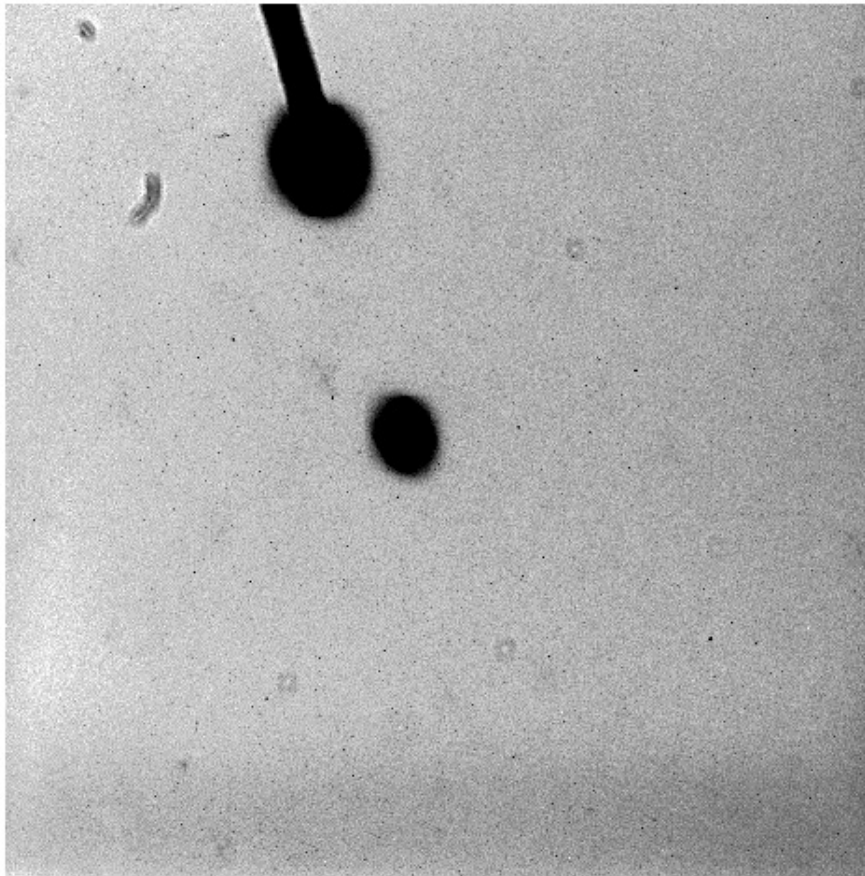
### 8.5.6 SBC Apertures

The SBC aperture is 1024 pixel square. There are no overscan pixels to consider. The x and y scales are 0.034 and 0.030 arcseconds/pixel leading to a coverage on the sky of 35 by 31 arcseconds. The reference point will initially be at (512,512). As with the CCDs we will maintain an SBC-FIX

aperture which will always have this same position even if SBC has to be altered. MAMA detectors slowly lose efficiency with each exposure, therefore the SBC reference point may be shifted if the initial position shows this effect to a measurable degree.

The (512,512) reference point falls at the same position in (V2,V3) as the HRC, namely (207, 471) and the x and y axis angles are -83.9 and 0.4 degrees.

Figure 8.5: HRC Coronagraphic finger and spots



The HRC aperture parameters are summarized in the following table.

Table 8.2: HRC Aperture Parameters

Aperture Name active area	Extent (arcsec)	Reference pixel	Reference V2,V3 (arcsec)	x-axis angle	y-axis angle
HRC 1024 × 1024	29 × 26	(531, 512)	(206,472)	-84.1	0.1
HRC-FIX 1024 × 1024	29 × 26	(531, 512)	(206,472)	-84.1	0.1
HRC-CORON1.8 200 × 200	6 × 5	(564,466) <sup>1</sup>	(205,471) <sup>1</sup>	-84.1	0.1
HRC-CORON3.0 200 × 200	6 × 5	(467,794) <sup>1</sup>	(208,479) <sup>1</sup>	-84.2	0.1
HRC-OCCULT0.8 200 × 200	6 × 5	(443,791)	(209,477)	-84.2	0.2
HRC-ACQ 200 × 200	6 × 5	(735,575)	(200,474)	-84.1	0.0
HRC-512 512 × 512	15 × 13	(276,256)	(214,465)	-84.1	0.2
HRC-SUB1.8 512 × 512	15 × 13	(570,468)	(205,471)	-84.1	0.1

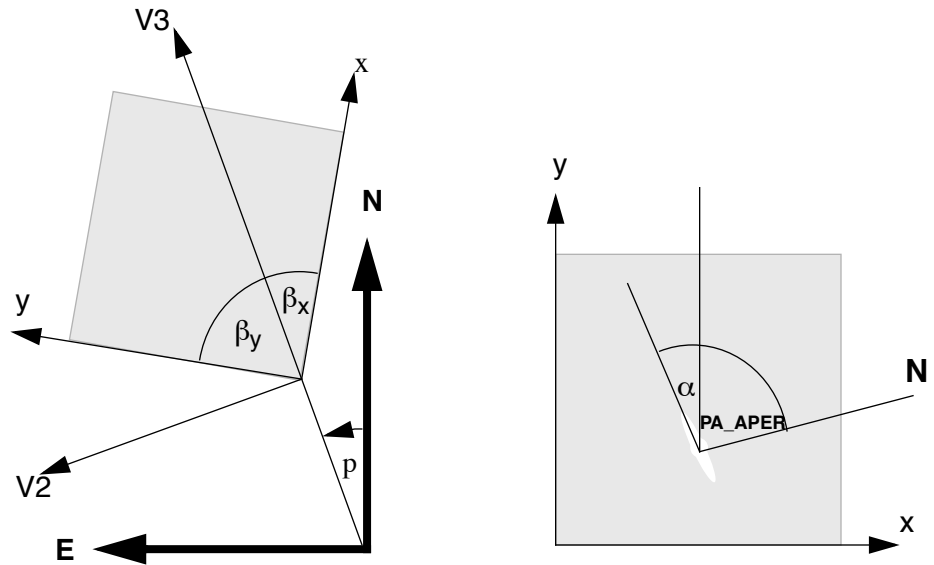
1. These values fluctuate and will be updated at the time of the observation.

## 8.6 Fixing Orientation on the Sky

Determining the orientation of an image requires knowledge of the telescope roll and the angle of the aperture relative to the telescope's coordinate frame. A target may need to be specially oriented on a detector, particularly when spectroscopy is to be performed.

All HST aperture positions and orientations are defined within an orthogonal coordinate system labelled V1,V2,V3, in which V1 is nominally along the telescope roll axis. Apertures are therefore in the V2,V3 plane. The V3 position angle  $p$  is defined as the angle of the projection of the V3 axis on the sky, measured from North towards East with the aperture denoting the origin. This is almost identical to the telescope roll angle. (There is a small difference between roll angles measured at the V1 axis and those measured at the aperture. This can amount to several tenths of a degree depending on the target declination.) When the position angle is zero, V3 points North and V2 points East. In the V2V3 coordinate system, aperture orientations are defined by  $\beta_x$  and  $\beta_y$ , the angles their x and y axes make with the V3 axis, measured in an anti-clockwise direction. (The value of  $\beta_x$  as illustrated would be considered negative.) Hence, the angles these axes make with North are found by adding the axis angles to the position angle.

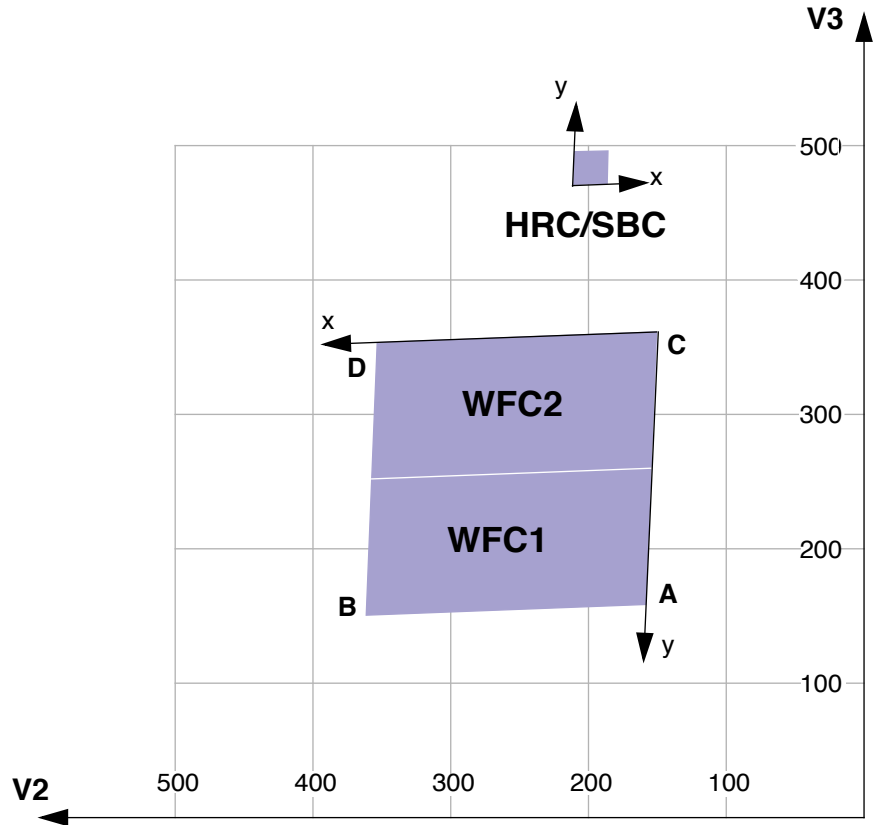
Figure 8.6: Aperture and image feature orientation



The science image header supplies the value of ORIENTAT, the angle the detector y axis makes with North, which is equal to  $p + \beta_y$ . Another angle keyword supplied is PA\_APER which is the angle the aperture y axis makes with North. Both angles are defined at the aperture so using them does not involve the displacement difference. Normally the aperture and detector y axes are parallel and so  $PA\_APER = ORIENTAT$ . Several STIS slit apertures were not aligned parallel to the detector axes and so this distinction was meaningful, but ACS has no slit apertures so this difference will probably not arise. In any case, we recommend to use PA\_APER.

Beyond establishing the direction of the aperture axes, it will often be required to know the orientation of a feature, such as the plane of a galaxy, within an image. Conversely, we need to know what direction within an image corresponds to North. To this end we define a feature angle  $\alpha$  within the aperture as measured on the science image, anti-clockwise from the y-axis so that it is in the same sense as the previously defined angles. For an orthogonal set of aperture axes the direction of this feature would be  $PA\_APER + \alpha$  and the image direction of North would be the value of  $\alpha$  which makes this angle zero, namely  $-PA\_APER$ , still measured in an anti-clockwise direction from the y axis.

Figure 8.7: ACS apertures in the V2/V3 reference frame. The readout amplifiers (A,B,C,D) are indicated on the figure. The WFC data products from the calibration pipeline will be oriented so that WFC1 (chip 1, which uses amps A and B) is on top. The HRC data products will also be oriented such that amps A and B are on top, but they will be inverted from WFC images with respect to the sky.



The  $x$  and  $y$  axes projected on the sky are not necessarily orthogonal. For all instruments prior to the ACS the departure from orthogonality has been negligible, but for the ACS the angle between the axes is about 85 degrees. Figure 8.7 realistically represents the alignment of the ACS apertures and shows that the apertures are not square. The  $x$  and  $y$  axes indicated are those that will be used for the science images. The  $V2, V3$  coordinates can be calculated from the  $x, y$  coordinates according to

$$V2 = V2_0 + s_x \sin \beta_x x + s_y \sin \beta_y y$$

$$V3 = V3_0 + s_x \cos \beta_x x + s_y \cos \beta_y y$$

where  $s_x$  and  $s_y$  are scales in arcsec per pixel along the image  $x$  and  $y$  axes.  $V2_0$  and  $V3_0$  are the coordinates of the aperture origin, but they do not enter into the angle calculations. Figure 8.7 shows that a rotation from  $x$  to  $y$  is in the opposite sense to a rotation from  $V2$  to  $V3$ . This will be the

arrangement for ACS apertures. This is significant in defining the sense of the rotation angles. For a direction specified by displacements  $\Delta x$  and  $\Delta y$  in the image, the angle  $\alpha$  is  $\arctan(-\Delta x/\Delta y)$ .

Because of the oblique coordinates, the angle  $\alpha_s$  on the sky will not be equal to  $\alpha$ . To calculate the sky angle, it is convenient to define another set of orthogonal axes  $x_s, y_s$ , similar to the V2V3 but rotated so that  $y_s$  lies along  $y$ , and  $x_s$  is approximately in the  $x$  direction. Let  $\omega = \beta_y - \beta_x$  be the angle between the projected detector axes and for simplicity let their origins be coincident. Then the transformation is

$$\begin{aligned}x_s &= s_x \sin \omega x \\y_s &= s_x \cos \omega x + s_y y\end{aligned}$$

By comparing differentials and defining  $\alpha_s$  as  $\arctan(-\Delta x_s/\Delta y_s)$  we find

$$\tan \alpha_s = \frac{s_x \sin \omega \sin \alpha}{s_y \cos \alpha - s_x \cos \omega \sin \alpha}$$

The equation as written will place the angle in the proper quadrant if the ATAN2 Fortran function or the IDL ATAN function is used. To get the true angle East of North, for a feature seen at angle  $\alpha$  in the image, calculate  $\alpha_s$  and add to PA\_APER.

The inverse relation is

$$\tan \alpha = \frac{s_y \sin \alpha_s}{s_x \sin(\alpha_s + \omega)}$$

To find the value of  $\alpha$  corresponding to North we need the value of  $\alpha_s$  such that  $\text{PA\_APER} + \alpha_s = 0$ . So substitute  $-\text{PA\_APER}$  for  $\alpha_s$  in the equation to get the angle  $\alpha$  in the image which corresponds to North. The values of the scales and axis angles for all instruments are maintained on an Observatory Science Group web page:

<http://www.stsci.edu/instruments/observatory/>

For the ACS apertures, the values in Table 8.3 have been derived from results of operating the ACS in the Refractive Aberrated Simulator. These should not be considered as true calibrations but they indicate some aperture features, such as the non-orthogonality of the aperture axes and the  $x$  and  $y$  scale differences for HRC and SBC.

Table 8.3: Plate scales and axis angles for the 3 ACS channels

	$s_x$	$s_y$	$\beta_x$	$\beta_y$	$\beta_y - \beta_x$
	arcsec/pixel		degrees		
WFC	.0494	.0494	92.2	177.5	85.3
HRC	.0284	.0248	-84.1	0.1	84.2
SBC	.0338	.0301	-85.4	-1.0	84.4

### 8.6.1 Determining Orientation for Phase II

A particular orientation is specified in an HST Phase II proposal using yet another coordinate system: U2,U3. These axes are opposite to V2 and V3, so, for example,  $U3 = -V3$ . The angle **ORIENT**, used in a Phase II proposal to specify a particular spacecraft orientation, is the position angle of U3 measured from North towards East. The direction of the V3 axis with respect to North is  $PA\_APER - \beta_y$  and so

$$ORIENT = PA\_APER - \beta_y \pm 180^\circ.$$

The IRAF task **rotate** in the package **images.geom** takes an image and rotates it counter-clockwise by a specified angle. To orient an image so that its y axis becomes North, the angle to specify is  $PA\_APER$ . The x axis will then point approximately 5 degrees North of East. Orients can be checked by using the Visual Target Tuner (VTT) in the APT.

---

## 8.7 Parallel Observations

### 8.7.1 Parallel Observing

Parallel observing allows HST to operate several instruments simultaneously, in addition to the instrument that executes the primary observations. While the primary instrument observes a fixed target at user-specified coordinates, the parallel instrument observes at coordinates 5 to 10 arcminutes away, depending on the parallel instrument. The HST field of view following SM3B (Figure 3.3 on page 30) shows the general locations of the instrument apertures adjacent to one another on the sky. Accurate relative positions for all instruments can be found on STScI's Observatory web page under "Pointing"<sup>1</sup>. The recommended method of determining the field of view for any instrument is the Visual Target Tuner (VTT). A Digital Sky Survey (or user supplied) image of the primary target area is displayed with an HST field of view overlay. Any desired coordinate and **ORIENT** combination for the primary target will then display the possible pointings of any instrument operated in parallel. If the primary exposure will execute at a known (absolute) orient, the VTT will display the exact field of view for any instrument executed in parallel. If the primary exposure will execute at a random (nominal) orient or range of orient values, the VTT allows the HST field-of-view to be rotated interactively about the primary pointing. The VTT can be an invaluable resource for parallel observing programs, especially those designed for or restricted to specific pointings for the parallel FOV.

---

1. Pointing page: <http://www.stsci.edu/instruments/observatory/taps.html>

Certain operating limits are in place to restrict use of configurations, modes, parameters, elements and requirements allowed for each instrument while used in parallel. Details on these limits are documented in the Cycle 14 *Call For Proposals*, Section 4.2: “Parallel Observations”. General information on ACS specific parallel operations are documented in the following sections for each of the three types of ACS parallel observing: coordinated, auto and pure.

### **ACS Coordinated Parallels**

Coordinated parallel observations are specified in the same Phase II observing program as the primary observations via the prime + parallel group containers in APT. A single ACS channel may be used for a coordinated parallel observation, with, and only with, another instrument. Unlike NICMOS, coordinated parallels cannot be used to operate any of the ACS channels simultaneously. ACS exposures may not be used as both the prime and parallel exposures within the same parallel container. In order to operate ACS channels simultaneously, the use of ACS auto-parallels are described in the following section. The filter choice for auto-parallels is restricted and thus implemented as auto-parallels instead of coordinated parallels.

In order to protect the ACS SBC detector from inadvertent over illumination, the ACS/SBC configuration may be used as a coordinated parallel only if an exact spacecraft orientation (ORIENTAtion) is specified, the coordinates of the parallel field are determined and the parallel target or field passes the same bright-object screening applied to SBC primary observations. The Visual Target Tuner will greatly assist in writing this type of ACS parallel program.

Currently ACS and WFPC2, used together in a coordinated parallel program, result in the ACS auto-parallel capability being disabled. This restriction is made to prevent potential conflicts between ACS buffer dumps and WFPC2 readouts. The user may attempt to restore autoparallels via PAREXP=MULTIPLE.

### **ACS Auto-Parallels**

The ACS auto-parallel capability is intended to increase the scientific return of the instrument by adding exposures with the parallel detector while interfering as little as possible with the observer's primary program. When either the WFC or HRC is the primary channel, and the exposure in that channel meets the requirements stated below, an auto-parallel observation will be automatically scheduled in the parallel channel during Phase II processing. Parallel detector exposures will be added automatically with the longest possible exposure time that does not interfere with the primary program. In order for an auto-parallel to be scheduled, the primary observation must meet the specifications that depend primarily on the exposure time and the filter selection of the primary exposure.

The user has three control options: This is done by selecting the PAREXP optional parameter. A user may either choose to explicitly add the auto-parallel by choosing PAREXP=MULTIPLE; choose to have no auto-parallel added by selecting PAREXP=NONE; or leave the special requirement set to the default, DEF. When DEF is selected, auto-parallel will be added according to the same primary exposure requirements as those for the MULTIPLE option. When MULTIPLE is selected an auto-parallel will be added for each CR-SPLIT part of the primary exposure (see Figure 8.8). There is a simple algorithm that the Phase II software follows in order to determine if an auto-parallel is feasible:

1. The primary exposure must be for an external target, in ACCUM mode and either in the WFC or HRC channel. It is not possible to observe simultaneously with the HRC and SBC, since they share the same optical train up to the flip mirror, and simultaneous operation of the WFC and SBC is not supported.
2. The primary exposure must be taken with a filter from the list of primary/auto-parallel filter combinations (Table 8.4). HRC and WFC share the same filter wheels, so the filter selection for the primary camera predetermines which filter will be used for the simultaneous observation in the other channel. (The HRC primary/WFC parallel filter combination will not always be the inverse of the WFC primary/HRC parallel combination, because the WFC & HRC optical paths are not diametrically opposite each other in the filter wheel).
3. The primary exposure time must be greater than the minimum exposure time, defined in Table 8.5. These values are calculated such that all of the commanding associated with the auto-parallel is scheduled during the exposure time of the primary CR-SPLIT portion.
4. The primary exposure is not allowed to have any EXPAND, MIN DUR, MAX DUR or RT ANALYSIS special requirements.

Table 8.4: Filter combinations for auto-parallel in the two cases of (i) HRC camera prime and (ii) WFC camera prime. Note that since the WFC and HRC apertures are not opposite each other on the filter wheels, filter pairs in columns 1 and 2 do not map to columns 3 and 4.

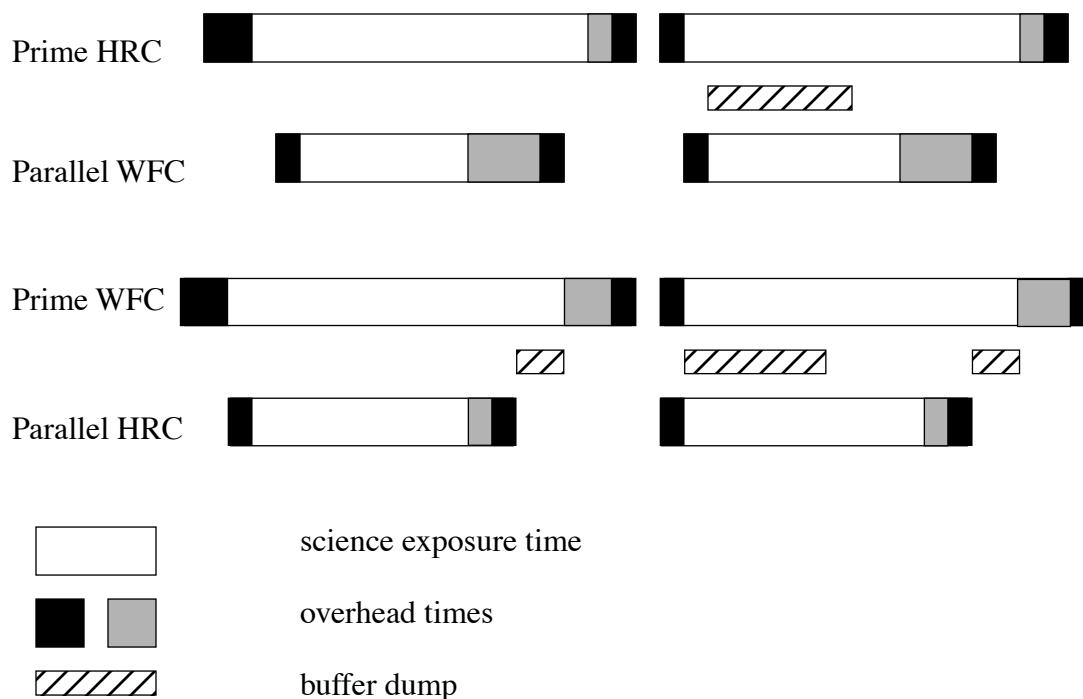
HRC Primary	WFC Auto-parallel	WFC Primary	HRC Auto-parallel
F892N	F775W	F475W	F850LP
F606W	F625W	F658N	F550M
F502N	F550M	G800L	F625W
G800L	F850LP	F502N	F775W
F555W	F606W	F606W	F555W
F775W	F502N	F850LP	G800L

HRC Primary	WFC Auto-parallel	WFC Primary	HRC Auto-parallel
F625W	G800L	F550M	F502N
F550M	F658N	F625W	F606W
F850LP	F475W	F775W	F892N
F330W	F660N	F660N	F330W
F250W	F814W	F814W	F250W
F220W	F435W	F435W	F220W

Table 8.5: Minimum primary exposure time (sec) to attach an auto-parallel for CR-SPLIT=n (if CR-SPLIT=NO then n=1, if CR-SPLIT not specified n=2)

primary exposure type	multiple auto-parallel scenario ( $n \geq 1$ )
HRC	$n \times 495$
WFC compressed	$n \times 406$
WFC uncompressed	$n \times 465$

Figure 8.8: Scheduling of Auto-parallels

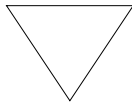


There are a few things to remember about auto-parallels:

- In order to avoid the addition of serial buffer dumps in the primary program, group short HRC exposures and long WFC exposures separately. It takes approximately 349 seconds to dump a WFC image from the buffer. When WFC is the parallel camera, this buffer dump

can occur during the following exposure if its exposure time is greater than ~339 seconds, otherwise a serial buffer dump must be added. This can be avoided by scheduling long WFC full-frame exposures together.

- auto-parallels will not be assigned when the number of exposure iterations specified for the primary exposure is greater than one. It is assumed that the observer will use exposure iterations to obtain coarse time resolution. These exposures will in most cases be too short for auto-parallel observations.
- WFC auto-parallels will be readout at GAIN=2 with one 2048×2048 CCD quadrant compressed. In some cases there may be partial data loss from the compression.




---

*This data loss will be considered routine and it will be the policy of STScI not to repeat observations scheduled as auto-parallels which exhibit partial data loss due to the data compression.*

---

### ACS Pure Parallels

In ACS pure parallel observations, an observation is taken with ACS on an essentially random area of the sky while another instrument is making prime observations. The WFC will be a prominent instrument in pure parallel observing due to its sensitivity and field of view. The HRC is also available for pure parallel observing, however no SBC pure parallels will be allowed due to bright object concerns.

Unlike the previous two types of parallel programs, pure parallels contain only parallel visits. Use of the GO/PAR proposal category will make any visit in the program a pure parallel.

The ACS default (archival) pure parallel program continued to execute for the community until midway through Cycle 13 when all of the "Default" HST archival pure parallel programs were discontinued to prolong the lifetime of transmitters on HST. This non-proprietary data currently comes from programs 9575, 9584 and 9701. A list of all pure parallel datasets in the HST archive is updated regularly at:

<http://www.stsci.edu/instruments/parallels/retrieve.html>.

Pure parallel observations are executed at every possible opportunity, although there are many constraints which can render pure parallels unschedulable in any given orbit. Pure parallels will always be given lower priority than primaries and are thus scheduled only on a non-interference basis.

### ACS Auto-Parallels with ACS Coordinated and ACS Pure Parallels

ACS auto-parallels can be added to ACS pure and ACS coordinated parallels by default if scheduling constraints allow. However auto-parallels cannot be added to observations that make use of EXPAND or MAX DUR special requirements. Therefore ACS pure parallels can either be crafted to expose for the maximum duration allowed in each individual orbit by using EXPAND/MAX DUR or have auto-parallels added, but not both.

---

## 8.8 Two-Gyro Guiding

At some future date HST may be operated with only two gyroscopes. A primary impact of operating with two gyros will be a reduction in the available observing time during an orbit, and a decrease in the times of year when a given target can be observed. Other potential impacts may include additional spacecraft jitter and degradation of the effective PSF, as well as slightly poorer pointing stability between different exposures..



---

*See the Two-Gyro Handbook for detailed information.*

---

# Overheads and Orbit-Time Determination

In this chapter . . .

9.1 Overview / 187
9.2 ACS Exposure Overheads / 188
9.3 Orbit Use Determination Examples / 192

This Chapter describes the overheads associated with ACS observations and gives examples showing how to determine the number of orbits your program will require.

---

## 9.1 Overview

After you establish the set of scientific exposures and any additional target-acquisition or calibration exposures that you require for your program, you are ready to determine the total number of orbits to request. Generally, this is a straightforward exercise involving compilation of the overheads on the individual exposures, packing the exposure plus overhead time into individual orbits, and tallying up the results to determine your total orbit request. In some cases, it may be an iterative process as you refine your exposure requests to more fully exploit the orbits.

The Phase I *Call for Proposals* includes proposal instructions that provide information on the Observatory policies and practices with respect

to orbit-time requests. The HST Primer provides specific advice on orbit determination. Below, we provide a summary of the ACS specific overheads and give several examples that illustrate how to calculate your orbit requirements for Phase I Proposals.

---

## 9.2 ACS Exposure Overheads

The overheads on exposures are summarized in Table 9.1 and Table 9.2. All numbers given are approximate; they do not differentiate in detail the overheads for different ACS modes and configurations. These overhead times are to be used (in conjunction with the actual exposure times and the instructions in the HST Primer) to estimate the total number of orbits for your proposal. After your HST proposal is accepted, you will be asked to submit a Phase II proposal to support scheduling of your approved observations. At that time you will be presented with actual, up-to-date overheads by the APT scheduling software. *Allowing sufficient time for overhead in your Phase I proposal is important; additional time to cover unplanned overhead will not be granted later.*

The following list presents important points for each type of overhead:

- **Generic (Observatory Level) Overheads:**
  - The first time you acquire an object you must include the overhead for the guide-star acquisition (6.1 min).
  - In subsequent contiguous orbits you must include the overhead for the guide-star reacquisition (5.7 min); if you are observing in the Continuous Viewing Zone (see the Phase I Proposal Instructions), no guide-star *reacquisitions* are required.
  - Time needs to be allowed for each deliberate movement of the telescope; e.g., if you are performing a target-acquisition exposure on a nearby star and then offsetting to your target, or if you are taking a series of exposures in which you move the target on the detector, you must allow time for the moves (20 sec to 60 sec depending on the size of the slew, see Table 9.1 and Table 9.2).
- **Onboard Target-Acquisition Overheads:**
  - On-board target acquisitions in general only need to be done to place the target under one of the coronagraphic spots.
  - An on-board target-acquisition needs to be done only once in a series of contiguous orbits (i.e., once per visit).
  - The drift rate induced by the Observatory is less than 10 milli-arc-sec per hour. Thermal drifts internal to ACS are less still.

- ***Scientific Exposures:***

- The overhead times are dominated by the time to move the filter wheel, the readout time (CCD), and any serial buffer dump that is necessary. Again, we stress that in Phase II the overheads will frequently be less, but it is important to plan Phase I using the conservative overheads given in Table 9.2 to ensure you will have adequate time for your scientific goals.

- ***Spectroscopy:***

- Each CCD spectroscopic observation is preceded by an imaging exposure used for calibration, with the exposure time 3 and 6 min. for grism and prism observations, respectively. SBC prism exposures are not preceded by an automatic calibration exposure. Technically this is an individual single exposure requiring all regular science exposure overheads. For the observer it represents, however, an additional overhead to include in the observation time budget, so we have included it in the table of instrument overhead times for science exposures. However if the observing program is already taking an appropriate broadband image, the automatic imaging and associated overheads preceding the spectroscopic grism or prism observations can be avoided by invoking the available-but-unsupported mode AUTOIMAGE=NO during the phase II preparations. More details can be found in the Phase II Instructions Handbook.

Table 9.1: Science Exposure Overheads: General

Action	Overhead
<b><i>Generic (Observatory Level)</i></b>	
Guide-star acquisition	Initial acquisition overhead = 6.1 min Reacquisitions on subsequent orbits = 5.7 min per orbit
Spacecraft moves	For offsets less than 1.5 arcmin and more than 10 arcsec = 1 min. For offsets between 10 arcsec and 1 arcsec = 0.5 min For offsets less than 1 arcsec in size = 20 sec

Table 9.2: ACS Science Exposure Overhead Times (minutes).

Exposure Type	WFC	HRC	SBC
<i>Mode: Accum</i>			
Single exposure or the first exposure in a series of identical exposures	4.0	2.5	1.7
Subsequent identical exposures in series (within an orbit)	2.5	1.0	0.7
Additional overhead for each serial buffer dump (added when WFC exposures are less than 339 sec long, or the buffer fills with short HRC or SBC exposures)	5.8	5.8	5.8
Predefined imaging exposure for prism spectroscopy	N/A	8.5	N/A
Predefined imaging exposure for grism spectroscopy	7	5.5	N/A
<i>Mode: Acq</i>			
For the specified acquisition exposure time, <i>tacq</i> , the total acquisition time is:	N/A	$3.5 + (2 \times tacq)$	N/A
<i>Additional Overheads</i>			
Additional overhead if switching over from HRC to SBC within an orbit		17.0	
Additional overhead if switching over from SBC to HRC within an orbit		14.0	

Note that identical exposures are generated automatically if the observer specifies the proposal optional parameters CR-SPLIT (for  $n > 1$ ) or PATTERN or if Number\_of\_Iterations  $> 1$ . If it is not specified, CR-SPLIT defaults to  $n=2$ . In general, identical exposures are defined here as exposures at the same target and with the same detector and the same filter(s). PATTERNS also involve slews and therefore slew overheads.

For ACQ mode, the overhead includes double the specified exposure time. The reason is that it is necessary to have two acquisition images, hence two exposures, in order to eliminate possible image defects which can interfere with target acquisition. The flight software ensures that two images are taken, the user does not need to specify them in the proposal.

The overhead time for serial buffer dumps arises in certain cases from the overheads associated with the on-board data management and switching over the cameras. The on-board buffer memory can hold no more than one WFC image. The next WFC image can be placed into the buffer only after the buffer dumps the previous image, which takes 349 sec. If the next exposure time is longer than 339 sec (for WFC) or 346 (for HRC; 16 HRC images may be taken before a buffer dump is triggered), the buffer

dump will occur during that exposure, and no overhead is imposed. However, if the next exposure time is shorter than 339 sec (WFC) or 346 sec (HRC), then the dump must occur between the two exposures. Sequences of many short HRC or SBC exposures can also lead to serial dumps when the buffer becomes full. In this case the buffer dump time becomes an overhead to be included into the orbit time budget. This overhead can severely constrain the number of short exposures one can squeeze into an orbit. Subarrays can be used to lower the data volume for some applications.

A serious penalty is imposed for toggling between SBC and HRC within an orbit. The time to switch over from SBC to HRC is 480 sec. The opposite switch takes 650 sec, and in both cases there is an additional overhead of 6 min. associated with buffer dump. This consumes a significant portion of the available orbital time. Thus, whenever possible, one should plan to use HRC and SBC in different orbits.

### 9.2.1 Subarrays

At the end of each exposure, data are read out into ACS's internal buffer memory where they are stored until they are dumped into HST's solid state data recorder. The ACS internal buffer memory holds 34 Mbyte or the equivalent of 1 full WFC frame or 16 HRC or SBC frames. Thus, after observing a full WFC frame, the internal buffer memory must be dumped before the next exposure can be taken. The buffer dump takes 349 sec and may not occur while ACS is being actively commanded. Of this time, 339 sec (for one WFC image) or 346 sec (for 16 HRC images) is spent dumping the image. The buffer dump cannot be done during the next exposure if the latter is shorter than 339 sec. If, however, the next exposure is less than 339 seconds the buffer dump will create an extra 5.8 minutes of overhead.

If your science program is such that a smaller FOV can be used, then one way of possibly reducing the frequency and hence overheads associated with buffer dumps is to use WFC subarrays. With subarrays, only a fraction of the detector is read out, a smaller volume of data per frame is stored in the buffer, and a larger number of frames can be stored before requiring a dump. Using subarrays not only reduces the amount of time spent dumping the buffer but in some cases may reduce the readout time, since only a portion of the detector is readout. We refer the user to Chapter 8 for a discussion of some of the limitations of subarrays. If the user elects to define a subarray of arbitrary size and location, allowed on an available-but-unsupported basis, then matching bias frames will not be automatically provided by STScI. Any bias frames specified by the user will typically be scheduled during the following occultation (i.e., they do not add to the overheads during visibility time). Dark frames and flat fields will be extracted from full frame images. In some special cases where a general subarray is cleverly defined so as to include a physical overscan region, no separate bias frames are needed.

## 9.3 Orbit Use Determination Examples

The easiest way to learn to compute total orbit time requests is to work through a few examples. Below we provide five different examples:

- Example 1 is a simple WFC image in one filter.
- Example 2 is a set of short WFC exposures that may require large overheads associated with buffer dumps.
- Example 3 is a one-orbit coronagraphic observation in two filters.
- Example 4 is a two-orbit observation using dithering.
- Example 5 is a one orbit WFC grism spectroscopic observation.

These examples represent fairly typical uses of ACS.

### 9.3.1 Sample Orbit Calculation 1:

Consider a target to be imaged with WFC in a given filter in one orbit. Using the Exposure Time Calculator (ETC), we find that we need 2400 sec of exposure time to reach the desired level of signal-to-noise ratio. Given that the observation must be split into a series of two exposures by CR-SPLIT (CR-SPLIT=2), we map the overheads and the science exposure times onto the orbit as follows:

Table 9.3: Orbit Calculation for Example

Action	Time (min.)	Explanation
<i>Orbit 1</i>		
Initial guide-star acquisition	6.1	Needed at start of observation of a new target
WFC overhead for the first exposure	4.0	Includes filter change, camera set-up, and readout
First science exposure	20.0	
WFC overhead for the subsequent science exposure in the series	2.5	Includes readout
The next science exposure in the series	20.0	
Total time for science exposures	40.0	
Total used time in the orbit	52.6	

Thus, the two WFC exposures totaling 2400 sec make full use of the typically available time in one orbit. The exposure times can be adjusted if the actual target visibility time differs from the derived total used time.

### 9.3.2 Sample Orbit Calculation 2

This example illustrates the impact of short WFC exposures on the useful time in the orbit. We have one orbit to observe a target with WFC in two filters, so the observation consists of two series, each with two identical CR-SPLIT exposures. The ETC has shown that at the minimally accepted signal-to-noise ratio the exposure time must be 540 sec for each of the filters, so each of the CR-SPLITS must be at least 270 sec long. For the target declination, we find that the visibility time is 55 min. The time budget for the orbit is then as follows:

Table 9.4: Orbit Calculation for Example 2

Action	Time (min.)	Explanation
<i>Orbit 1</i>		
Initial guide-star acquisition	6.1	Needed at start of observation of a new target
WFC overhead for the first exposures in two series	$2 \times 4 = 8$	Includes filter change, camera set-up, and readout
WFC overhead for subsequent exposures in each of the two series	$2 \times 2.5 = 5$	Includes readout
Additional overhead for all but the last exposures in the orbit	$5.8 \times 3 \approx 17$	Needed to dump the buffer because the next exposure is too short (shorter than 339 sec) to accommodate the dump time.
Science exposures	$4 \times 4.5 = 18$	
Total time for science exposures	18	
Total used time in the orbit	54	

Comparing with the previous example, we see that although with the adopted minimum exposure times we can squeeze the observation into one orbit, the efficiency of the orbit use is very low because of the large overheads associated with buffer dumps. However, if we increase each of the four exposure times so that they are larger than 339 sec, we avoid these additional overheads. This would free  $\sim 17$  min. of the orbit time for science, which allows us to almost double the science exposure time (35 min. instead of 18 min.) and thus significantly improve signal-to-noise.

Similarly, a subarray can be used to readout only a fraction of the detector, allowing more frames to be stored in the buffer before requiring a dump. In this example, using four WFC1-1K subarrays for 4 short ( $t < 339$ s) exposures would save 176s in readout time and 1047s in dump time. This frees up  $\sim 20$  minutes of orbit time to be used for science.

### 9.3.3 Sample Orbit Calculation 3:

This example demonstrates the orbit calculation for a coronagraphic observation. We want to obtain coronagraphic images of a star in two filters, F250W and F606W. The ETC has shown that the exposure times adequate for our scientific goals are 5 min. in F606W and 30 min. in

F250W. From the orbit visibility table (see the HST Primer) we find that at the target declination of 15 degrees the target visibility time is 52 min. With CR-SPLIT=2, we thus have to accommodate in that period 35 min. of four science exposures grouped in two series. The orbit calculation goes like this:

Table 9.5: Orbit Calculation for Example 3

Action	Time (min.)	Explanation
<i>Orbit 1</i>		
Initial guide-star acquisition	6.1	Needed at start of observation of a new target
Target acquisition	$3.5+(2 \times 0.1)=3.7$	Point-source acquisition on target
HRC overhead for the first exposures in the series	$2 \times 2.5=5$	Includes filter change, camera set-up, and readout
HRC overhead for the subsequent exposures in the series	$2 \times 1=2$	Includes readout
Science exposures in F606W	$2 \times 2.5=5$	
Science exposures in F250W	$2 \times 15=30$	
Total time for science exposures	35	
Total used time in the orbit	~51.8	

The derived total used time in the orbit shows that our target can indeed be imaged in the selected filters in one orbit. Since there remains 3 min. of unused time, we can adjust our exposure times to make full use of the available time.

### 9.3.4 Sample Orbit Calculation 4:

This example illustrates the orbit calculation for a WFC observation with the ACS box pattern, which implements imaging at four offset pointings. The goal of the observation is to obtain a dithered image of a field in such a way that would allow us to bridge the 50-pixel interchip gap between the WFC CCDs in the combined image. Given the WFC plate scale of 0.05 arcsec/pix, this requires that the offsets in the dithering pattern are larger than 2.5 arcsec. Each offset will then take 0.5 min. to move the spacecraft from one pointing in the pattern to another. We have determined that the exposure time necessary to reach the desired signal-to-noise ratio is 80 min. The visibility time at our target declination is 58 min. In this observation we do not want to rely on cosmic ray removal provided by the dithering data reduction package, and set CR-SPLIT=2 to be able to remove cosmic rays from the four individual images separately. As a result, the orbit calculation will involve a series of 8 exposures (two

exposures at each of the four pointings in the dithering pattern) split across two orbits:

Table 9.6: Orbit Calculation for Example 4

Action	Time (min.)	Explanation
<i>Orbit 1</i>		
Initial guide-star acquisition	6.1	Needed at start of observation of a new target
WFC overhead for the first exposures in the series	4	Includes filter change, camera set-up, and readout
WFC overhead for the subsequent 3 exposures in the series	$3 \times 2.5 = 7.5$	Includes readout
Spacecraft slew	0.5	To offset from the first to the second pointing
Four science exposures	$4 \times 10 = 40$	Exposures at the first two pointings in the dither pattern
Total time for science exposures	40	
Total used time in the orbit	58.1	
<i>Orbit 2</i>		
Guide-star re-acquisition	5.7	Needed at start of a new orbit to observe the same target
WFC overhead for the remaining exposures in the series	$4 \times 2.5 = 10$	Includes readout
Spacecraft slews	$2 \times 0.5 = 1$	To offset to the third and fourth pointings
Four science exposures	$4 \times 10 = 40$	Exposures at the second two pointings in the dither pattern
Total time for science exposures	40	
Total used time in the orbit	56.7	

The total used time in the first orbit comes out a little bit larger than the visibility time. However, given the conservative nature of the adopted overhead times as well as a bit of flexibility in the adopted signal-to-noise ratio, the difference is not significant. It is to be remembered that the purpose of the above exercises is to estimate how many orbits to request for our science program rather than to exactly design the observation.

### 9.3.5 Sample Orbit Calculation 5:

This example illustrates the orbit calculation for a simple 30 min. WFC grism spectroscopic observation broken down by CR-SPLIT=2 into a series of two exposures.

Table 9.7: Orbit Calculation for Example 5

Action	Time (min.)	Explanation
<i>Orbit 1</i>		
Initial guide-star acquisition	6.1	Needed at start of observation of a new target
Predefined imaging exposure for grism spectroscopy	7	Needed to co-locate the targets and their spectra in the FOV
WFC overhead for the first science exposure in the series	4.0	Includes filter change, camera set-up, and readout
WFC overhead for the subsequent science exposure in the series	2.5	Includes readout
Two science exposures	$2 \times 15.0 = 30$	
Total science exposure time	30.0	
Total used time in the orbit	49.6	

Unlike similar imaging exposures, here we have to take into account an additional imaging exposure before the sequence of spectroscopic exposures, which takes 10 min. off the available orbit time.



PART III:

# Supporting Material

---

The chapters in this Part present more detailed material in support of the User's Guide. Included is the imaging reference material.



## CHAPTER 10:

# Imaging Reference Material

### In this chapter . . .

10.1 Introduction / 200	HRC/F550M / 224
10.2 Using the Information in this Chapter / 200	HRC/F555W / 225
WFC/F435W / 203	HRC/F606W / 226
WFC/F475W / 204	HRC/F625W / 227
WFC/F502N / 205	HRC/F658N / 228
WFC/F550M / 206	HRC/F660N / 229
WFC/F555W / 207	HRC/F775W / 230
WFC/F606W / 208	HRC/F814W / 231
WFC/F625W / 209	HRC/F850LP / 232
WFC/F658N / 210	HRC/F892N / 233
WFC/F660N / 211	HRC/G800L / 234
WFC/F775W / 212	HRC/PR200L / 235
WFC/F814W / 213	HRC/CLEAR / 236
WFC/F850LP / 214	SBC/F115LP / 237
WFC/G800L / 215	SBC/F122M / 238
WFC/CLEAR / 216	SBC/F125LP / 239
HRC/F220W / 217	SBC/F140LP / 240
HRC/F250W / 218	SBC/F150LP / 241
HRC/F330W / 219	SBC/F165LP / 242
HRC/F344N / 220	SBC/PR110L / 243
HRC/F435W / 221	SBC/PR130L / 244
HRC/F475W / 222	10.3 Distortion in the ACS / 248
HRC/F502N / 223	

In this Chapter, we provide imaging reference material, in support of the information presented in Chapter 6.

---

## 10.1 Introduction

This chapter provides reference material to help you select your filter and detector configuration and determine your observing plan (e.g., total required exposure time, and number of exposures). This chapter is, for the most part, organized by *filter* and *detector*. For each imaging mode the following are provided:

- Plots of integrated system throughput as a function of wavelength.
- Plots of the time needed to achieve a desired signal-to-noise ratio vs. magnitude for all filters for a point source and a one arcsec<sup>2</sup> extended source.
- Tables of color corrections  $AB_v$  to go from Johnson V magnitude to AB magnitude.

---

## 10.2 Using the Information in this Chapter

### 10.2.1 Sensitivity Units and Conversions

This chapter contains plots of throughputs for each imaging mode. “Determining Count Rates from Sensitivities” on page 102 explains how to use these throughputs to calculate expected count rates from your source.

The first figure for each imaging mode gives the integrated system throughput. This is the combination of the efficiencies of the detector and of the optical elements in the light path. The throughputs in this handbook are based in part on ground test data. Although, at the time of writing the overall detector efficiency curve and most filter throughputs have been adjusted based on in-flight data. The throughput is defined as the number of detected counts per second per cm<sup>2</sup> of telescope area relative to the incident flux in photons per cm<sup>2</sup> per second. For the CCD “counts” is the number of electrons detected. For the MAMA, “counts” is the number of valid events processed by the detector electronics after passing through the various pulse-shape and anti-coincidence filters. In both cases the detected counts obey Poisson statistics. The throughput includes all obscuration effects in the optical train (e.g., due to the HST secondary). Comparisons of the throughput between ACS and the other instruments can be found in “Which Instrument to Use?” on page 41.

To recalculate the throughput with the most recent CCD QE tables in synphot, you can create total-system-throughput tables (instrument plus OTA) using the synphot calcband task. Calcband takes any valid obsmode command string as input and produces an STSDAS table with two columns

of data called “wavelength” and “throughput” as its output. For example, to evaluate the throughput for the F475W filter and the WFC detector, chip 1, you would use the command **calcband acs,wfc1,f475w sdssg\_thpt**. The resulting throughput table is stored in `sdssg_thpt`.

## 10.2.2 Signal-To-Noise

For each imaging mode, plots are provided to estimate the signal-to-noise ratio (S/N) for a representative source. The first figure shows S/N for point sources (GAIN=1). The second figure shows S/N for uniform extended sources of area  $1 \text{ arcsec}^2$ .

The different line styles in the S/N figures delineate regions where different sources of noise dominate. A particular source of noise (readnoise for example) is presumed to dominate if it contributes more than half the total noise in the observations.

The point- and extended-source S/N figures are shown for average and low sky levels. For point sources, an aperture size of  $5 \times 5$  pixels has been used for the WFC,  $9 \times 9$  pixels for HRC and  $15 \times 15$  pixels for the SBC S/N evaluation. For extended sources a  $1 \text{ arcsec}^2$  aperture was used. For the CCD the read noise has been computed assuming a number of readouts  $\text{NREAD} = \text{integer}(t / 1000 \text{ s})$ , where  $t$  is the exposure time, with a minimum  $\text{NREAD}=2$ . That is, each exposure has a minimum  $\text{CR-SPLIT}=2$ . Different line styles in the figures are used to indicate which source of noise dominates.

To the left of the vertical line in the SBC S/N plots, the count rate from the source exceeds the  $150 \text{ counts sec}^{-1} \text{ pix}^{-1}$  local count rate limit. This is computed from the model PSF, which gives 14 to 22% of the flux in the central pixel.

In situations requiring more detailed calculations (non-stellar spectra, extended sources, other sky background levels, unknown target V magnitude, etc.), the ACS [Exposure-Time Calculator](#) should be used.

Follow these steps to use the signal-to-noise plots:

1. Determine the AB magnitude of your source at the wavelength of interest. There are several ways to do this.
  - Examine Table 10.1, 10.2 or 10.3 and find  $\text{AB}_V$  for the desired spectral type and filter. Sum the V magnitude of the target and  $\text{AB}_V$  derived from the table.
  - Alternatively, compute  $\text{ABMAG} (=V+\text{AB}_V)$  from the source flux, using the relation  $\text{ABMAG} = -2.5 \log f_V - 48.60$ , or  $\text{ABMAG} = -2.5 \log f_\lambda - 5 \log \lambda - 2.406$ .
2. Find the appropriate plot for the filter in question, and locate  $V+\text{AB}_V$  on the horizontal axis. Then read off the signal-to-noise ratio for the desired exposure time, or vice-versa.

The “x” characters at the top of each plot indicate the onset of saturation, in the case of the CCD. The “x” shows where the total number of counts exceeds the 16-bit buffer size of 65,535.

Note that the plots show the S/N as a function of source magnitude for exposure times as short as 0.1s, although the minimum exposure time for the WFC CCD channel is 0.5s.

### 10.2.3 Point Spread Functions

All information about the PSF are based on the modeled encircled energy data presented in “ACS Point Spread Functions” on page 54.

## WFC/F435W

### Description

Johnson B filter.

Figure 10.1: Integrated System Throughput for WFC/F435W

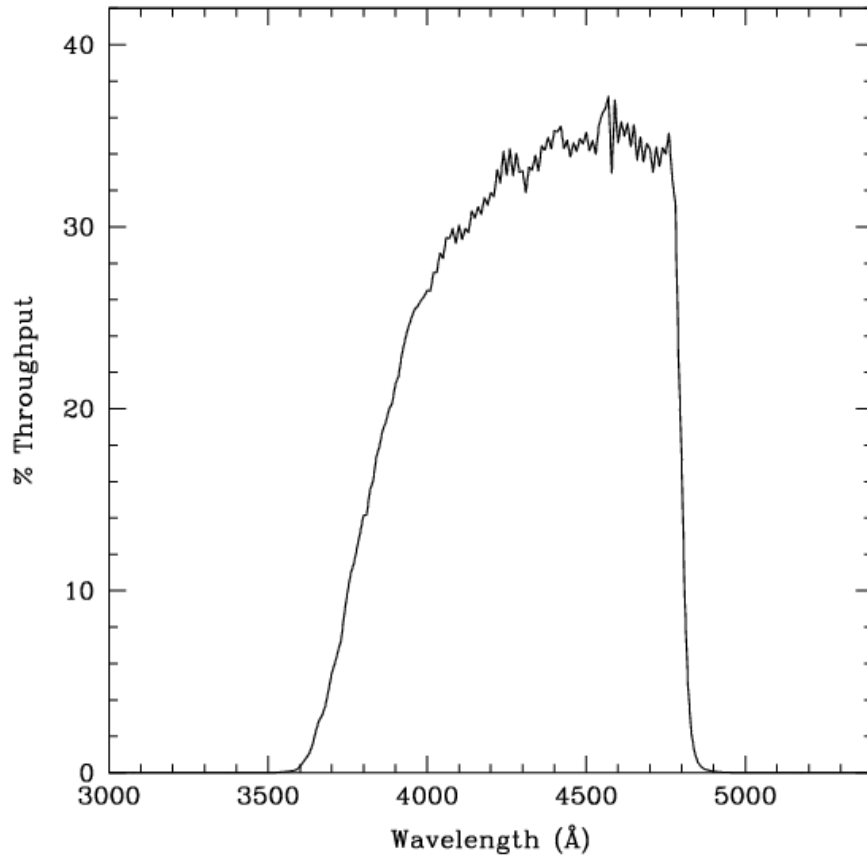


Figure 10.2: Point Source S/N vs.  $V+AB_v$  for the WFC/F435W filter. Top curves are for low sky; bottom curves are for average sky.

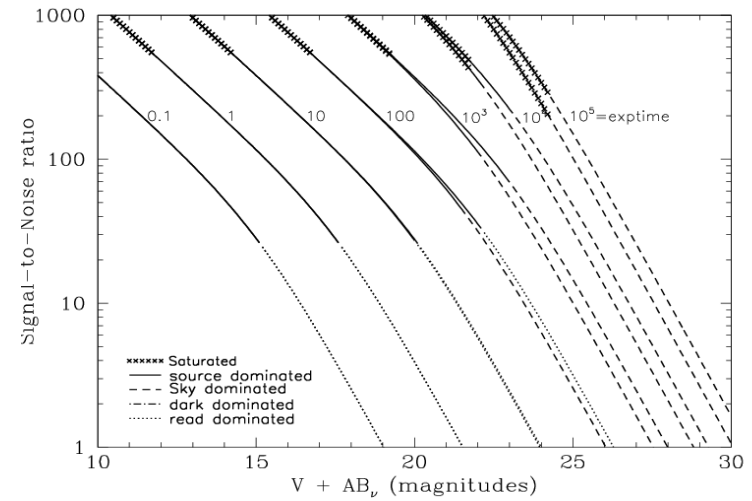
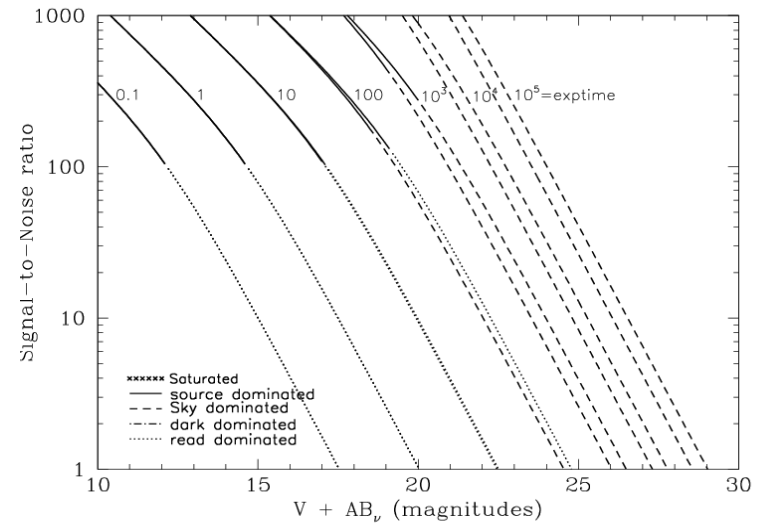


Figure 10.3: Extended Source S/N vs.  $V+AB_v$  for the WFC/F435W filter. Top curves are for low sky and bottom curves are for average sky for a 1 arcsec<sup>2</sup> area.



## WFC/F475W

### Description

Sloan Digital Sky Survey g filter.

Figure 10.4: Integrated System Throughput for WFC/F475W

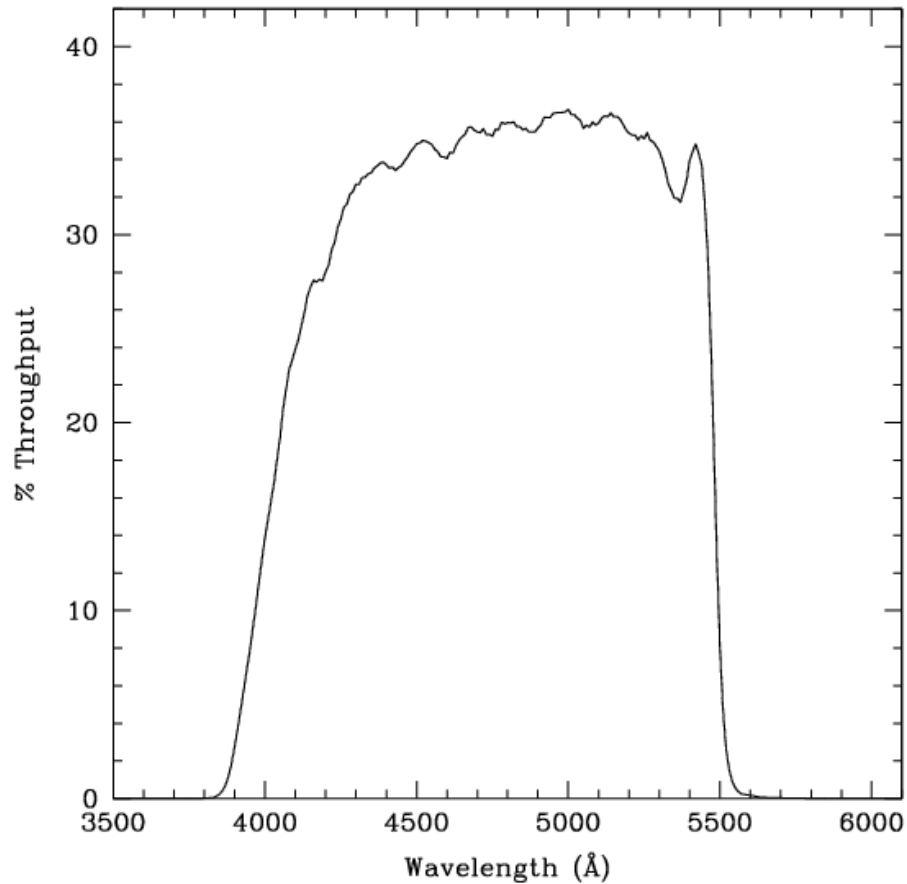


Figure 10.5: Point Source S/N vs.  $V+AB_v$  for the WFC/F475W filter. Top curves are for low sky; bottom curves are for average sky.

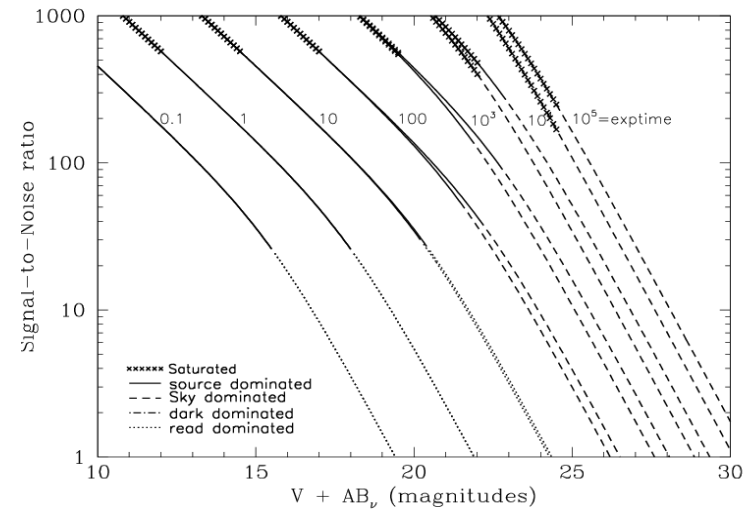
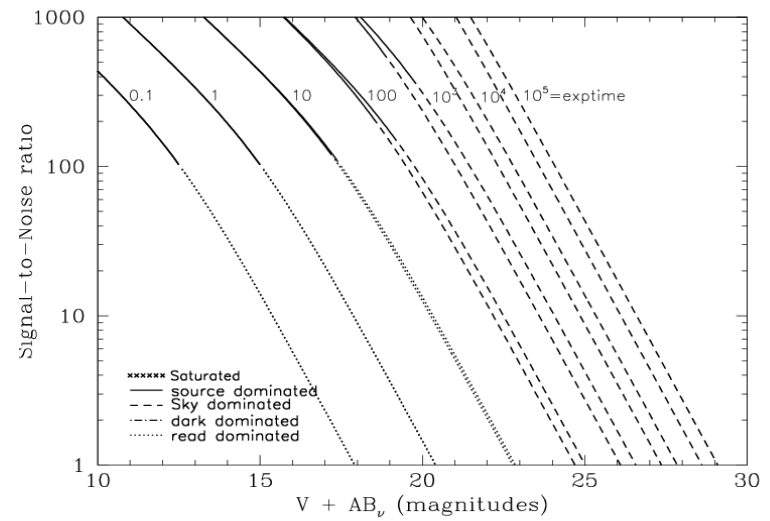


Figure 10.6: Extended Source S/N vs.  $V+AB_v$  for the WFC/F475W filter. Top curves are for low sky and bottom curves are for average sky for a 1 arcsec<sup>2</sup> area.



## WFC/F502N

### Description

OIII filter.

Figure 10.7: Integrated System Throughput for WFC/F502N

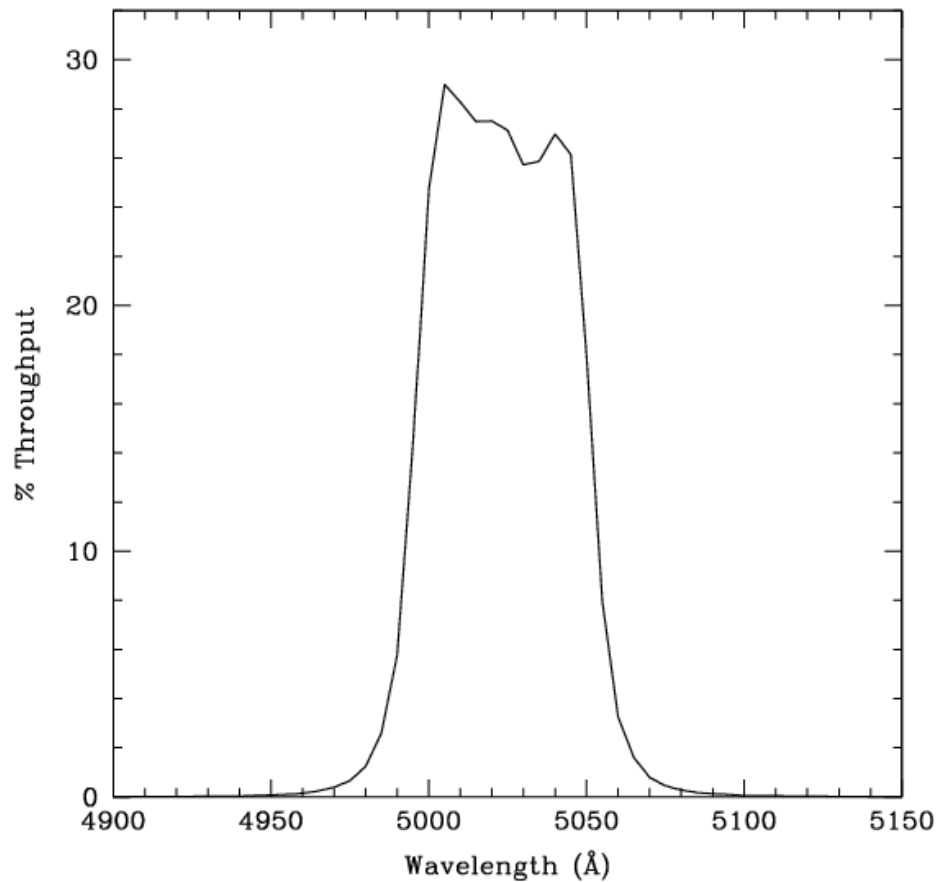


Figure 10.8: Point Source S/N vs.  $V+AB_v$  for the WFC/F502N filter. Top curves are for low sky; bottom curves are for average sky.

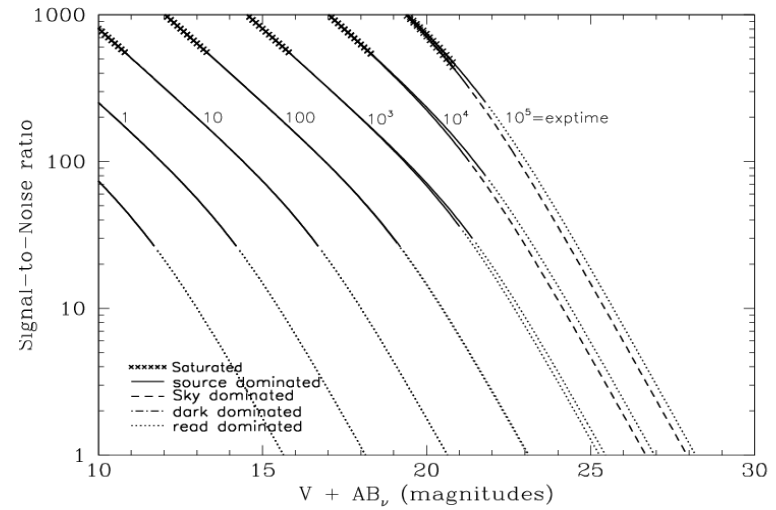
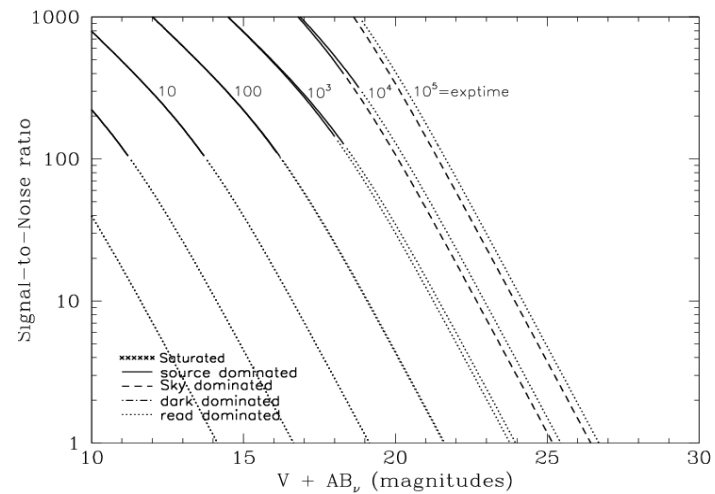


Figure 10.9: Extended Source S/N vs.  $V+AB_v$  for the WFC/F502N filter. Top curves are for low sky and bottom curves are for average sky for a 1 arcsec<sup>2</sup> area.



# WFC/F550M

## Description

Narrow V filter.

Figure 10.10: Integrated System Throughput for WFC/F550M

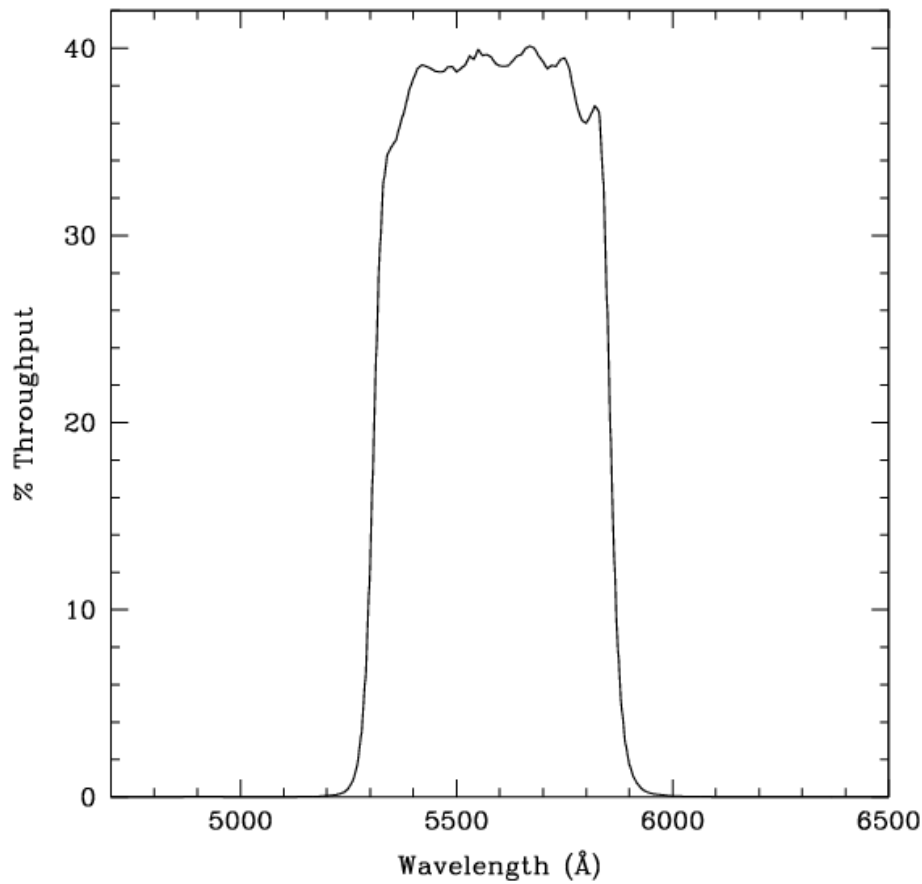


Figure 10.11: Point Source S/N vs.  $V+AB_V$  for the WFC/F550M filter. Top curves are for low sky; bottom curves are for average sky.

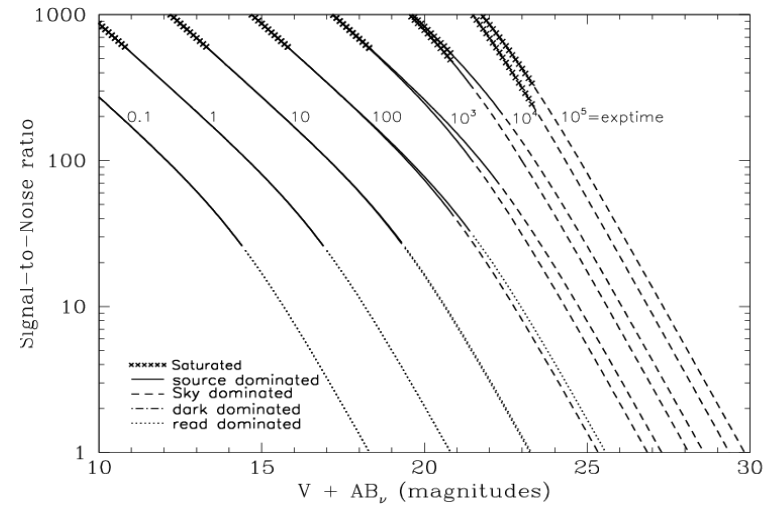
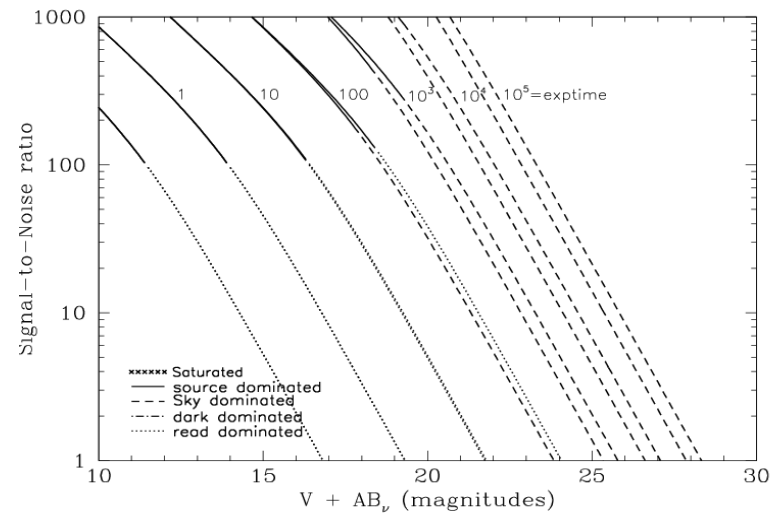


Figure 10.12: Extended Source S/N vs.  $V+AB_V$  for the WFC/F550M filter. Top curves are for low sky and bottom curves are for average sky for a 1 arcsec<sup>2</sup> area.



## WFC/F555W

### Description

Johnson V filter.

Figure 10.13: Integrated System Throughput for WFC/F555W

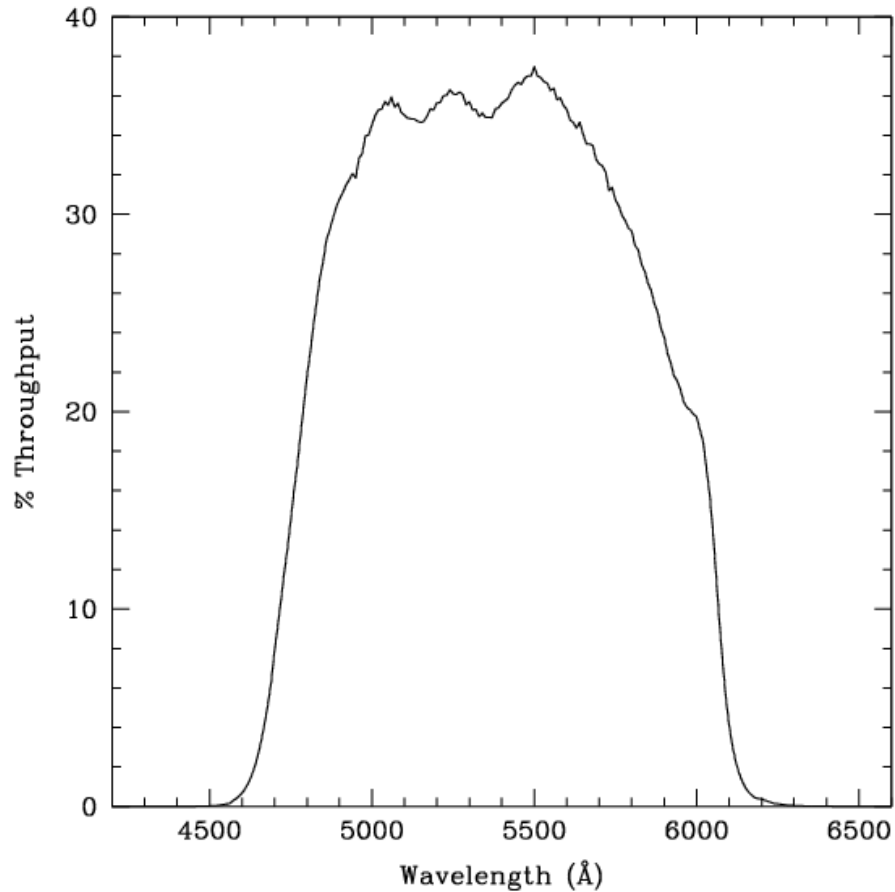


Figure 10.14: Point Source S/N vs.  $V+AB_v$  for the WFC/F555W filter. Top curves are for low sky; bottom curves are for average sky.

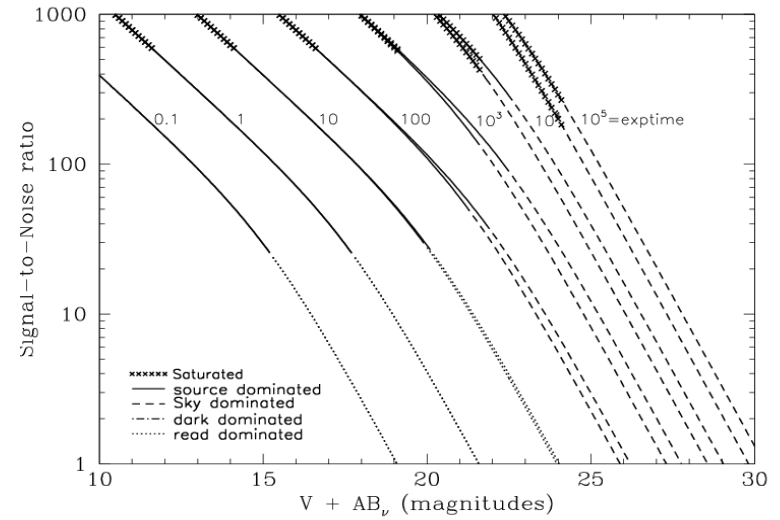
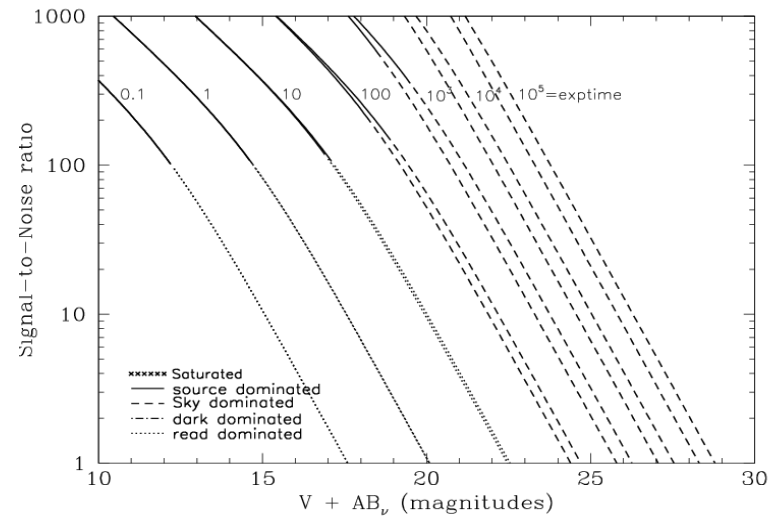


Figure 10.15: Extended Source S/N vs.  $V+AB_v$  for the WFC/F555W filter. Top curves are for low sky and bottom curves are for average sky for a 1 arcsec<sup>2</sup> area.



## WFC/F606W

### Description

Broad V filter.

Figure 10.16: Integrated System Throughput for WFC/F606W

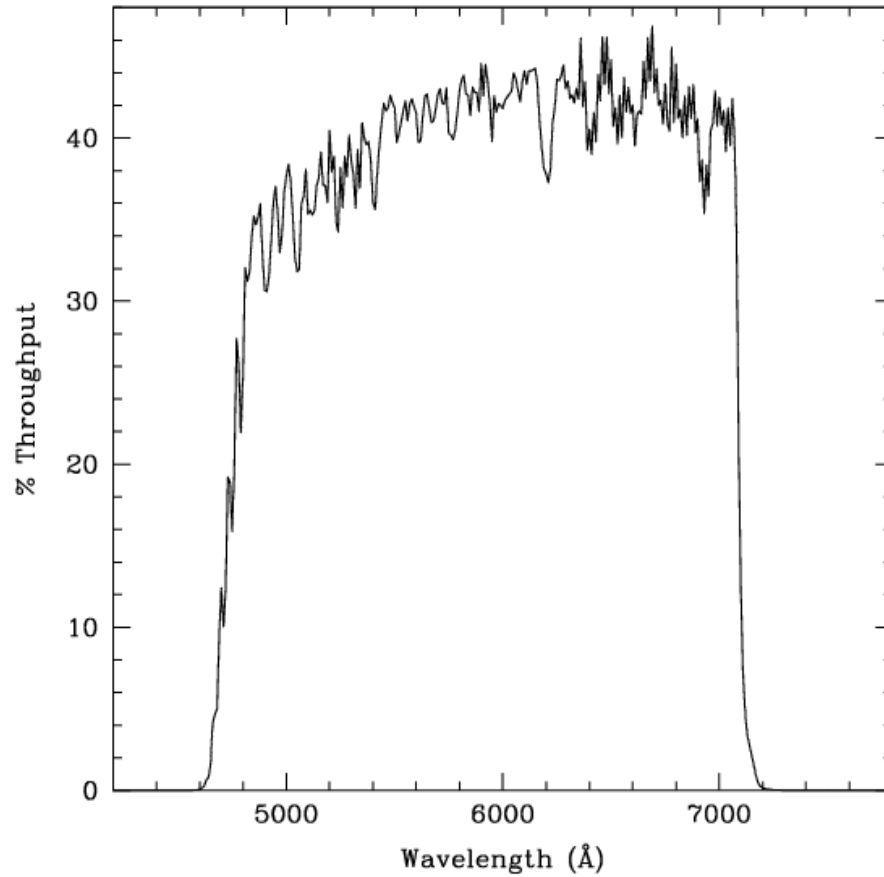


Figure 10.17: Point Source S/N vs.  $V+AB_v$  for the WFC/F606W filter. Top curves are for low sky; bottom curves are for average sky.

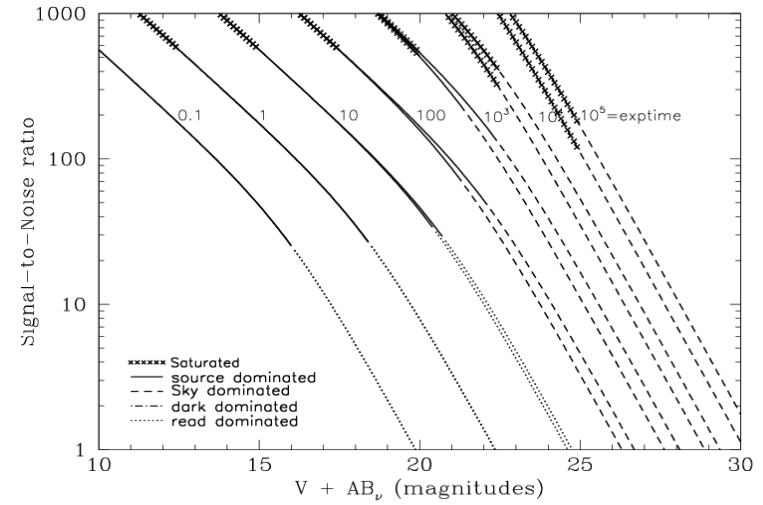
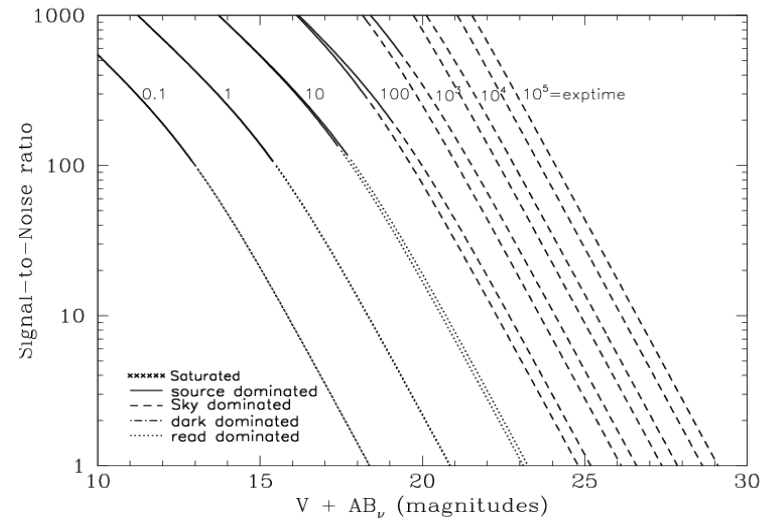


Figure 10.18: Extended Source S/N vs.  $V+AB_v$  for the WFC/F606W. Top curves are for low sky and bottom curves are for average sky for a  $1 \text{ arcsec}^2$  area.



## WFC/F625W

### Description

Sloan Digital Sky Survey r filter.

Figure 10.19: Integrated System Throughput for WFC/F625W

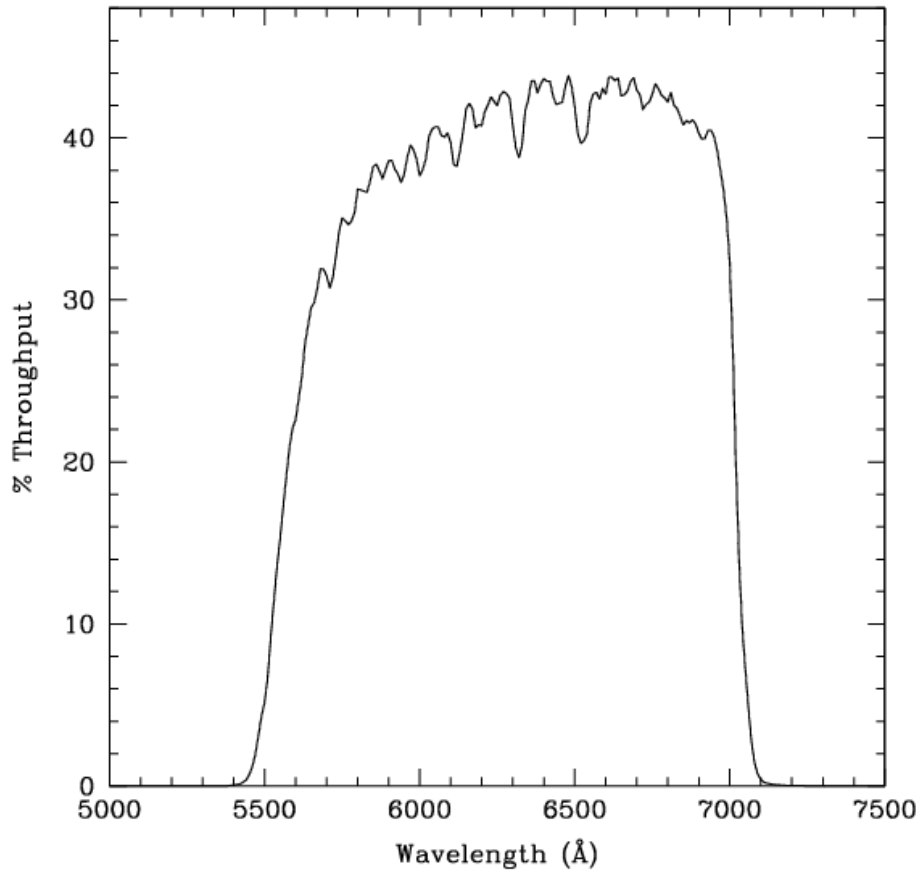


Figure 10.20: Point Source S/N vs.  $V+AB_V$  for the WFC/F625W filter. Top curves are for low sky; bottom curves are for average sky.

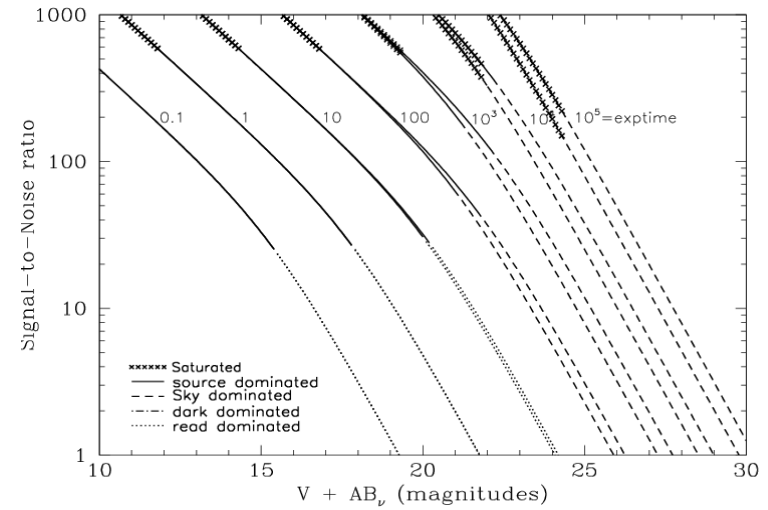
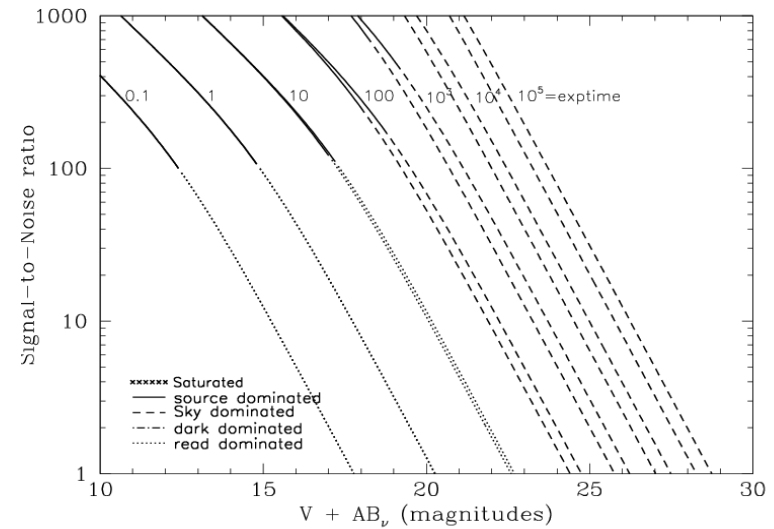


Figure 10.21: Extended Source S/N vs.  $V+AB_V$  for the WFC/F625W filter. Top curves are for low sky and bottom curves are for average sky for a 1 arcsec<sup>2</sup> area.



## WFC/F658N

### Description

H $\alpha$  filter.

Figure 10.22: Integrated System Throughput for WFC/F658N

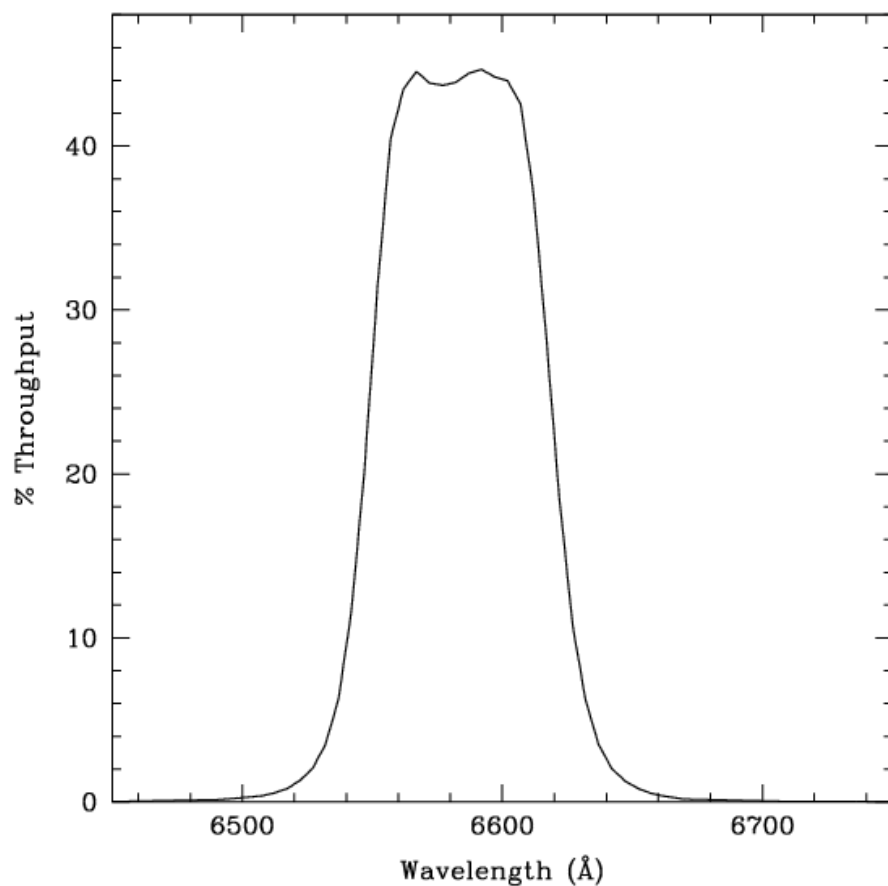


Figure 10.23: Point Source S/N vs.  $V+AB_V$  for the WFC/F658N filter. Top curves are for low sky; bottom curves are for average sky.

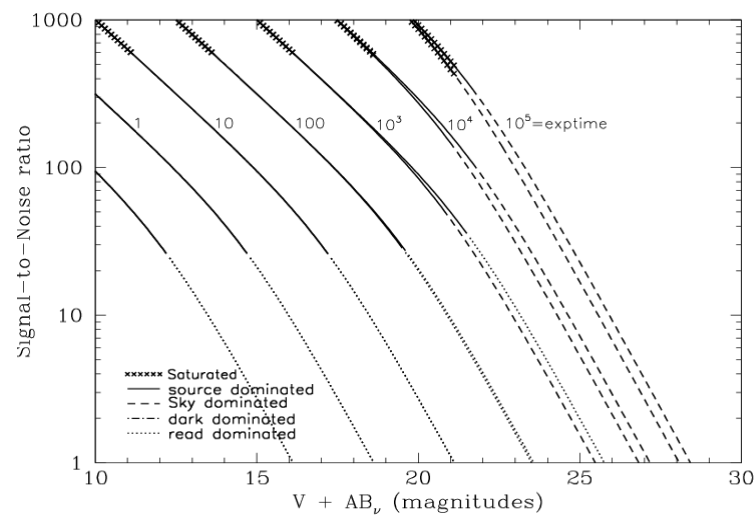
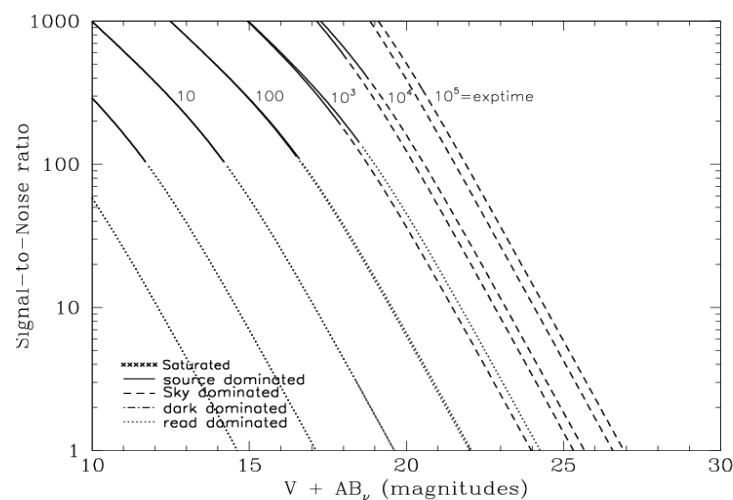


Figure 10.24: Extended Source S/N vs.  $V+AB_V$  for the WFC/F658N filter. Top curves are for low sky and bottom curves are for average sky for 1 arcsec<sup>2</sup> area.



## WFC/F660N

### Description

NII filter.

Figure 10.25: Integrated System Throughput for WFC/F660N

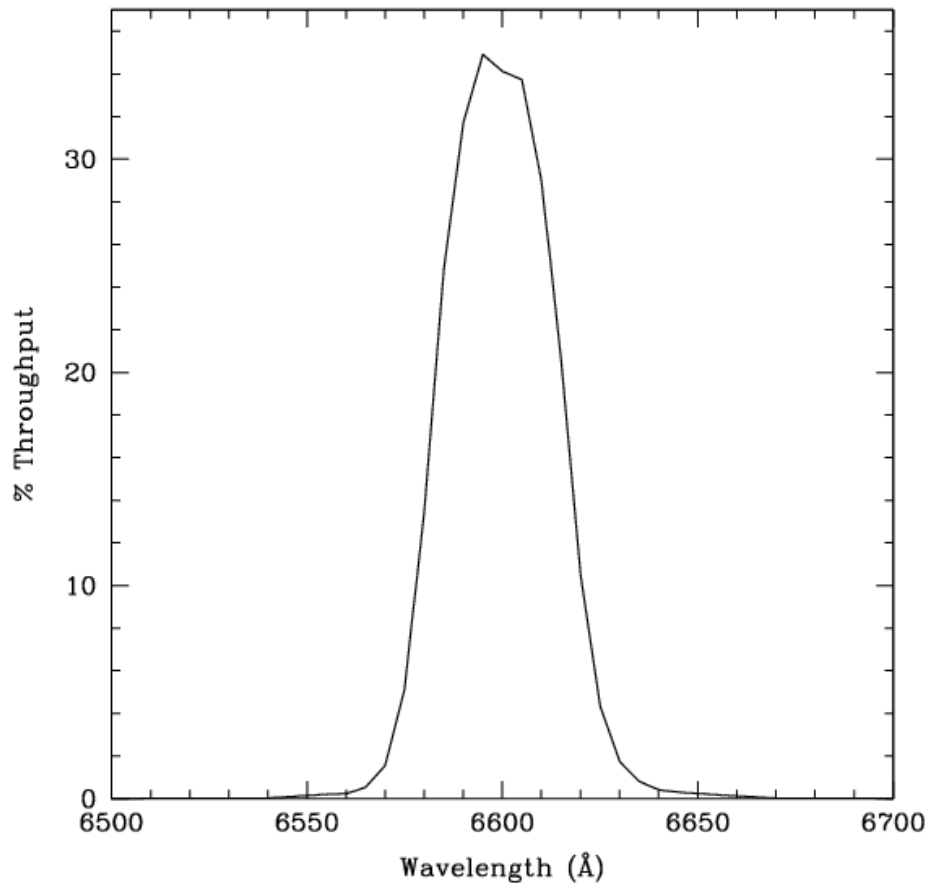


Figure 10.26: Point Source S/N vs.  $V+AB_V$  for the WFC/F660N filter. Top curves are for low sky; bottom curves are for average sky.

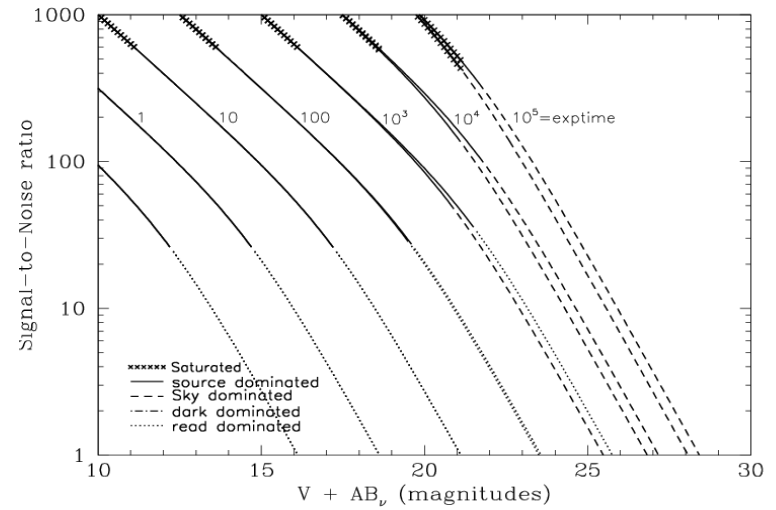
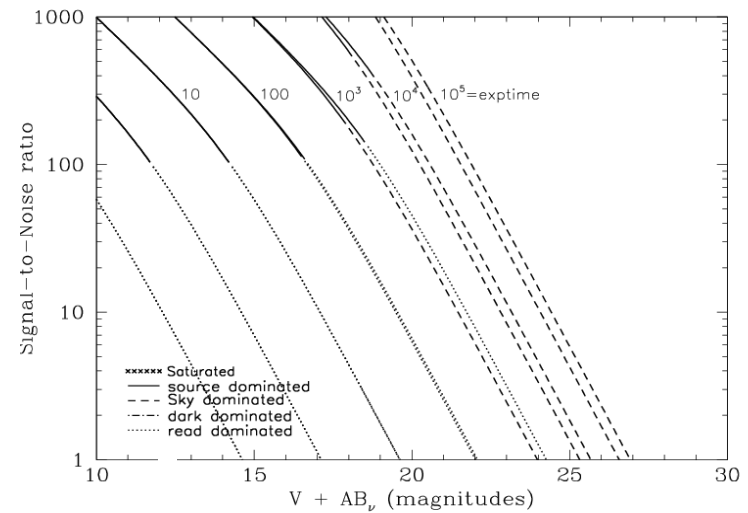


Figure 10.27: Extended Source S/N vs.  $V+AB_V$  for the WFC/F660N filter. Top curves are for low sky and bottom curves are for average sky for a 1 arcsec<sup>2</sup> area.



## WFC/F775W

### Description

Sloan Digital Sky Survey i filter

Figure 10.28: Integrated System Throughput for WFC/F775W

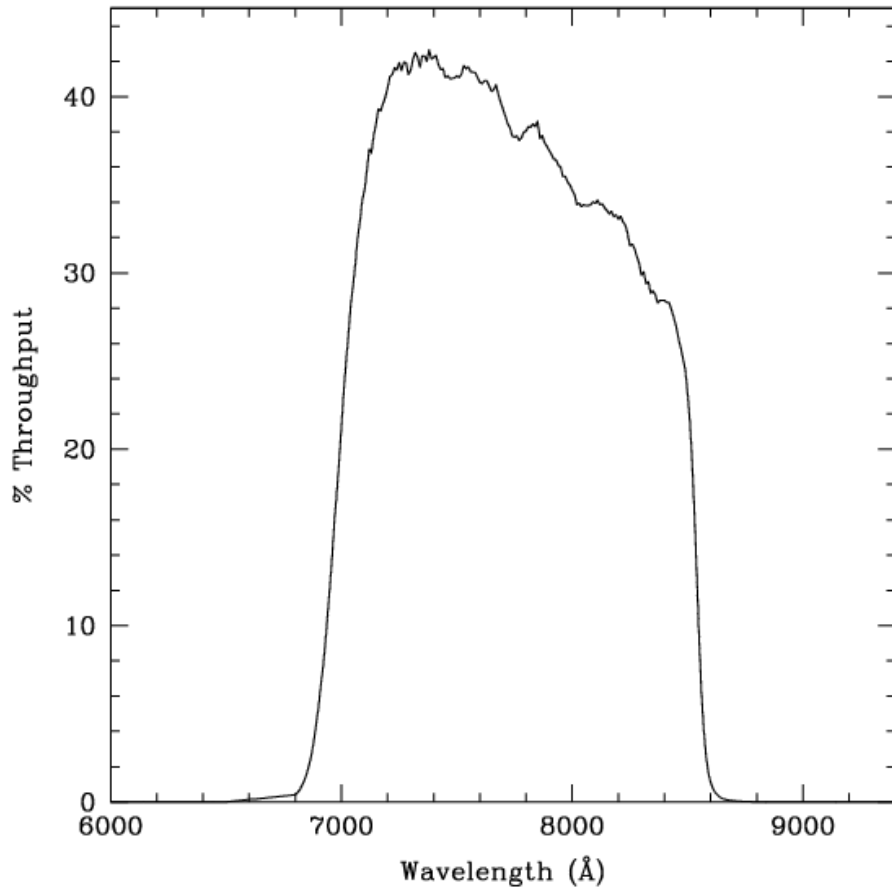


Figure 10.29: Point Source S/N vs.  $V+AB_V$  for the WFC/F775W filter. Top curves are for low sky; bottom curves are for average sky.

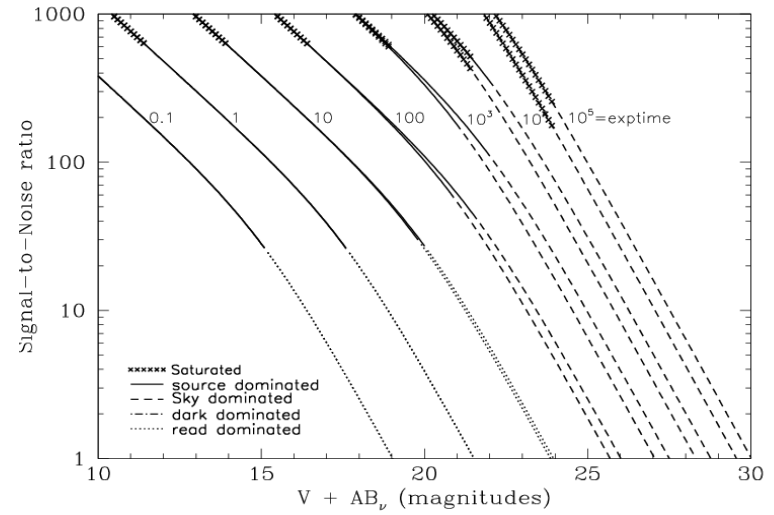
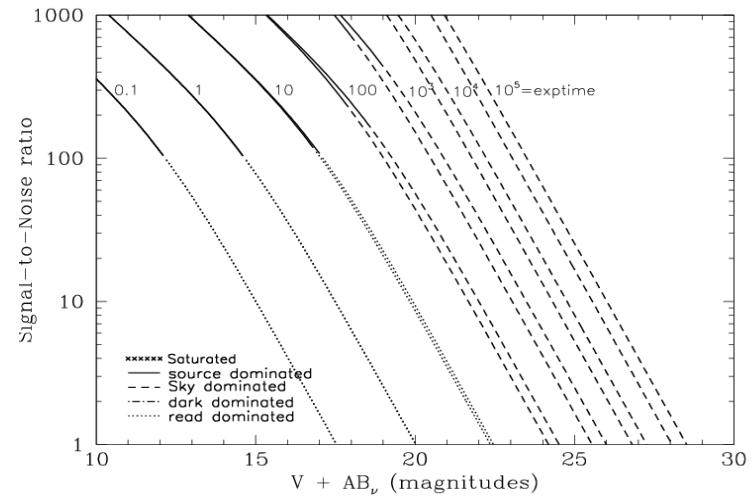


Figure 10.30: Extended Source S/N vs.  $V+AB_V$  for the WFC/F775W filter. Top curves are for low sky and bottom curves are for average sky for a 1 arcsec<sup>2</sup> area.



## WFC/F814W

### Description

Broad I filter.

Figure 10.31: Integrated System Throughput for WFC/F814W

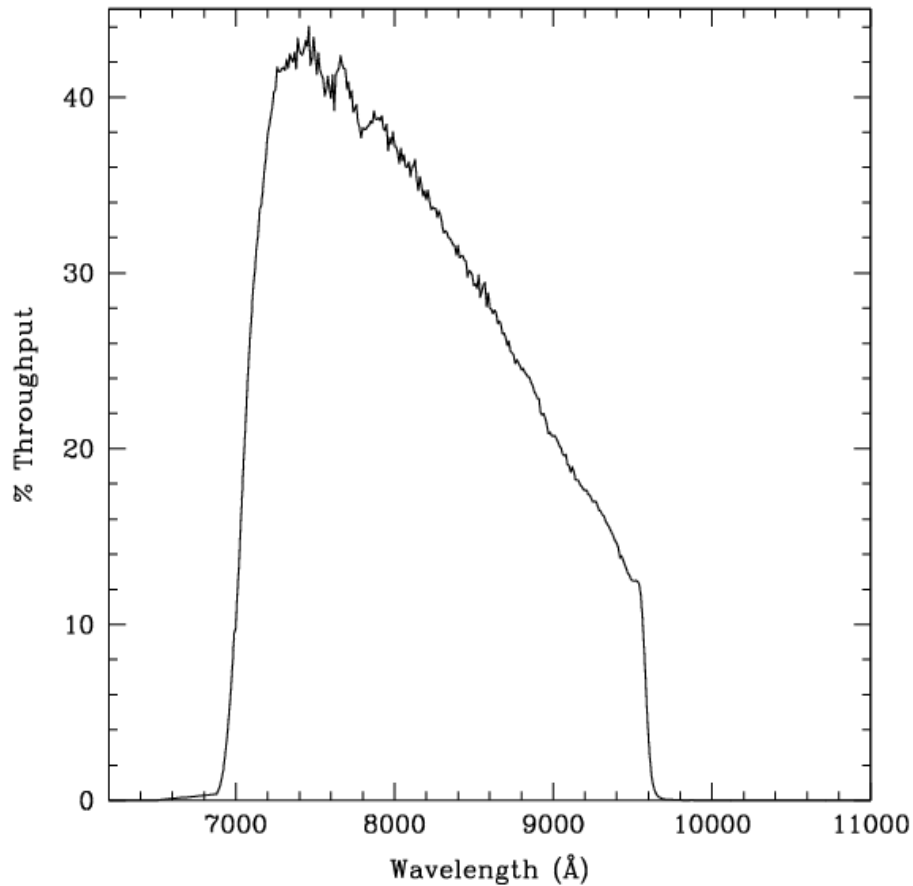


Figure 10.32: Point Source S/N vs.  $V+AB_V$  for the WFC/F814W filter. Top curves are for low sky; bottom curves are for average sky.

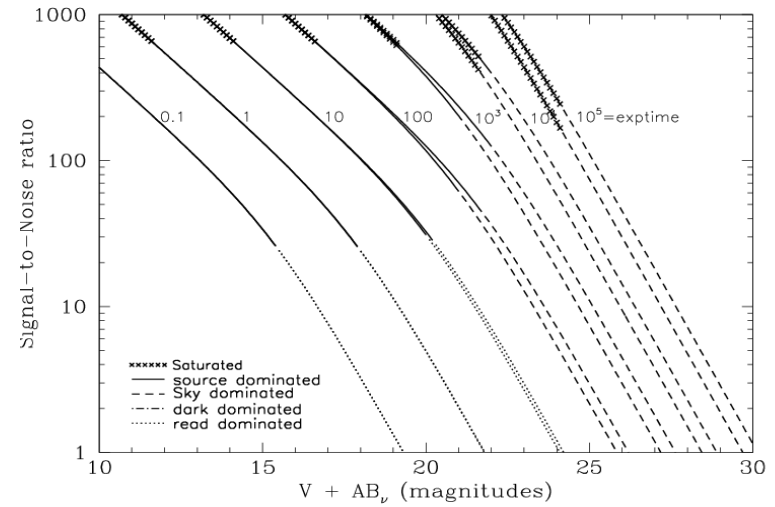
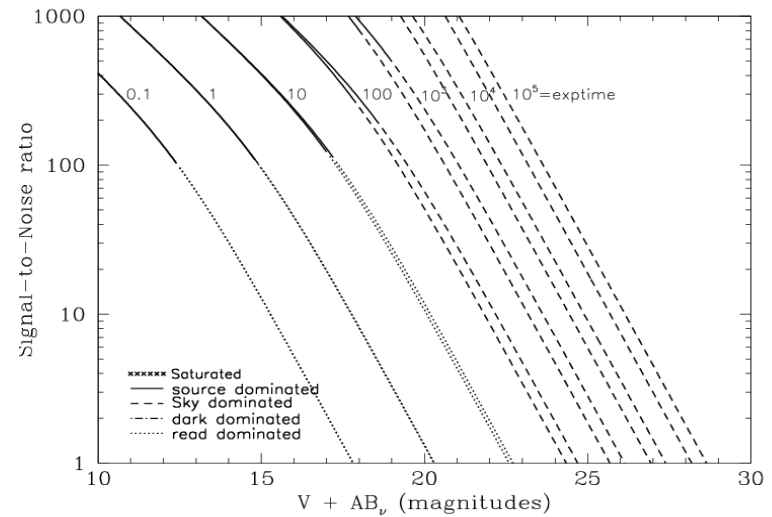


Figure 10.33: Extended Source S/N vs.  $V+AB_V$  for the WFC/F814W filter. Top curves are for low sky and bottom curves are for average sky for a 1 arcsec<sup>2</sup> area.



# WFC/F850LP

## Description

Sloan Digital Sky Survey z filter.

Figure 10.34: Integrated System Throughput for WFC/F850LP

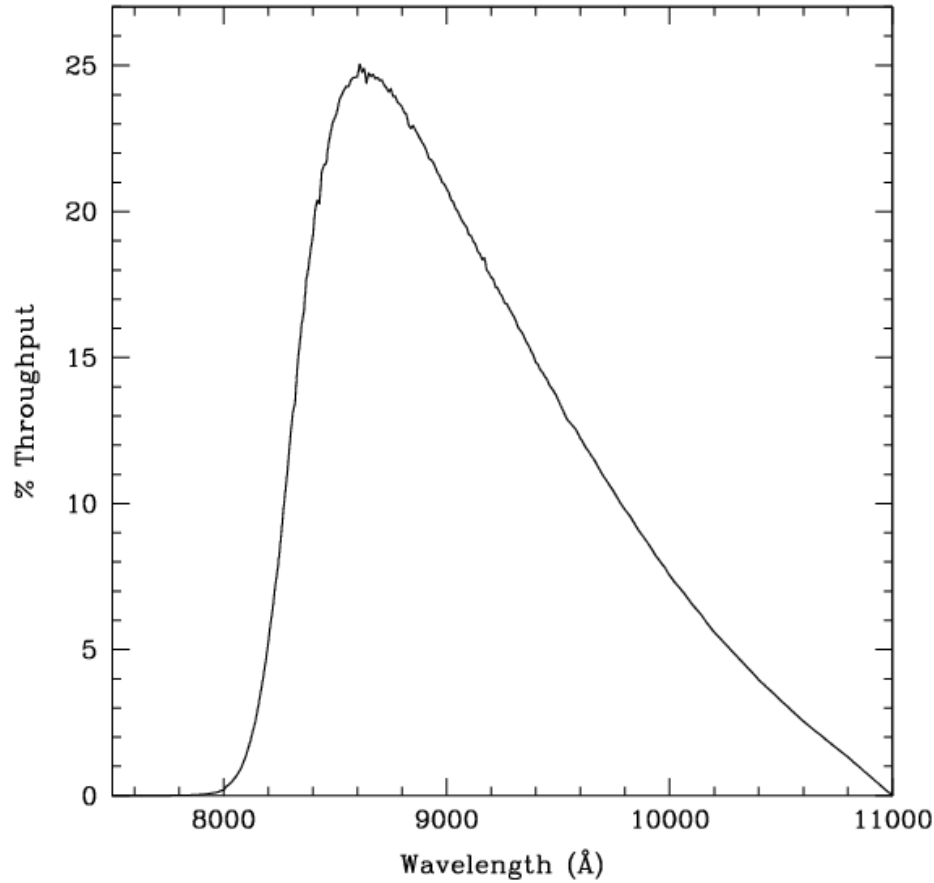


Figure 10.35: Point Source S/N vs.  $V+AB_V$  for the WFC/F850LP filter. Top curves are for low sky; bottom curves are for average sky.

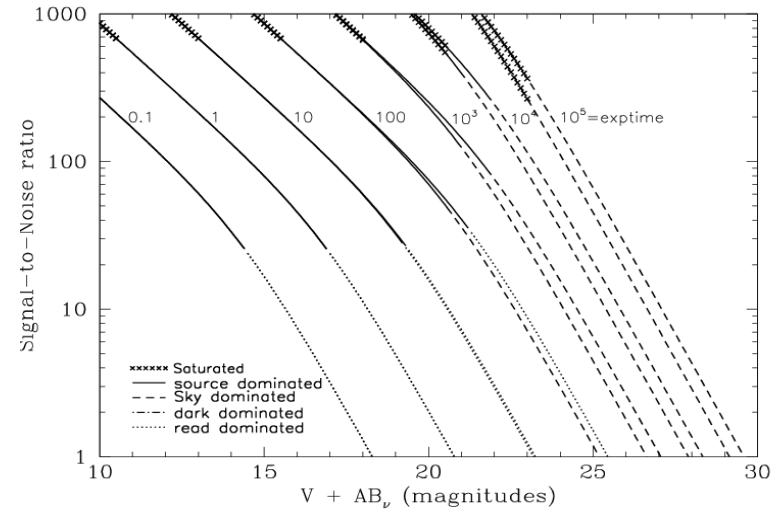
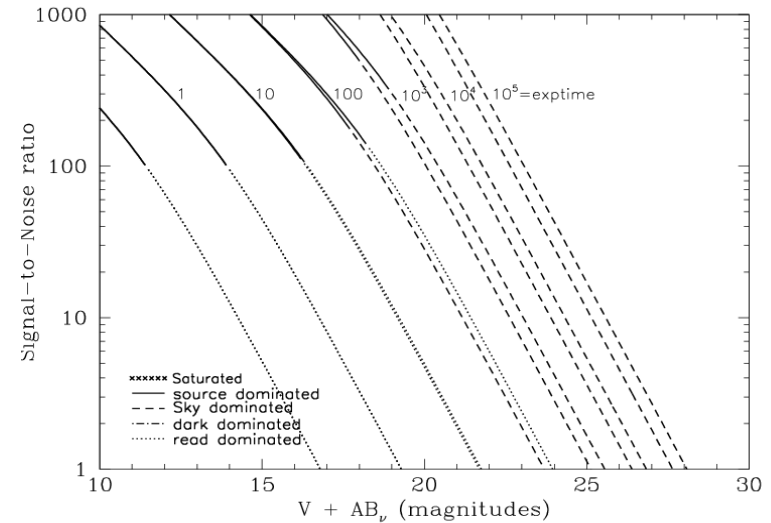


Figure 10.36: Extended Source S/N vs.  $V+AB_V$  for the WFC/F850LP filter. Top curves are for low sky and bottom curves are for average sky for a  $1 \text{ arcsec}^2$  area.



## WFC/G800L

### Description

Grism.

Figure 10.37: Integrated System Throughput for WFC/G800L

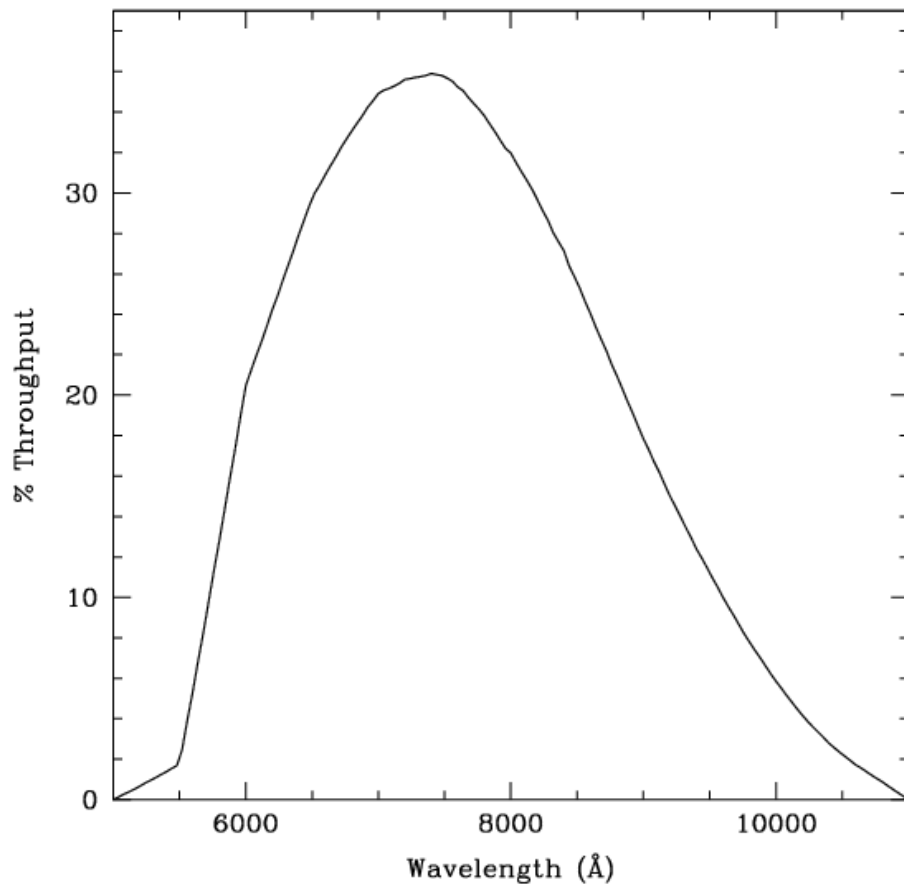


Figure 10.38: Point Source S/N vs.  $V+AB_v$  for the WFC/G800L filter. Top curves are for low sky; bottom curves are for average sky.

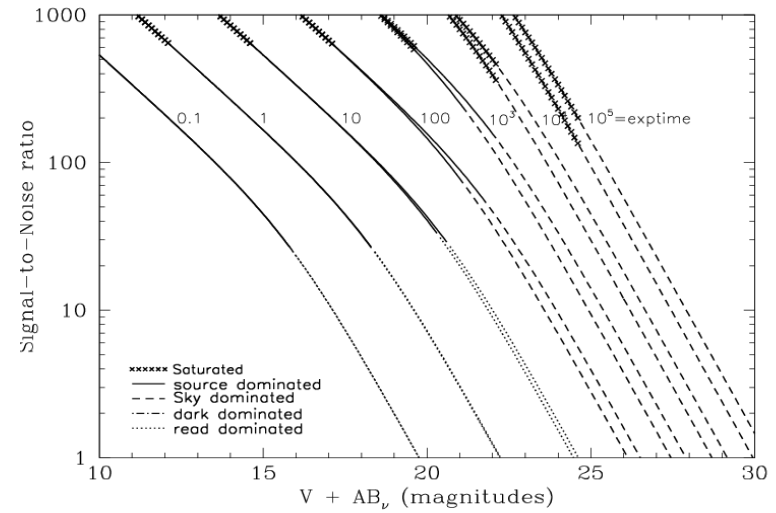
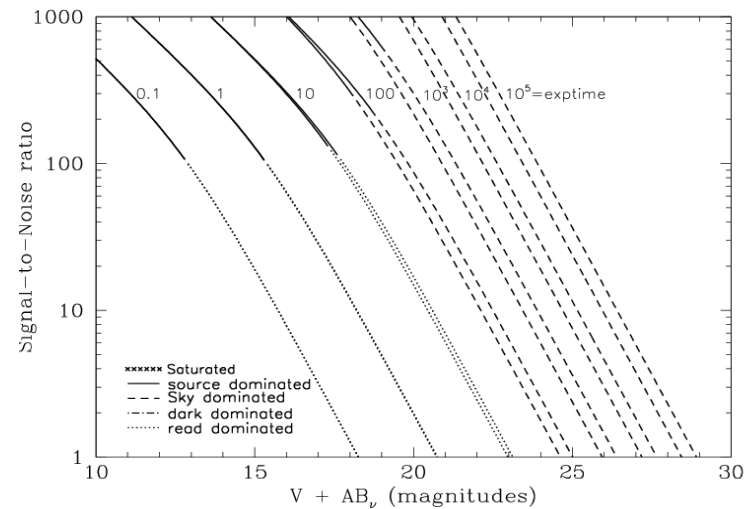


Figure 10.39: Extended Source S/N vs.  $V+AB_v$  for the WFC/G800L filter. Top curves are for low sky and bottom curves are for average sky for a  $1\text{arcsec}^2$  area.



## WFC/CLEAR

### Description

Clear filter.

Figure 10.40: Integrated System Throughput for WFC/Clear

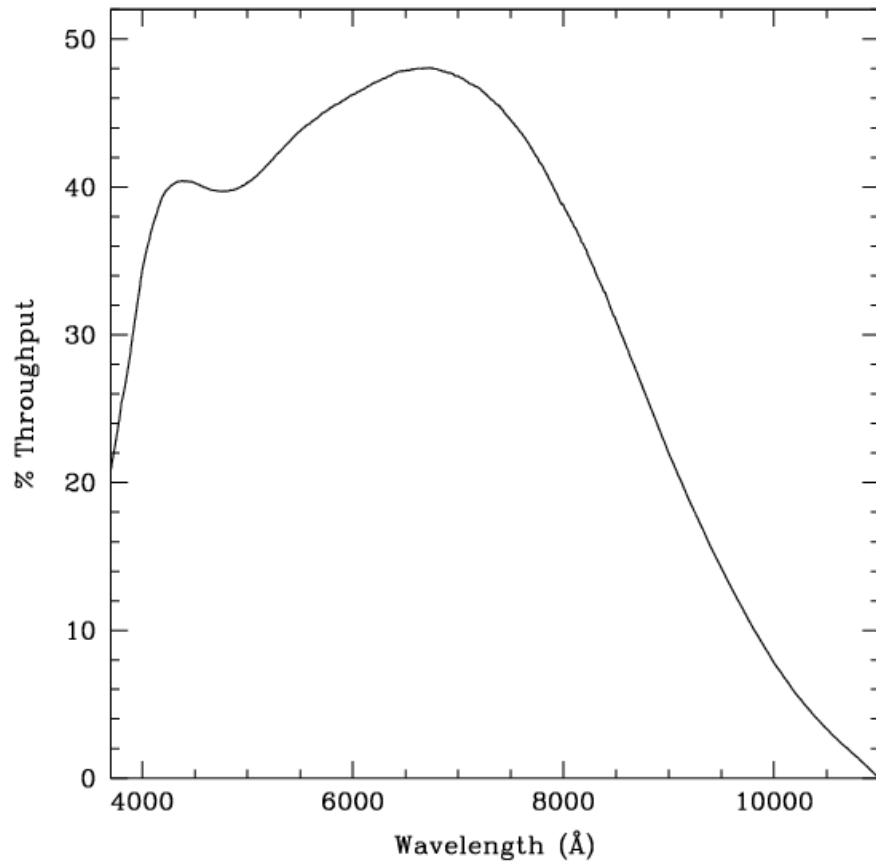


Figure 10.41: Point source S/N vs.  $V+AB_v$  for the WFC/Clear filter. Top curves are for low sky; bottom curves are for average sky.

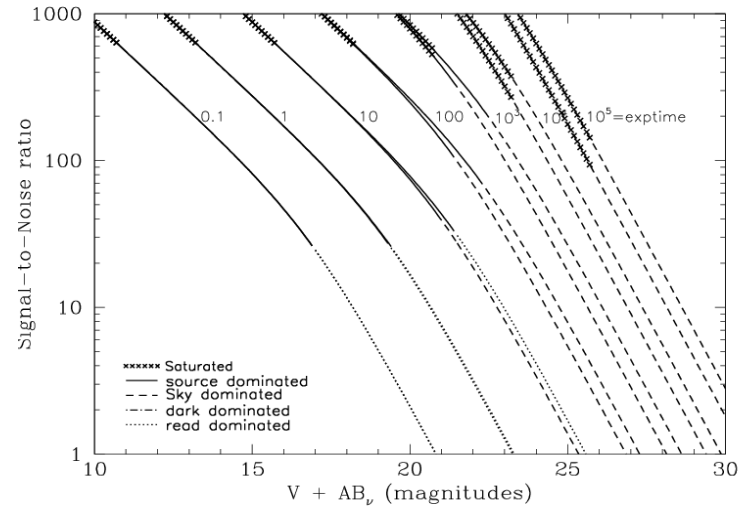
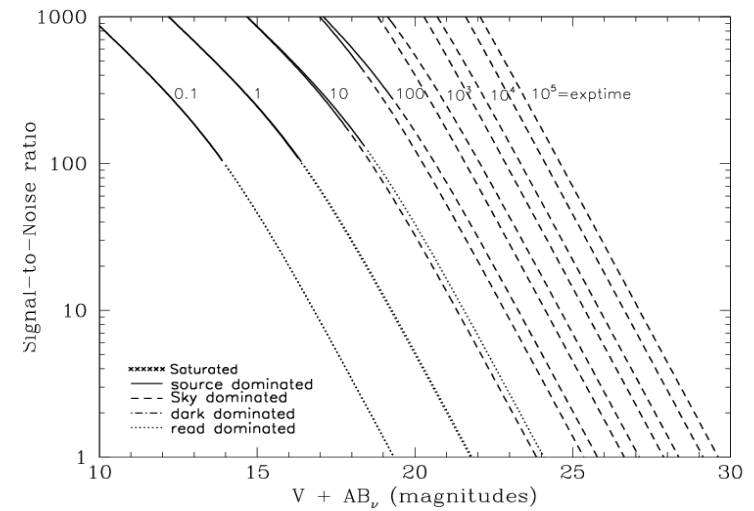


Figure 10.42: Extended source S/N vs.  $V+AB_v$  for the WFC/Clear filter. Top curves are for low sky and bottom curves are for average sky for a 1 arcsec<sup>2</sup> area.



## HRC/F220W

### Description

Near-UV filter.

Figure 10.43: Integrated System Throughput for HRC/F220W

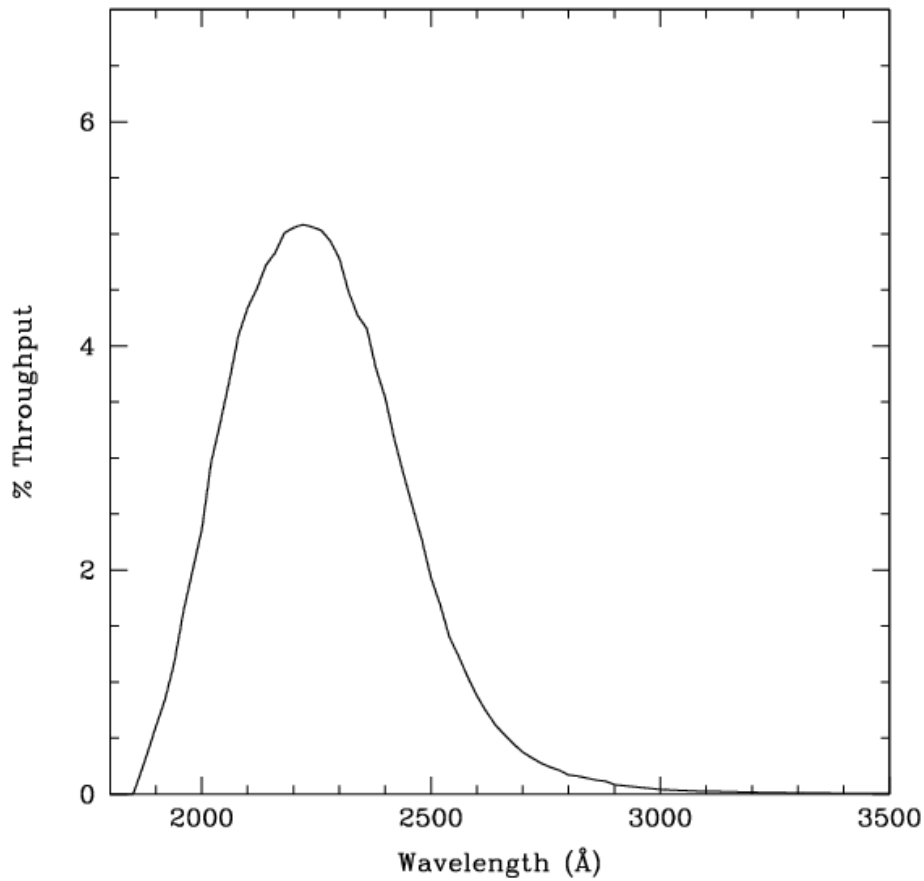


Figure 10.44: Point source S/N vs.  $V+AB_V$  for the HRC/F220W filter. Top curves are for low sky; bottom curves are for average sky.

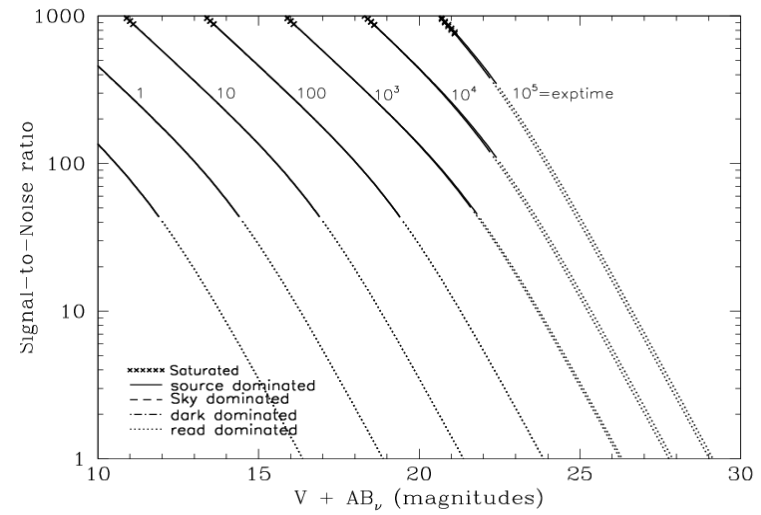
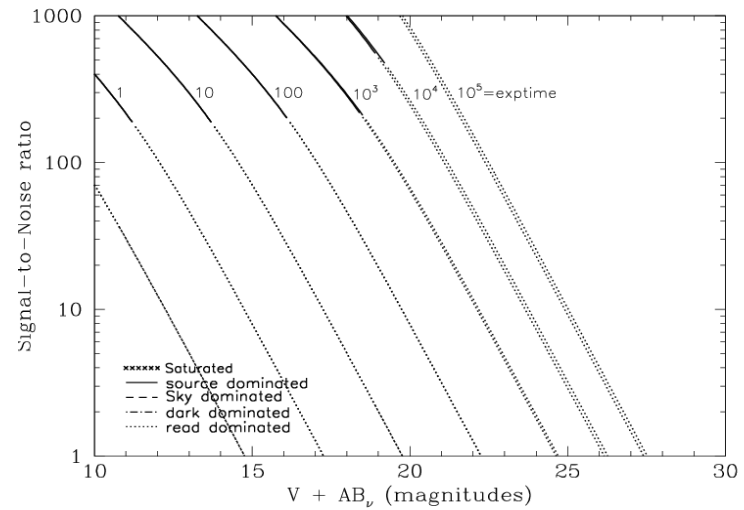


Figure 10.45: Extended source S/N vs.  $V+AB_V$  for the HRC/F220W filter. Top curves are for low sky and bottom curves are for average sky for a 1 arcsec<sup>2</sup> area.



## HRC/F250W

### Description

Near-UV filter.

Figure 10.46: Integrated System Throughput for HRC/F250W

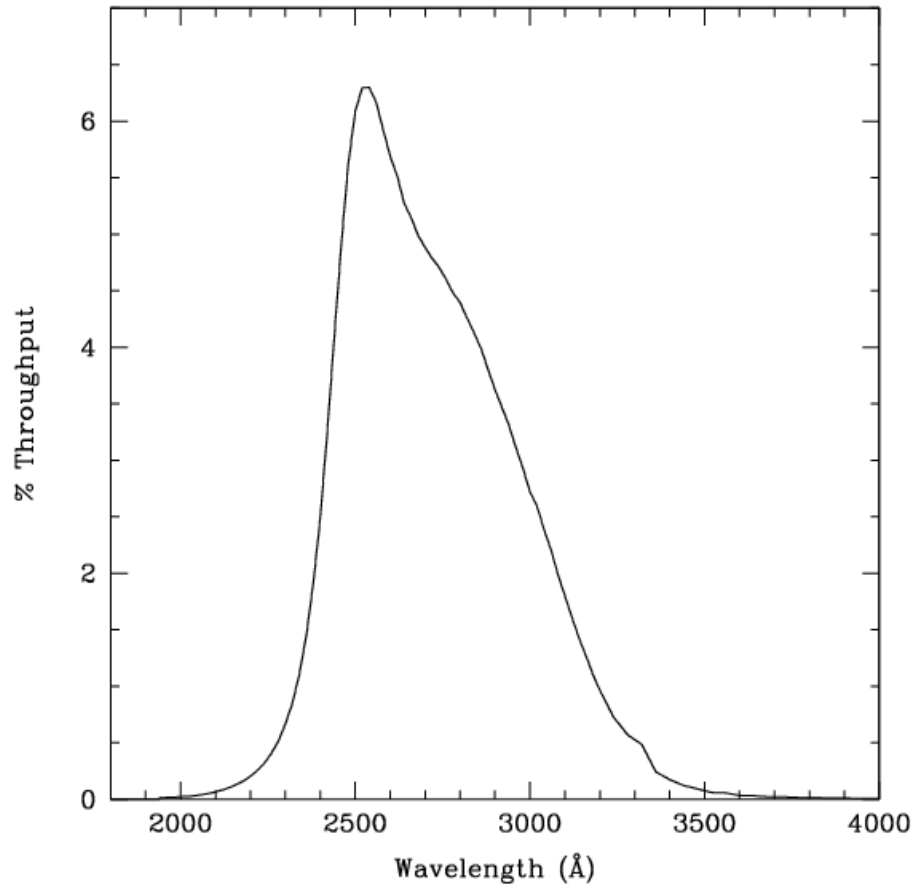


Figure 10.47: Point Source S/N vs.  $V+AB_V$  for the HRC/F250W filter. Top curves are for low sky; bottom curves are for average sky.

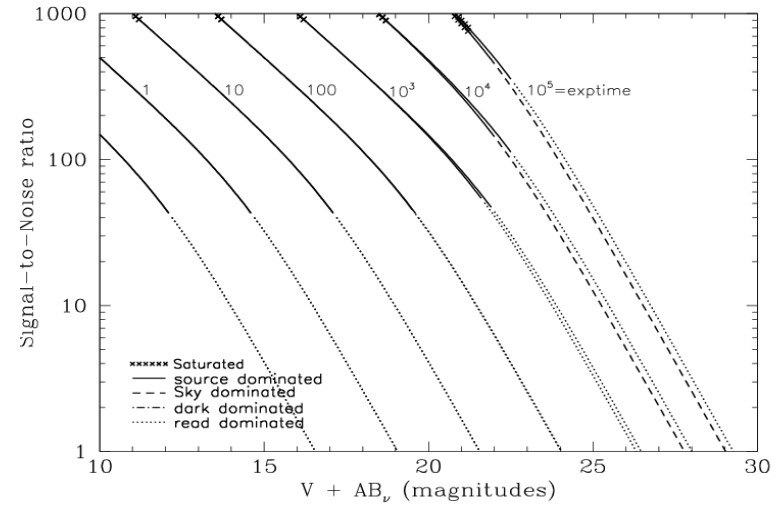
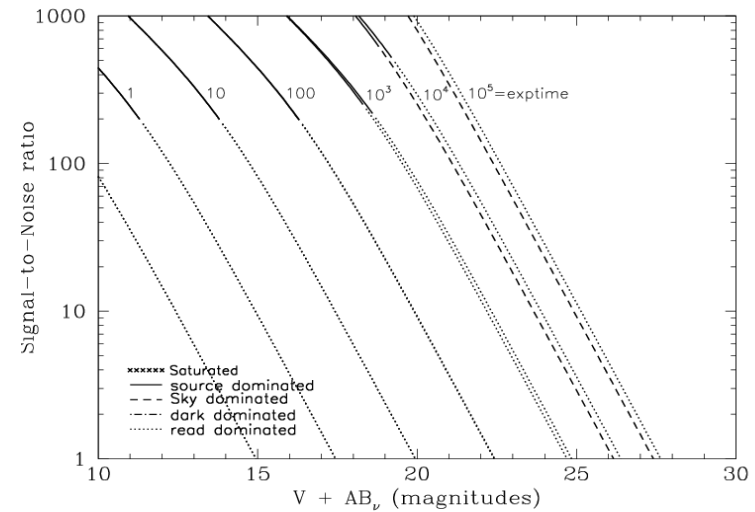


Figure 10.48: Extended Source S/N vs.  $V+AB_V$  for the HRC/F250W filter. Top curves are for low sky and bottom curves are for average sky for a 1 arcsec<sup>2</sup> area.



## HRC/F330W

### Description

HRC u filter.

Figure 10.49: Integrated System Throughput for HRC/F330W

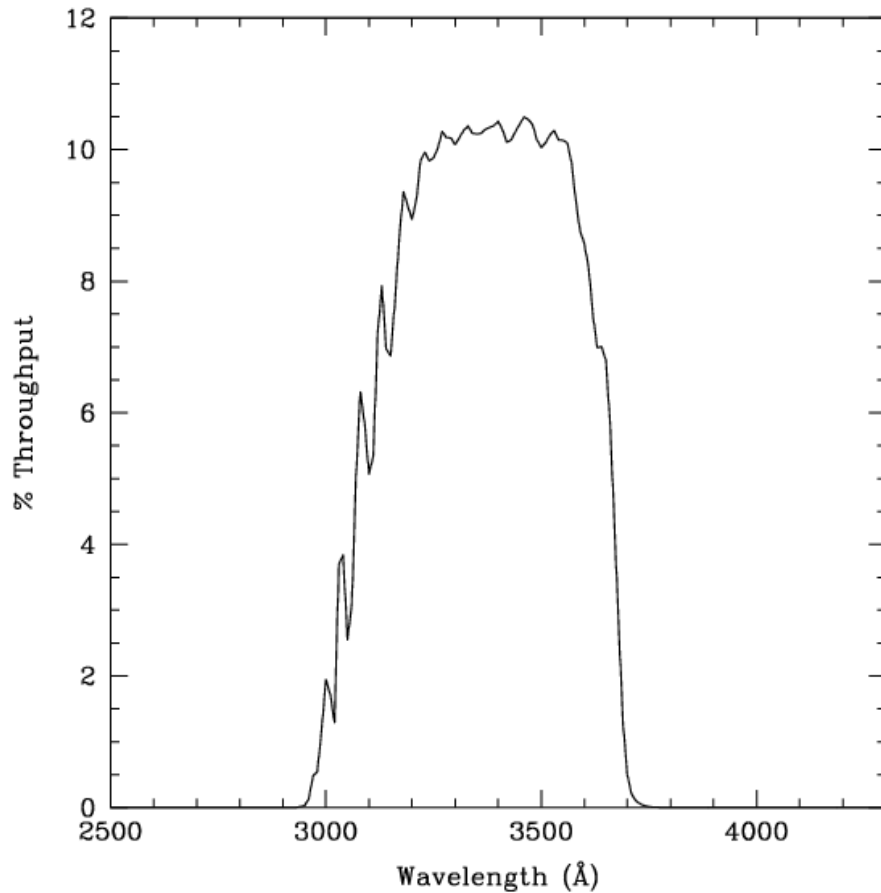


Figure 10.50: Point Source S/N vs.  $V+AB_V$  for the HRC/F330W filter. Top curves are for low sky; bottom curves are for average sky.

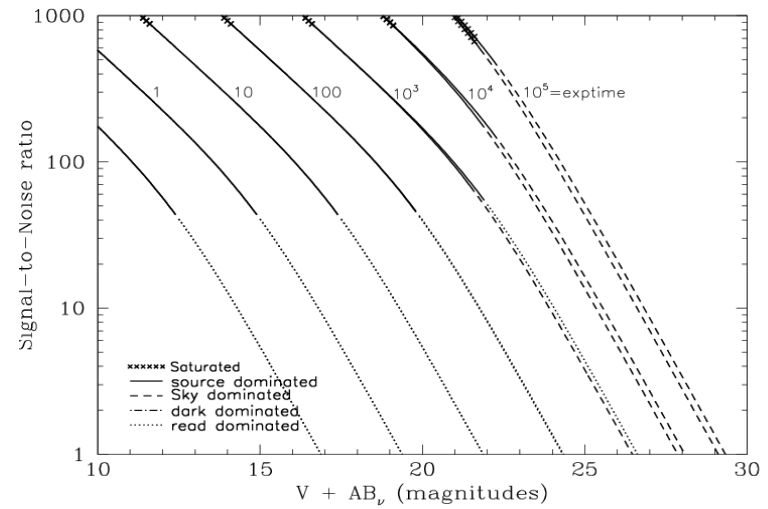
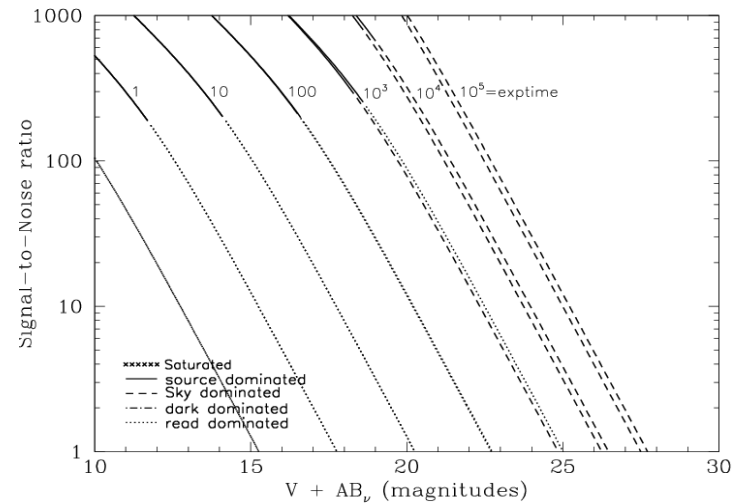


Figure 10.51: Extended Source S/N vs.  $V+AB_V$  for the HRC/F330W filter. Top curves are for low sky and bottom curves are for average sky for a 1 arcsec<sup>2</sup> area.



# HRC/F344N

## Description

NeV filter.

Figure 10.52: Integrated System Throughput for HRC/F344N

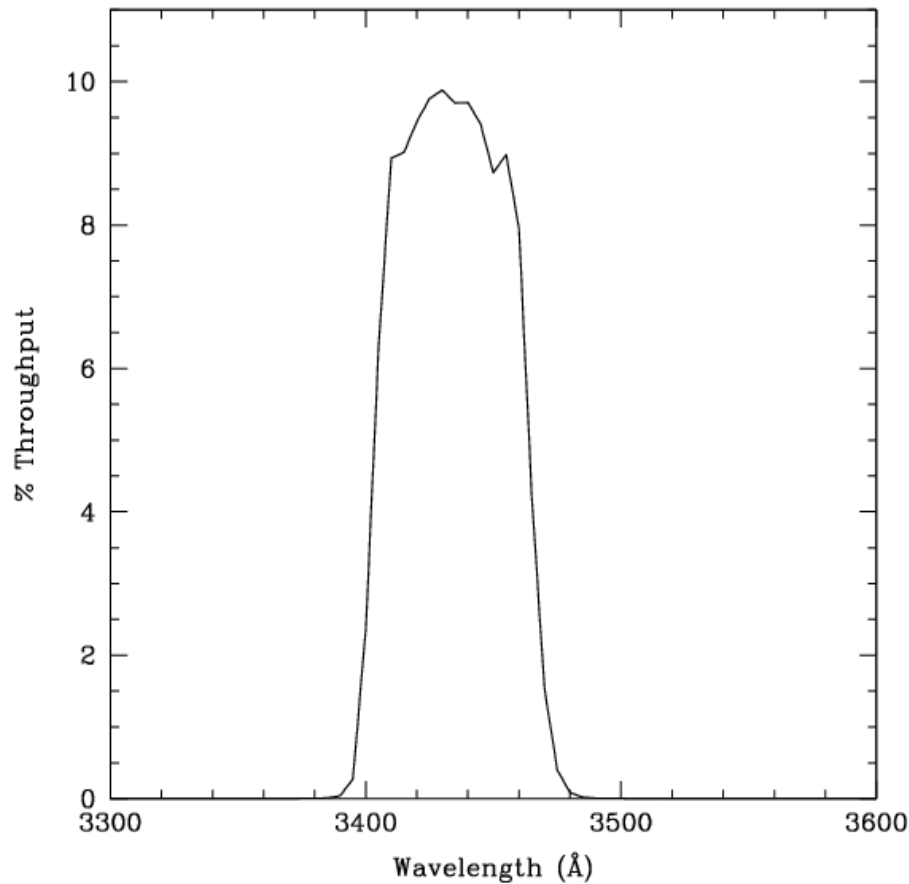


Figure 10.53: Point Source S/N vs.  $V+AB_V$  for the HRC/F344N filter. Top curves are for low sky; bottom curves are for average sky.

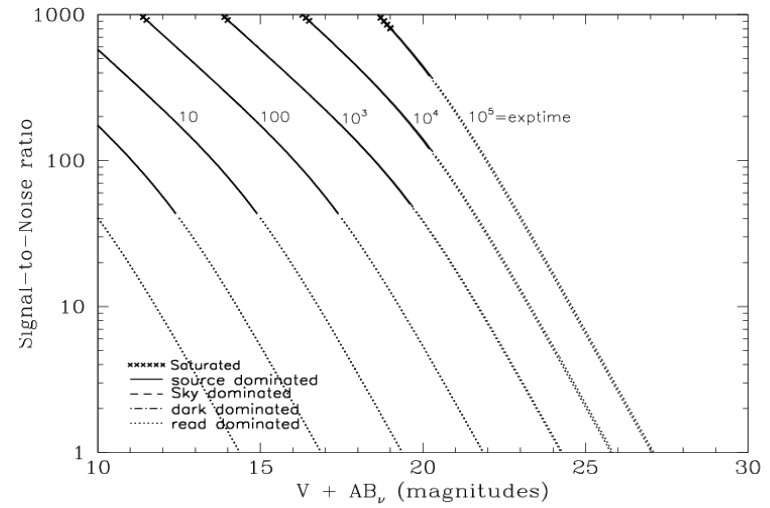
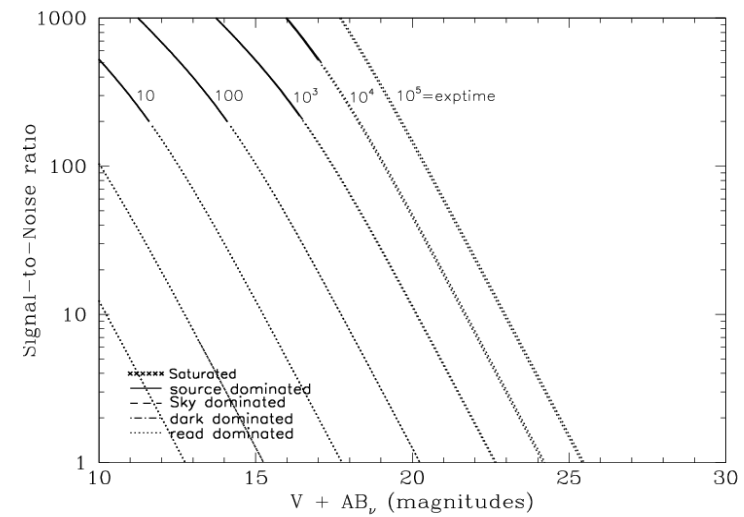


Figure 10.54: Extended Source S/N vs.  $V+AB_V$  for the HRC/F344N filter. Top curves are for low sky and bottom curves are for average sky for a 1 arcsec<sup>2</sup> area.



## HRC/F435W

### Description

Johnson B filter.

Figure 10.55: Integrated System Throughput for HRC/F435W

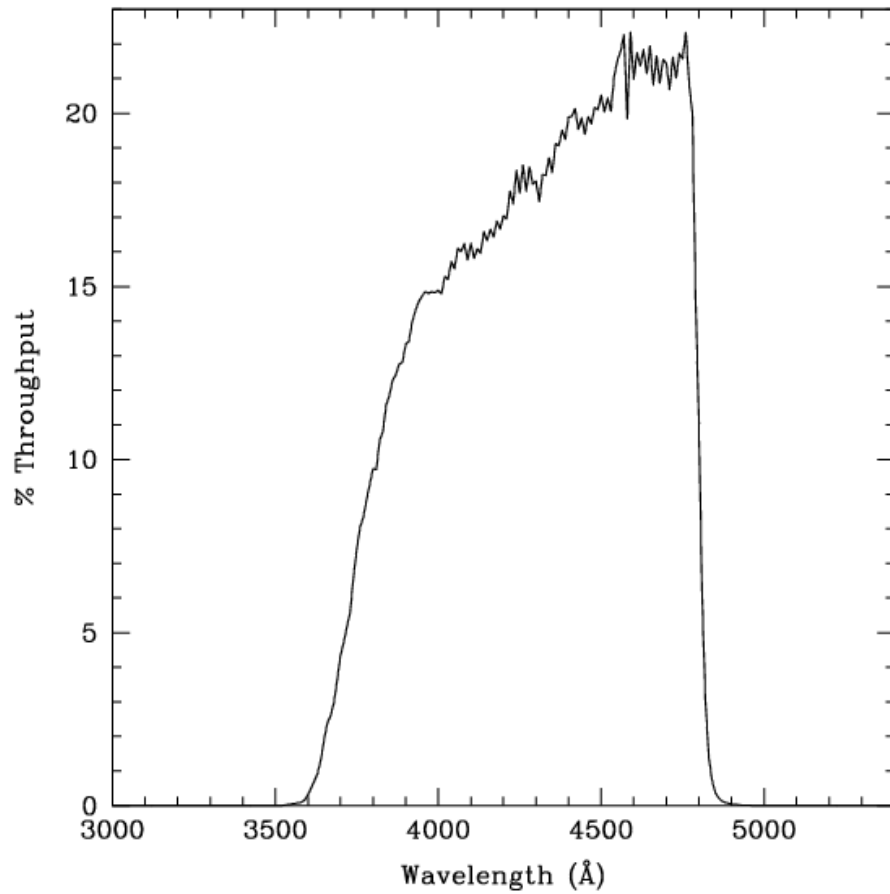


Figure 10.56: Point Source S/N vs.  $V+AB_V$  for the HRC/F435W filter. Top curves are for low sky; bottom curves are for average sky.

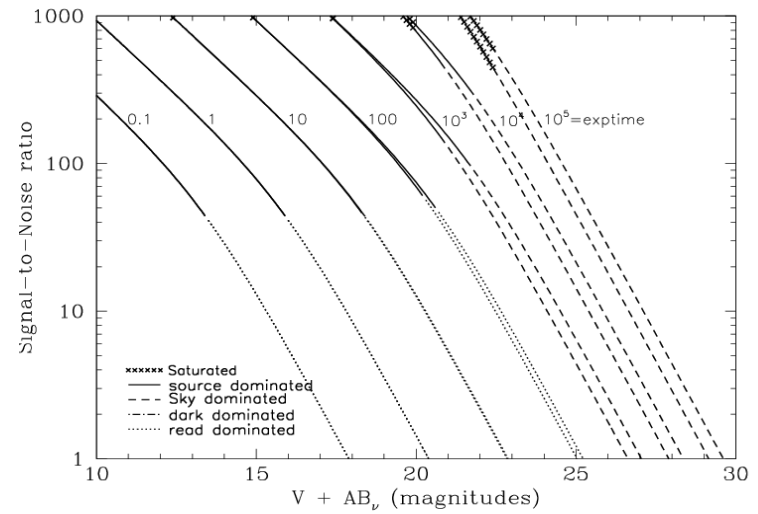
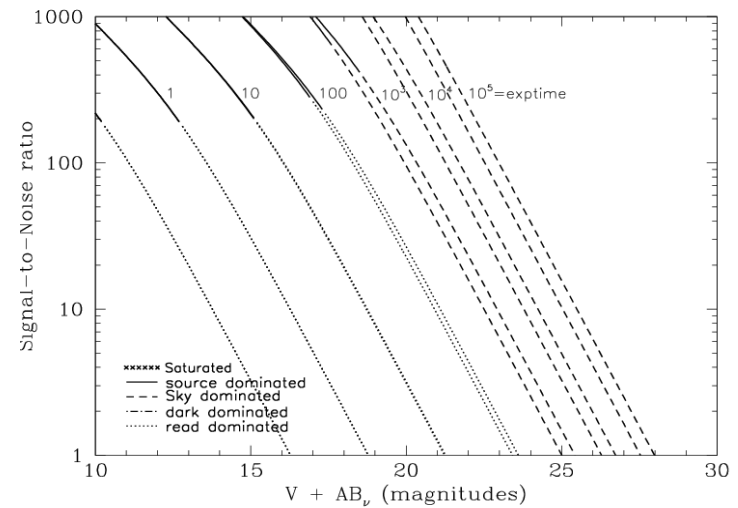


Figure 10.57: Extended Source S/N vs.  $V+AB_V$  for the HRC/F435W filter. Top curves are for low sky and bottom curves are for average sky for a 1 arcsec<sup>2</sup> area.



## HRC/F475W

### Description

Sloan Digital Sky Survey g filter.

Figure 10.58: Integrated System Throughput for HRC/F475W

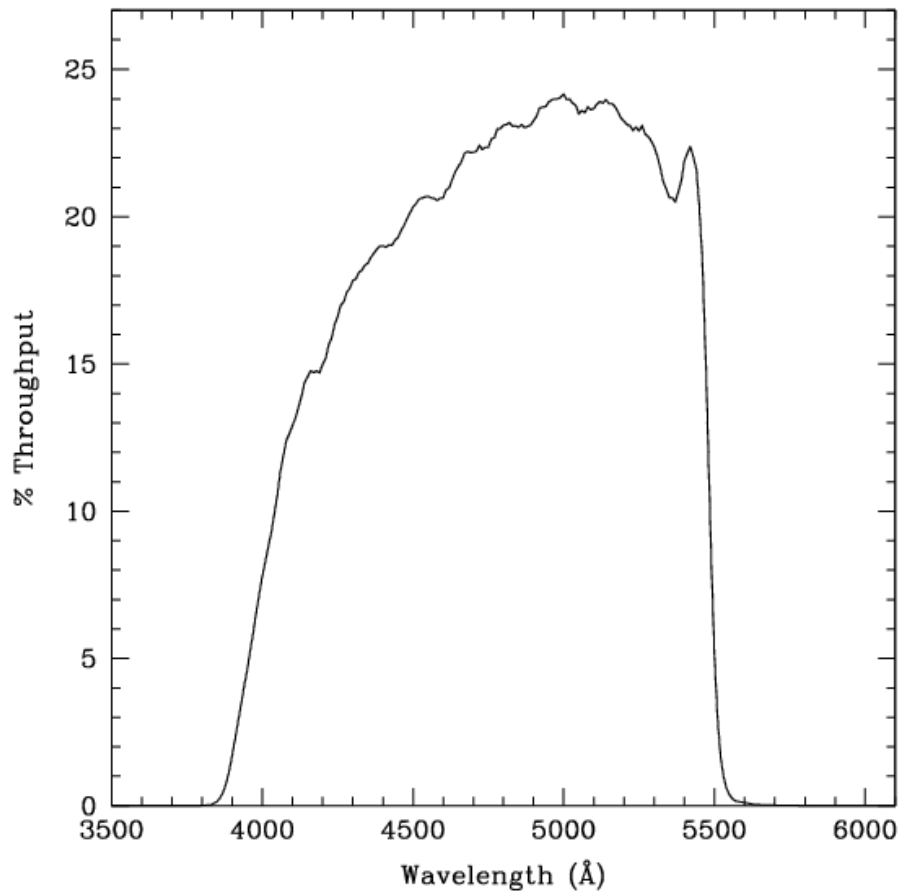


Figure 10.59: Point Source S/N vs.  $V+AB_V$  for the HRC/F475W filter. Top curves are for low sky; bottom curves are for average sky.

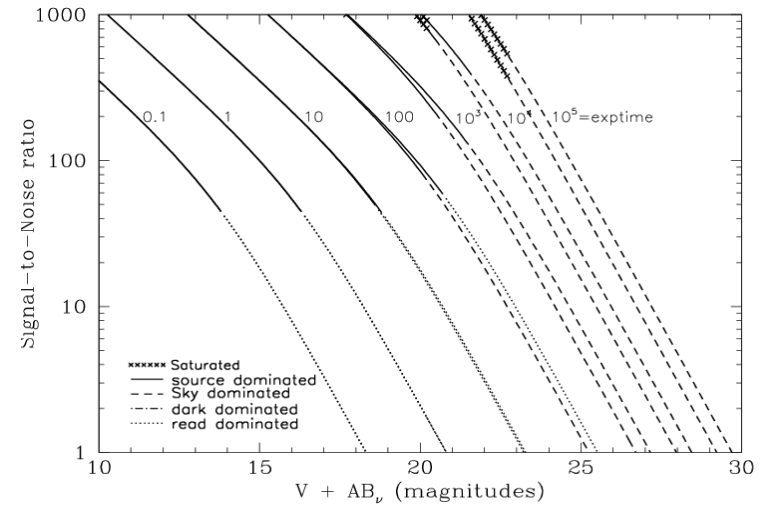
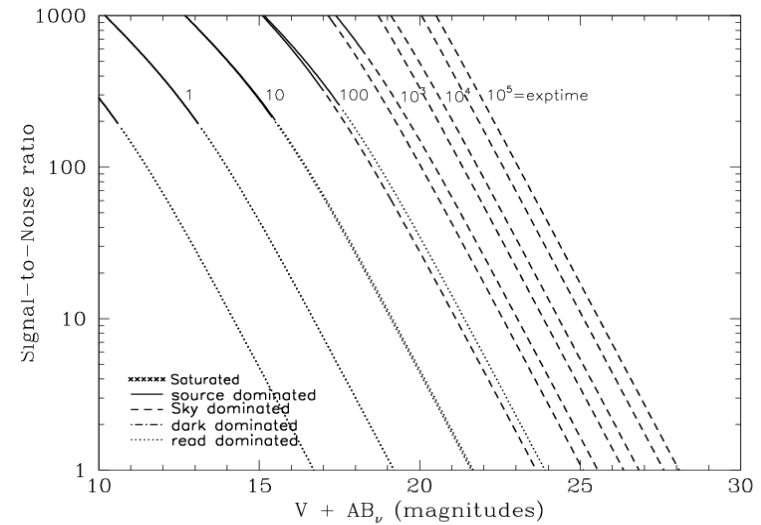


Figure 10.60: Extended Source S/N vs.  $V+AB_V$  for the HRC/F475W filter. Top curves are for low sky and bottom curves are for average sky for a 1 arcsec<sup>2</sup> area.



## HRC/F502N

### Description

OIII filter.

Figure 10.61: Integrated System Throughput for HRC/F502N

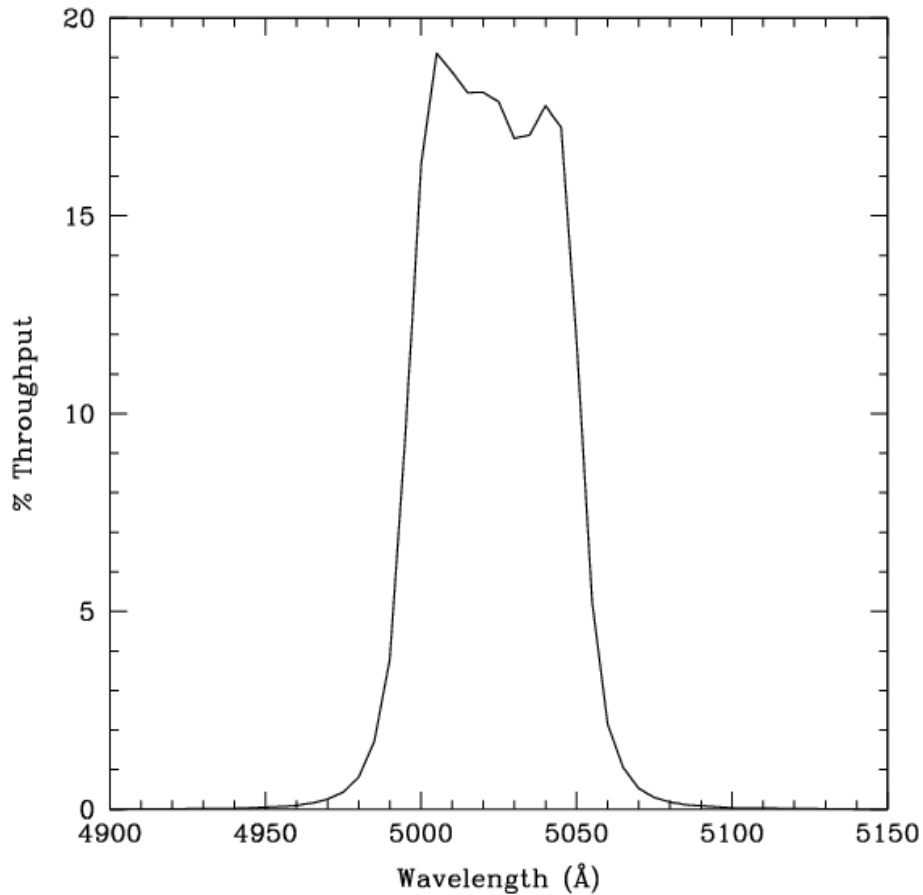


Figure 10.62: Point Source S/N vs.  $V+AB_V$  for the HRC/F502N filter. Top curves are for low sky; bottom curves are for average sky.

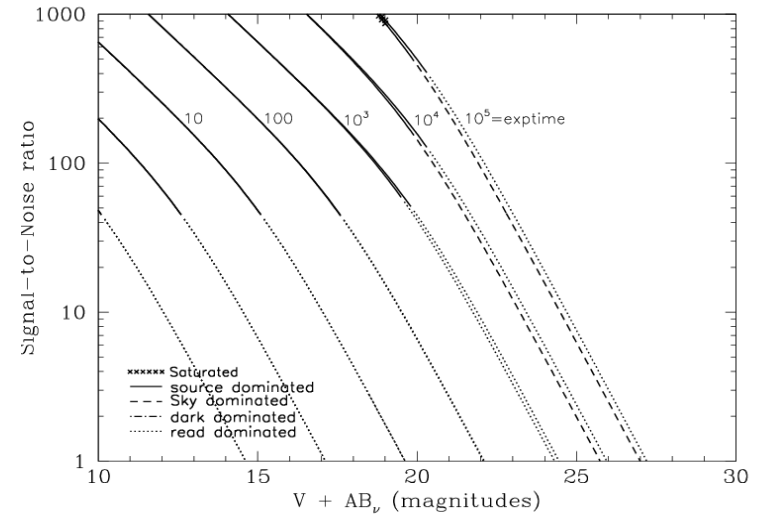
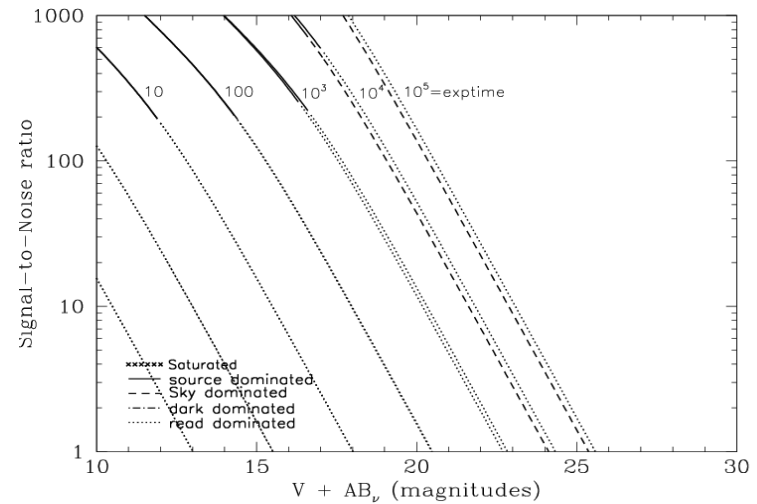


Figure 10.63: Extended Source S/N vs.  $V+AB_V$  for the HRC/F502N filter. Top curves are for low sky and bottom curves are for average sky for a 1 arcsec<sup>2</sup> area.



# HRC/F550M

## Description

Narrow V filter.

Figure 10.64: Integrated System Throughput for HRC/F550M

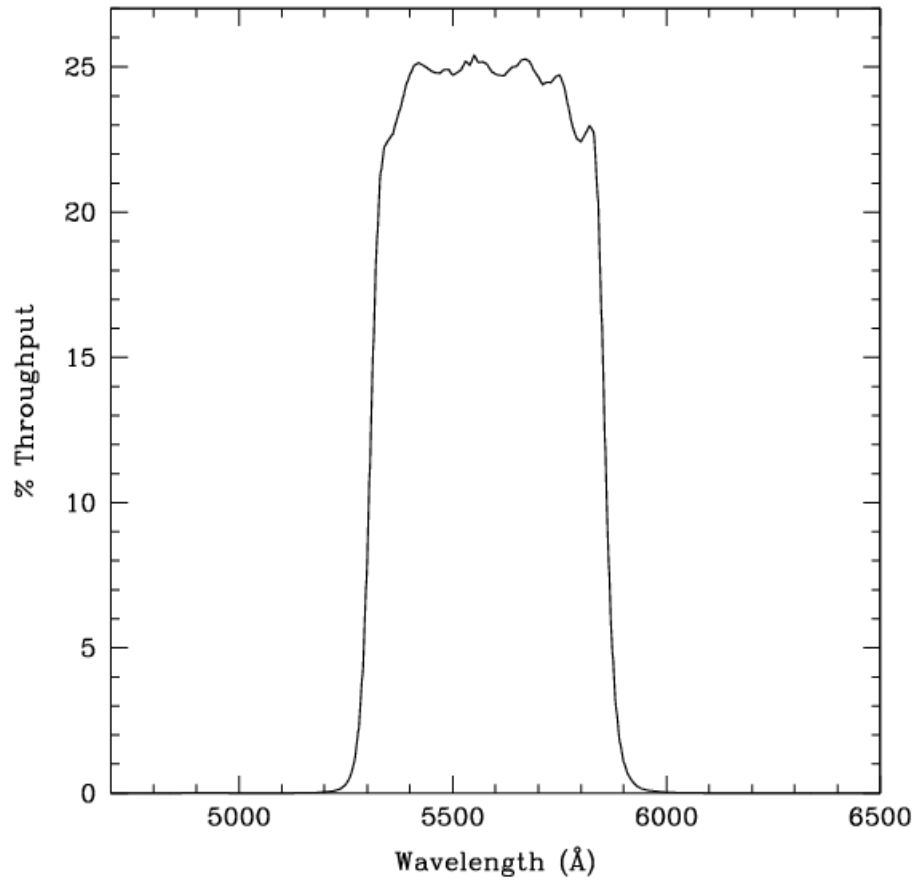


Figure 10.65: Point Source S/N vs.  $V+AB_V$  for the HRC/F550M filter. Top curves are for low sky; bottom curves are for average sky.

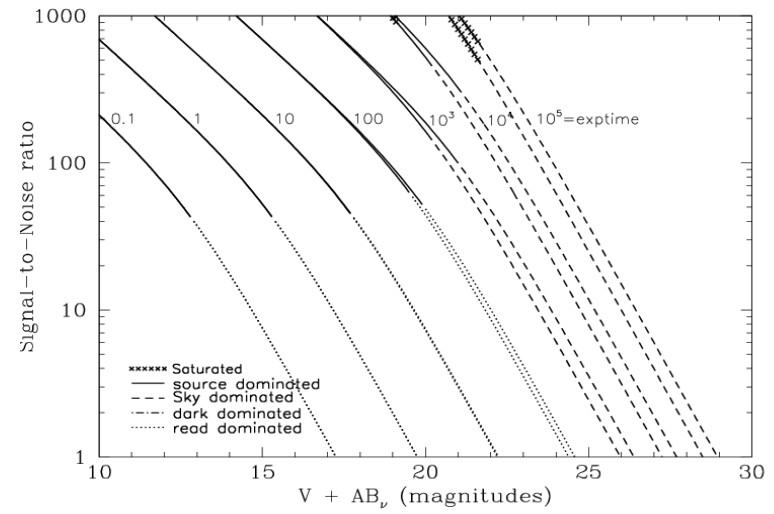
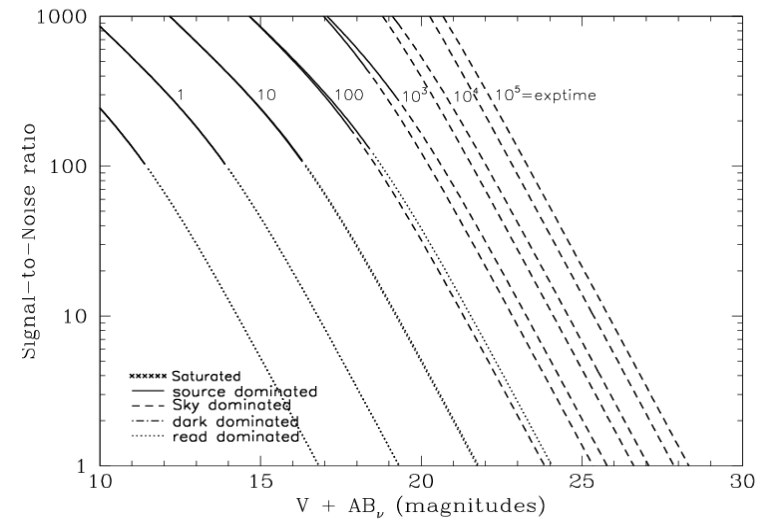


Figure 10.66: Extended Source S/N vs.  $V+AB_V$  for the HRC/F550M filter. Top curves are for low sky and bottom curves are for average sky for a 1 arcsec<sup>2</sup> area.



## HRC/F555W

### Description

Johnson V filter.

Figure 10.67: Integrated System Throughput for HRC/F555W

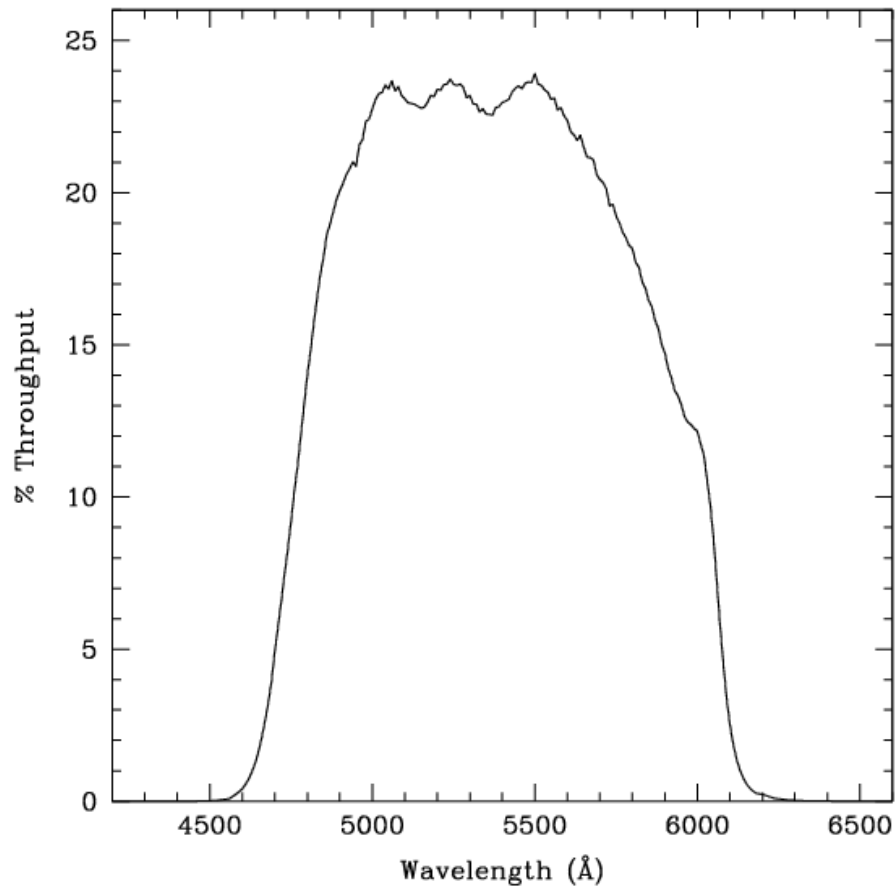


Figure 10.68: Point Source S/N vs.  $V+AB_V$  for the HRC/F555W filter. Top curves are for low sky; bottom curves are for average sky.

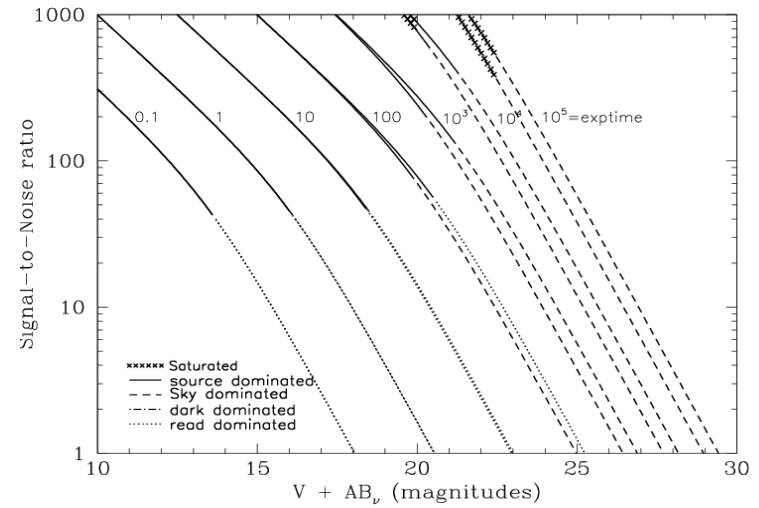
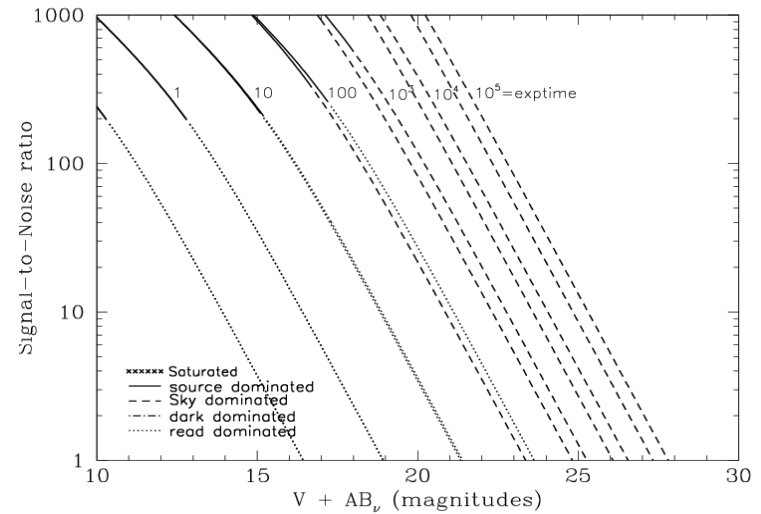


Figure 10.69: Extended Source S/N vs.  $V+AB_V$  for the HRC/F555W filter. Top curves are for low sky and bottom curves are for average sky for a 1 arcsec<sup>2</sup> area.



# HRC/F606W

## Description

Broad V filter.

Figure 10.70: Integrated System Throughput for HRC/F606W

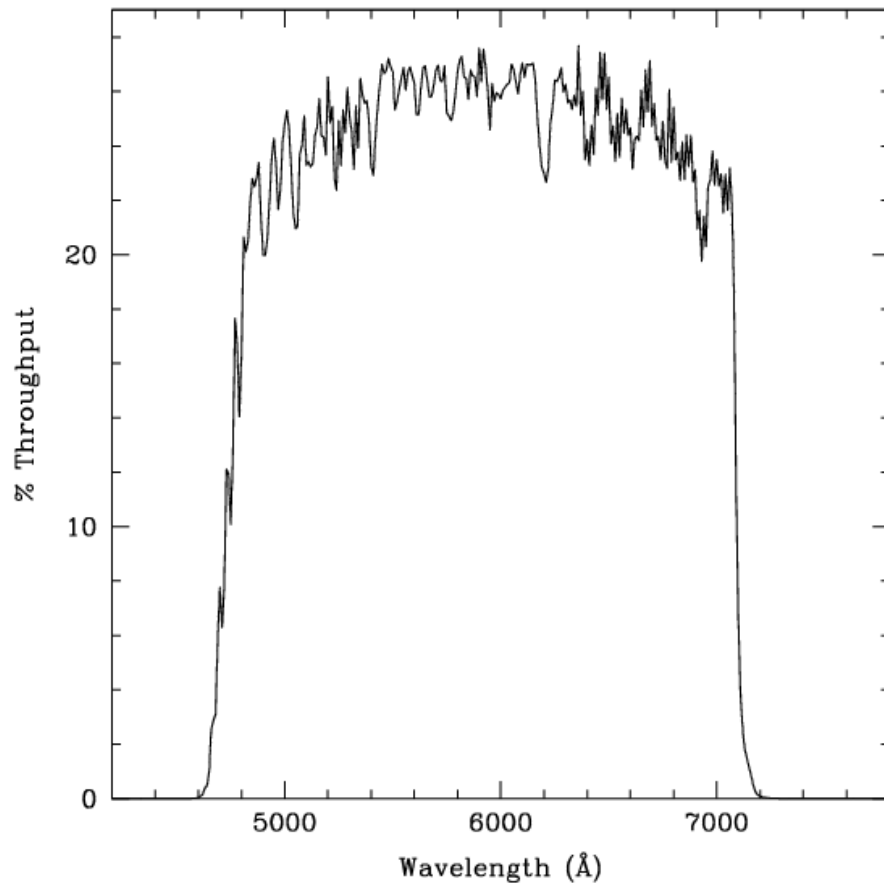


Figure 10.71: Point Source S/N vs.  $V+AB_V$  for the HRC/F606W filter. Top curves are for low sky; bottom curves are for average sky.

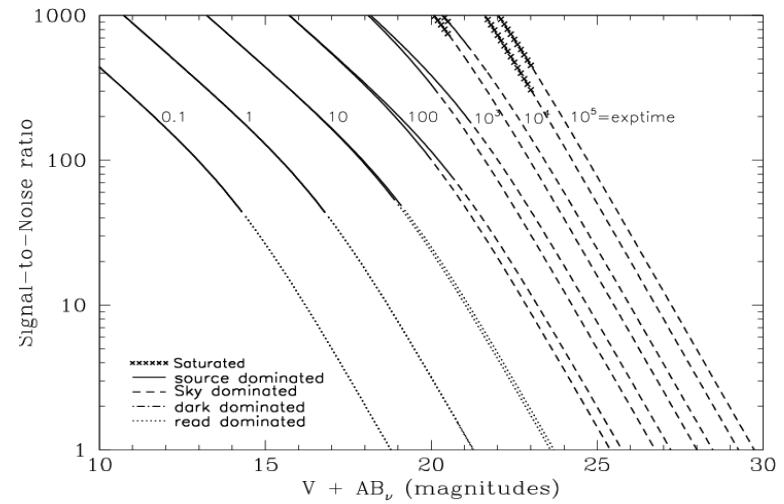
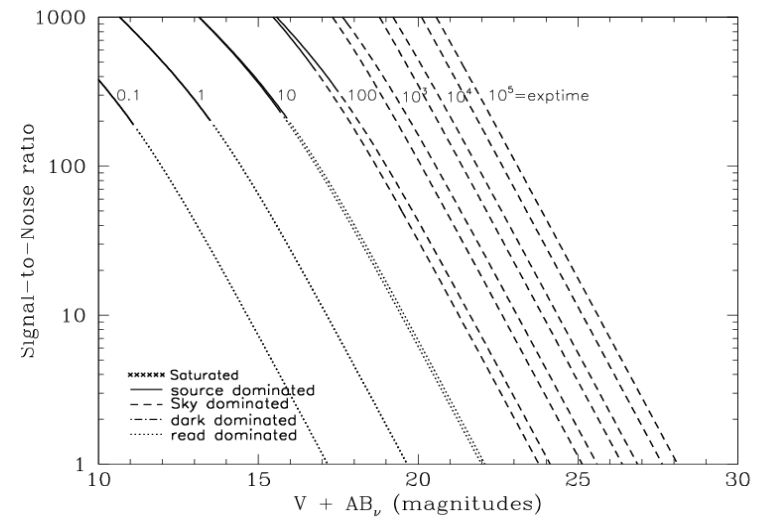


Figure 10.72: Extended Source S/N vs.  $V+AB_V$  for the HRC/F606W filter. Top curves are for low sky and bottom curves are for average sky for a 1 arcsec<sup>2</sup> area.



## HRC/F625W

### Description

Sloan Digital Sky Survey r filter.

Figure 10.73: Integrated System Throughput for HRC/F625W

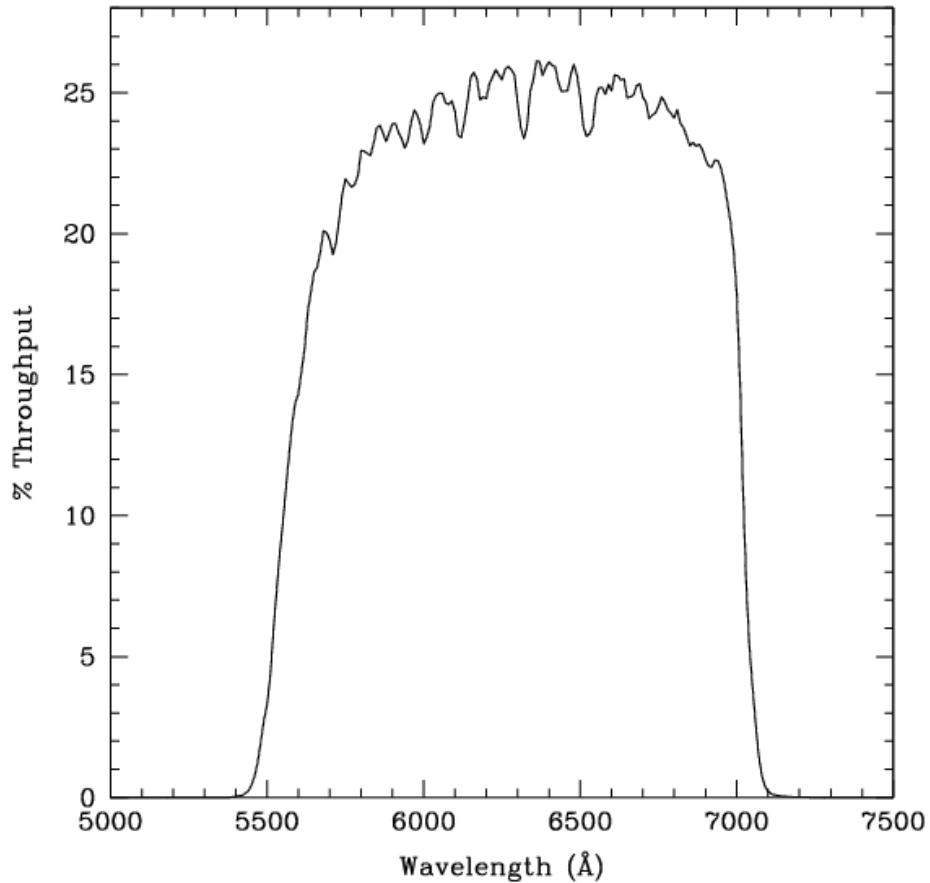


Figure 10.74: Point Source S/N vs.  $V+AB_v$  for the HRC/F625W filter. Top curves are for low sky; bottom curves are for average sky.

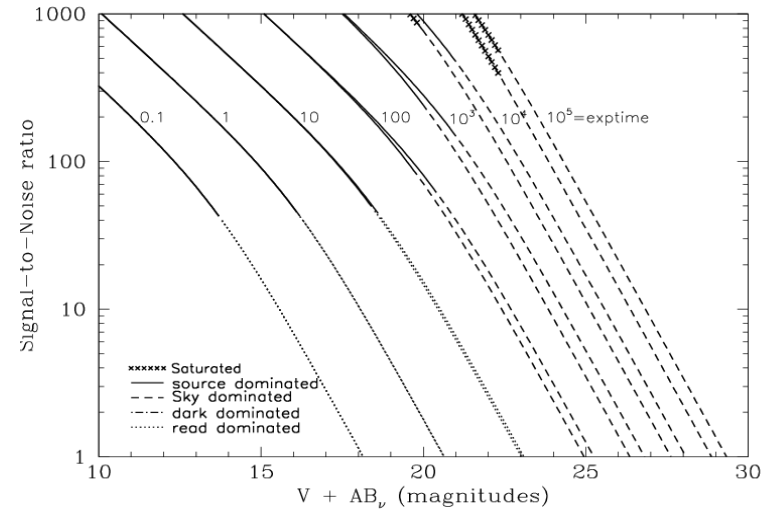
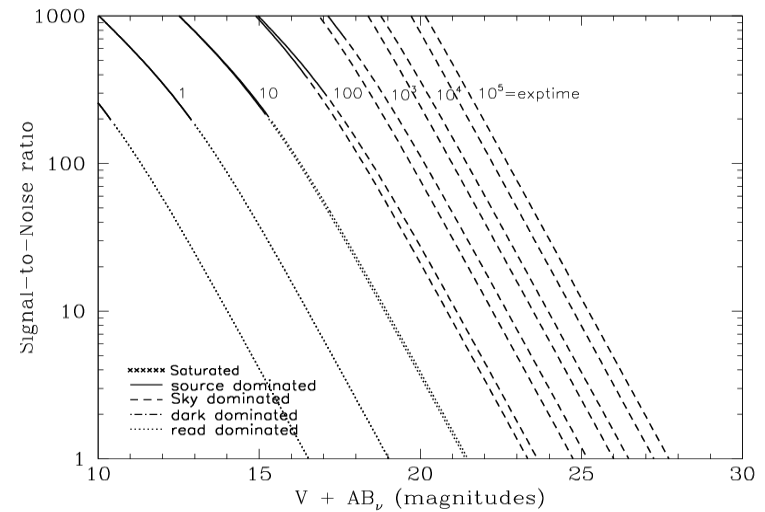


Figure 10.75: Extended Source S/N vs.  $V+AB_v$  for the HRC/F625W filter. Top curves are for low sky and bottom curves are for average sky for a 1 arcsec<sup>2</sup> area.



# HRC/F658N

## Description

H $\alpha$  filter.

Figure 10.76: Integrated System Throughput for HRC/F658N

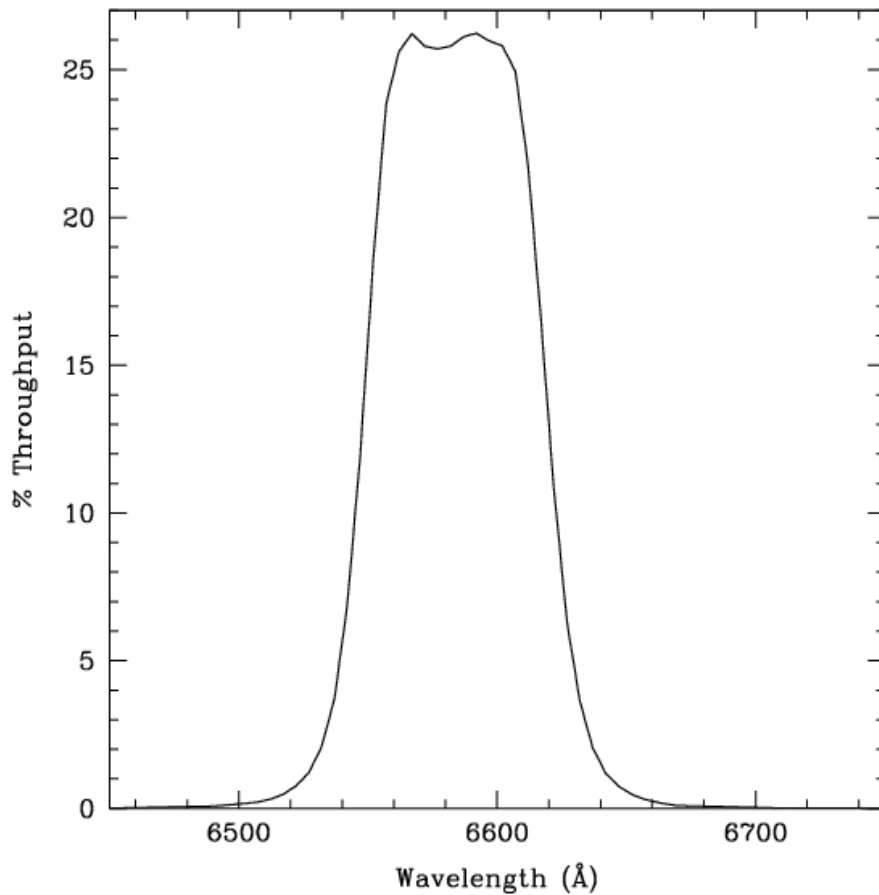


Figure 10.77: Point Source S/N vs.  $V+AB_V$  for the HRC/F658N filter. Top curves are for low sky; bottom curves are for average sky.

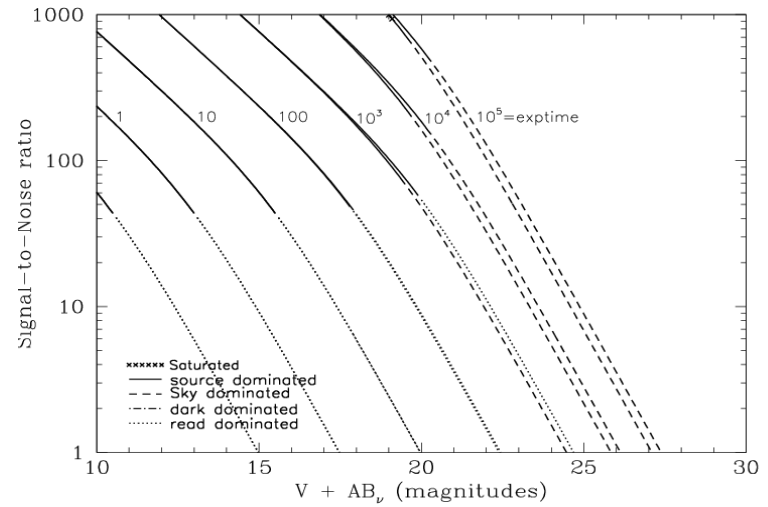
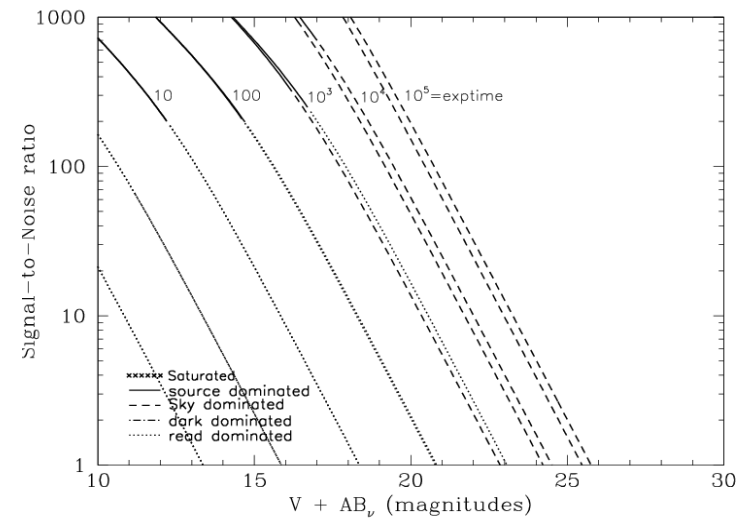


Figure 10.78: Extended Source S/N vs.  $V+AB_V$  for the HRC/F658N filter. Top curves are for low sky and bottom curves are for average sky for a 1 arcsec<sup>2</sup> area.



## HRC/F660N

### Description

NII filter.

Figure 10.79: Integrated System Throughput for HRC/F660N

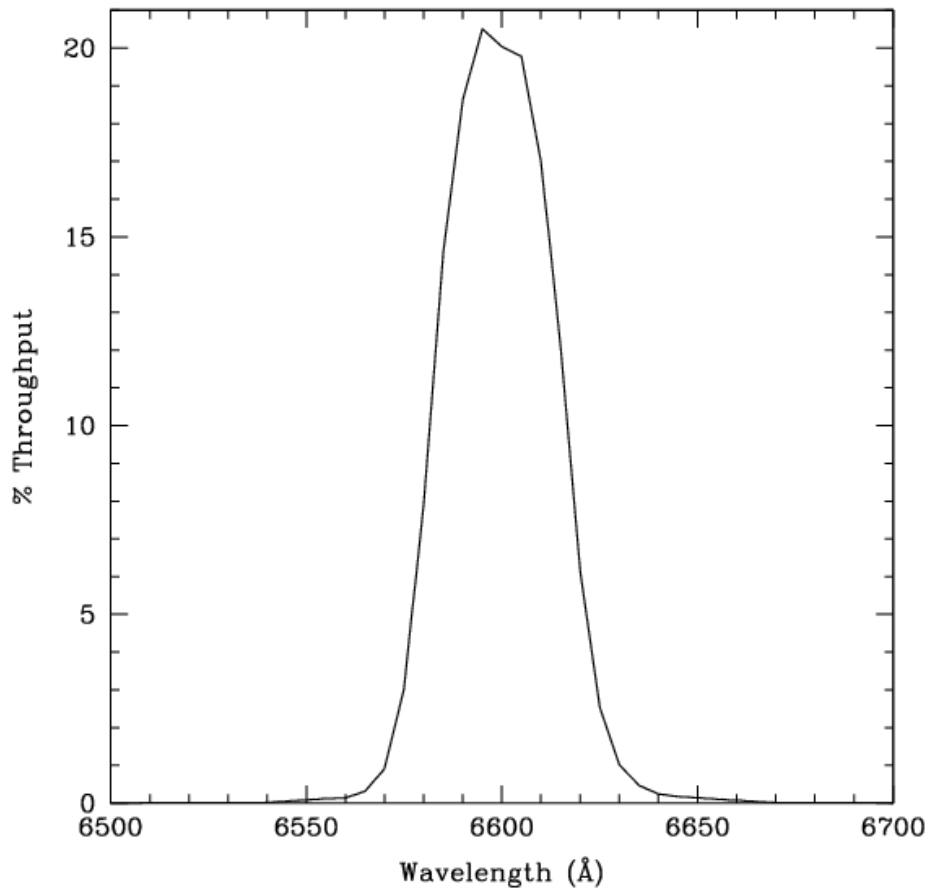


Figure 10.80: Point Source S/N vs.  $V+AB_V$  for the HRC/F660N filter. Top curves are for low sky; bottom curves are for average sky.

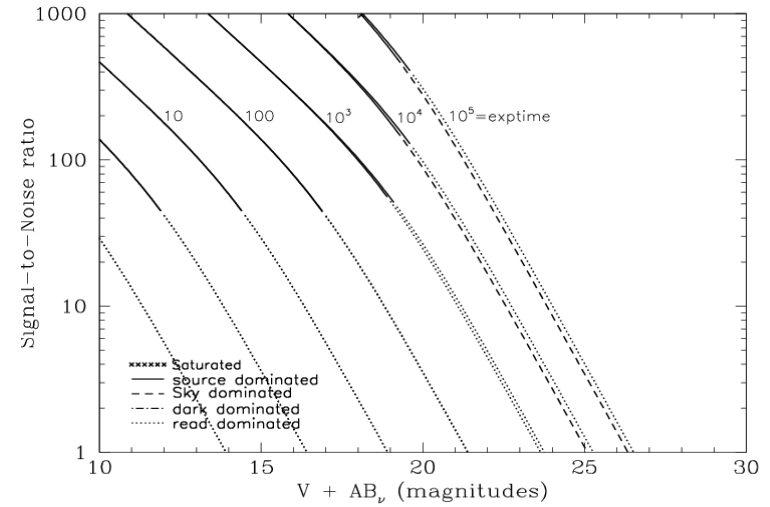
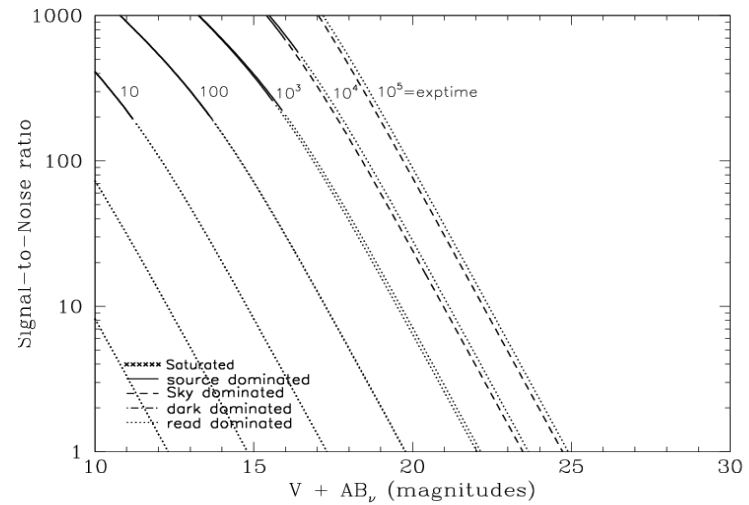


Figure 10.81: Extended Source S/N vs.  $V+AB_V$  for the HRC/F660N filter. Top curves are for low sky and bottom curves are for average sky for a 1 arcsec<sup>2</sup> area.



# HRC/F775W

## Description

Sloan Digital Sky Survey i filter.

Figure 10.82: Integrated System Throughput for HRC/F775W

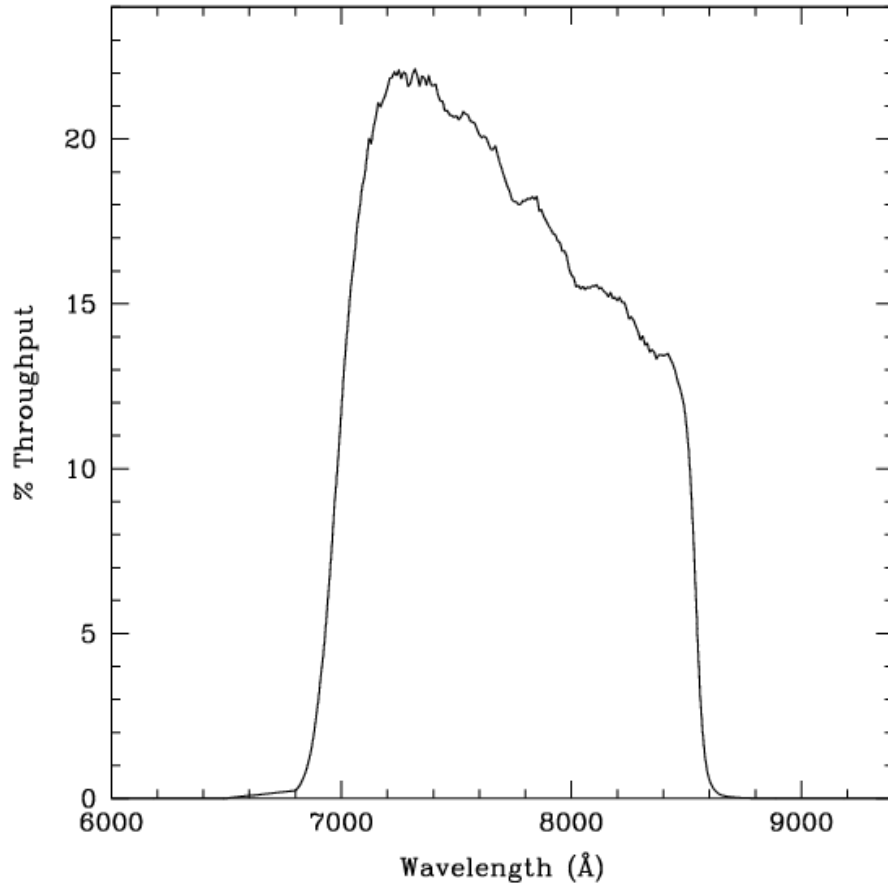


Figure 10.83: Point Source S/N vs.  $V+AB_V$  for the HRC/F775W filter. Top curves are for low sky; bottom curves are for average sky.

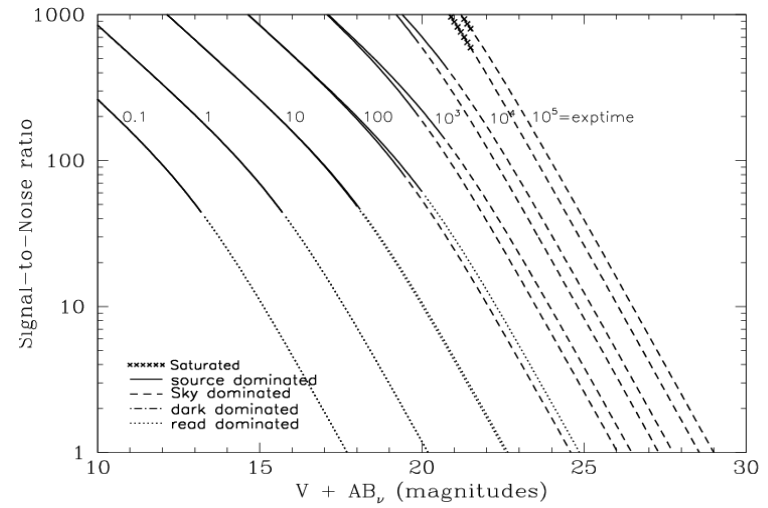
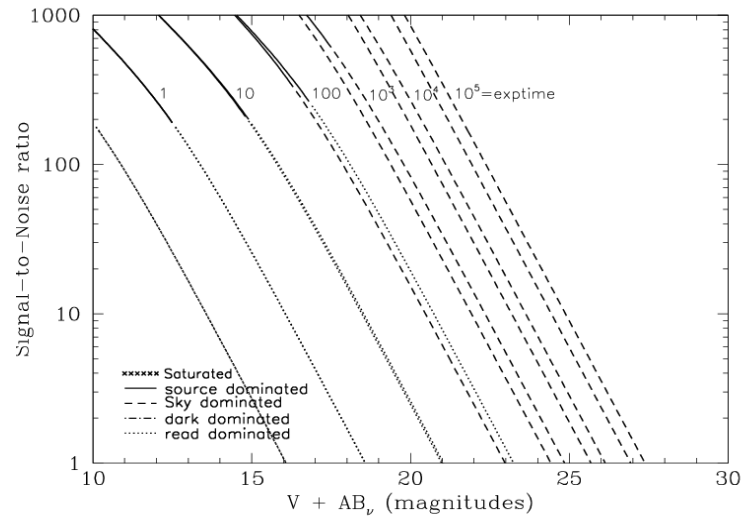


Figure 10.84: Extended Source S/N vs.  $V+AB_V$  for the HRC/F775W filter. Top curves are for low sky and bottom curves are for average sky for a 1 arcsec<sup>2</sup> area.



## HRC/F814W

### Description

Broad I filter.

Figure 10.85: Integrated System Throughput for HRC/F814W

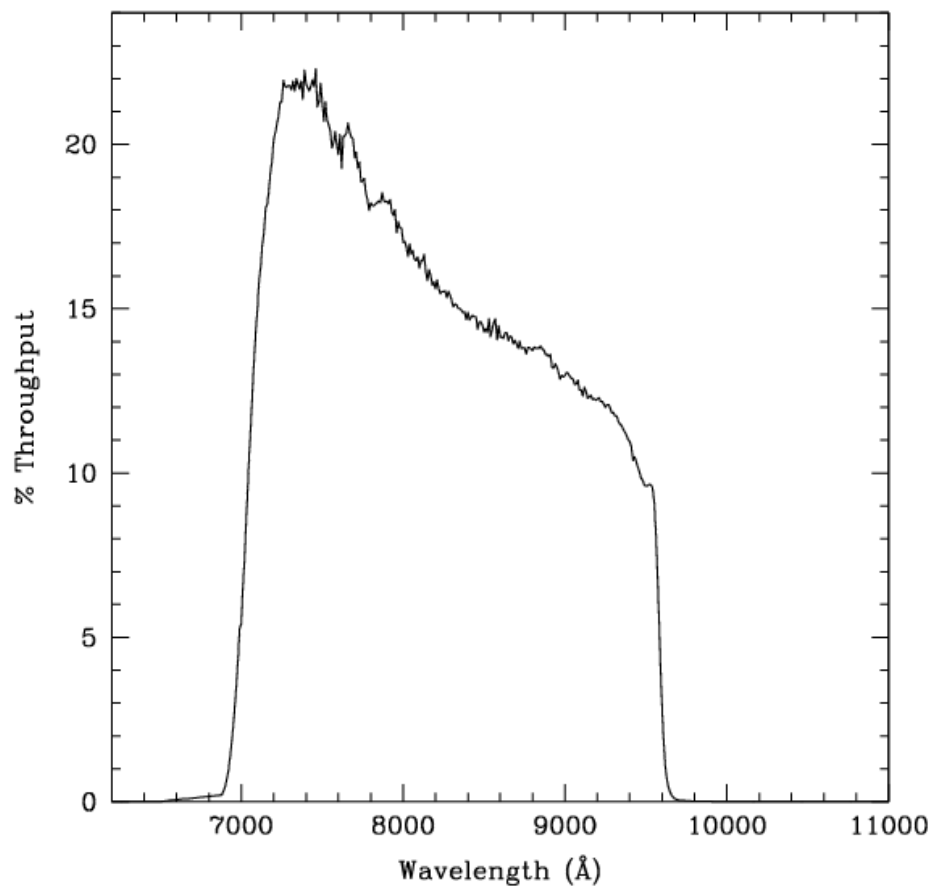


Figure 10.86: Point Source S/N vs.  $V+AB_V$  for the HRC/F814W filter. Top curves are for low sky; bottom curves are for average sky.

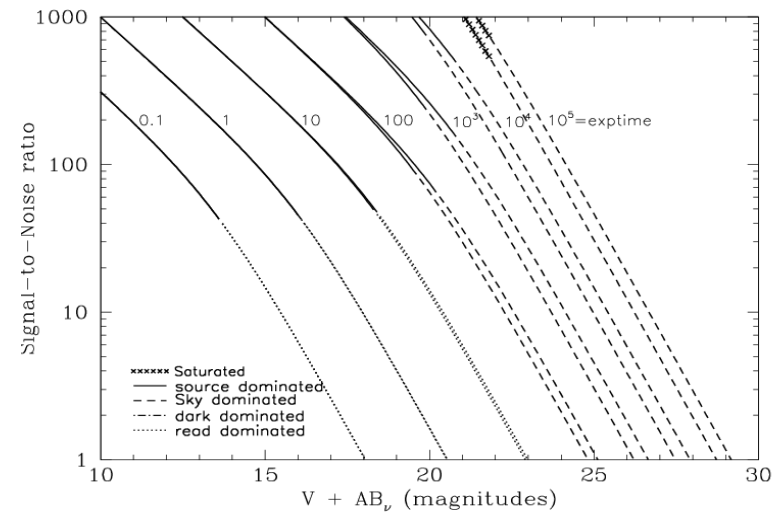
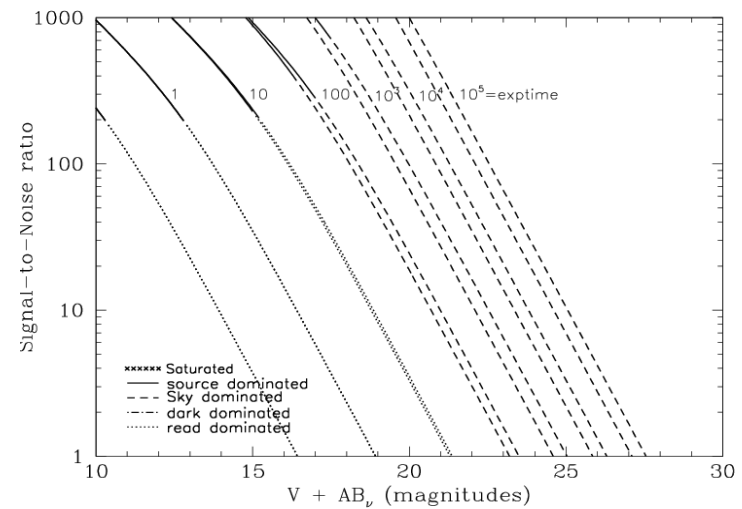


Figure 10.87: Extended Source S/N vs.  $V+AB_V$  for the HRC/F814W filter. Top curves are for low sky and bottom curves are for average sky for a 1 arcsec<sup>2</sup> area.



# HRC/F850LP

## Description

Sloan Digital Sky Survey z filter.

Figure 10.88: Integrated System Throughput for HRC/F850LP

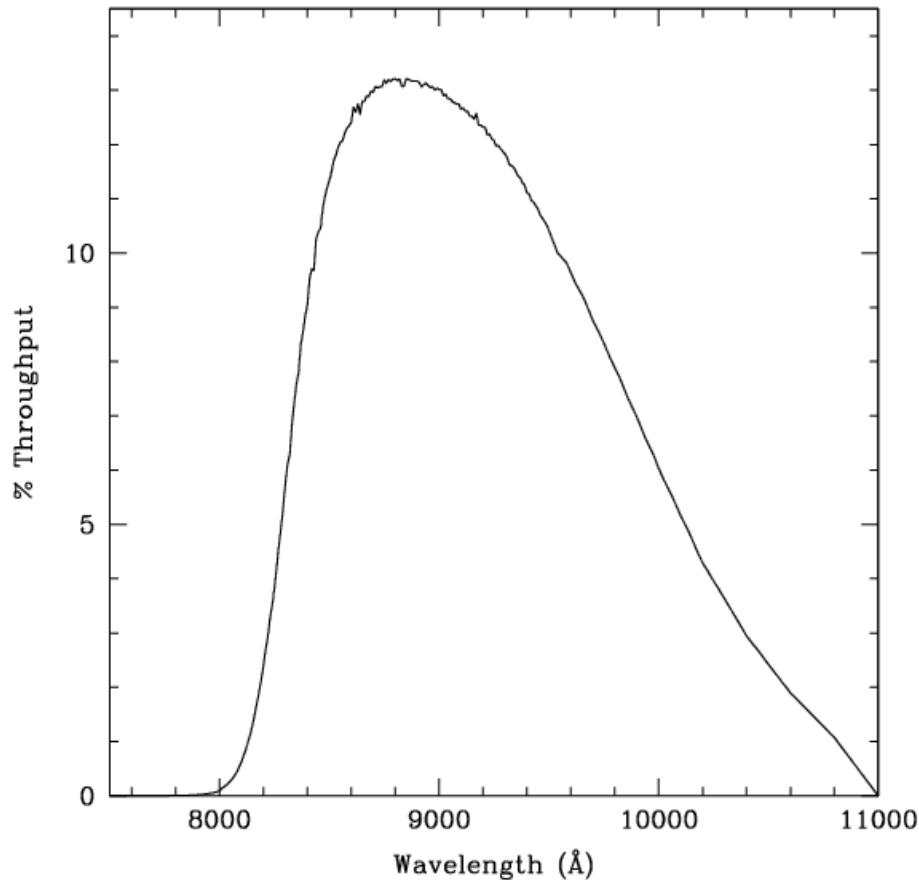


Figure 10.89: Point Source S/N vs.  $V+AB_V$  for the HRC/F850LP filter. Top curves are for low sky; bottom curves are for average sky.

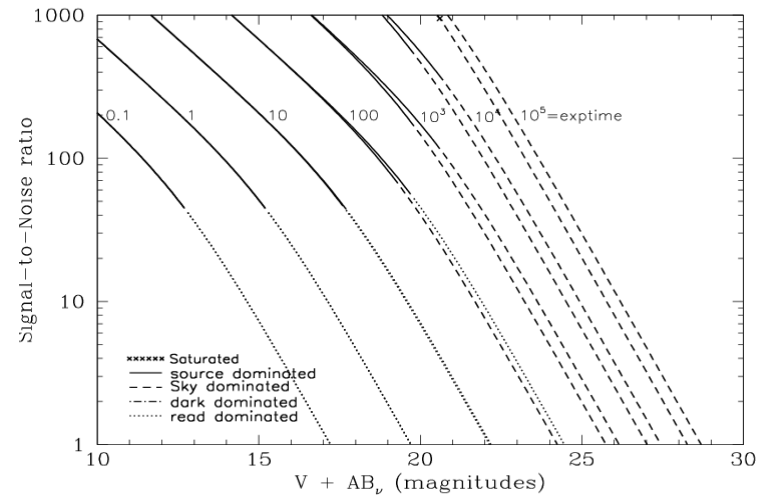
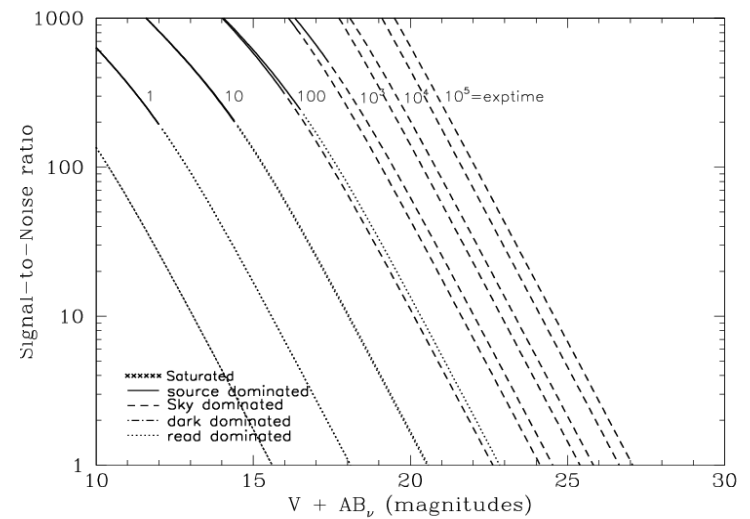


Figure 10.90: Extended Source S/N vs.  $V+AB_V$  for the HRC/F850LP filter. Top curves are for low sky and bottom curves are for average sky for a 1 arcsec<sup>2</sup> area.



## HRC/F892N

### Description

Methane filter.

Figure 10.91: Integrated System Throughput for HRC/F892N

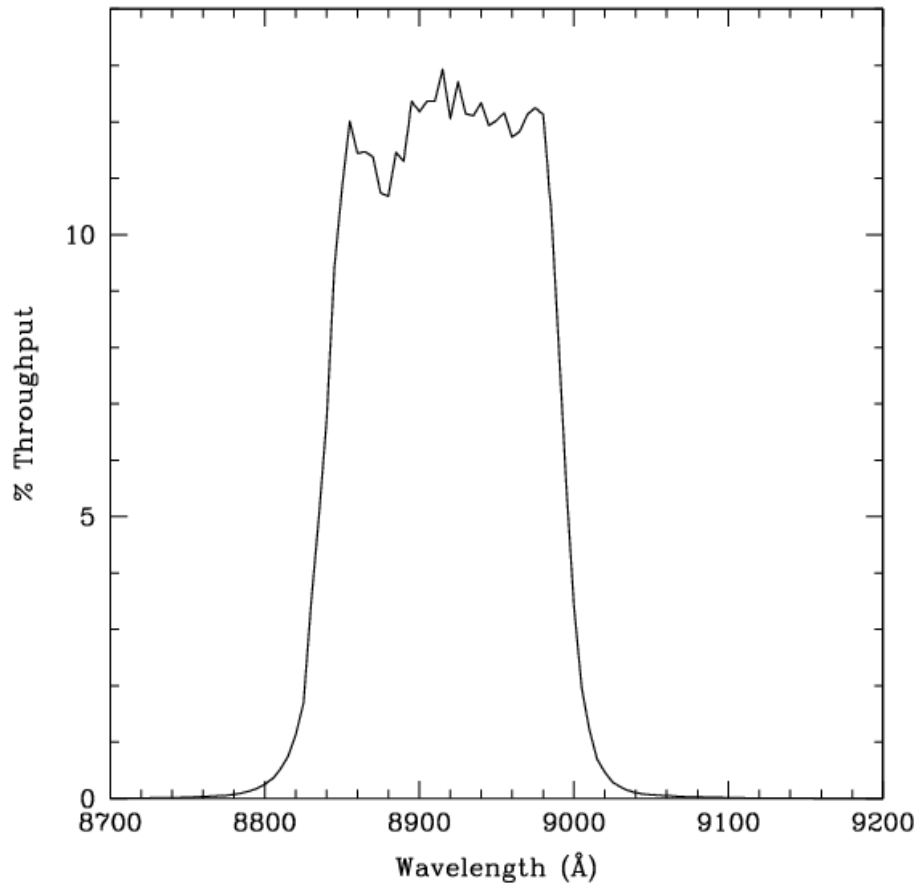


Figure 10.92: Point Source S/N vs.  $V+AB_V$  for the HRC/F892N filter. Top curves are for low sky; bottom curves are for average sky.

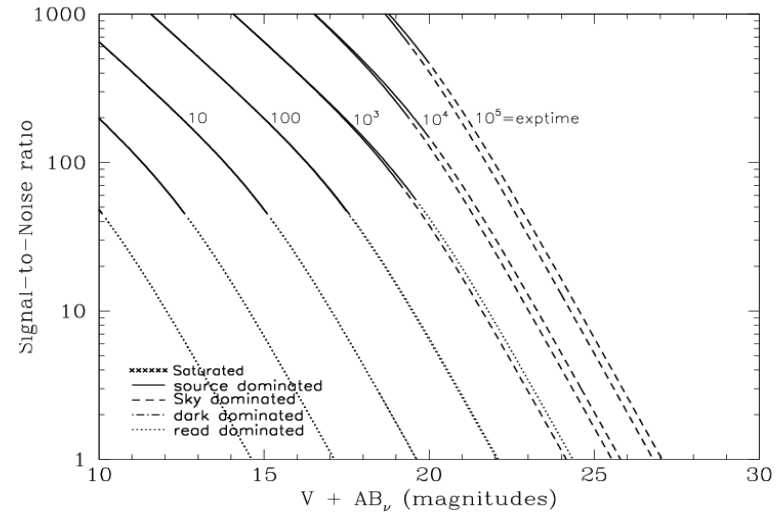
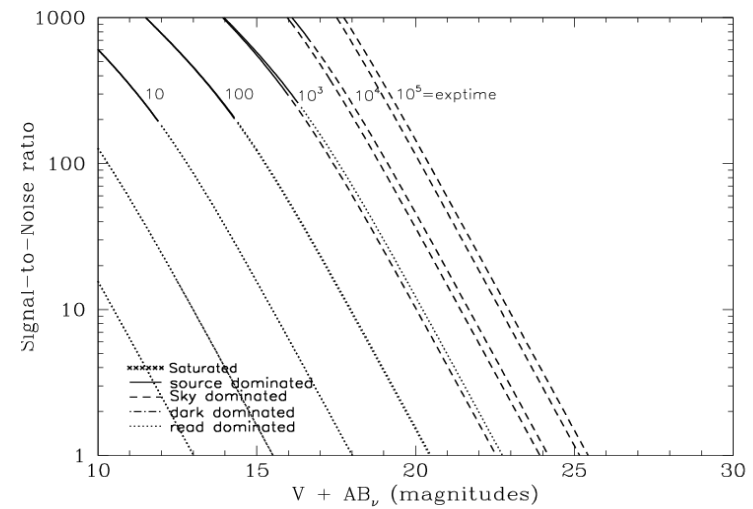


Figure 10.93: Extended Source S/N vs.  $V+AB_V$  for the HRC/F892N filter. Top curves are for low sky and bottom curves are for average sky for a 1 arcsec<sup>2</sup> area.



## HRC/G800L

### Description

Grism.

Figure 10.94: Integrated System Throughput for HRC/G800L

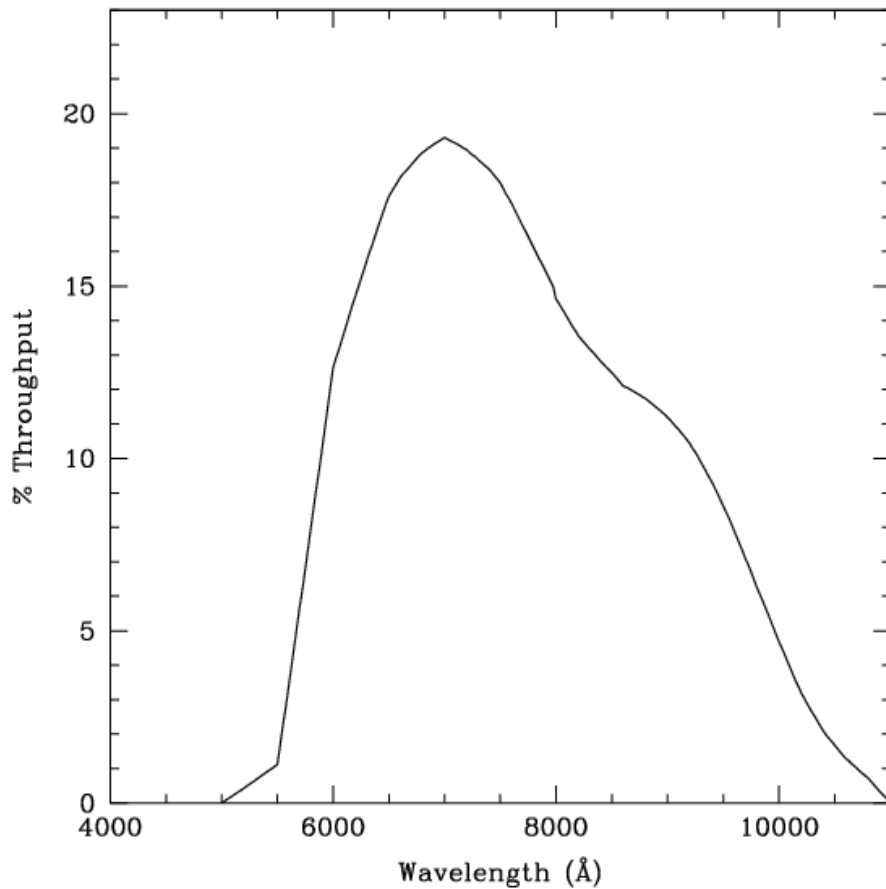


Figure 10.95: Point Source S/N vs.  $V+AB_v$  for the HRC/G800L filter. Top curves are for low sky; bottom curves are for average sky.

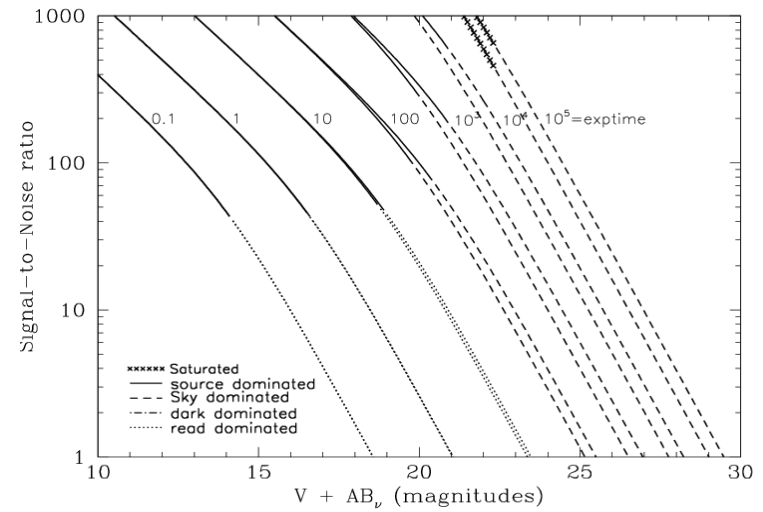
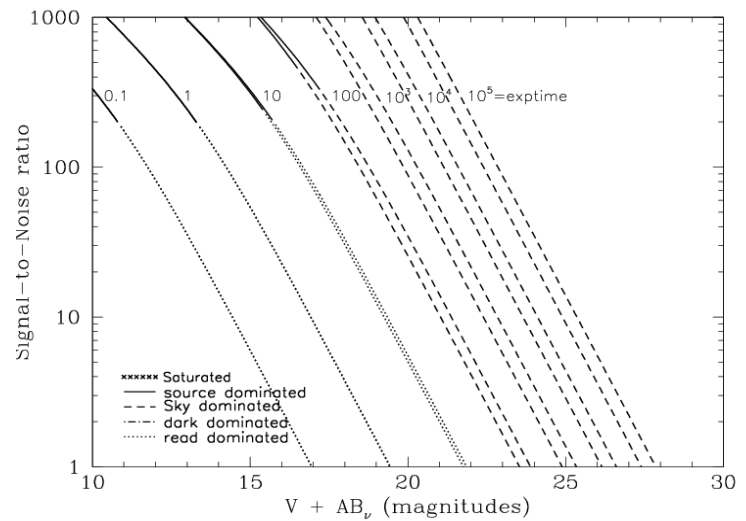


Figure 10.96: Extended Source S/N vs.  $V+AB_v$  for the HRC/G800L filter. Top curves are for low sky and bottom curves are for average sky for a 1 arcsec<sup>2</sup> area.



## HRC/PR200L

### Description

HRC Prism.

Figure 10.97: Integrated System Throughput for HRC/PR200L

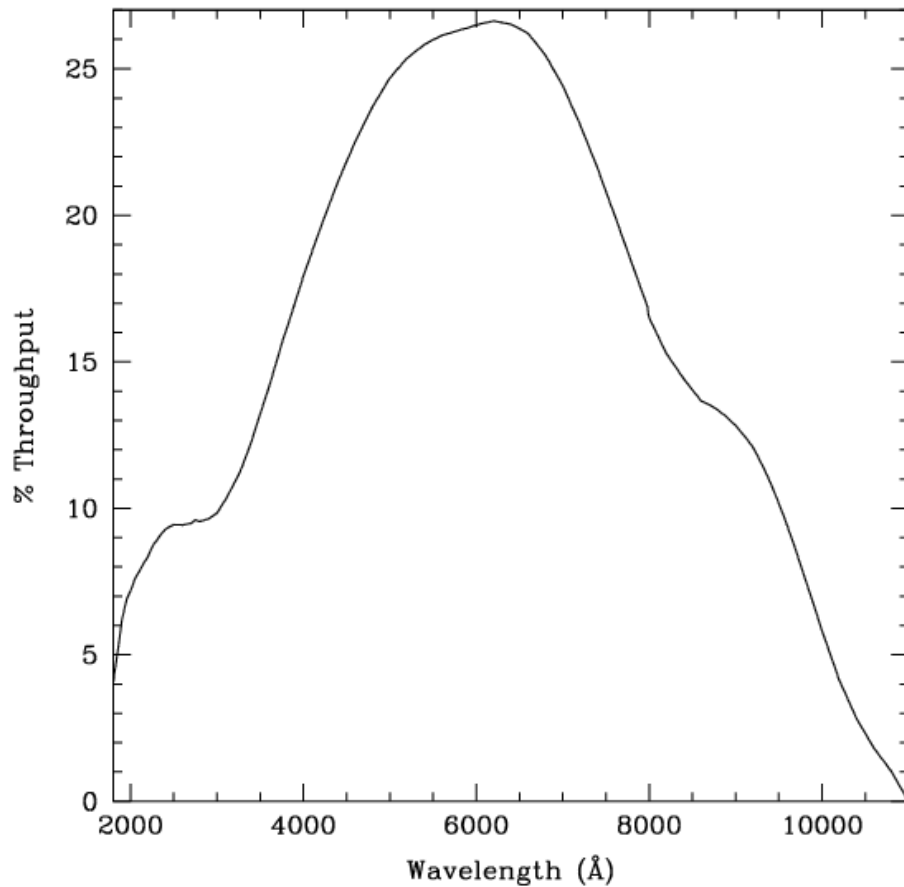


Figure 10.98: Point Source S/N vs.  $V+AB_v$  for the HRC/PR200L filter. Top curves are for low sky; bottom curves are for average sky.

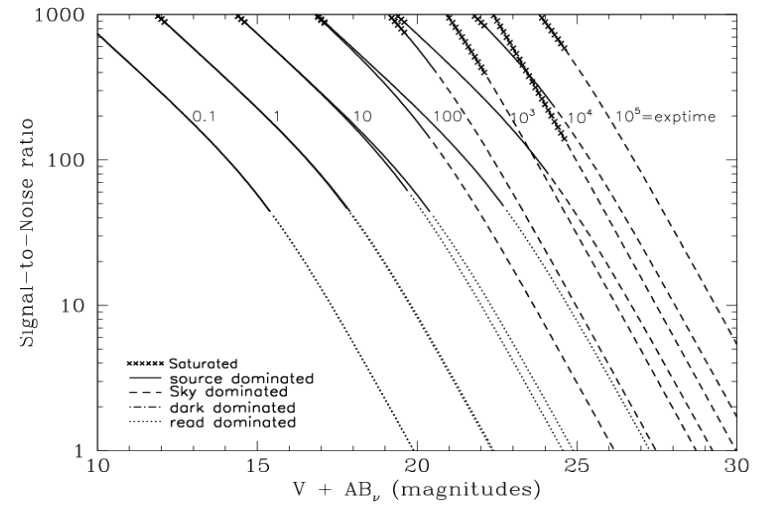
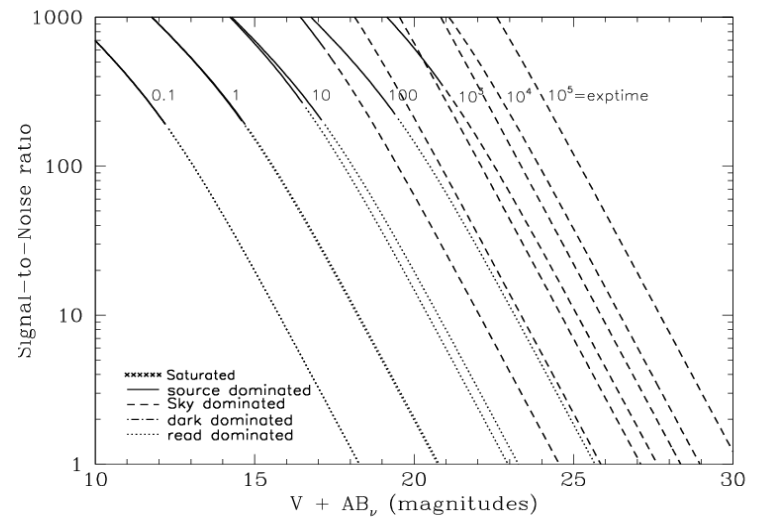


Figure 10.99: Extended Source S/N vs.  $V+AB_v$  for the HRC/PR200L filter. Top curves are for low sky and bottom curves are for average sky for a 1 arcsec<sup>2</sup> area.



## HRC/CLEAR

### Description

HRC Clear Filter.

Figure 10.100: Integrated System Throughput for HRC/Clear

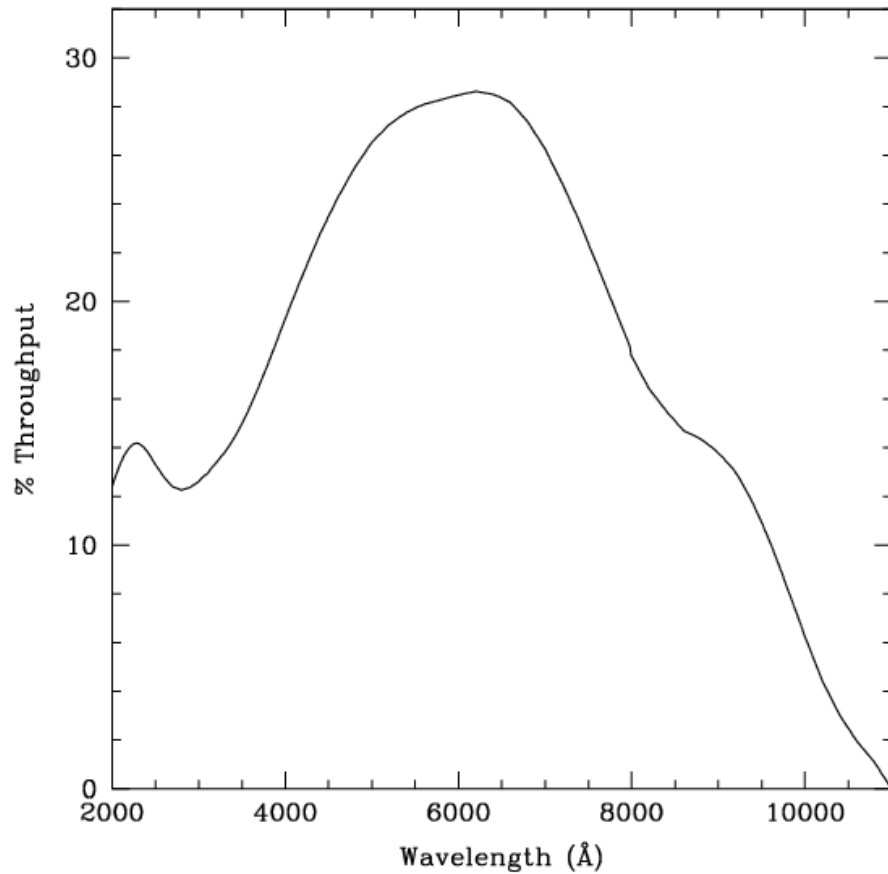


Figure 10.101: Point Source S/N vs.  $V+AB_V$  for the HRC/Clear filter. Top curves are for low sky; bottom curves are for average sky.

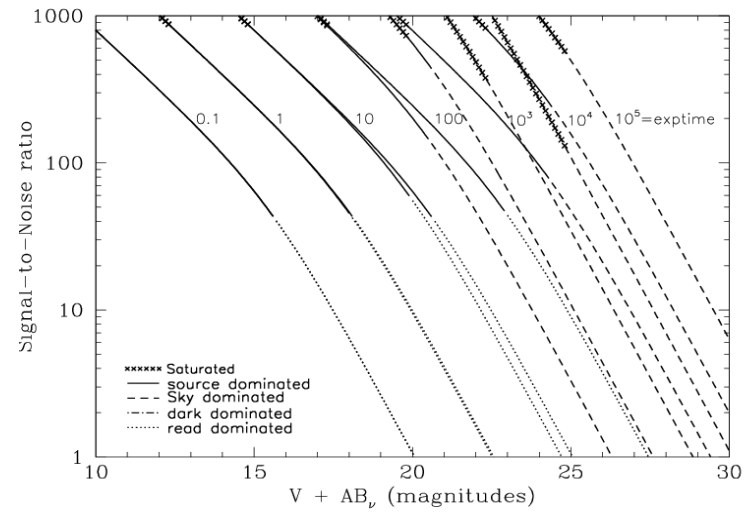
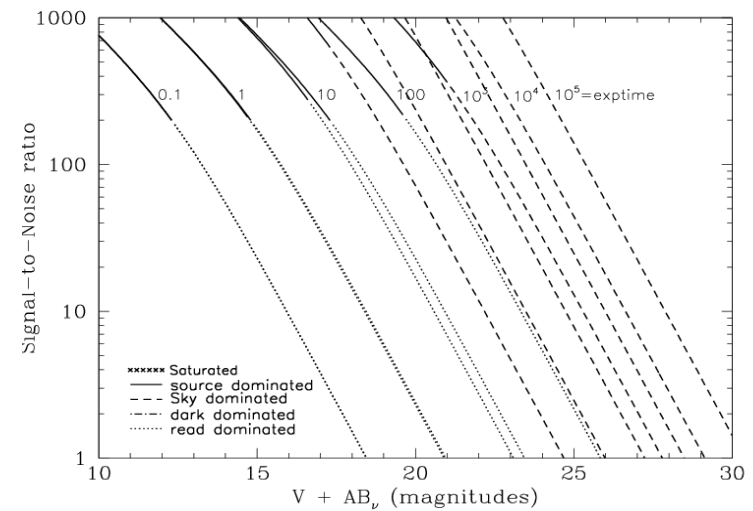


Figure 10.102: Extended Source S/N vs.  $V+AB_V$  for the HRC/Clear filter. Top curves are for low sky and bottom curves are for average sky for a 1 arcsec<sup>2</sup> area.



## SBC/F115LP

### Description

MgF<sub>2</sub> filter.

Figure 10.103: Integrated System Throughput for SBC/F115LP

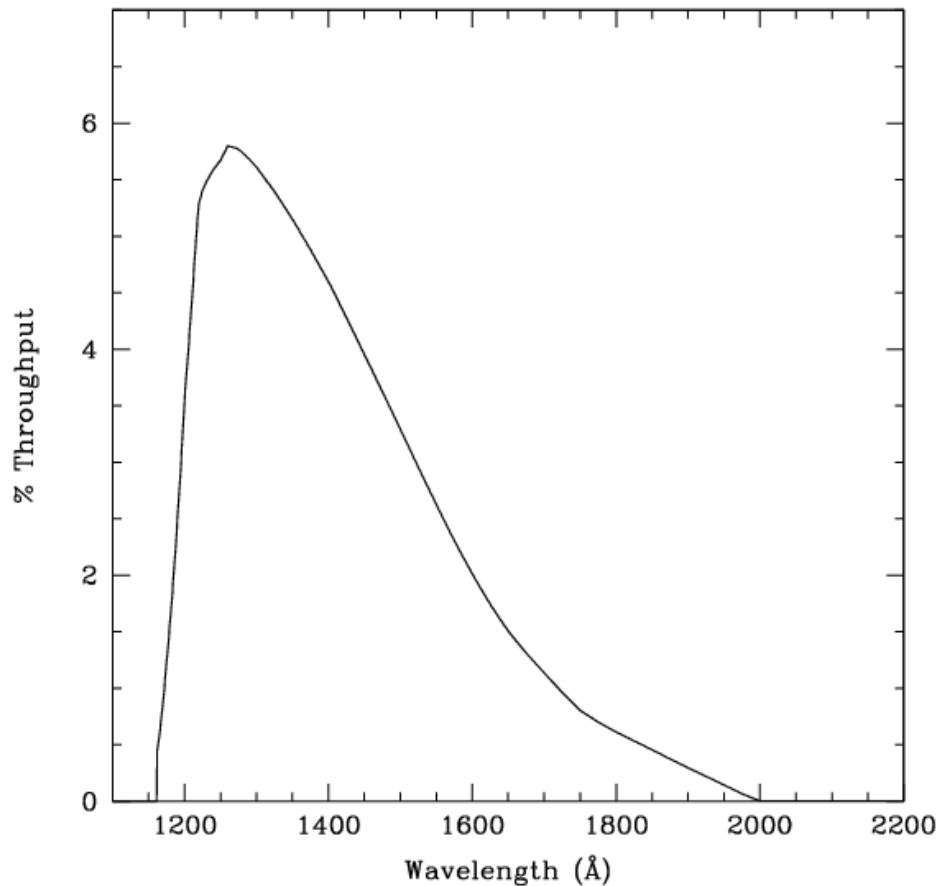


Figure 10.104: Point Source S/N vs.  $V+AB_V$  for the SBC/F115LP filter. Top curves are for low sky; bottom curves are for average sky.

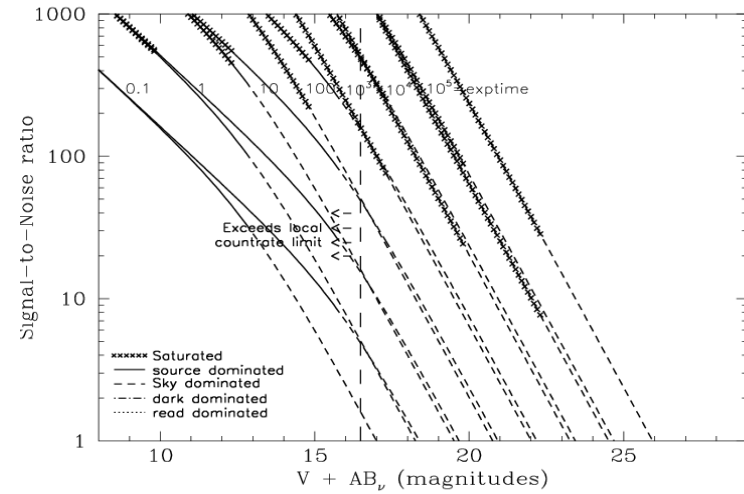
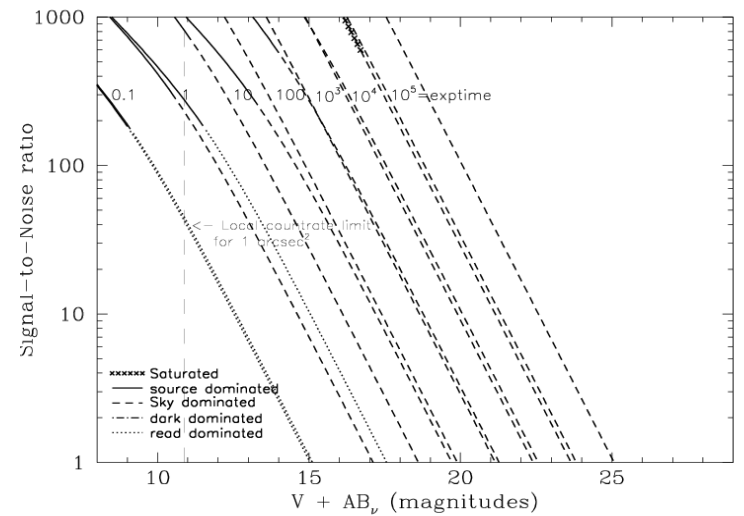


Figure 10.105: Extended Source S/N vs.  $V+AB_V$  for the SBC/F115LP filter. Top curves are for low sky and bottom curves are for average sky for a 1 arcsec<sup>2</sup> area.



# SBC/F122M

## Description

Lyman  $\alpha$  filter.

Figure 10.106: Integrated System Throughput for SBC/F122M

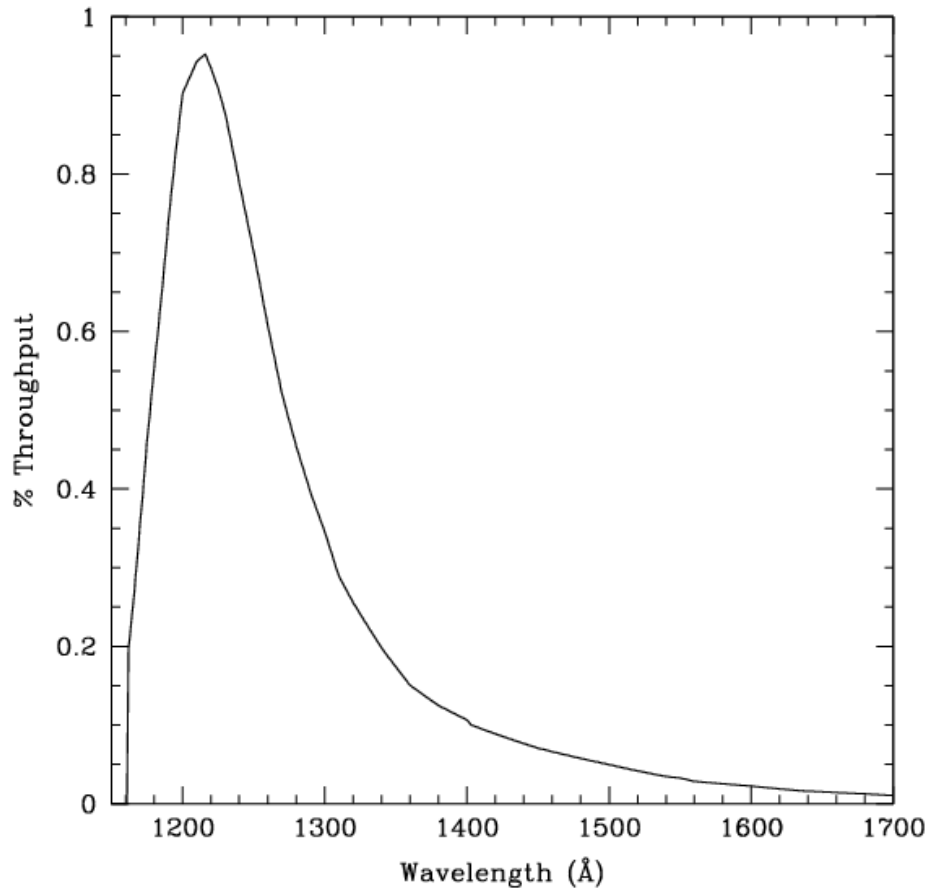


Figure 10.107: Point Source S/N vs.  $V+AB_V$  for the SBC/F122M filter. Top curves are for low sky; bottom curves are for average sky.

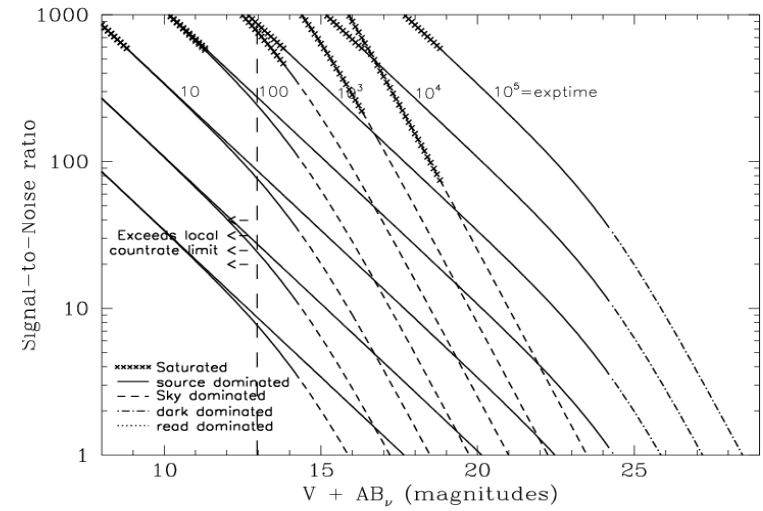
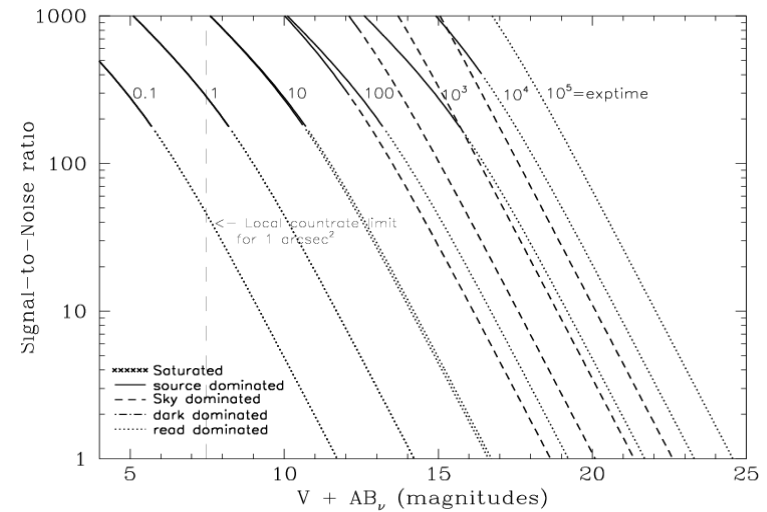


Figure 10.108: Extended Source S/N vs.  $V+AB_V$  for the SBC/F122M filter. Top curves are for low sky and bottom curves are for average sky for a 1 arcsec<sup>2</sup> area.



## SBC/F125LP

### Description

CaF<sub>2</sub> filter.

Figure 10.109: Integrated System Throughput for SBC/F125LP

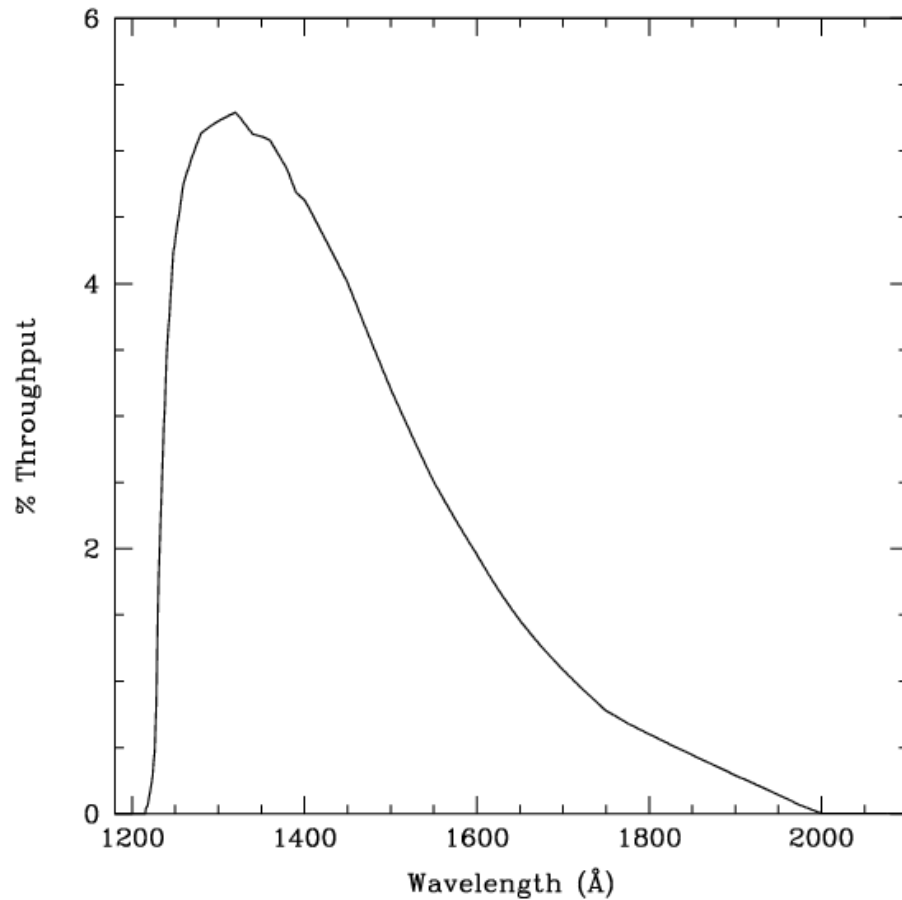


Figure 10.110: Point Source S/N vs.  $V+AB_V$  for the SBC/F125LP filter. Top curves are for low sky; bottom curves are for average sky.

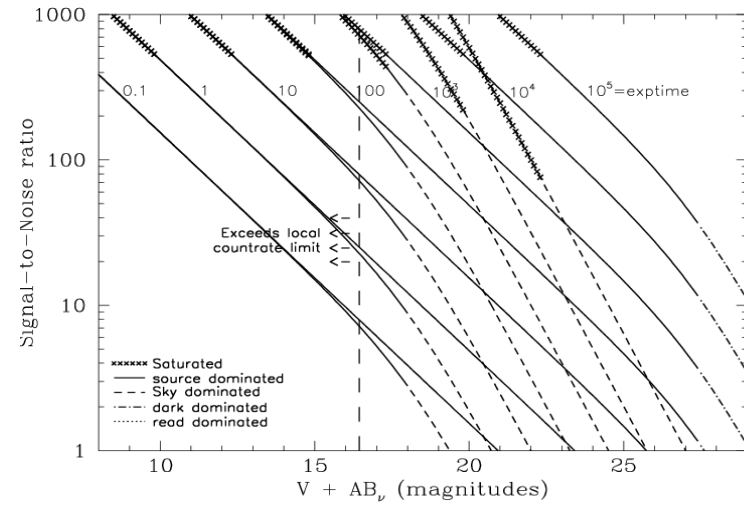
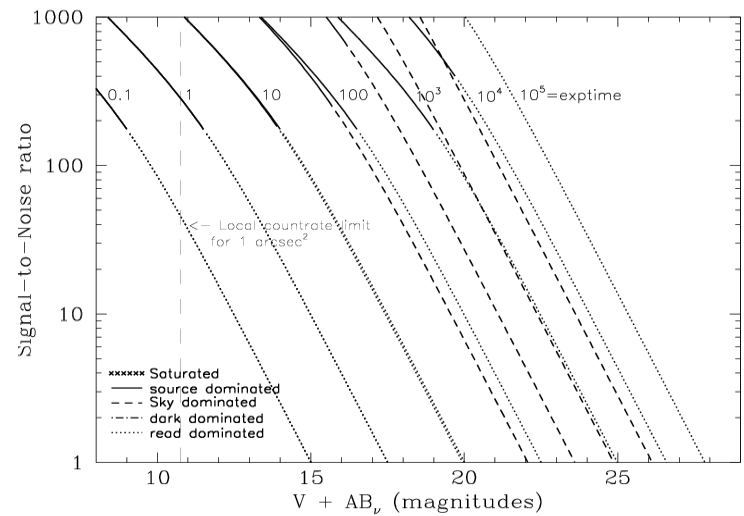


Figure 10.111: Extended Source S/N vs.  $V+AB_V$  for the SBC/F125LP filter. Top curves are for low sky and bottom curves are for average sky for a 1 arcsec<sup>2</sup> area.



# SBC/F140LP

## Description

BaF<sub>2</sub> filter.

Figure 10.112: Integrated System Throughput for SBC/F140LP

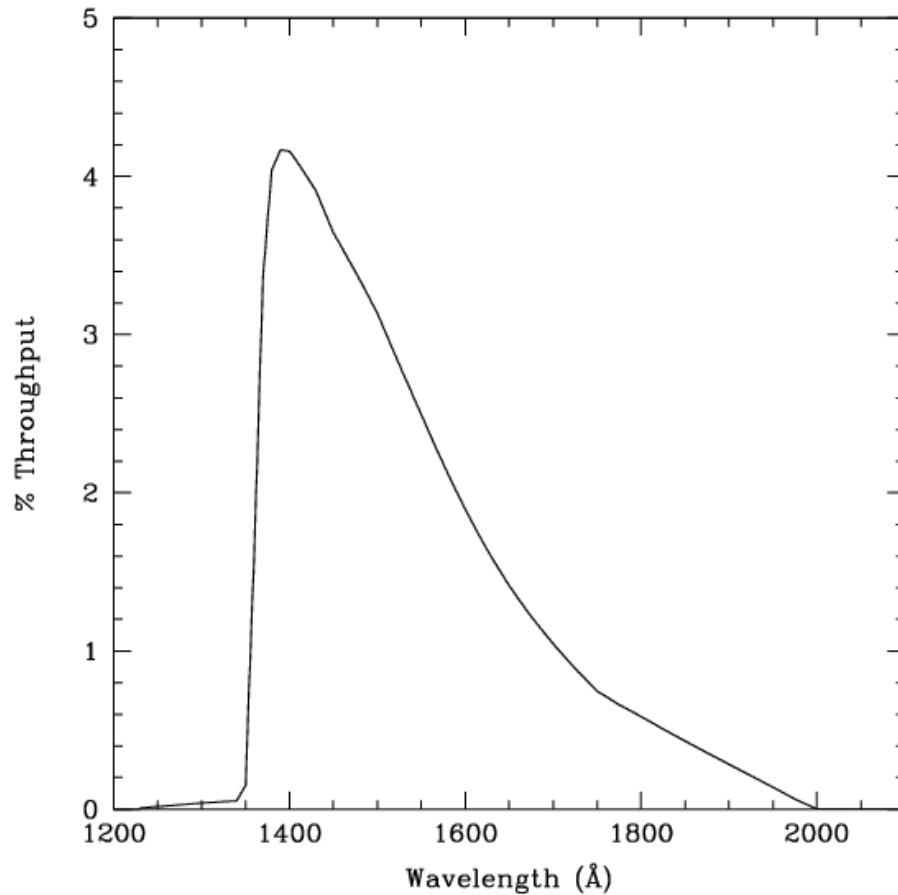


Figure 10.113: Point Source S/N vs.  $V+AB_V$  for the SBC/F140LP filter. Top curves are for low sky; bottom curves are for average sky.

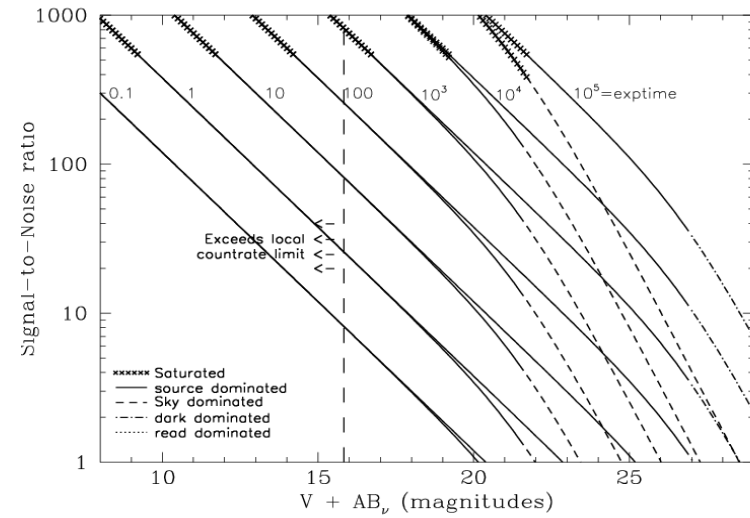
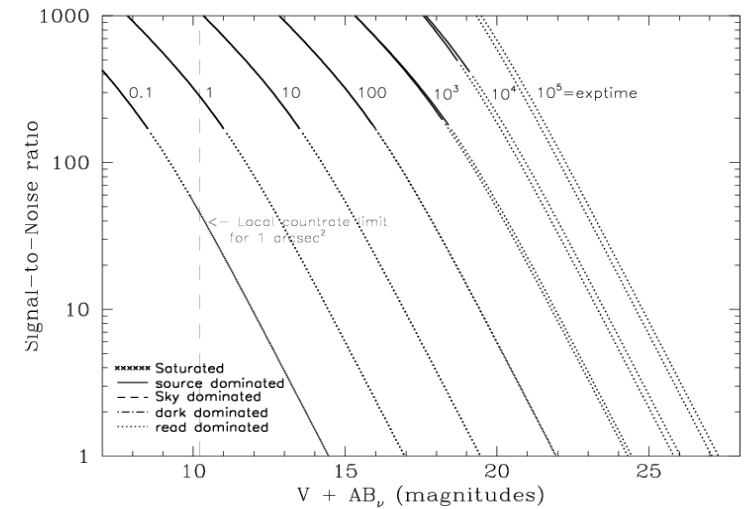


Figure 10.114: Extended Source S/N vs.  $V+AB_V$  for the SBC/F140LP filter. Top curves are for low sky and bottom curves are for average sky for a 1 arcsec<sup>2</sup> area.



## SBC/F150LP

### Description

Crystal Quartz filter.

Figure 10.115: Integrated System Throughput for SBC/F165LP

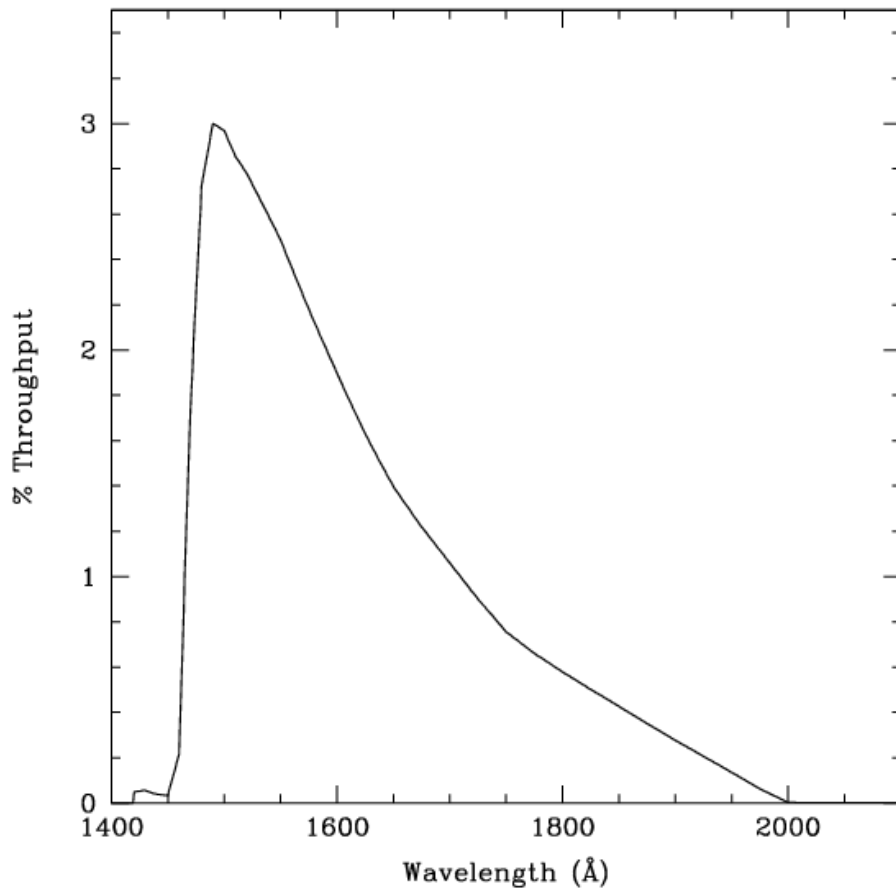


Figure 10.116: Point Source S/N vs.  $V+AB_V$  for the SBC/F150LP filter. Top curves are for low sky; bottom curves are for average sky.

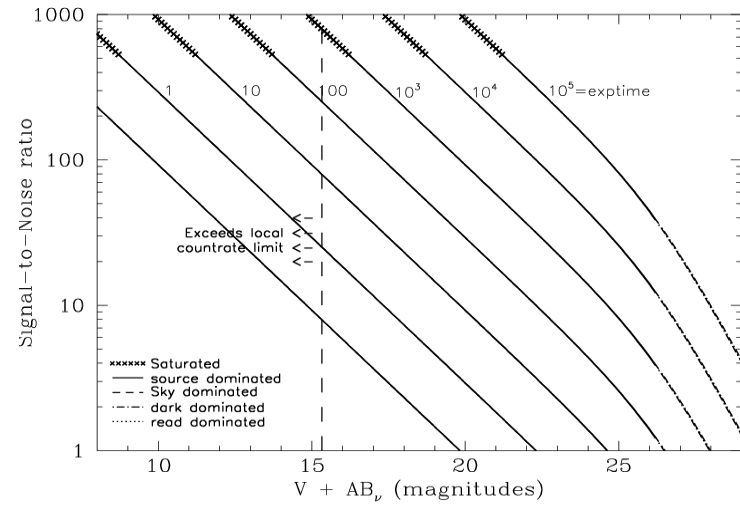
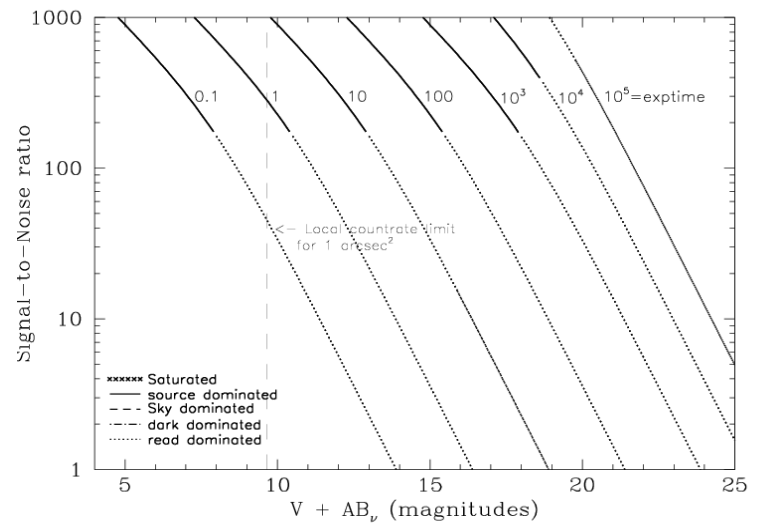


Figure 10.117: Extended Source S/N vs.  $V+AB_V$  for the SBC/F150LP filter. Top curves are for low sky and bottom curves are for average sky for a 1 arcsec<sup>2</sup> area.



## SBC/F165LP

### Description

Dynasil filter.

Figure 10.118: Integrated System Throughput for SBC/F165LP

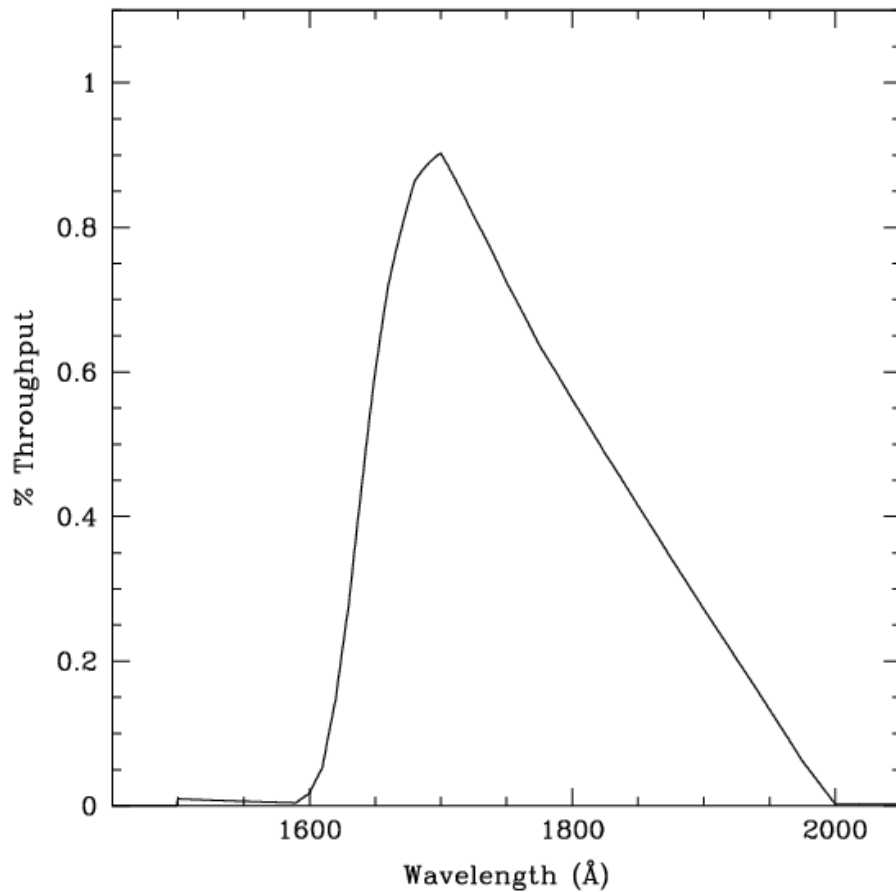


Figure 10.119: Point Source S/N vs.  $V+AB_V$  for the SBC/F165LP filter. Top curves are for low sky; bottom curves are for average sky.

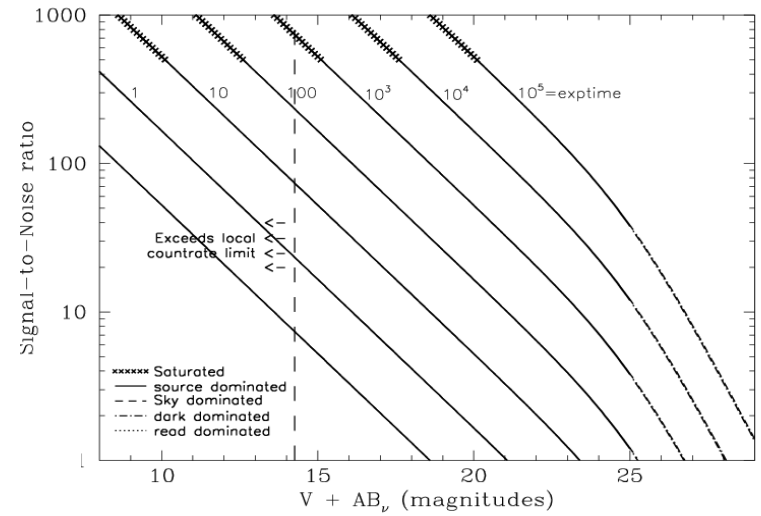
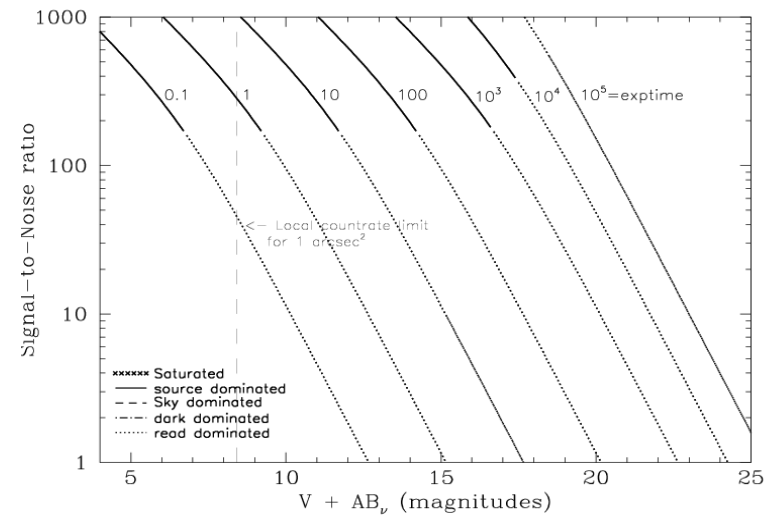


Figure 10.120: Extended Source S/N vs.  $V+AB_V$  for the SBC/F165LP filter. Top curves are for low sky and bottom curves are for average sky for a  $1 \text{ arcsec}^2$  area.



## SBC/PR110L

### Description

LiF<sub>2</sub> Prism.

Figure 10.121: Integrated System Throughput for SBC/PR110LP

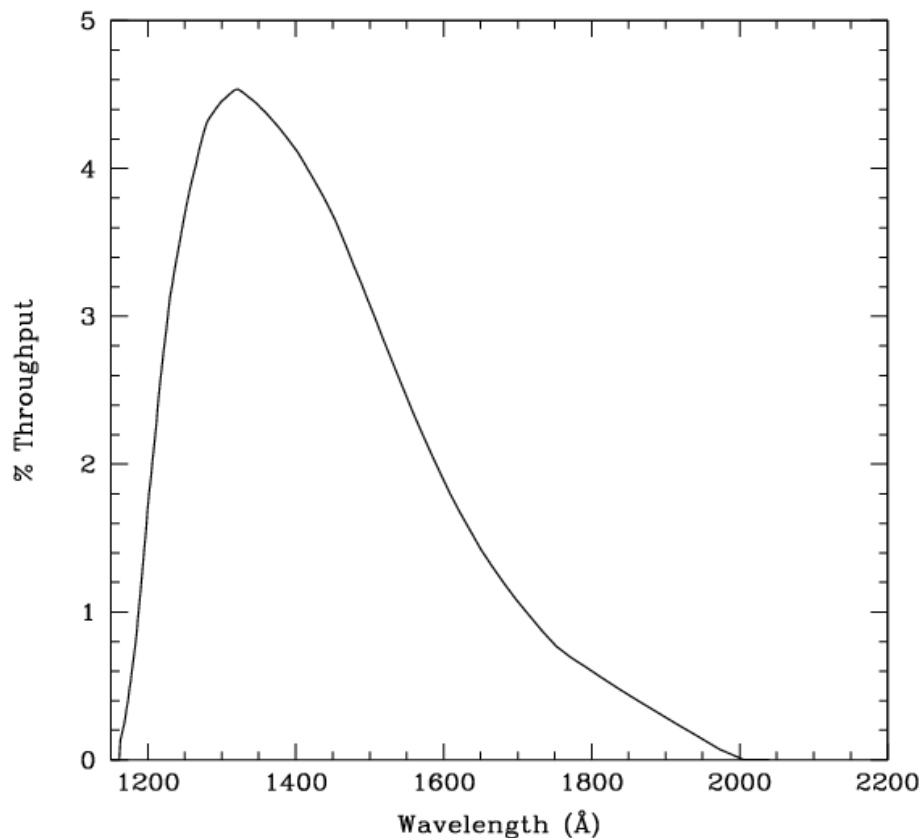


Figure 10.122: Point Source S/N vs.  $V+AB_V$  for the SBC/PR110LP filter. Top curves are for low sky; bottom curves are for average sky.

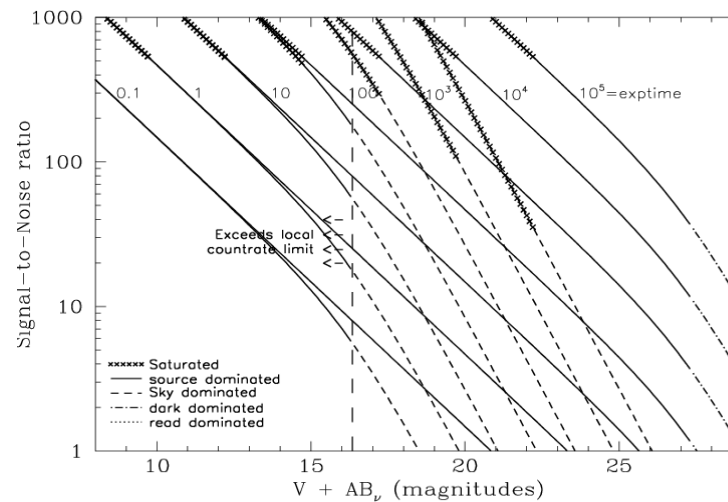
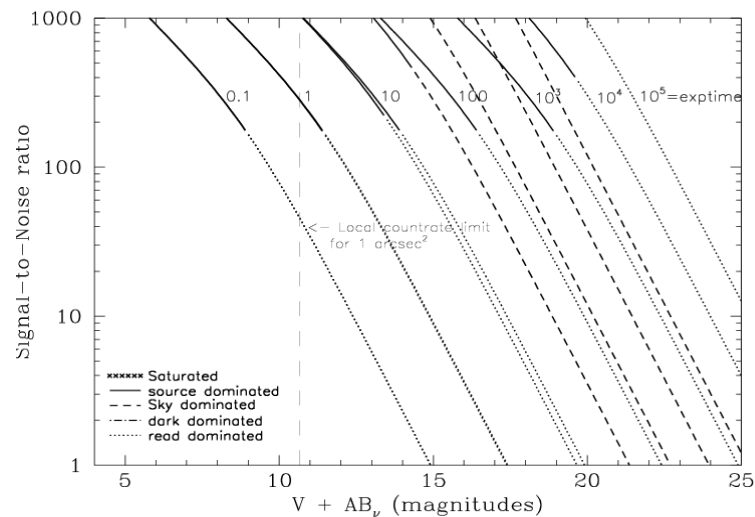


Figure 10.123: Extended Source S/N vs.  $V+AB_V$  for the SBC/PR110LP filter. Top curves are for low sky and bottom curves are for average sky for a 1 arcsec<sup>2</sup> area.



# SBC/PR130L

## Description

CaF<sub>2</sub> Prism.

Figure 10.124: Integrated System Throughput for SBC/PR130LP

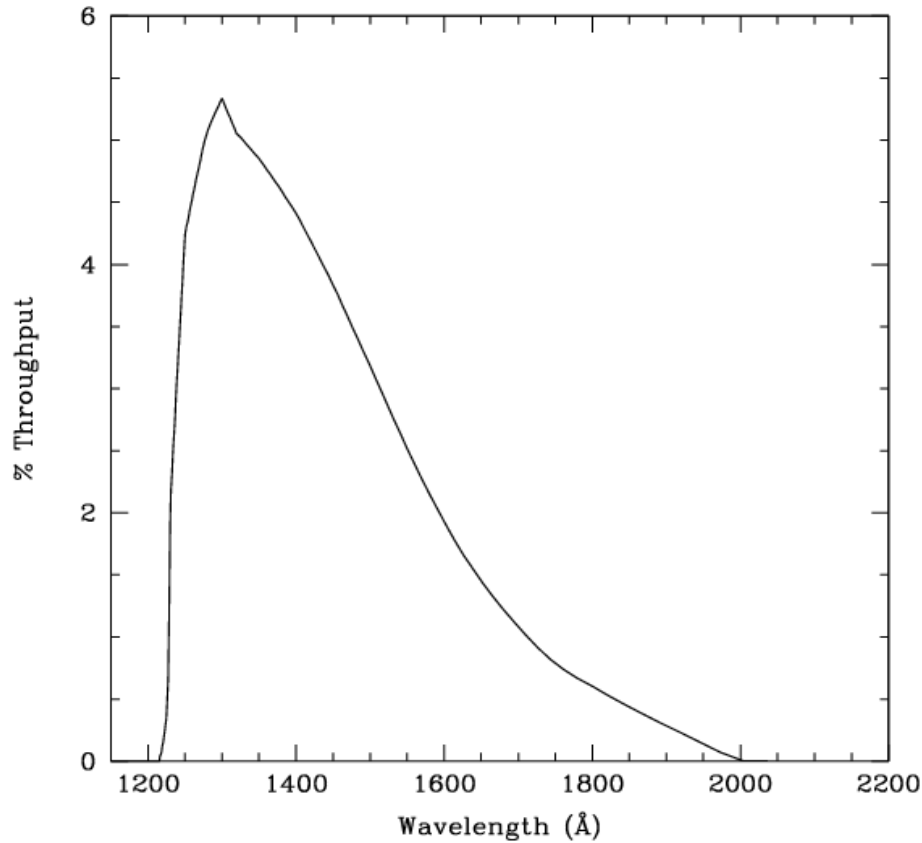


Figure 10.125: Point Source S/N vs.  $V+AB_V$  for the SBC/PR130LP filter. Top curves are for low sky; bottom curves are for average sky.

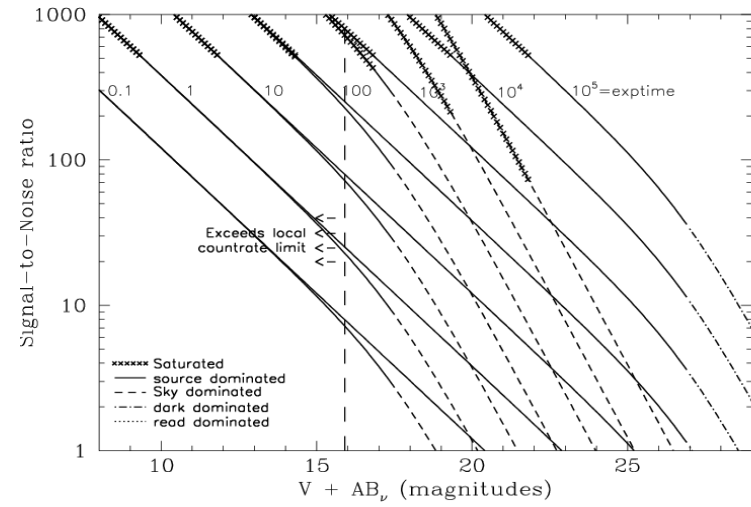


Figure 10.126: Extended Source S/N vs.  $V+AB_V$  for the SBC/PR130LP filter. Top curves are for low sky and bottom curves are for average sky for a 1 arcsec<sup>2</sup> area.

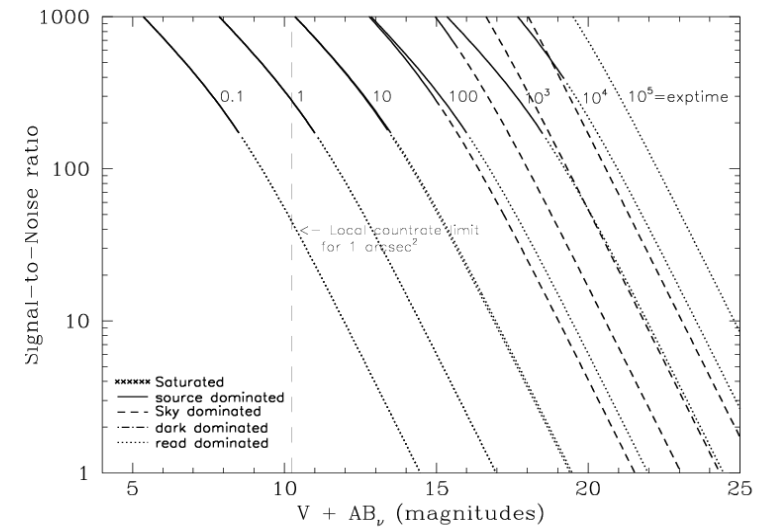


Table 10.1: Color Corrections  $AB_V$  to go from Johnson V Magnitude to AB Magnitude for the WFC

Spectrum	F435W	F475W	F502N	F550M	F555W	F606W	F625W	F658N	F660N	F775W	F814W	F850LP	F892N	G800L	CLEAR
<b>AvgSky</b>	0.62	0.33	0.21	-0.04	0.05	-0.10	-0.22	-0.24	-0.27	-0.40	-0.42	-0.47	-0.47	-0.35	-0.05
<b>LowSky</b>	0.52	0.26	0.14	-0.03	0.03	-0.07	-0.15	-0.18	-0.20	-0.26	-0.27	-0.30	-0.31	-0.23	0.00
<b>O5V</b>	-0.44	-0.28	-0.15	0.05	-0.04	0.12	0.27	0.38	0.39	0.67	0.75	1.00	0.98	0.55	0.04
<b>B0V</b>	-0.43	-0.28	-0.17	0.06	-0.04	0.12	0.29	0.40	0.39	0.64	0.71	0.94	0.92	0.54	0.04
<b>A0V</b>	-0.07	-0.08	-0.07	0.02	0.00	0.08	0.15	0.33	0.29	0.35	0.39	0.48	0.48	0.29	0.14
<b>A5V</b>	0.04	-0.01	-0.03	0.00	0.00	0.06	0.10	0.22	0.16	0.23	0.25	0.31	0.30	0.19	0.13
<b>F2V</b>	0.26	0.12	0.05	-0.01	0.02	0.00	-0.03	0.00	-0.03	-0.05	-0.05	-0.04	-0.05	-0.04	0.06
<b>G2V</b>	0.54	0.28	0.14	-0.03	0.04	-0.07	-0.16	-0.16	-0.17	-0.30	-0.31	-0.34	-0.34	-0.26	0.00
<b>K0V</b>	0.77	0.40	0.19	-0.06	0.05	-0.12	-0.25	-0.31	-0.31	-0.42	-0.44	-0.47	-0.49	-0.37	-0.04
<b>M0V</b>	1.41	0.80	0.67	-0.14	0.11	-0.33	-0.59	-0.84	-0.84	-1.21	-1.31	-1.55	-1.52	-1.09	-0.53
<b>M6V</b>	1.72	0.89	0.71	-0.18	0.12	-0.40	-0.66	-1.17	-1.15	-2.11	-2.34	-2.80	-2.74	-1.96	-1.27
<b>O7I</b>	-0.40	-0.25	-0.13	0.04	-0.03	0.11	0.25	0.35	0.35	0.63	0.70	0.94	0.92	0.52	0.05
<b>B0I</b>	-0.34	-0.21	-0.11	0.03	-0.03	0.10	0.22	0.31	0.31	0.52	0.58	0.77	0.75	0.43	0.05
<b>F0III</b>	0.19	0.07	0.00	0.00	0.01	0.01	0.01	0.06	0.03	0.06	0.06	0.07	0.05	0.04	0.10
<b>G0III</b>	0.63	0.32	0.15	-0.03	0.04	-0.09	-0.19	-0.24	-0.25	-0.36	-0.38	-0.43	-0.45	-0.31	-0.02
<b>K2III</b>	1.13	0.57	0.33	-0.07	0.07	-0.19	-0.37	-0.48	-0.48	-0.68	-0.72	-0.83	-0.89	-0.60	-0.17
<b>M0III</b>	1.56	0.80	0.56	-0.12	0.11	-0.33	-0.58	-0.74	-0.75	-1.24	-1.35	-1.59	-1.62	-1.12	-0.55
<b>M6III</b>	1.65	0.92	1.19	-0.12	0.18	-0.64	-0.95	-1.20	-1.15	-2.91	-3.24	-3.89	-3.74	-2.83	-2.10
<b>Elliptical</b>	0.95	0.51	0.34	-0.07	0.07	-0.19	-0.36	-0.48	-0.48	-0.81	-0.92	-1.07	-1.18	-0.72	-0.27
<b>Sa</b>	0.80	0.45	0.30	-0.06	0.07	-0.18	-0.36	-0.54	-0.51	-0.75	-0.84	-0.94	-1.05	-0.66	-0.24
<b>Sb</b>	0.81	0.44	0.27	-0.06	0.06	-0.18	-0.34	-0.50	-0.48	-0.75	-0.85	-0.97	-1.09	-0.66	-0.24
<b>Sc</b>	0.08	0.00	-0.71	0.07	-0.03	-0.17	-0.26	-1.76	-0.84	0.40	0.77	1.67	1.26	0.20	0.08
<b>Starburst E(B-V) 0.51-0.60</b>	0.41	0.24	-0.02	0.00	0.04	-0.22	-0.39	-1.38	-0.87	-0.59	-0.67	-0.75	-0.80	-0.56	-0.23
<b>Starburst E(B-V)&lt;0.1</b>	0.23	0.05	-0.96	0.09	-0.03	-0.10	-0.14	-1.16	-0.35	-0.15	-0.19	-0.18	-0.23	-0.16	-0.03
<b>Sun</b>	0.58	0.30	0.17	-0.03	0.04	-0.07	-0.17	-0.17	-0.20	-0.26	-0.27	-0.27	-0.28	-0.23	0.01
<b>Vega</b>	-0.12	-0.11	-0.07	0.02	0.00	0.08	0.16	0.35	0.32	0.39	0.43	0.56	0.49	0.32	0.14

Table 10.2: Color Corrections  $AB_V$  to go from Johnson V Magnitude to AB Magnitude for the HRC

Spectrum	F220W	F250W	F330W	F344N	F435W	F475W	F502N	F550M	F555W	F606W	F625W	F658N	F660N	F775W	F814W	F850LP	F892N	G800L	PR200L	Clear
AvgSky	3.56	2.58	2.01	1.89	0.63	0.32	0.21	-0.04	0.05	-0.09	-0.22	-0.24	-0.27	-0.39	-0.42	-0.47	-0.47	-0.35	0.21	0.29
LowSky	5.31	3.37	1.84	1.72	0.65	0.33	0.22	-0.04	0.05	-0.11	-0.24	-0.27	-0.30	-0.45	-0.48	-0.55	-0.30	-0.39	0.18	0.26
O5V	-1.53	-1.24	-0.86	-0.81	-0.44	-0.26	-0.15	0.04	-0.04	0.11	0.27	0.38	0.39	0.66	0.76	1.02	0.98	0.55	-0.45	-0.57
B0V	-1.16	-0.98	-0.72	-0.69	-0.44	-0.27	-0.17	0.06	-0.04	0.11	0.28	0.40	0.39	0.63	0.72	0.96	0.92	0.54	-0.31	-0.41
A0V	1.75	1.54	1.19	1.16	-0.06	-0.08	-0.07	0.02	0.00	0.07	0.15	0.33	0.29	0.35	0.39	0.48	0.48	0.29	0.33	0.39
A5V	2.60	2.15	1.41	1.35	0.05	-0.01	-0.03	0.00	0.00	0.05	0.10	0.22	0.16	0.23	0.25	0.31	0.29	0.19	0.36	0.43
F2V	3.49	2.52	1.45	1.35	0.27	0.11	0.05	-0.01	0.02	0.00	-0.03	0.00	-0.03	-0.05	-0.05	-0.04	-0.05	-0.04	0.31	0.38
G2V	5.66	3.29	1.63	1.63	0.55	0.26	0.14	-0.03	0.04	-0.06	-0.15	-0.16	-0.17	-0.30	-0.31	-0.34	-0.34	-0.26	0.25	0.33
K0V	6.82	4.47	2.39	2.26	0.78	0.38	0.19	-0.06	0.05	-0.11	-0.24	-0.31	-0.31	-0.42	-0.44	-0.47	-0.49	-0.37	0.23	0.31
M0V	7.73	5.93	3.90	3.76	1.40	0.76	0.67	-0.14	0.12	-0.31	-0.58	-0.84	-0.84	-1.20	-1.32	-1.57	-1.52	-1.09	-0.24	-0.15
M6V	7.30	6.31	4.31	4.23	1.71	0.84	0.71	-0.18	0.13	-0.37	-0.65	-1.17	-1.15	-2.09	-2.37	-2.83	-2.75	-1.98	-0.99	-0.90
O7I	-0.33	-0.55	-0.60	-0.56	-0.40	-0.24	-0.13	0.04	-0.03	0.10	0.25	0.35	0.35	0.62	0.71	0.96	0.92	0.51	-0.11	-0.14
B0I	-0.72	-0.69	-0.55	-0.54	-0.34	-0.20	-0.11	0.03	-0.03	0.09	0.22	0.31	0.31	0.51	0.59	0.78	0.75	0.43	-0.15	-0.21
F0III	3.69	2.75	1.58	1.47	0.20	0.06	0.00	0.00	0.01	0.01	0.01	0.06	0.03	0.06	0.06	0.07	0.05	0.04	0.34	0.42
G0III	6.58	4.21	2.24	2.13	0.63	0.31	0.15	-0.03	0.04	-0.08	-0.19	-0.24	-0.25	-0.36	-0.38	-0.43	-0.45	-0.31	0.24	0.32
K2III	8.43	6.56	3.78	3.56	1.13	0.54	0.33	-0.07	0.07	-0.17	-0.36	-0.48	-0.48	-0.67	-0.73	-0.84	-0.89	-0.60	0.11	0.19
M0III	7.71	7.02	5.14	5.01	1.55	0.76	0.56	-0.11	0.12	-0.31	-0.57	-0.74	-0.75	-1.23	-1.36	-1.61	-1.62	-1.12	-0.25	-0.17
M6III	6.27	6.17	4.45	4.28	1.67	0.89	1.19	-0.12	0.18	-0.60	-0.93	-1.20	-1.15	-2.88	-3.29	-3.93	-3.74	-2.87	-1.83	-1.75
Elliptical	5.20	4.63	2.82	2.63	0.95	0.48	0.34	-0.07	0.07	-0.17	-0.36	-0.48	-0.48	-0.80	-0.93	-1.08	-1.18	-0.72	0.01	0.09
Sa	4.35	3.53	2.38	2.34	0.80	0.43	0.30	-0.06	0.07	-0.17	-0.35	-0.54	-0.51	-0.75	-0.85	-0.94	-1.05	-0.66	0.03	0.11
Sb	3.73	3.10	2.11	2.16	0.81	0.42	0.27	-0.06	0.07	-0.17	-0.34	-0.50	-0.48	-0.74	-0.86	-0.98	-1.09	-0.66	0.02	0.10
Sc	2.09	1.15	0.15	-0.07	0.07	-0.01	-0.70	0.07	-0.03	-0.17	-0.25	-1.76	-0.85	0.34	0.77	12.85	9.95	0.19	0.22	0.285
Starburst E(B-V) 0.51-0.60	1.82	1.63	1.13	1.14	0.41	0.23	-0.02	0.00	0.04	-0.21	-0.38	-1.38	-0.87	-0.59	-0.68	-0.76	-0.80	-0.57	0.00	0.05
Starburst E(B-V)<0.1	0.98	0.95	0.81	0.80	0.22	0.04	-0.96	0.09	-0.03	-0.10	-0.14	-1.16	-0.35	-0.15	-0.20	-0.18	-0.23	-0.16	0.11	0.16
Sun	5.67	3.55	1.83	1.72	0.58	0.28	0.17	-0.03	0.04	-0.06	-0.16	-0.17	-0.20	-0.26	-0.27	-0.27	-0.28	-0.23	0.27	0.36
Vega	1.65	1.48	1.18	1.14	-0.10	-0.10	-0.07	0.02	0.00	0.08	0.16	0.35	0.32	0.38	0.44	0.56	0.49	0.32	0.33	0.39

Table 10.3: Color Corrections  $AB_V$  to go from Johnson V Magnitude to AB Magnitude for the SBC

Spectrum	F115LP	F122M	F125LP	F140LP	F150LP	F165LP	PR110L	PR130L
<b>AvgSky</b>	12.00	14.41	11.83	11.23	10.60	9.25	11.81	11.81
<b>LowSky</b>	-1.78	-2.95	2.73	6.80	10.34	9.00	-1.27	2.69
<b>O5V</b>	-2.07	-2.18	-2.04	-1.96	-1.91	-1.82	-2.05	-2.04
<b>B0V</b>	-1.64	-1.53	-1.69	-1.67	-1.63	-1.54	-1.66	-1.69
<b>A0V</b>	2.65	3.88	2.47	2.09	1.91	1.82	2.51	2.46
<b>A5V</b>	5.41	7.44	5.24	4.65	4.05	3.14	5.23	5.22
<b>F2V</b>	7.91	10.17	7.74	7.14	6.51	5.18	7.72	7.71
<b>G2V</b>	13.82	16.35	13.65	13.05	12.42	11.07	13.63	13.63
<b>K0V</b>	10.07	10.43	10.00	9.79	9.61	9.31	10.01	9.99
<b>M0V</b>	11.58	11.94	11.50	11.29	11.11	10.81	11.51	11.49
<b>M6V</b>	12.06	12.42	11.98	11.77	11.59	11.29	11.99	11.97
<b>O7I</b>	-0.57	-0.42	-0.61	-0.68	-0.70	-0.71	-0.59	-0.61
<b>B0I</b>	-0.80	-0.61	-0.87	-0.83	-0.78	-0.75	-0.82	-0.86
<b>F0III</b>	7.81	10.09	7.63	7.04	6.41	5.07	7.62	7.61
<b>G0III</b>	9.80	10.16	9.72	9.52	9.34	9.03	9.74	9.72
<b>K2III</b>	13.32	13.68	13.24	13.04	12.86	12.55	13.26	13.24
<b>M0III</b>	11.07	11.42	10.99	10.78	10.60	10.30	11.00	10.98
<b>M6III</b>	10.37	10.73	10.29	10.09	9.91	9.61	10.31	10.29
<b>Elliptical</b>	6.24	6.71	6.11	6.08	5.98	5.90	6.18	6.10
<b>Sa</b>	5.66	6.23	5.52	5.42	5.27	5.06	5.59	5.52
<b>Sb</b>	4.63	5.18	4.49	4.38	4.27	4.24	4.56	4.49
<b>Sc</b>	2.87	3.52	2.71	2.60	2.45	2.32	2.78	2.71
<b>Starburst E(B-V) 0.51-0.60</b>	2.68	3.31	2.52	2.44	2.35	2.13	2.60	2.52
<b>Starburst E(B-V)&lt;0.1</b>	1.33	1.88	1.18	1.13	1.09	1.06	1.25	1.18
<b>Sun</b>	12.00	11.78	12.29	11.79	11.21	10.02	12.02	12.28
<b>Vega</b>	2.74	3.95	2.56	2.20	2.04	1.91	2.61	2.56

## 10.3 Distortion in the ACS

The ACS detectors exhibit more distortion than previous HST instruments. The principal reason for this is that the optics have been designed with a minimum number of components, consistent with correcting for the spherical aberration induced by the OTA, without introducing coma. The result is a high throughput, but focal surfaces far from normal to the principal rays. The WFC detector is tilted at 22 degrees giving an elongation of 8% while the HRC and SBC have a 25 degree tilt leading to an elongation of 12%. In each case, the scales in arcseconds per pixel are smaller along the radial direction of the OTA field of view than along the tangential direction.

The orientations of the ACS detector edges are approximately in line with the V2 and V3 coordinate axes of the telescope. Consequently, the eigenaxes of the scale transformation are along the diagonals for WFC and the apertures and pixels appear non-rectangular in the sky projection. For the HRC and SBC the situation is even more irregular because the aperture diagonals do not lie along a radius of the HST field of view. Figure 8.7 shows the ACS apertures in the telescope's V2V3 reference frame. For a telescope roll angle of zero this would correspond to an on-sky view with the V3 axis aligned with North and the V2 with East.

If these were the only distortions they would not really present much difficulty. Their impact on photometry and mosaicing or dithering could be simply computed. A more problematic effect is the variation of scale across each detector. For the WFC this amounts to a change of 10% from corner to corner. For the HRC and SBC this variation is only about 1% as they cover much smaller fields of view. The area on the sky covered by a WFC pixel varies by about 18% from corner to corner, allowance for which must be made in photometry of extended objects. Dithering and mosaicing are complicated by the fact that an integral pixel shift near the center of the detector will translate into a non-integral displacement for pixels near the edges. Even this is not a fundamental difficulty, but will imply some computational complexity in registering images and will depend on an accurate measurement of distortions.

The results presented here are derived from on-sky measurements. For WFC and HRC multiple pointings of 47 Tucanae were taken through the F475W filter, resulting in several thousand star location measurements. These were analyzed to express the distortion as quartic polynomials. The residuals of the fit to these polynomials are of order 0.2 pixels, much larger than the errors. Correction images describing these residuals are now supplied and used in CALACS to bring the final errors down to about 0.01 pixels. Additionally, an area of open cluster NGC 188, for which astrometric data are available, was used to establish the exact location and orientation of the aperture in telescope coordinates. At the same time, the

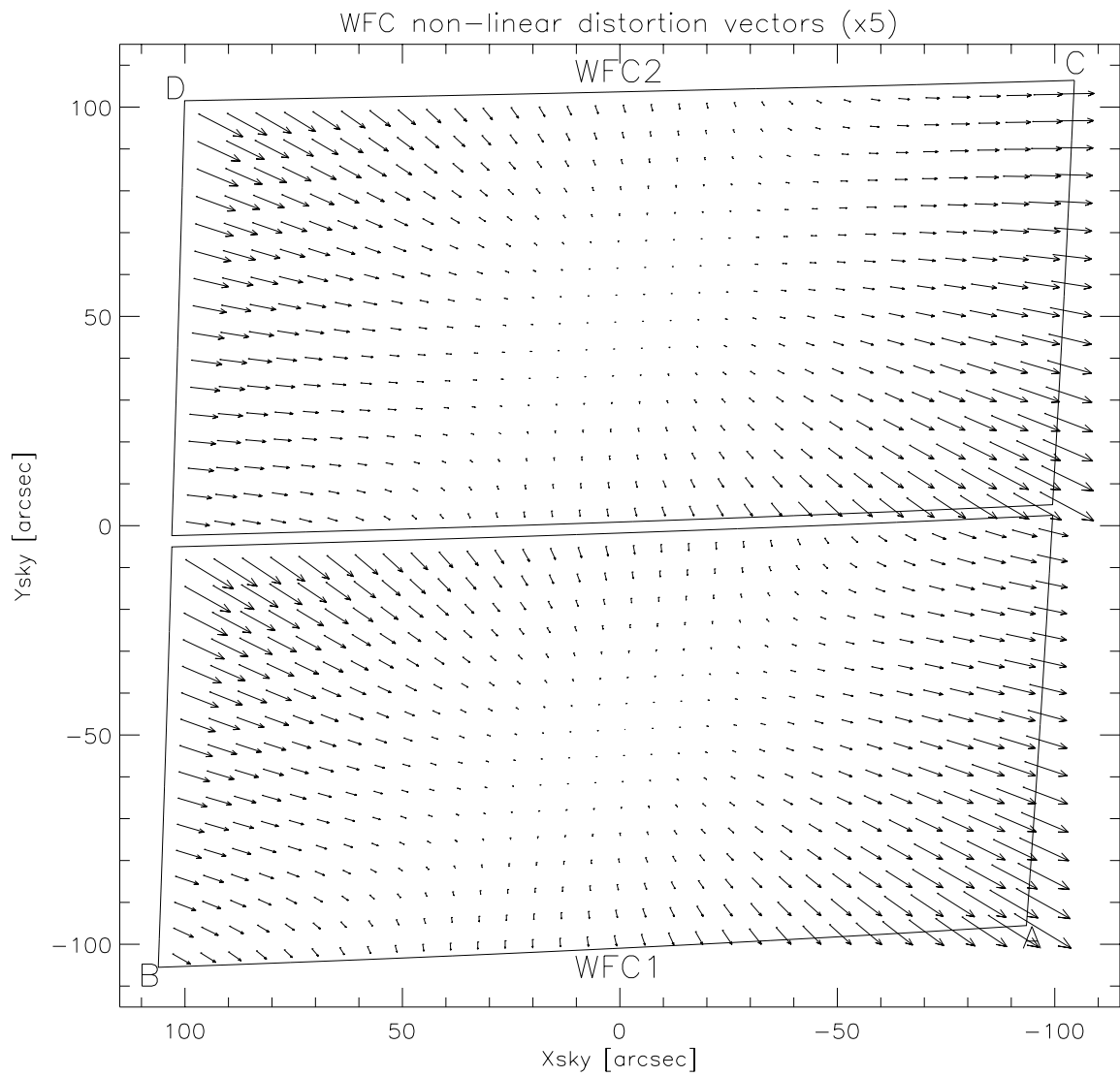
scale factors were confirmed. For the SBC, the distortion measurement used the target NGC 6681 and filter F125LP. The alignment was established by observing this same target with the HRC and SBC consecutively to establish the relative locations. The SBC position was thereby derived from the HRC position.

### 10.3.1 WFC

The rhombus shape of the WFC is evident in Figure 8.7. The angle between the x and y axes is 84.9 for WFC1 and 86.1 for WFC2. The WFC distortion is illustrated in Figure 10.127, a vector displacement diagram which shows the contribution of the non-linear part of a quadratic fit to the data. The vectors represent the displacements and have been scaled up by a factor of 5 for display. The corner displacements are about 82 pixels. The principal effect is the diagonal variation of scale.

At the center of chip WFC1 the scale in the x direction is 0.0493 arcsec/pixel and 0.0486 in the y direction. For WFC2 these figures are 0.0498 and 0.0503. Between the corner of WFC nearest to the V1 axis and the diagonally opposite corner, the overall scale increases by 10%. WFC1 forms a slightly distorted rectangle 201 by 100 arcseconds in size while WFC2 is 203 by 103 arcseconds. There is a 2.5 arcsecond gap between the two chips.

Figure 10.127: Non-linear component of the WFC Distortion. Note that this figure is rotated 180° with respect to the pipeline calibration products, where WFC2 is the lower half of the detector.

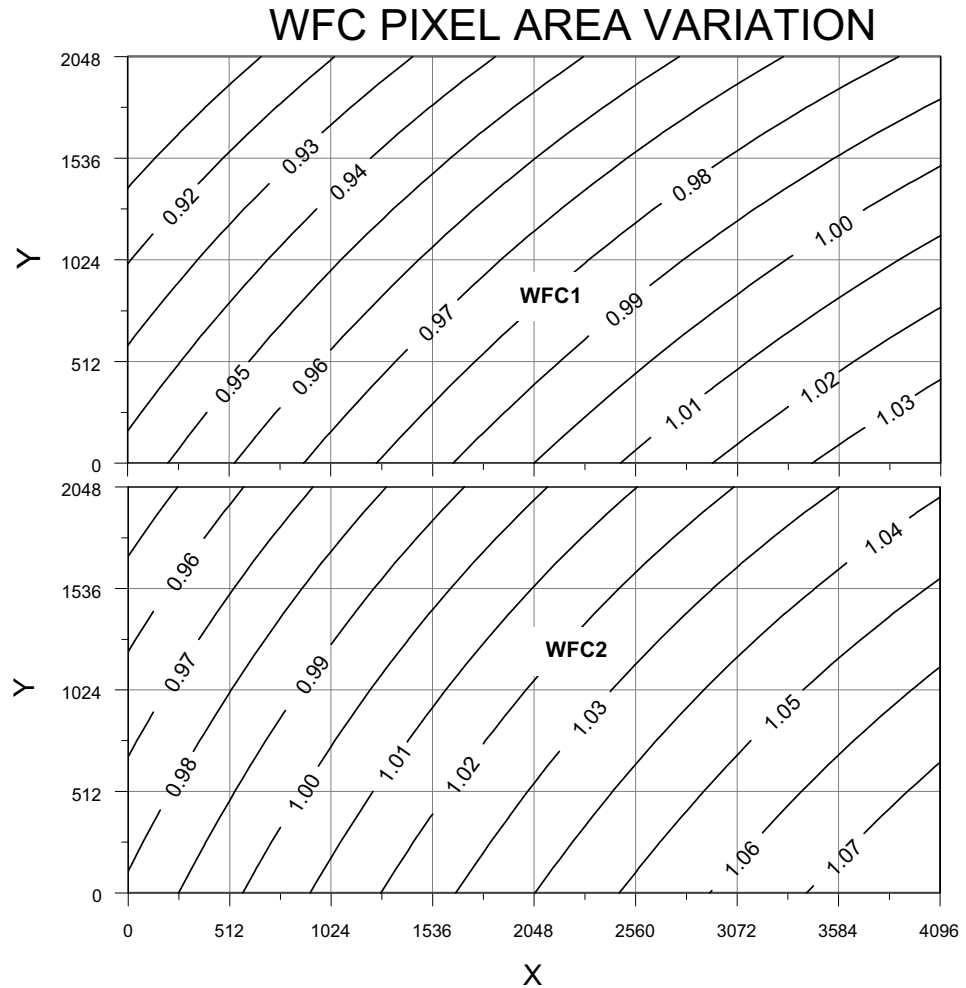


The resulting variation of the projected pixel area on the sky requires corrections to the photometry of point objects. A contour plot of relative pixel size across the WFC normalized to the central pixel, is shown in Figure 10.128. The range of area is from 0.89 to 1.08 times the central value.

### 10.3.2 HRC

The High Resolution Channel has its edges aligned approximately along the V2 and V3 axes. In this case, the center of the aperture lies on a line passing through the V2V3 origin and making an angle of 22 degrees with the V3 axis. The diagonal of the aperture does not correspond to a radius of the HST field of view. So the distortion has no particular symmetry with respect to the detector axes. Again, because the focal plane, and therefore the detector plane is 25 degrees away from the plane normal to the light path, the scales along the axes differ by 14%. However, since the HRC is less than 30 arcsec across, the scale variation over the field is much less than for the WFC, being about 1%. At the center the x and y scales are 0.0284 and 0.0248 arcsec/pixel respectively. The average scales across the middle of the detector are 0.02842 and 0.02485 arcsec/pixel making the x and y widths 29.1 and 25.4 arcsec. The slightly non-square projected aperture shape is evident in Figure 8.7. The angle between the x and y axes on the sky is 84.2 degrees. A vector plot of the deviation from linearity is given in Figure 10.129 in which the deviations have been magnified by a factor of 10 for illustrative purposes. The largest deviation is 4.9 pixels in the top left corner and corresponds to about 0.1 arcsec. The variation of pixel size across the HRC to be used for photometric correction of point sources is shown in Figure 10.130. The maximum deviation from the central value is just over 2%.

Figure 10.128: Variation of the WFC effective pixel area with position in detector coordinates.



### 10.3.3 SBC

The Solar Blind Channel contains the MAMA detector. It is centered close to the HRC position in the V2V3 plane and has a slightly larger field of view, about 35 by 31 arcseconds. The scales and distortions have now been measured directly. The maximum distortion displacement is about 2 pixels or 0.06 arcseconds. The HRC and SBC both have much smaller areas than the WFC. In the x direction the scale is 0.0338 arcsec/pixel while in the y direction it is 0.0301. Like the HRC, the SBC exhibits a 13% difference between x and y scales with a variation across the aperture of a little over 2%.

Figure 10.129: HRC Distortion

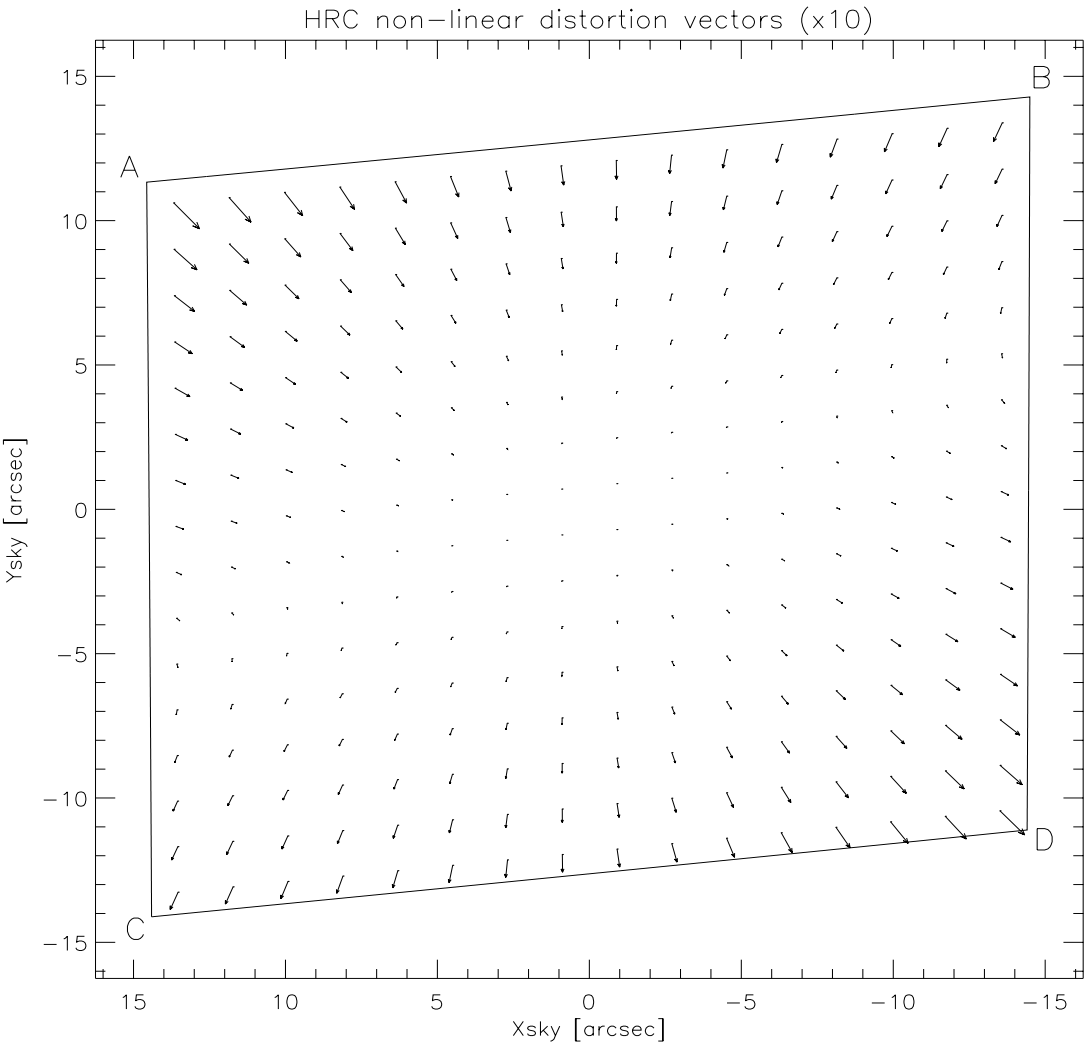
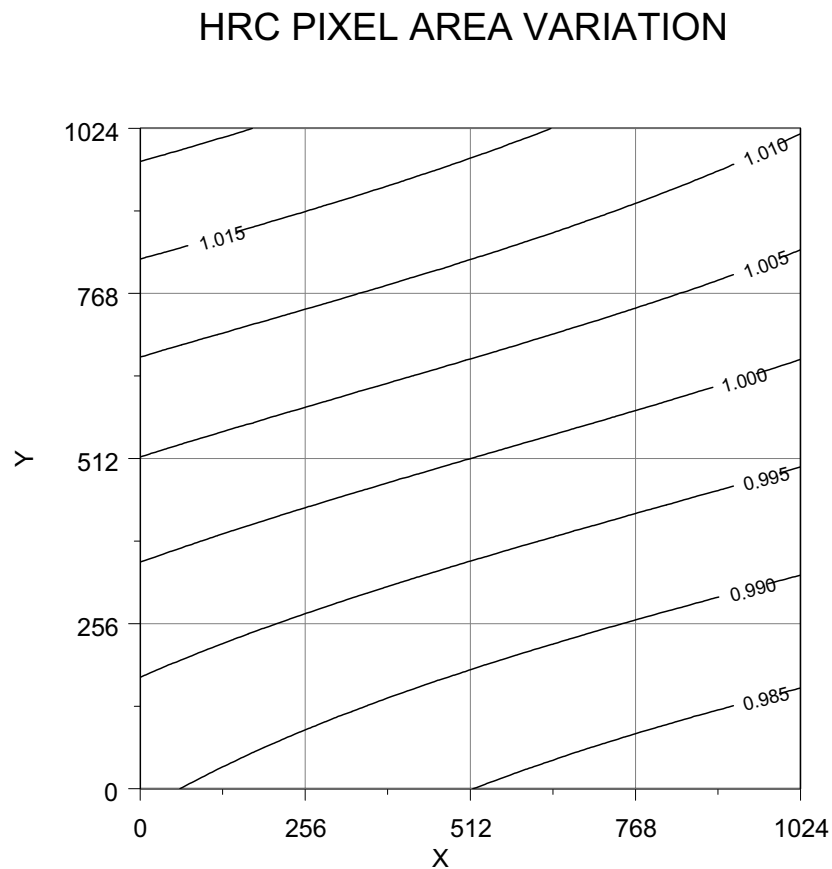


Figure 10.130: Variation of the HRC effective pixel area with position in detector coordinates.



### 10.3.4 Summary

All values presented here are based on in-flight measurements taken during SMOV. Formerly they were based on Ball Aerospace optical simulator measurements. The new values are quite close to the previously published numbers in that scale factors have changed by less than 1% and the aperture locations moved by only a few arcseconds.



PART IV:

# Calibration

---

The Chapters in this Part describe the calibration of ACS. They include an overview of the pipeline calibration process, expected accuracies for data taken in Cycle 12, and plans for calibrating and verifying the instrument's performance.



# Pipeline Calibration

In this chapter . . .

11.1 Overview / 257 11.2 ACS Pipeline / 263 11.3 ACS Data Products / 266
--

This Chapter describes the ACS pipeline’s calibration software, CALACS and MultiDrizzle. Developed at STScI, CALACS removes instrumental signatures, combines CR-SPLIT or REPEAT-OBS exposures and updates certain header keyword values when calibrating ACS data. MultiDrizzle completes the calibration process by removing uncalibrated hot-pixels and cosmic-rays when combining associated images and by removing geometric distortion from all images when creating a final calibrated, possibly combined, product. This chapter is meant only as a high level overview. The “HST Data Handbook for ACS” version 3.0, July 2004, provides a more thorough discussion of data reduction and analysis issues for ACS.

---

## 11.1 Overview

### 11.1.1 On The Fly Reprocessing (OTFR)

All data taken by HST are run through STScI’s calibration pipeline. This consists of two main software systems, the Operations Pipeline Unified System (OPUS) and the Data Archive and Distribution System (DADS). Raw spacecraft telemetry from Goddard Spaceflight Center (GSFC) is transmitted to STScI in the form of POD files. When a user requests data

from the archive through Starview or the archive web interface, OTFR uses these POD files as input to the OPUS step named Generic Conversion generating the uncalibrated “raw” data. CALACS and MultiDrizzle is then run by OPUS to process the uncalibrated data, using specific ACS reference images and tables from the Calibration Data Base System (CDBS), into calibrated data. DADS populates a database from these data that is accessible to users via StarView. DADS then distributes any data requested for download to the user completing the OTFR process.

OTFR is now the standard way to process data requested from the STScI archive. It provides the best calibrated products by reprocessing the raw spacecraft telemetry files through OPUS “on the fly” for distribution each time any data is requested. Exceptions to this include observations expected to be heavily requested by the community for which the archive will maintain current calibrated versions for quicker access.

The most appropriate versions of the ACS reference files are used by CALACS and Multidrizzle each time OTFR is run. Since reference files such as CCD biases and darks are frequently updated, OTFR will use different reference files depending on the date of reprocessing. The user waits until the contemporaneous reference files are in place, and requests the data via StarView. Dark and bias reference files will be updated on a regular basis (usually within 2-3 weeks). The uncalibrated and calibrated data’s header keywords are updated with the filenames of the reference files used during that specific OTFR run.

OTFR also enables the user to avoid downloading outdated archived data due to the software changes made for bug fixes, improved algorithms, new capabilities or header keyword changes. Once a code change is made, OTFR will reprocess and distribute the corrected data using the latest software versions available.

OTFR can distribute all files associated with an ACS observation, including raw and uncalibrated. It will also allow the users to select certain parts of the dataset for download, such as only the uncalibrated or only the calibrated data, when the user does not need all the products.

### 11.1.2 When is OTFR not Appropriate or Sufficient?

Although OTFR produces a data product which will be suitable for many uses there are several occasions when it is not ideal and offline interactive processing by the user is required. The main most frequent reasons for this are:

- Running CALACS or Multidrizzle with personal versions of reference files
- Running CALACS with non-default calibration switch values

- Running Multidrizzle with improved pointing information or other non-default parameter settings

OTFR will always use the most appropriate ACS calibration reference files by default. In order to use non-default calibration reference files, manual re-calibration is required. The calibration reference file keywords in the uncalibrated data need to be updated manually with the non-default filenames before running CALACS.

The selection criteria in table 11.1 are used to set the values for the calibration switch header keywords in uncalibrated ACS data. In order to use non-default calibration switch values, manual re-calibration is required. The calibration switches in the uncalibrated data need to be updated with the non-default values before running CALACS.

A few of the calibration capabilities, specifically an analogue-to-digital conversion correction controlled by ATODCORR, and a correction for shutter shading (gradient of exposure time at short values) as controlled by SHADCORR are not invoked. These capabilities are supported in CALACS code, but instrument characterization has shown that these corrections are fortunately not needed for ACS, and supporting reference files do not exist. The switches for these should therefore always be left as OMIT.

Table 11.1: Calibration Switch Selection Criteria

Switch	Description	Criteria
DQICORR	Data Quality Array Initialization	DEFAULT = "PERFORM" If OBSMODE = ACQ then "OMIT"
ATODCORR	Analog to Digital Correction	DEFAULT = "OMIT"
BLEVCORR	Overscan Region Subtraction	DEFAULT = "PERFORM"
BIASCORR	Bias Subtraction	DEFAULT = "PERFORM"
FLSHCORR	Post Flash Subtraction	DEFAULT = "OMIT"
CRCORR	Cosmic Ray Rejection	If CRSPLIT $\geq$ 2 then "PERFORM" If CRSPLIT < 2 then "OMIT"
DARKCORR	Dark Subtraction	DEFAULT = "PERFORM"
FLATCORR	Flat Field Division	DEFAULT = "PERFORM"
SHADCORR	Shutter Shading Correction	DEFAULT = "OMIT"
PHOTCORR	Photometric Processing	DEFAULT = "PERFORM"
RPTCORR	Repeat Processing	DEFAULT = "OMIT" If NRPTXP > 1 then "PERFORM"
EXPSCORR	Full calibration of individual exposures in an association	DEFAULT = "PERFORM"

Switch	Description	Criteria
DRIZCORR	Dither processing and distortion correction	DEFAULT = " <b>PERFORM</b> "
GLINCORR	Global Non-Linearity Correction	SBC DEFAULT = " <b>PERFORM</b> "
LFLGCORR	Local and Global Non-Linearity Flagging in DQ Array	SBC DEFAULT = " <b>PERFORM</b> "

The goal of the ACS pipeline is to provide data calibrated to a level suitable for initial evaluation and analysis for all users. Observers frequently require a detailed understanding of the calibrations applied to their data and the ability to repeat, often with improved calibration products, the calibration process at their home institution. Therefore, the CALACS and PyDrizzle packages used in this pipeline can also be used to calibrate ACS data off-line and are available within the STSDAS system. In addition, the calibration reference files (e.g. flat fields) are available from the HST Archive via the [Archive web pages](#). The most recent version of STSDAS, which includes CALACS and MultiDrizzle, can be downloaded at [http://www.stsci.edu/resources/software\\_hardware/stsdas](http://www.stsci.edu/resources/software_hardware/stsdas). A tutorial for running CALACS can also be viewed at <http://www.stsci.edu/hst/acs/analysis>.

Many ACS datasets will not have multiple exposures at the same pointing. The increasing prevalence of hot pixels, particularly in the WFC camera, make dithering in most cases highly desirable. This use of dithering circumvents the algorithms built into CALACS for detecting and removing cosmic-rays. To address this problem, the task MultiDrizzle, originally designed to be run interactively (Koekemoer et al. 2002 HST Calibration Workshop), has been developed to run within OTFR. It will be used in OTFR to process all ACS datasets and remove hot-pixels and cosmic-rays from all associated ACS images, regardless of whether they were dithered or taken as CR-SPLIT or REPEAT-OBS pointings, while also correcting for geometric distortion.

MultiDrizzle provides a single-step interface to the complex suite of operations originally performed by the tasks in the STSDAS dither package. These are used for initial image registration, creation of a clean median image, transformation back to the input image plane, creation of cosmic ray masks, and final drizzling. The goal of MultiDrizzle is to provide a high-level task which has an extensive suite of user-adjustable parameters which, if left at their default values, will allow the task to perform all these steps in a single operation with no user intervention. At the same time, the parameters allow the user a large amount of flexibility in controlling the relevant aspects of these steps, in case the default parameters are not sufficient for specific scientific applications. MultiDrizzle relies on PyDrizzle extensively to control the operation of the

task 'drizzle' which performs the actual distortion correction and image combination.

MultiDrizzle relies on the image header world coordinate system (WCS) to deduce the image-to-image offsets. However, user-supplied offsets may also be applied in a flexible way in offline use, offsets computed using whatever tasks the user finds most appropriate and suitable for their data. For OTFR use, though, image header WCS information for images taken as part of a defined association generally provides image registration good enough for initial analysis.

The most recent version of MultiDrizzle, updated since the last release of STSDAS, can be downloaded from:

[http://www.stsci.edu/resources/software\\_hardware/pydrizzle](http://www.stsci.edu/resources/software_hardware/pydrizzle)

In addition, examples of using Multidrizzle with ACS data, along with available documentation, can be found at:

<http://www.stsci.edu/hst/acs/analysis/drizzle>.

### 11.1.3 Distortion Correction and Dither Combining

All ACS data will automatically be corrected for distortion during standard pipeline processing using a task called PyDrizzle called from MultiDrizzle. PyDrizzle relies on the IDCTAB reference file for the description of the distortion model. It also understands the ACS association tables to allow Multidrizzle to combined dithered observations in the pipeline. Observation sets which use CR-SPLIT or REPEAT-OBS options for a single pointing or use the dither patterns provided in the proposal instructions will be automatically associated for combining in the pipeline. Programs which rely on explicit POS TARG commands will NOT be associated in the pipeline, resulting in separately calibrated image for each position. PyDrizzle, as called by MultiDrizzle, automatically produces images which are both astrometrically and photometrically accurate regardless of whether they were taken as part of an association or as a single exposure. Calibrated individual images, with the \_flt.fits extension (FLT files) are also produced by the pipeline and are used as the input for MultiDrizzle.

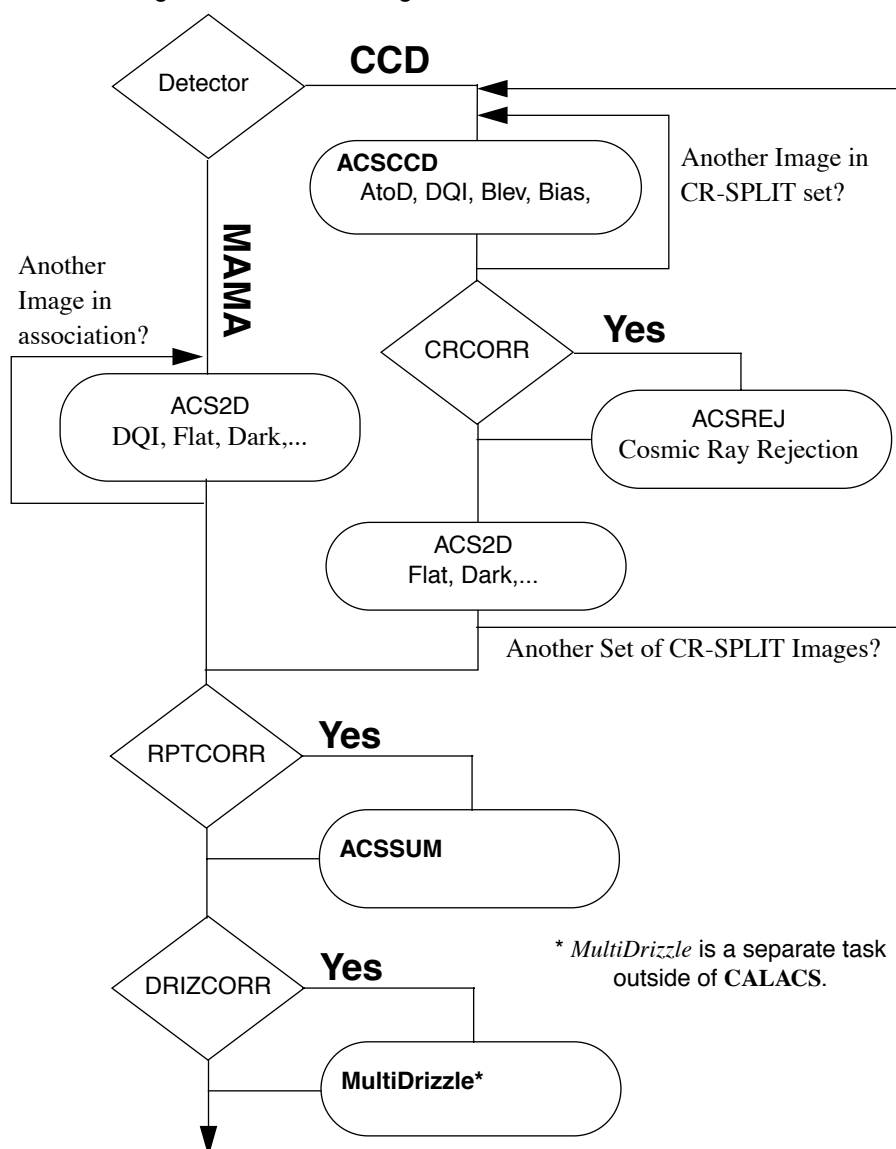
It is important to note that PyDrizzle, when combining dithered images, does NOT remove cosmic-rays. MultiDrizzle was developed to perform this additional work of removing cosmic-rays from associated images, relying on PyDrizzle to perform the actual distortion correction and image combination.

For ACS WFC observations, both WFC chips will be combined into a single image in the output by PyDrizzle. All ACS distortion-corrected, possibly dither-combined, images will have a single SCI extension, a weight (WHT) extension, and a context (CTX) extension, replacing the standard SCI, ERR and DQ arrays in the CALACS calibrated products. The WHT extension records the combined input weights for each output

pixel. In standard processing, the values will be the effective exposure time for each output pixel. The CTX extension encodes information about which input image contributes to a specific output pixel. This is done using a bitmask for each output pixel where ‘bit set’ means that the image, in the order they were combined, contributed with non-zero weight to that output pixel. The context image starts as a 32-bit integer image but is extended as a cube with additional 32-bit deep planes as required to handle all the input images.

Processing comments are recorded in the trailer file for the DRZ image, including which version of drizzle was used, what parameters were used, and which images were combined (if dithered). The same default parameters, however, are used for all observations in the pipeline. These parameters were chosen to avoid introducing any scale changes, or shifts relative to the original point while returning a corrected product oriented with North aligned with the Y axis for most ACS images. The size of a single, distortion-corrected image, prior to rotating it to align with North, can be found in Table 11.2. These products will be properly corrected for distortion. However, for dithered observations, the combination may not be ideal as many defects resulting from small pointing errors may still be present. Subsequent reprocessing with PyDrizzle or MultiDrizzle offline, using updated image registration, may be required to obtain the desired scientific value. PyDrizzle and MultiDrizzle can be obtained as part of STSDAS, which requires the PyRAF environment to run. These packages can also be obtained from the [STSDAS web](#) pages.

Figure 11.1: Flow Diagram for ACS data shown with CALACS task names.



## 11.2 ACS Pipeline

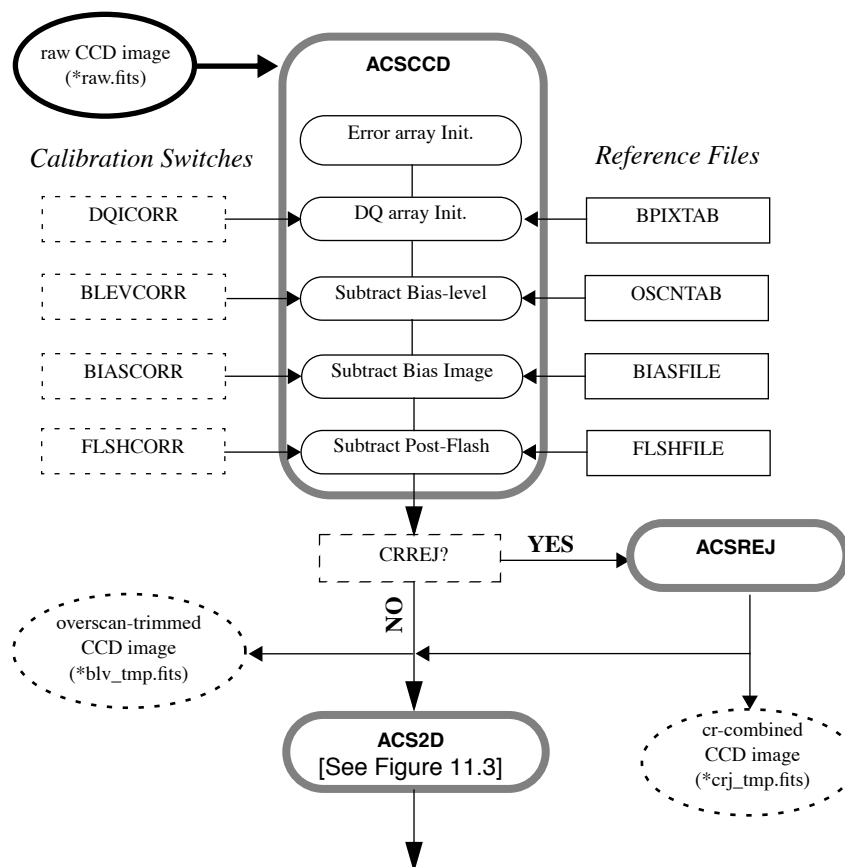
The ACS calibration pipeline consists of 2 major packages run one after the other: namely, CALACS and MultiDrizzle. The CALACS package itself consists of 4 calibration tasks which can all be run separately on individual exposures. Since ACS can also produce associated data, such as CR-SPLIT or REPEAT-OBS exposures, the task **CALACS** can be used to process these associated exposures, or even individual exposures, automatically by calling the 4 individual tasks in the package as needed. The PyDrizzle package then processes the output from CALACS, both

single exposures and associated datasets. These tasks apply the basic calibrations necessary for ACS data. The flow of data through the ACS pipeline, and what decisions are made while working with associated data, can be seen in Figure 11.1.

The following calibration steps are performed in order for ACS data:

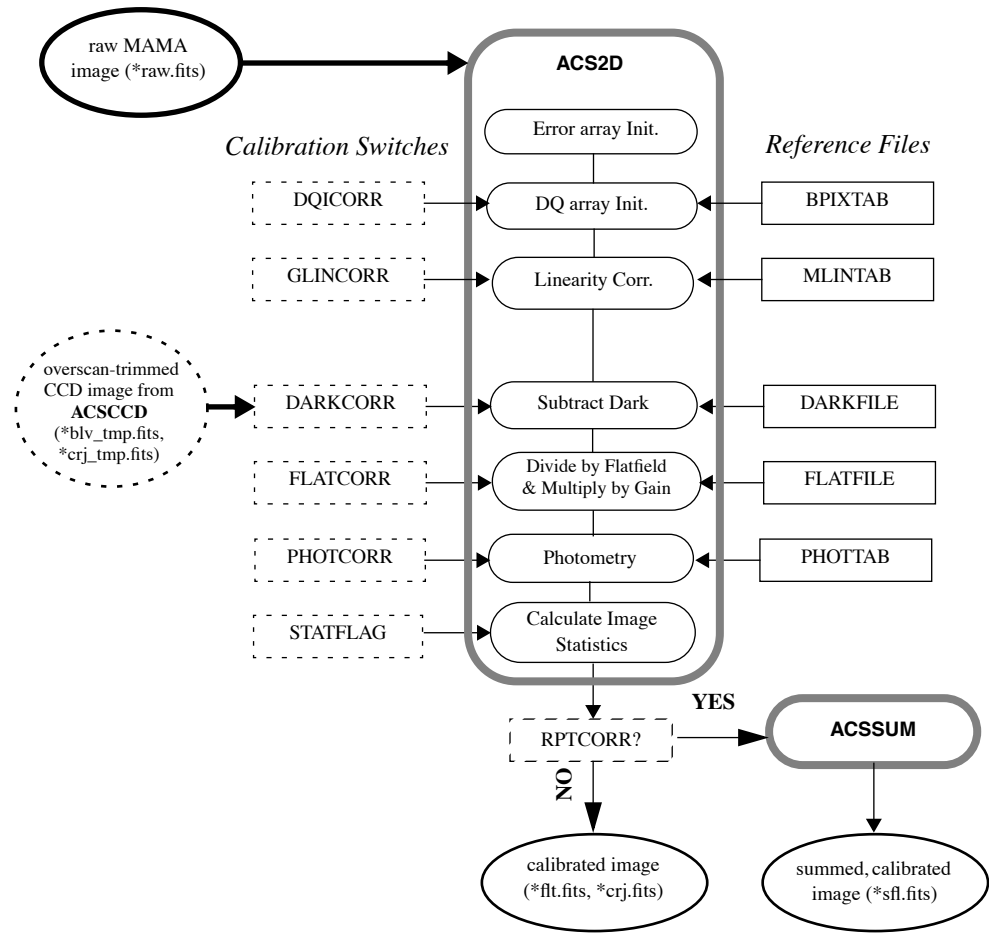
1. Calculate a noise model for each pixel and record estimated noise value in error array
2. Flag known bad pixels and saturated pixels in the data quality array
3. Subtract bias-level determined from overscan regions (CCD data only)
4. Subtract bias image (CCD data only)
5. Subtract post flash image (CCD data only)
6. Perform cosmic-ray rejection and combination of CR-SPLIT data (CCD data only)
7. Perform global linearity corrections (MAMA data only)
8. Scale and subtract dark image and calculate mean dark value
9. Perform flat-fielding
10. Calculate values for photometry keywords
11. Calculate image statistics
12. Remove cosmic-rays, combine associated observations, and apply distortion correction (using MultiDrizzle)

Figure 11.2: Flow diagram for CCD data in CALACS



As shown in Figure 11.1, the calibration tasks have been split to handle CCD-specific calibrations separately from those steps which can be applied to any ACS data. MAMA data obtained from the SBC do not have the overscan regions found in CCD data, and therefore those steps pertaining to the use of the overscan regions were split into a separate task. The initial processing performed on CCD data alone is shown in Figure 11.2, with the result being processed like the rest of the ACS data through the processing steps shown in Figure 11.3.

Figure 11.3: Flow diagram for MAMA and CCD data in CALACS.

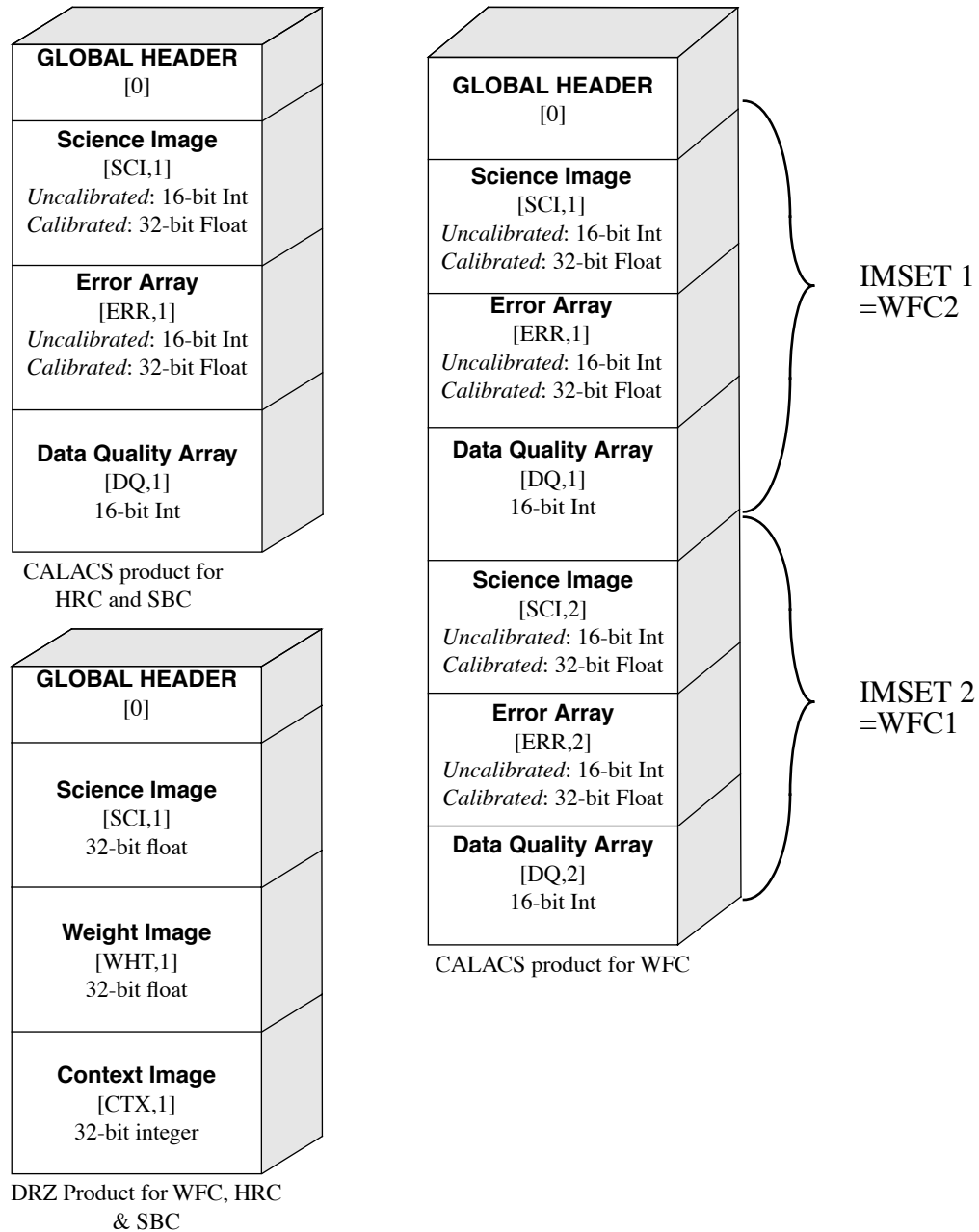


## 11.3 ACS Data Products

The inputs for CALACS processing come out of the Generic Conversion stage of OTFR and include:

- raw exposure - FITS formatted, 16-bit integer data (see Figure 11.4)
- association table (only for associated data)
- trailer file from Generic Conversion (optional for reprocessing)

Figure 11.4: Data formats for Calibrated and Drizzled ACS Modes. Note that for calibrated data, WFC1 (chip 1) corresponds to extension [SCI,2] (or equivalently, extension [4]).



### Processing Single Exposures with CALACS

Processing single exposures will result in the creation of a single fully calibrated ACS exposure. Figure 11.4 illustrates the basic format used to store ACS images, however, differences exist between uncalibrated and calibrated observations. A single, uncalibrated (RAW) ACS exposure starts out with a Primary header plus, for each chip, a SCI extension with the data

in 16-bit integer format, an empty ERR extension, and a DQ extension which may or may not have 16-bit integer data. CALACS then processes this observation using the steps outlined in Figure 11.2 and Figure 11.3 to generate the fully calibrated (FLT) image. This FLT image consists of a Primary header, and again for each chip, a SCI extension with 32-bit float data, an ERR extension with 32-bit float data, and a DQ extension with 16-bit integer data. The data in the calibrated SCI extension and the corresponding ERR extension have units of ELECTRONS, after accounting for the gain correction performed during the flat-field correction.

### Processing Associated Exposures with CALACS

The CALACS will also recognize and correctly process CR-SPLIT or REPEAT-OBS exposures by interpreting the association table and determining which exposures should be combined during calibration. As illustrated in Figure 11.1, REPEAT-OBS exposures are individually processed to create an FLT file for each input exposure, then those FLT images are summed to create the final (SFL) product. However, since these exposures are not run through ACSREJ, no cosmic-ray rejection is performed when REPEAT-OBS images are summed together to form the final SFL product.

Input RAW exposures taken for a CR-SPLIT association, on the other hand, are only calibrated using ACSccd, then they are combined into a single exposure during cosmic-ray rejection with ACSREJ. The final calibration steps are then run on cosmic-ray cleaned products to produce the final calibrated, cosmic-ray cleaned (CRJ) image. Thus, processing an association results in a single CALACS-calibrated product created from combining the individual exposures in the association.

Since the same processing is performed on combined images as single exposures, the data in the calibrated SCI extension and the corresponding ERR extension also have units of ELECTRONS for both REPEAT-OBS and CR-SPLIT data.

### MultiDrizzle Processing in the Pipeline

The final calibration performed during pipeline processing corrects for the geometric distortion and pixel area effects in the flat-fielded calibrated observations produced by CALACS. It also removes cosmic-rays and combines all associated observations, whether taken as CR-SPLIT, REPEAT-OBS or dither patterns, into a single distortion-corrected product. Both steps are performed using MultiDrizzle in the pipeline with the flat-fielded (FLT) files from CALACS as input.

A single ACS exposure calibrated by CALACS results in an FLT file. This image can be processed by MultiDrizzle only by running PyDrizzle to remove the effects of the geometric distortion to produce a drizzle calibrated (DRZ) images. This DRZ image is a multi-extension FITS file with the format shown in Figure 11.4 for the DRZ product. The SCI

extension contains the distortion-corrected data as 32-bit float data. The weight image gets stored as a WHT extension in the form of 32-bit float data, while the final CTX extension contains the 32-bit integer data for the context data.

Associations can be produced for dither patterns, CR-SPLIT, or REPEAT-OBS exposures or a combination of CR-SPLIT or REPEAT-OBS exposures at each point in a dither pattern. CALACS, though, will always produce an FLT image for each input in the association, regardless of the pointing, while CRJ or SFL images will also be produced for each CR-SPLIT or REPEAT-OBS pointing, respectively. MultiDrizzle processes only the FLT images from the association to remove the cosmic-rays, apply the correction for geometric distortion, then combine them into a single combined DRZ product with the same format as a single calibrated exposure. More details on this can be found in Chapter 4 of the “HST Data Handbook for ACS”.

## 11.4 System Requirements for ACS Data

The large size of ACS WFC exposures may present problems for observers using ACS, especially when dealing with data that requires associations. Raw ACS exposures which serve as input to the pipeline have the sizes given in Table 11.2.

The total size of a WFC image includes both the SCI arrays, while the HRC and SBC detectors only have one chip/array. The file sizes given in Table 11.2 presume that both the SCI array and DQ array are populated with short integer values, but that the ERR array is NULL with all pixels having a value of zero. During processing, the SCI arrays are converted to floating point data from the input integer data. The ERR array also is populated with floating point values. The size of the calibrated images become quite large, as noted in Table 11.2. The final size of the distortion corrected images, though, can be considerably larger due to the expansion to account for the distortion, as noted in the last column of Table 11.2. The final image size as produced by OTFR can be up to 50% larger than the distortion corrected size since most ACS images get rotated to align the Y axis with North. Thus, the final size depends on the initial orientation of the image, but will never be smaller than the value listed in Table 11.2.

Table 11.2: Final sizes of unrotated calibrated ACS exposures for each detector.

Detector	Size of raw FITS file ( $S_{\text{raw}}$ )	Size of calibrated FITS file ( $S_{\text{cal}}$ )	Size of unrotated DRZ file ( $S_{\text{drz}}$ ) <sup>1</sup>
WFC (2 Chips)	68.7 MB	168 MB	215MB
HRC (1 Chip)	4.4 MB	10.5 MB	16MB
SBC (1 detector)	4.2MB	10.5 MB	16MB

1. This size assumes no dither offset or scale change.

While the size of the final calibrated HRC or SBC exposures are comparable to those of STIS or WFPC2, the ACS WFC exposures are over 16 times as large. In addition, the following equation should be used to estimate the minimum amount of free storage that should be available during processing of associated ACS data:

$$D_{min} = (1 + n) \cdot S_{cal} + n \cdot S_{raw} + (2.1 + p^2) \cdot S_{drz}$$

where:

- $D_{min}$  is the minimum free disk space required for processing,
- $S_{cal}$  is the size of the calibrated exposure (from Table 11.2),
- $S_{raw}$  is the size of the raw exposure (from Table 11.2), and
- $n$  is the number of exposures in each CR-SPLIT set or REPEAT-OBS set.
- $S_{drz}$  is the size of the distortion corrected, dither combined (if needed) exposure (from Table 11.2).
- $p$  is the percentage shift (in pixels) across all dither positions.

### Size of Reference Files for Re-Processing

Another additional concern when processing ACS observations may be the amount of storage taken for reference files. For ACS WFC observations, a complete set of reference files could exceed 520MB by themselves. HRC and SBC reference files, in comparison, only require about 45MB of disk space.

### Speed of Pipeline Processing

Some observers will eventually want to re-calibrate their ACS data locally. Reprocessing HRC or SBC data will not put a burden on most computing systems since the data sizes are relatively small, both for the science data and for the reference files. Processing ACS WFC observations, on the other hand, will require more computing power, both in terms of CPU runtime and disk space. Great care has been taken to minimize the memory requirements of the pipeline software to accommodate most computing configurations. Even so, CALACS requires up to 130MB of memory, while PyDrizzle requires up to 400MB to process WFC data. This involves relying on line-by-line I/O to read the input data and reference files, placing an extra burden on the I/O capabilities of the computing system.

Overall, though, an Ultra-10 class workstation (300 MHz, 512MB RAM) can still run CALACS to process ACS WFC data in reasonable times; namely, about 13 minutes for a CR-SPLIT=2 ACS/WFC association or about 4.5 minutes for a single ACS/WFC exposure. The PyDrizzle processing only requires working on the output image, not all individual input images, thus requiring only about 5 minutes to process a single

ACS/WFC exposure itself. These results can be scaled by the processor speed for the computing system, resulting in even more acceptable runtimes for faster, newer workstations.



# Calibration Accuracies

In this chapter . . .

12.1 Summary of Accuracies / 273
----------------------------------

In this Chapter we describe the accuracies that can be expected from ACS observations.

---

## 12.1 Summary of Accuracies

In the tables below we list the accuracy that we expect to achieve from the planned calibration program. These estimates reflect the current understanding of the instrument and may need to be updated once additional calibration data have been obtained and thoroughly analyzed. Updates will be available on the ACS web pages (under “[Calibration Plan](#)”). Although data will be analyzed according to our list of calibration priorities, all calibration data are immediately public and accessible through the HST archive so that users in need of extremely accurate or urgent results will be able to carry out their own calibration. The values quoted here are the results of pre-launch measures, of observations taken during SMOV, and of observations taken as part of the Cycles 11 and 12 calibration program.

The extensiveness of our calibrations will also depend, in part, on the science programs selected by the proposers and the TAC. Clearly, we will spend little or no time calibrating filters or capabilities that are not requested by observers. We have selected a subset of the filters as those that we expect to receive heavy use; the accuracy numbers quoted here for photometric measurements are for WFC/F435W, WFC/F475W, WFC/F555W, WFC/F606W, WFC/F625W, WFC/F775W, WFC/F814W,

WFC/F850LP, HRC/F330W, HRC/F435W, HRC/F475W, HRC/F555W, HRC/F606W, HRC/F625W, HRC/F775W, HRC/F814W and HRC/F850LP. The remaining filters may be subject to moderately higher levels of uncertainty.

The accuracies tabulated assume that the Poisson noise in the data is negligible. Clearly, low-S/N data will have accuracies dominated by this unavoidable noise source.

Table 12.1: WFC Accuracies

Attribute	Accuracy	Limiting factor
Relative Astrometry within a chip	0.25 pixel	Calibration & stability of geometric distortion
Relative astrometry between chips	0.5 pixel	Stability
Absolute astrometry	1"	Guide Star, Catalog uncertainties
Absolute Photometry	3%	Absolute Calibration, standards
Relative Photometry within an image	1%	Flat-field characterization or characterization of geometric distortion.
Repeated photometry of same star	0.3%	Stability of Flatfield
Transformation to Standard Magnitude Systems	0.02 mag SDSS 0.025 mag WFPC2 0.03 mag BVRI	DQE curve determination Color terms
Polarimetry	1%	
Wavelength Calibration	20Å grism	Accuracy of dispersion solution
Grism Spectrophotometry	6%	

The values listed here are meant to reflect typical applications, in special circumstances it is possible to do much better (or worse as the case may be). For example, a program designed to perform differential time-series photometry has demonstrated photometric stability of 0.06% for 519 WFC exposures spanning 7 days using GAIN=2, pointing maintained to the same pixel throughout, and for strongly saturated (!) stars providing a low Poisson limit.

Table 12.2: HRC Accuracies

Attribute	Accuracy	Limiting factor
Relative Astrometry within the field	0.1 pixel	Calibration & stability of geometric distortion
Absolute astrometry	1"	Guide Star, Catalog uncertainties
Absolute Photometry	2%	Absolute Calibration, standards
Relative Photometry within an image	1%	Flat-field characterization or characterization of geometric distortion.
Repeated photometry of same star	0.3%	Stability of Flatfield
Transformation to Standard Magnitude Systems	0.02 mag SDSS 0.025 mag WFPC2 0.03 mag BVRI	DQE curve determination Color terms
Polarimetry	1%	
Wavelength Calibration	12Å grism	Accuracy of dispersion solution
Grism Spectrophotometry	10%	

Table 12.3: SBC Accuracies

Attribute	Accuracy	Limiting factor
Relative Astrometry within the field	0.25 pixel	Calibration & stability of geometric distortion
Absolute astrometry	1"	Guide Star, Catalog uncertainties
Absolute Photometry	5%	Absolute Calibration, standards
Relative Photometry within an image	2%	Flat-field characterization or characterization of geometric distortion.
Repeated photometry of same star	1%	Stability of Flatfield
Wavelength Calibration	1 pixel prisms	Accuracy of dispersion solution
Prism Spectrophotometry	20%	



# Calibration Plans

## In this chapter . . .

13.1 Ground Testing and Calibration / 278
13.2 SMOV Testing and Calibration / 278
13.3 Cycle 11 Calibration / 280
13.4 Cycle 12 Calibration / 282
13.5 Cycle 13 Calibration / 284
13.6 Cycle 14 Calibration / 285

In this Chapter we describe the current status of ACS calibrations, as well as plans for the Cycle 14 period of primary interest in this Handbook.

At the time of writing, the analysis of SMOV (Servicing Mission Orbital Verification) and most Cycle 11 data has been completed. Most of the Cycle 12 calibration observations have been obtained, and calibrations of fundamental items such as geometrical distortions and absolute sensitivity are well in hand. Details and results for low use modes are being actively pursued.

For further information please access the STScI web page for ACS, and/or consult the [Helpdesk](#) for staff input to specific questions.

---

## 13.1 Ground Testing and Calibration

Ground calibration and testing was a prime responsibility of the ACS Investigation Definition Team (Principal Investigator Holland Ford, JHU) and was carried out at Ball Aerospace in Colorado. Thermal vacuum (and supplemental dry-nitrogen environment) testing in which orbital conditions were simulated was conducted pre-launch at Goddard Space Flight Center. Filter transmission curves, and detector quantum efficiency curves, were derived at GSFC and JHU. These tests characterized the basic properties of the optics, the detectors, and the mechanisms. During ground calibration the highest priority was given to those measurements essential to establish that instrument design specs were being met, and to those measurements that could not be obtained on-orbit. Most of the non-unique ground test data were superseded by on-orbit measurements as part of the STScI Cycle 11 calibration plan. Successive cycles of the calibration program both maintain routine calibrations (such as providing darks and biases and tracking evolving CTE) and also brings maturity to determinations of the overall QE and low-frequency flat fields.

---

## 13.2 SMOV Testing and Calibration

The primary goal of the SMOV3B was a timely commissioning of the HST observatory for normal science operations. For ACS this has included basic testing of the instrument functionality as well as testing/setting of the focus (internal and external), measuring the sensitivity in all filters, establishing the geometric distortion and plate scale, quantifying the point spread function for each camera, and adjusting flat fields to properly capture low-frequency variations for which ground calibrations are always difficult. Data from SMOV proposals are non proprietary and fully accessible through the HST archive. We list below the program IDs and proposal titles. Details of the Phase II programs may be found via: <http://presto.stsci.edu/public/propinfo.html>. Some programs are of very limited technical interest (e.g., Science data buffer check--9003), while others (e.g., WFC flat field stability--9018) collected large amounts of data in standard filters on objects of potential archival science interest.

Table 13.1: ACS SMOV Proposals

Proposal ID	Titles
8947	CCD Daily Monitoring
8948	CCD CTE Test
8992	ACS ERO Program
9002	ACS Dump Test & Verification of Memory Loads
9003	ACS Science Data Buffer Check
9004	ACS Calibration Lamp Checkout Contingency
9005	CCD Functional
9006	CCD Temperature Set Point Determination
9008	ACS MAMA Initial Turnon & Anomalous Recovery Procedure
9009	ACS MAMA Fold Analysis
9010	SMOV Contamination Plan
9011	ACS to FGS Fine Alignment
9012	HRC Coronagraphic Acquisition
9013	ACS Coarse Corrector Alignment
9014	ACS Fine Corrector Alignment
9015	ACS Image Quality Verification
9016	HRC Coronagraph Repeatability
9017	ACS Image Stability Verification
9018	WFC Flat Field Stability
9019	HRC Flat Field Stability
9020	Preliminary ACS Sensitivity
9022	SBC Dark Current Measurement
9023	ACS SBC Image Quality Verification
9024	SBC Flat Field uniformity
9025	Scattered Light in Coronagraphic Obs
9026	ACS Ramp Filter Test
9027	ACS SBC Geometric Distortion Calibration
9028	CCD Geometric Distortion
9029	ACS Grism/Prism Performance Check
9031	ACS CCD hot pixel annealing
9032	ACS CCD Flash calibration
9574	Focus Monitor

## 13.3 Cycle 11 Calibration

The SMOV calibration and testing period extended for roughly two months taking routine monitoring of ACS performance through April 2002. With the nominal start of Cycle 11 at July 1, 2002 and with a desire not to define the final calibration program for Cycle 11 until some flight experience from SMOV could be obtained, a decision was made to break the Cycle 11 calibration into two parts: (1) an interim program continuing routine monitoring (darks, biases) and extending characterization in areas not well covered by SMOV, and (2) the standard full program expected to start in July 2002 and run for one year. Tables 13.2 and 13.3 list program IDs and titles for the interim and standard Cycle 11 calibrations respectively.

### 13.3.1 Calibration Priorities

As for any instrument the ACS calibration plan represents a compromise between the desire to calibrate the instrument as well as possible and the availability of finite resources both in terms of primary HST orbits and in terms of human resources at STScI. The list of priorities that guided the Cycle 11 calibration planning was:

1. *Monitor the Health and Safety of the Instrument.* This includes obtaining all data necessary to verify that the instrument is performing as planned and to insure a useful lifetime as extended as possible.
2. *Update and Maintain Pipeline Reference Files.* Dark, biases, flat fields and sensitivities used in the pipeline calibration need to be accurate and current. Information on newly released reference files is announced via the Space Telescope Analysis Newsletter and posted on the ACS web page. The updated list of recommended reference files to be used with each data set is available through the HST Archive, and will be automatically applied when calibrated data are requested from the Archive.
3. *Characterization of Optical Performance.* The point spread function and its variation across the field of view needs to be carefully determined as a function of wavelength.
4. *Characterization of detectors.* This includes charge transfer effects, long wavelength fringing, hot pixel growth, etc.

Table 13.2: Cycle 11 ACS Interim Calibrations

Proposal ID	Proposal Title
9558	CCD Monitor
9559	Focus Monitor
9560	CCD Linearity Check
9561	Internal CTE Monitor
9562	Internal Flat Field Stability
9563	Photometric Stability
9564	UV Earth Flats
9565	Contamination Monitor
9566	CCD Hot Pixel Annealing
9567	SBC Dark Current
9568	Grism/Prism Calibration

Table 13.3: Cycle 11 ACS Standard Calibrations

Proposal ID	Proposal Title
9647	CCD Daily Monitor Part I
9648	External CTE Monitor
9649	ACS internal CTE monitor
9650	CCD Hot Pixel Annealing
9651	ACS CCD Flash Calibration
9652	SBC Dark Current
9653	ACS MAMA Initial Turn-on and Anomalous Recovery Procedure
9654	ACS photometric Stability
9655	ACS Post-SMOV UV Contamination Monitor
9656	Stability of the ACS CCD: geometry, flat fielding, photometry
9657	ACS Internal Flat Field Stability
9658	UV Earth Flats
9659	Gain Dependence of Biases
9660	Earth Bright Limb Calibration
9661	ACS Polarization Calibration
9662	HRC+WFC Shutter Stability Test
9663	Focus Monitoring

Proposal ID	Proposal Title
9664	SDSS Primary Standards
9665	Extreme Red Stars
9666	Photometric Transformations
9667	ACS PSF Characterization
9668	ACS Coronagraph Wavelength Dependence
9669	ACS Coronagraph stability and vignetting
9670	UV and Narrow Band Filter Red Leak Check
9671	ACS Ramp Filter Check
9672	Grism/Prism Calibration
9673	CCD Daily Monitor (9674 & 9675 continue this)

The Cycle 11 calibration program was intended to most effectively balance the needs of the community for obtaining excellent science results from the instrument with the limited resources available (e.g., a nominal limit of 10% time available for calibration). Common uses of the instrument were fully calibrated.

## 13.4 Cycle 12 Calibration

The goal of the Cycle 12 calibration plan was to complete the definition of the ACS calibration by refining the measure of a number of important parameters of the instrument. These included the geometric distortions, L-flats, sky flats, and the quantum efficiency of the two CCD detectors. Monitoring programs followed hot pixels, the stability of bias and dark reference frames, the photometric calibration stability, and tracking the degradation of photometric performance due to CTE losses induced by the continued exposure to cosmic radiation.

The Cycle 12 calibration plan started on October 2003 and Table 13.4 lists the programs.

Table 13.4: Cycle 12 ACS Standard Calibrations

Proposal ID	Proposal Title
10042	CCD Daily monitor
10043	External CTE Monitor
10044	Internal CTE Monitor
10045	SBC Dark Current and Recovery
10046	CCD Hot Pixel Annealing
10047	UV Contamination Monitor
10048	Stability of Photometry, Geometrical Distortions and Flat Fields
10049	Internal Flats
10050	UV Earth Flats
10051	Bias Reference Files for Sub-arrays
10052	CCD Postflash Verification
10054	Photometric Zero Points
10055	Polarization Calibrations
10056	Calibration of Photometry of Extreme Red Sources
10057	Ramp Filter Wavelengths and L-Flats
10058	Grism/Prism Calibrations

The CCD daily monitoring program continued to provide dark and bias frames to build the corresponding bi-weekly reference files. Separate programs provided bias reference files for subarrays, and measured the SBC detector's dark current and stability. The CTE monitoring program characterized the CCDs' CTE losses as a function of time, field crowding and background levels, and defined recipes to calibrate them. Also, accurate measures and monitoring of available post-flash background levels were made to allow its use in future cycles in mitigating CTE losses. Annealing of CCD hot pixels continued as during Cycle 11, and possible contamination to the UV throughput was monitored. The photometric zero points of all cameras will be further refined through observations now obtained of four spectro-photometric standard stars. The photometric calibration for compact or point sources with very red spectral energy distribution was checked through observations of extreme red stars. The stability of the photometric calibration, geometrical distortions and flat fielding will also be measured and monitored through dedicated programs. Polarization calibrations were taken to fully characterize the internal polarization of the instrument. Data to support accurate wavelength measures and L-flats for the ramp filters were acquired. The plan also included accurate measures of the wavelength calibration of the grism and the prism.

## 13.5 Cycle 13 Calibration

The goal of the Cycle 13 calibration plan is to continue refining the definition of the ACS calibration by measuring a number of important parameters of the instrument, but with a level of resource commitment in orbits that will be lower for areas exhibiting excellent stability to date. These include the geometric distortions, L-flats, sky flats, and the quantum efficiency of the two CCD detectors. Monitoring programs followed hot pixels, the stability of bias and dark reference frames, the photometric calibration stability, and tracking the degradation of photometric performance due to CTE losses induced by the continued exposure to cosmic radiation. New observations will be aimed at testing the wavelength stability of primary filters and further refining the measure of their bandpasses, and continuing to build up polarimetric calibration.

The Cycle 13 calibration plan will start on October 2004 and Table 13.5 lists the currently planned programs.

Table 13.5: Cycle 13 ACS Standard Calibrations

Proposal ID	Proposal Title
10367	CCD Daily monitor
10368	External CTE Monitor
10369	Internal CTE Monitor
10370	CCD Hot Pixel Annealing
10371	CCD Postflash Verification
10372	SBC MAMA Recovery
10373	UV Contamination Monitor and SBC Dark Current
10374	ACS Photometric Stability
10375	Stability of Photometry, Geometrical Distortions and Flat Fields
10376	Internal Flats
10377	UV Earth Flats
10378	Polarization Calibrations

The CCD daily monitoring program will continue to provide dark and bias frames to build the corresponding bi-weekly reference files. The CTE monitoring program will continue to characterize the CCDs' CTE losses as a function of time, field crowding and background levels, and define recipes to calibrate them. Also, rough measures and monitoring of available post-flash background levels were made to allow its use in future cycles in mitigating CTE losses (these observations do not -- and will not

for Cycle 14 -- constitute calibrations sufficient for reducing science data). Annealing of CCD hot pixels will continue as during Cycles 11 and 12, and possible contamination to the UV throughput will be monitored, although less frequently. Observations will be obtained to further define zeropoints, and to check filter bandpasses. The photometric calibration for compact or point sources with very red spectral energy distribution will be provided through observations of extreme red stars. The stability of the photometric calibration, geometrical distortions and flat fielding will also be measured and monitored through dedicated programs. Polarization calibrations will fully characterize the internal polarization of the instrument.

---

## 13.6 Cycle 14 Calibration

The Cycle 14 calibration program will be developed in detail during mid-2005 at which time: (1) instrument performance will have been tracked for three years on-orbit; (2) the results from Cycles 11 and 12 and, at least in part, Cycle 13 calibration programs will be known with documented results; (3) feedback will be available from the community on the effectiveness of ACS calibrations to date; (4) the approved Cycle 14 science program and implied instrument use will be known.

The goal of the Cycle 14 calibration program will again be to optimally support science results from the community while balancing the program with available resources (HST orbits and staff analysis time). Routine calibrations such as darks will be carried forward at the proper cadence. Resources will also be allocated for further characterization of capabilities and calibration of science observations as required in response to evolution of either performance or needs reflected in the science program as a whole.

In special circumstances proposers may wish to request additional orbits for the purpose of calibration. These can be proposed in two ways and should be for calibrations that are not likely to be in the core calibration programs. An example of a non-core calibration would be one that needs to reach precision levels well in excess of those outlined in Tables 12.1, 12.2 or 12.3.

The first type of special calibration would simply request additional orbits within a GO program for the purpose of calibrating the science data to be obtained (see Section 4.3 of the *Call for Proposals*). In this case the extra calibration would only need to be justified on the basis of the expected science return of the GO's program.

The second type of special calibration would be performed as a general service to the community via Calibration Proposals (Section 3.6 of *Call for Proposals*). In this case the calibration observations should again be outside the core responsibilities of the ACS group to perform, and furthermore should be directed at supporting general enhancement of ACS

capabilities with the expectation of separately negotiated deliverables if time and/or funding are granted.

Proposers interested in obtaining either type of special calibration should consult with Instrument Scientists from the ACS Group via questions to the Help Desk at least 14 days before the proposal deadline in order to ascertain if the proposed calibrations would be done at STScI in the default program.

Observations obtained for calibration programs will generally be flagged as non-proprietary.

# Glossary

The following terms and acronyms are used in this Handbook.

**A-D:** Analog to digital

**ABMAG:**  $-2.5 \log (F_{\nu}) - 48.60$  where  $F_{\nu}$  is the flux from the source in  $\text{erg cm}^{-2} \text{sec}^{-1} \text{Hz}^{-1}$

**AB<sub>ν</sub>:** Correction to ABMAG to account for the fact that the source spectrum is not constant in  $F_{\nu}$  ( $\text{ABMAG} = V + \text{AB}_{\nu}$ )

**ABC:** Aberrated Beam Coronagraph

**ACS:** Advanced Camera for Surveys

**APT:** Astronomer's Proposal Tools

**BOP:** Bright-Object Protection

**calacs:** ACS calibration pipeline software

**CCD:** Charge Coupled Device. Solid-state, light detecting device

**CDBS:** Calibration Data Base System for maintaining reference files and tables used to calibrate HST observational datasets.

**CP:** Call for Proposals

**CR:** Cosmic ray

**CR-SPLIT:** Division of a CCD exposure into shorter exposures to be used for cosmic ray rejection

**CS:** Contact Scientist

**CTE:** Charge transfer efficiency

**CVZ:** Continuous viewing zone

**DQ:** Data quality

**DN:** Data number

**ETC:** Exposure Time Calculator. ETCs are web-based tools which can be accessed through the ACS web pages.

**ERO:** Early release observations

**FAQ:** Frequently asked questions

**FGS:** Fine Guidance Sensors

**FITS:** Flexible Image Transport System. A generic IEEE and NASA defined standard file format used for storing image data.

**FOC:** Faint Object Camera

**FOS:** Faint Object Spectrograph

**FOV:** Field of view

**FSW:** Flight software

**FTP:** File Transfer Protocol. Basic tool used to retrieve files from a remote system. Ask your system manager for information about using FTP.

**FUV:** Far ultraviolet (~912-2000Å)

**FWHM:** Full width at half maximum

**GEIS:** Generic Edited Information Set. Multigroup format used by STS-DAS for storing some HST image data.

**GHRS:** Goddard High-Resolution Spectrograph

**GO:** General Observer

**GSC:** Guide Star Catalog

**GTO:** Guaranteed Time Observer

**HDA:** Hubble Data Archive

**Help Desk:** Facility for getting help on HST related topics via email. [help@stsci.edu](mailto:help@stsci.edu).

**HRC:** High Resolution Channel

**HSP:** High-Speed Photometer

**HST:** Hubble Space Telescope

**HUT:** Hopkins Ultraviolet Telescope

**ICD:** Interface control document. Defines data structures used between software or systems to ensure compatibility.

**IDT:** Investigation Definition Team

**IHB:** Instrument Handbook

**IR:** Infrared

**IRAF:** Image Reduction and Analysis System. The environment in which STSDAS operates.

**IS:** Instrument Scientist

**ISR:** Instrument Science Report

**IUE:** International Ultraviolet Explorer

**K:** Degree Kelvin

**LMC:** Large Magellanic Cloud

**MAMA:** Multi-Anode Microchannel Array

**MCP:** Microchannel Plate

**ND:** Neutral density

**NICMOS:** Near-Infrared Camera and Multi-Object Spectrograph

**NUV:** Near ultraviolet ( $\sim 2000\text{--}4000\text{\AA}$ )

**OSS:** Observation Support System

**OTA:** Optical Telescope Assembly

**OTFC:** On-the-Fly Calibration

**OTFR:** On-the-Fly Recalibration

**PC:** Program Coordinator

**Phase I proposal:** A proposal for observing time on HST

**Phase II program:** An approved HST program; includes precise detail of how program is to be executed

**PI:** Principal investigator

**PSF:** Point-spread function.

**PyRAF:** version of IRAF implemented in the Python language

**QE:** Quantum efficiency

**QEH:** Quantum efficiency hysteresis

**QSO:** Quasi-stellar object

**RA:** Right ascension

**reference file:** data file containing ACS parameters or calibration information which is used by the calibration pipeline

**rms:** Root mean square

**SAA:** South Atlantic anomaly

**SBC:** Solar-Blind Channel

**SITe:** Scientific Image Technologies; company that designed the ACS CCDs

**SMOV:** Servicing Mission Observatory Verification

**S/N:** Signal-to-noise ratio

**ST-ECF:** Space Telescope European Coordinating Facility

**STAN:** Space Telescope Analysis Newsletter

**STIS:** Space Telescope Imaging Spectrograph

**STMAG:** STScI magnitude system;  $-2.5 \log (F_{\lambda}) - 21.10$  where  $F_{\lambda}$  is the flux from the source in  $\text{erg cm}^{-2} \text{sec}^{-1} \text{\AA}^{-1}$

**STScI:** Space Telescope Science Institute

**STSDAS:** Space Telescope Science Data Analysis System. The complete suite of IRAF data analysis and calibration routines used to process HST data.

**SV:** Science verification. Process of taking observations that can be used for HST instrument calibration.

***synphot:*** STSDAS synthetic photometry (IRAF) software package

**TAC:** Telescope Allocation Committee

**TIR:** Technical Instrument Report

**URL:** Uniform resource locator. Address for WWW.

**UV:** Ultraviolet

**WFC:** Wide-Field Channel

**WF/PC:** Wide Field/Planetary Camera

**WFPC2:** Wide Field Planetary Camera-2. Replacement for WF/PC installed during first servicing mission of December 1993.

**WWW:** World Wide Web. Hypertext-oriented method for finding and retrieving information over the Internet.

# Index

## A

- AB(nu) 106, 201, 245
- Aberrated Beam Coronagraph 70
- Aberration Correction 24
- ABMAG 103, 201
- ACCUM mode
  - HRC 160
  - SBC 161
  - WFC 158
- Accuracies
  - HRC 275
  - SBC 275
  - WFC 274
- ACQ mode
  - effective neutral density filters 162
  - HRC 162
- Analysis 289
- Annealing
  - HRC 139
  - WFC 139
- Apertures
  - HRC 161, 175
  - SBC 175
  - WFC 158, 169
- A-to-D Converter
  - HRC 131, 160
  - WFC 131, 158
- Auto-Parallels 182

## B

- Bandpass 37, 103, 203
- Blooming 131
- BOP

- exceeding bright object limits 154
  - screening 153, 154
  - solar system objects 154
- Bright Object Protection 149
  - global limit 151
  - limiting V magnitudes 152
  - local limit 151
- Buffer
  - compression 158
  - HRC 161
  - internal memory 28
  - overheads 158
  - SBC 162

## C

- CALACS
  - flow diagram CCD 265
  - Switches 259
- Calibration
  - accuracies 273
  - ground testing 278
  - lamps 27
  - non-science exposures 34
  - outsourcing 285
  - pipeline 257
  - polarizers 64
  - SMOV3B 278
- Call for Proposals (CP) 8
- Capabilities
  - coronagraphy 22
  - imaging 21
  - polarimetry 22
  - spectroscopy 22
- CCDs

HRC. See HRC  
 WFC. See WFC  
 CDBS 258  
 Charge Transfer Efficiency 140  
 Comparison of Instruments 41  
 Coordinated Parallels 182  
 Coronagraph  
   design 70  
 Coronagraphy  
   exposure time calculation 85  
   Lyot stop 70  
   occulting finger 72  
   occulting masks 70  
   PSF 82  
   target acquisition 161, 162  
 Cosmic Rays  
   HRC 136  
   WFC 136  
 Cosmic rays 136  
 Count Rate Limits  
   SBC 144, 149  
 CR-SPLIT 163, 165, 183, 190  
 CTE 16, 140  
 Cycle 12  
   calibration plan 282  
 Cycle 13  
   calibration plan 284  
   scheduling policies 12  
 Cycle 14  
   calibration plan 285  
**D**  
 Dark Current  
   HRC 126  
   SBC 144  
   WFC 126  
 Data 288, 289  
 Data Number (DN) 128, 158, 160  
 Data Quality (DQ) 269  
 Data Storage  
   buffer size 29  
 Data Transfer 28  
 Data Volume 16  
 Detectors  
   HRC. See HRC

SBC. See SBC  
 WFC. see WFC  
 Dithering  
   goals 162  
   strategy 163  
   STSDAS dither package 164  
 Documentation  
   FAQs 9  
   requesting 9  
   world wide web 10  
 Drizzle 167  
 Dynamic Range 168  
**E**  
 Earthshine 114, 122  
 Encircled Energy  
   models 56  
 Exposure Time Calculator (ETC) 101  
   bright object limits 152  
   examples 118  
   sky backgrounds 122  
 Exposures  
   calibration 34  
   overheads 190  
   target-acquisition 34  
 Extinction 117  
**F**  
 FAQs 9  
 Field of View (FOV)  
   HRC 22, 41, 175  
   HST 30  
   SBC 22, 41, 175  
   WFC 21, 41, 169  
 Filter Wheel  
   SBC 26  
   WFC/HRC 26  
 Filters 27, 37, 102  
   HRC/F220W 216, 217  
   HRC/F250W 218  
   HRC/F330W 219  
   HRC/F344N 220  
   HRC/F435W 221  
   HRC/F475W 222

- HRC/F502N 223
- HRC/F550M 224
- HRC/F555W 225
- HRC/F606W 226
- HRC/F625W 227
- HRC/F658N 228
- HRC/F660N 229
- HRC/F775W 230
- HRC/F814W 231
- HRC/F850LP 232
- HRC/F892N 233
- HRC/G800L 234
- HRC/PR200L 235
- Johnson-Cousins 50
- narrow-band 50
- Ramp Filters
  - HRC 52
  - WFC 50
- SBC Summary Table 38
- SBC/F115LP 237
- SBC/F122M 238
- SBC/F125LP 239
- SBC/F140LP 240
- SBC/F150LP 241
- SBC/F165LP 242
- SBC/PR110LP 243
- SBC/PR130LP 244
- Sloan Digital Sky Survey 50
- WFC/F435W 203
- WFC/F475W 204
- WFC/F502N 205
- WFC/F550M 206
- WFC/F555W 207
- WFC/F606W 208
- WFC/F625W 209
- WFC/F658N 210
- WFC/F660N 211
- WFC/F775W 212
- WFC/F814W 213
- WFC/F850LP 214
- WFC/G800L 215
- WFC/HRC Summary Table 37
- Flat Field
  - general 259
  - HRC 131
  - SBC 148
  - WFC 129
- Fringing 127
- Full Well 41, 131
- Full Width Half Maximum (FWHM)
  - HRC 51
  - WFC 49
- G**
- Gain
  - HRC 128, 160
  - WFC 128
- Geocoronal emission 116
- Geometric Distortion
  - HRC 251
  - PSF 58
  - temporal changes 163
  - WFC 49
- Ground Testing 278
- H**
- Help Desk 9
- Hot Pixels 137
- HRC
  - ACCUM 160
  - accuracies 275
  - ACQ mode 162
  - apertures 161, 175
  - A-to-D converter 160
  - buffer 161
  - characteristics 51, 126
  - coating 126
  - cosmic rays 136
  - dark current 126
  - description 23
  - flat field 131
  - fringing 127
  - full well 131
  - full width half maximum (FWHM) 51
  - gain 160
  - hot pixels 137
  - multiple electron events 52, 142
  - occulting masks 176
  - physical overscan 128
  - plate scale 180
  - point spread function 56

QEH 127  
 ramp filters 160  
 read noise 126  
 readout 128  
 red leaks 52  
 saturation 131  
 spectral response 127  
 subarrays 161  
 virtual overscan 128

**I****Imaging**

caveats 46  
 filters 36, 52, 53  
 HRC detector 51  
 limiting magnitude 48  
 saturation 49  
 SBC detector 53  
 signal-to-noise 49  
 throughput 47  
 WFC detector 49

Instrument 290

Integrated System Throughput 47

**L****Lamps**

deuterium 27  
 tungsten 27

Light Paths 25, 26

Limiting Magnitudes 48

**Linearity**

CCDs 169  
 SBC 149

LOW-SKY 116

Lyot Stop 70

**M**

Magnitude 289

MAMA. See SBC

Memory. See Buffer

**N**

NICMOS

characteristics 41

comparison 43

Non-linearity

SBC 149

**O****Observing Considerations**

coronagraph 28

dithering 28

pattern 28

Observing Strategy 165

**Observing Techniques**

coronagraphy 85

On-The-Fly-Reprocessing (OTFR) 257

**Optical Path**

HRC/SBC 26

WFC 25

**Optics**

coronagraph 24

corrective optics 24

fold mirror 24

HRC/SBC 24

spherical aberration 24

WFC 24

Orbit-Time Determination 189

ORIENT 178

**Orientation**

computing 177

ORIENTAT 178

PA\_APER 178

**Overheads**

buffer size 190

examples 192

types 187

**P****Parallel Observations**

coordinated parallels 182

pointing 181

pure parallels 185

visual target tuner 181

Parallel Observing 29

Patterns 162

Phase I

- bright object limits 152
  - preparation 6, 29, 157
- Phase II
  - bright object limits 152
  - preparation 8
- Photometry
  - accuracy 274
  - encircled energy 56, 103
  - zero point 103
- Pipeline
  - data products 266
  - see calacs 289
  - storage requirements 269
- Pivot Wavelength 103
- Pixel Response Function (PRF) 55
- Plate Scale 180
- Point Spread Function (PSF)
  - HRC 56
  - WFC 56
- Pointing Stability 165
- Polarimetry
  - Calibration 64
  - filters 66, 68
  - FOV 67
  - throughput 64
- Policy
  - CCD
    - auto-parallels 14
  - SBC
    - bright-object protection 12
    - coronagraph 24
    - parallel observing 13
- Post-flash 27
- Precision 273
- Proposal 289
  - BOP 149
  - exposure time 33
  - feasibility 33
  - Phase I 8
  - Phase II 8
  - subarrays 34
  - tradeoffs 32
- Proposals
  - calibration exposures 34
- PSF
  - coronagraphy 82
  - encircled energy 56

- geometric distortion 58
  - HRC halo 52
  - models 55
  - PRF 55
  - residual aberrations 59
  - SBC halo 54
  - TinyTIM 54, 55
  - WFC halo 51
- Pure Parallels
  - pure parallel program 185

## Q

- Quantum Efficiency Hysteresis 127

## R

- Ramp Filters
  - aperture location 160
  - apertures 171
  - See Filters
- Read Noise 41
- Readout Time 23, 190
- Red Leaks
  - HRC 52
  - SBC 54

## S

- Saturation
  - CCDs 131
  - SBC 145
- SBC
  - ACCUM mode 142, 161
  - Accuracies 275
  - accuracies 275
  - apertures 175
  - BOP 155
  - buffer 162
  - characteristics 53, 144
  - description 23
  - flat field 148
  - global count rate 149
  - limiting count rates 150
  - local count rate 149
  - microchannel plate 143
  - PSF 54, 145
  - red leaks 54

- repeller wire 54, 143
- signal-to-noise ratio 147
- spectral response 144
- Scheduling
  - SBC considerations 12
- Sensitivity
  - HRC/G800L 93, 94
  - HRC/PR 200L 95
  - WFC/G800L 90, 91, 92
- Shutter 132
- Signal-to-Noise 109
- sky background 122
- SMOV3B
  - proposals 278
- Solar System Objects 154
- South Atlantic Anomaly 12
- Spectral Response. See Imaging throughput 47
- Spectroscopy
  - HRC 91
  - SBC 94
  - WFC 89
- ST-ECF
  - help desk 9
- STIS 12
  - characteristics 41
  - comparison 44
  - filter curves 45
- Subarrays
  - amplifier 159
  - coronagraph 161
  - data volume 159
  - HRC 161
  - overscan 159
- Synphot 102

**T**

- Target ACQ
  - accuracy 28
  - aperture 28
  - coronagraph 28
  - ramp filters 28
- Terms used in this manual 287
- TinyTIM 54, 55
- Tools 287
- Transmission Curves

- broad-band filters 39
- medium-band filters 39
- narrow-band filters 40
- SBC filters 40
- SDSS filters 39

## U

- Undersampling 49, 51
- User Support
  - help desk 9

## W

- WFC
  - ACCUM 158
  - accuracies 274
  - apertures 158, 169
  - characteristics 49, 126
  - cosmic rays 136
  - dark current 126
  - description 23
  - flat field 129
  - fringing 127
  - full well 131
  - full width half maximum (FWHM) 49
  - hot pixels 137
  - physical overscan 128
  - plate scale 180
  - point spread function 56
  - QEH 127
  - ramp filters 160
  - read noise 126
  - readout 128
  - saturation 131
  - spectral response 127
  - virtual overscan 128
- WFC/HRC Summary Table 103
- WFPC2
  - characteristics 41
  - comparison 42
  - filter curves 43
- WWW pages 9

## Z

- Zodiacal Light 116, 122



